THE UNIVERSITY *of* EDINBURGH

Improving engraftment for cell therapy in cholangiopathies

Mark Macmillan-John

Doctor of Philosophy – The University of Edinburgh 2023

Table of Contents

Declaration

I declare that this thesis has been composed by myself and represents my own work. The experiments herein were performed by me alone except where explicitly stated otherwise in the text. This thesis has not been submitted for any other degree or professional qualification and does not exceed the word limit of 100,000 words set by the College of Medicine and Veterinary Medicine.

Mark Macmillan 01/02/2023

Acknowledgements

I would like to thank my supervisors Professor Stuart Forbes and Dr. Luke Boulter for their guidance and support during my PhD. I feel incredibly grateful to have worked in such a successful lab, I believe that I have been given every opportunity for success during my PhD, which is an incredibly fortunate position to have been in.

I count myself lucky to have received all the help I have during this process. I am blessed that so many people have treated me with kindness and limitless patience, in particular Daniel Rodrigo-Torres, Sofia Ferreira-Gonzalez, Victoria Gadd, Alastair Kilpatrick, Ben. Dwyer, Candice Ashmore-Harris, Janet Man and Rhona Aird. I have learned so much and hope I can repay this by passing on the knowledge that has been imparted to me.

I have also been fortunate to have guidance from the ECAT team throughout my PhD. Professors Neil Henderson, Andrew Jackson, Amanda Drake and Sarah Stock have all contributed to my development and I will always count myself privileged to have had the opportunity to have had access to their guidance.

I would also like to mention my family; my wife Jeeva who has helped me to see the bigger picture during more challenging times. I'm sure I would not have completed this without her support. My mother who has always maintained unwavering faith in me, which has been comforting when my self-belief has been tried.

There are people whom I never have and never shall meet, that I also have gratitude for. I feel blessed to have access to the wisdom of those who have come before me. The view is dizzying when standing on the shoulders of giants.

Finally, I thank God if there is anything well that I have done, it is surely his. Trust in the LORD with all your heart; do not depend on your own understanding (Proverbs 3;5).

Abstract

The cholangiopathies are a group of conditions associated with injury to the bile ducts in the liver. Recent murine studies have demonstrated the potential of hepatic progenitor cells (HPC) as cell therapy for the treatment of cholangiopathies.

The biliary engraftment of HPC in the *Krt19Cre^{ER}Mdm2 $^{fl/fl}$ Rag2$^{-/-}$ Il2rg$^{-/-}$* mouse model of cholangiopathy is poor at present, this could limit the progression of this therapy to the clinic. The aim of this thesis is to improve biliary engraftment of human HPC in the *Krt19Cre^{ER}Mdm2 $^{fl/fl}$ Rag2$^{-/-}$ Il2rg$^{-/-}$* model of cholangiopathy.

The identification of specific markers in the biliary system which were upregulated in injury was made. Using this information, markers were targeted with receptors upregulated in the plasma membrane of transplanted human HPC.

To identify a marker, the expression of biliary specific proteins SCTR, CD44, TFF2, CCL2, CXCL1 and CXCL2 was investigated in the *Krt19Cre^{ER}Mdm2 $^{fl/fl}$ Rag2$^{-/-}$ Il2rg$^{-/-}$* model. CXCL2 was upregulated in injury and had higher expression in the biliary ducts when compared with hepatocytes. A proteomic analysis was also performed which did not yield additional targets, however it did identify two novel biliary specific proteins in ANXAV and MYH14.

The receptor for CXCL2 is CXCR2. In this thesis we demonstrated CXCR2 is not normally expressed in HPC. It was shown that HPC could be transduced to express CXCR2 and GFP using a lentivirus construct.

CXCR2 and GFP expressing HPC were transplanted into the *Krt19Cre^{ER}Mdm2 $^{fl/fl}$ Rag2$^{-/-}$ Il2rg$^{-/-}$* model of cholangiopathy. Transplanted cells were demonstrated to engraft in close proximity to the bile ducts. When compared with GFP only HPC, CXCR2 GFP HPC were found adjacent to fewer ducts but in larger numbers. The potential for developing a homing system for transplantation of HPC in the cholangiopathies is demonstrated in this thesis.

Lay abstract

The bile ducts allow bile to flow from the liver, where it is produced, to the bowel, where it is used to aid digestion. Conditions which specifically injure the bile ducts are known as the cholangiopathies. Cholangiopathies may all progress to cause the liver to fail. In such cases liver transplantation, in which a patient's liver is replaced by a liver which is donated from another person following death.

There are limited livers available for transplantation, therefore alternate treatments are desired. Cell therapies in which cells (donor) are injected into patients (recipients) in the hope of regenerating the bile ducts, have shown promise in recent years in mouse models of cholangiopathy.

Despite the initial positive results associated with cell therapy, only few cells reach the bile ducts. Improvements in delivering cells to the bile ducts are therefore required prior to using this treatment in humans.

One method for improving cell delivery to the ducts is altering donor cells, such that they express proteins on their surface which can interact with proteins in the body of the recipient. Selecting proteins which interact with proteins in the bile ducts of the recipients may improve the ability of donor cells to arrive at the ducts.

In this thesis a catalogue of proteins present in the bile ducts is produced. After selecting a protein present in the bile ducts, namely CXCL2, a homing mechanism was developed. CXCR2, which interacts with CXCL2, was placed on the surface of donor cells intended for transplantation. CXCR2 cells were then transplanted into a mouse with injury to the bile ducts and were demonstrated to engraft near the bile ducts.

This research has demonstrated the potential to develop homing systems in cells used for cell therapy in the cholangiopathies.

List of Abbreviations

AAV	Adeno-associated virus
ABCB11	ATP-binding cassette subfamily B member 11
ABCG	ATP-binding cassette transporter
ACH	Acetylcholine
ACKR2	Atypical chemokine receptor 2
ADHLSC	Adult derived human stem/progenitor cells
ADP	Adenosine diphosphate
Adv. DMEM	Advanced Dulbecco's modified eagle medium
AE2	Anion exchange protein 2
AIDS	Acquired immune deficiency syndrome
ALA	δ-aminolaevulinate
ALP	Alkaline phosphatase
ALT	Alanine aminotransferase
ASBT	Apical sodium dependent bile transporter
ASGPR	Asialoglycoprotein receptor
AST	Aspartate Aminotransferase
ATP	Adenosine triphosphate
ATP8B1	ATPase Phospholipid Transporting 8B1
AQP-1	Aquaporin-1
BDL	Bile duct ligation
BEC	Biliary epithelial cells
BNHS	Biotinyl-N-hydroxy-succinimide
BSA	Bovine serum albumin
BSEP	Biliary salt export protein
cAMP	Cyclic adenosine monophosphate
CBD	Common bile duct
CCl_4	Carbon tetrachloride
CCL2/7	C-C chemokine ligand 2/7
CCR2	C-C chemokine receptor 2
CD24/44/133	Cluster of differentiation 24/44/133
cIAP	Cellular inhibitor of apoptosis proteins
CF	Cystic fibrosis

CFTR	Cystic fibrosis transmembrane conductance regulator
CMV	Cytomegalovirus
CX3CL1	CX3 chemokine ligand 1
CX3CR1	CX3 chemokine receptor 1
CXCL1/2	C-X-C chemokine ligand 1/2
CXCR2/4/5	C-X-C chemokine receptor type 2/4/5
DAB	3,3'-Diaminobenzidine
DAPI	4′,6-diamidino-2-phenylindole
DBD	Donation after brain death
DCA	Deoxycholate
DCD	Donation after circulatory death
DDC	3,5-diethoxycarbonyl-1,4-dihydrocollidine
DTT	Dithiothreitol
E. COLI	Escherichia Coli
EDTA	Ethylenediaminetetraacetic acid
EGTA	Ethyleneglycol-bis-N,N,N′,N′-tetraacetic acid
ERCP	Endoscopic retrograde cholangiopancreatography
FACS	Fluorescence activated cell sorting
FCS	Fetal calf serum
FSC	Forward scatter
GAPDH	Glyceraldehyde 3-phosphate dehydrogenase
GFP	Green fluorescent protein
GLP1R	Glucagon like peptide receptor 1
GLDH	Glutamate dehydrogenase
GMEM	Glasgow modified eagle medium
HA	Hyaluronic acid
HEK 293T	Human embryonic kidney 293T
HEPES	N-2-hydroxyethylpiperazine-N-2-ethane sulfonic acid
HPC	Hepatic progenitor cells
IL2rg	Interleukin 2
IVC	Inferior vena cava
KIF3A	Kinesin-like proteins 3a
KRT19	Keratin 19

LAM	Lipid associated macrophages
LCA	Lithocholate
LDM	Liver digest media
LDS	Lithium dodecyl sulphate
LMOD1	Leiomodin 1
LPM	Liver perfusion media
LPS	Lipo-polysaccharide
M3	Muscarinic receptor 3
MDR2/3	Multi drug resistant protein 2/3
MDM2	Mouse double minute homologue 2
MOPS	3-N-morpholinopropanesulfonic acid
MSC	Mesenchymal stem cells
MYH14	Non-muscle myosin IIc
NAFLD	Non-alcoholic fatty liver disease
NHSB	N-Hydroxysulfosuccinimide biotin
NOTCH	Neurogenic locus notch homolog protein
NTCP	Sodium taurocholate co-transporting polypeptide
OATP	Organic anion transporter
OLT	Orthoptic liver transplant
PEI	Polyethylenimine
PerCP	Peidinin chlorophyll
PBC	Primary biliary cholangitis
PBS	Phosphate buffered saline
PGM5	Phosphoglucomutase-like protein 5
PK2DLI	Polycystic kidney disease 2 like 1 protein
PPIA	Peptidylprolyl isomerase A
PS	Phosphatidylserine
PSC	Primary sclerosing cholangitis
PTC	Percutaneous transhepatic cholangiography
qPCR	Quantitative polymerase chain reaction
RAG2	Recombination activating gene 2
RFP	Red fluorescent protein
RIPA	Radioimmunoprecipitation assay

SCT	Secretin
SCTR	Secretin receptor
SDF1	Stromal derived factor 1
SLex	sialyl-Lewisx
SIRT	Selective internal radiation therapy
SMAC	Second mitochondria-derived activator of caspase
SOX	Sex determining region Y-Box Transcription Factor
SSC	Side scatter
SSTR2	Somatostatin receptor 2
TAA	Thioacetamide
TACE	Trans-arterial chemo-embolization
TBG	Thyroxine binding globulin
TBS	Tris-buffered saline
TFF2	Trefoil factor 2
TGF-β1	Transforming growth factor beta 1 (TGF-β1)
TGF-RII	Transforming growth factor beta receptor II
TJP2	Tight junction protein 2
TPM1/2	Tropomyosin alpha-1/2
TRPV4	Transient receptor potential cation 4
UDCA	Ursodeoxycholate
UDP	Uridine diphosphate glucose
VCAM-1	Vascular cell adhesion molecule 1
ZNF830	Zinc finger protein 830

List of figures

List of tables

Chapter 1: Introduction

1.1 The biliary system

The biliary system consists of a branching network of epithelialised ducts, which extend from the bile canaliculi, formed by hepatocytes, to the duodenum at the ampulla of Vater. It holds the important function of acting as a conduit for transportation of bile from the liver into the bowel. Bile is essential to bowel function, facilitating the digestion and absorption of fats and fat-soluble vitamins, whilst also acting as a means by which the liver can excrete waste metabolites.

The parenchyma of the liver is arranged into lobules, which contain rows of hepatocytes separated by channels for blood, hepatic sinusoids (Figure 1.1B). Hepatocytes and sinusoids are arranged in a hexagonal shape around a central draining vein. In the outer corners of the hexagon, branches of the hepatic artery, portal vein and bile ducts are present within connective tissue; together these structures form a portal triad. Blood passes from the artery and portal vein in the corners of the hexagon through the sinusoids, towards the draining central vein. The sinusoids are lined by fenestrated, interrupted epithelial cells, which allow proteins and small cells to pass from the blood into the underlying space of Disse between the endothelial cells and the hepatocytes. The space of DIsse contains hepatic stellate cells. Stellate cells are thought to be important for immune response within the liver, whilst also having a role to play in the development of hepatic fibrosis[1]. Associated with the endothelium are resident hepatic macrophages known as Kupffer cells [2].

The biliary drainage system flows in the opposite direction of blood in the hepatic lobules, from the areas closest to the central vein to the bile ducts in the corners of the lobule[3]. Bile is initially produced by hepatocytes and is excreted into biliary canaliculi, which form between hepatocytes. These canaliculi are contained by tight junctions at their edges, which form between the plasma membranes of neighbouring hepatocytes.

On approaching the portal triads, canaliculi drain into ducts lined with BEC, known as Canals of Hering. These are most commonly found at the interface between the hepatic parenchyma and the portal triads; however, they may also extend into the hepatic parenchyma, albeit separated by a dedicated basement membrane. Once inside the portal triad, ducts connect forming interlobular ducts. Ducts continue to join and enlarge eventually forming septal ducts, which in turn form area ducts [4].

Grossly, the human liver can be divided into eight segments. Each segment, in classical anatomy, has a single lobar portal triad containing: a portal vein, hepatic artery branch and a segmental duct supplying it. Segmental ducts form from the convergence of the area ducts and combine to produce anterior, and posterior sectoral ducts, however this anatomy is variable. The sectoral ducts combine to form the right and left main ducts, which in turn form the common hepatic duct at the hepatic hilum (Figure 1.1A). Area ducts and those larger and distal contain peribiliary glands, which extend from the lumen of the bile duct into the surrounding connective tissue and produce mucus.

In the extrahepatic portion of the liver, the common hepatic duct is joined by the cystic duct, which connects the gallbladder to the rest of the biliary tree. At this point, another name change occurs as the common bile duct (CBD) is formed (Figure 1.1A). The CBD traverses the head of the pancreas and opens into the second part of the duodenum through the ampulla of Vater, thus allowing bile to enter the small bowel.

In order for bile to transit through the biliary system, it is essential that bile is contained by the biliary epithelium and does not leak into the hepatic parenchyma, particularly as components of bile can be toxic to cells[5]. BEC are held together by tight intercellular junctions, impassable to cells proteins and large molecules. This creates two aspects of the BEC cell membrane, one facing the bile, the apical side, and one the hepatic parenchyma, the basolateral side. The apical aspect of BEC are exposed to bile, and produce a layer of bicarbonate rich fluid, which acts as a barrier between the bile and the BEC for protection, known as the bicarbonate umbrella.

The blood supply of the liver is complicated by the fact that it comes from two sources, namely the hepatic artery and portal vein. The portal vein carries blood from the bowel, which is poor in oxygenation, whilst rich in nutrients. The bowel is extensively colonised by bacteria; therefore, the portal vein can be a conduit for toxins and microorganisms to enter the liver. Hepatocytes are equipped to process the nutrient rich blood, metabolising fats, and carbohydrates for further storage or use, and producing multiple essential proteins from amino acids. The Kupffer cells, which are present on the endothelium can monitor the blood for pathogens, which have entered via the gut, before entering the systemic circulation. As the portal vein provides relatively poorly oxygenated blood, the liver also receives supply from the hepatic artery.

The biliary system has no significant role in the metabolism of drugs, and nutrients, and therefore, only receives blood from the hepatic artery through a network of arterioles known as the peribiliary plexus (Figure 1.1C). This is an important distinction for clinical practice as injuries to the hepatic artery can lead to biliary injury without causing significant damage to the hepatic parenchyma [6, 7]. A further distinction can be made between the intra- and extra-hepatic ducts in terms of blood supply, with the intrahepatic ducts receiving supply from the hepatic artery proper whilst the extrahepatic ducts are supplied from a branch of the common hepatic artery, the gastroduodenal artery.

Figure 1.1 Structure of the biliary system within the liver.

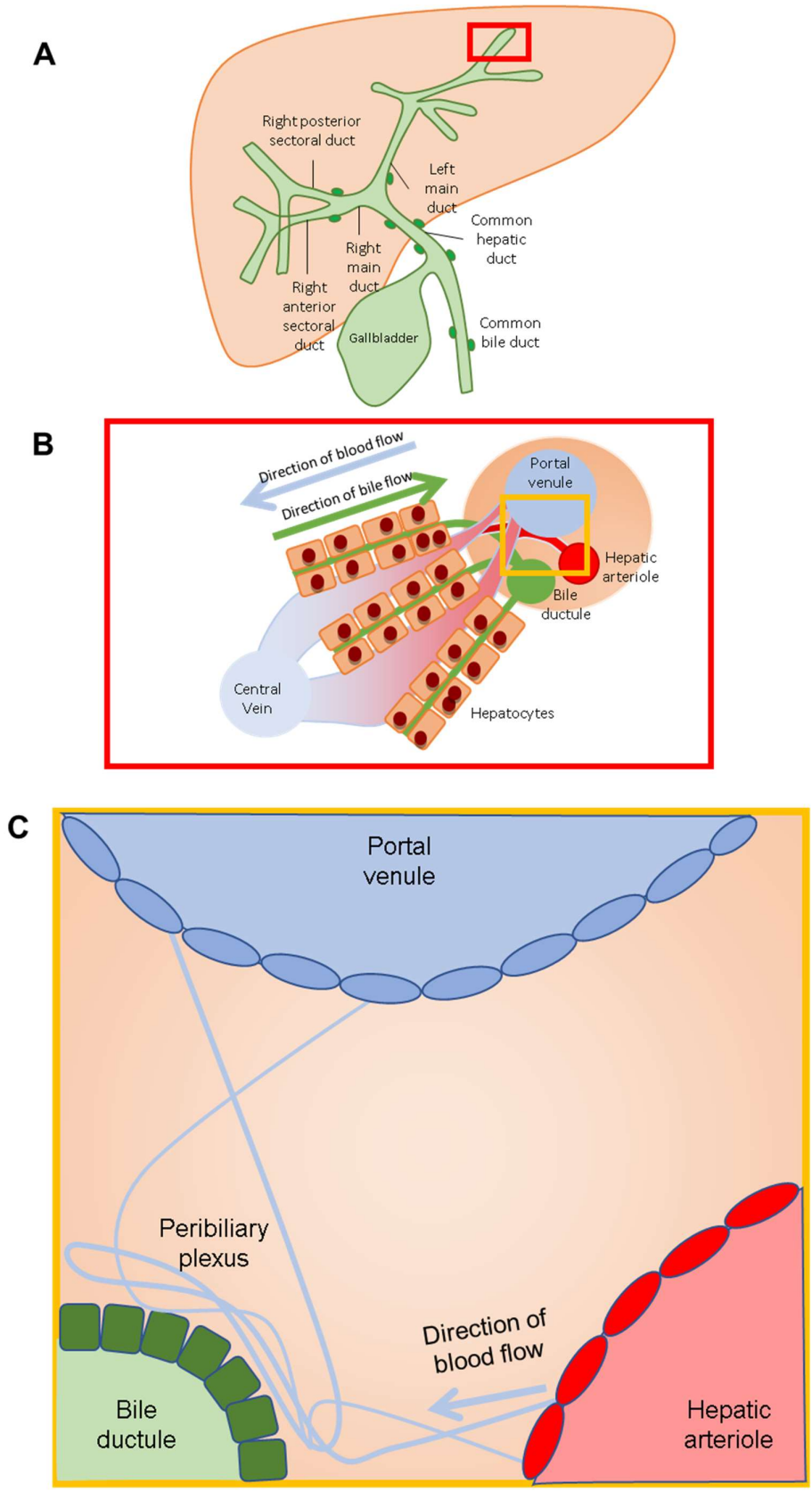

Figure 1.1 Structure of the biliary system within the liver.

A: Schematic demonstrating the gross anatomy of the biliary tree.

B: Arrangement of the portal triads in relation to hepatocytes biliary canaliculi and hepatic sinusoids.

C: View of the portal triads demonstrating branches of the hepatic artery and vein, a biliary ductule and the peribiliary plexus.

1.2 Intra- and extrahepatic ducts

Although the biliary system forms a continuous tract, it is constituted of subsections, which have distinct functions, anatomical features, and embryological origins. The clearest separation that can be made is between intrahepatic ducts, which lie within the liver, and extrahepatic ducts, which do not.

Intrahepatic BEC have a cuboidal appearance whilst the extrahepatic ducts have a columnar configuration[8], which may reflect a more secretory phenotype. In addition, intrahepatic ductular cells are more likely to have smaller overall cell volume, and higher nucleus-to-cytoplasm ratio. Cells with such appearances are known as small BEC in contrast to large BEC.

Embryologically, both the intra and extrahepatic ducts develop from the ventral foregut as part of the hepatic diverticulum[9]. As gestation progresses, the hepatic bud, which will give rise to the liver, forms at the cranial- and ventral-most part of the diverticulum. At the caudal end, the hepatic diverticulum is hollow, and will form the extrahepatic biliary tree and ventral pancreas.

The intrahepatic ducts develop from mesenchymal cells, which surround the developing portal vein and venules known as the ductal plate. Within the ductal plate, cells aggregate parallel to the portal veins. As the clumps become larger, they develop lumina, which begin to connect and form ducts. This process occurs in a hilar to peripheral direction, at partum, the most peripheral biliary ducts have not yet become patent [10]. As the ducts develop, they produce angiogenic factors, which cause the development of hepatic arterioles, and a capillary network adjacent to the bile ducts known as the peribiliary plexus[11]. This aspect of development illustrates the importance of the relationship between the biliary system and the hepatic artery.

The extrahepatic ducts develop from the caudal part of the hepatic diverticulum, which in contrast to ductal plate development, is hollow from inception, remaining so throughout gestation[12]. During in utero growth, the primitive extrahepatic duct elongates as the hepatic bud grows and fills the right upper quadrant of the embryonic abdomen. Following gestation, peribiliary glands develop as outpouchings from the extrahepatic biliary system.

In addition to the structural differences in the development of the intra- and extrahepatic biliary system, there are also distinctions in transcriptional regulators that drive

development. SOX9 (Sex determining region Y-Box Transcription Factor 9) is thought to be integral to the development of the intrahepatic ducts, whilst SOX17 is expressed in precursors of the extrahepatic biliary system [13, 14]. Poncy and co-workers in 2015, demonstrated paucity of intrahepatic ducts in mice with *Sox9* and *Sox4* knocked out; however, the hilar and extrahepatic ducts were not affected [15]. Uemura et al showed that insufficiency of Sox17 led to extrahepatic biliary duct defects, without significantly affecting the intrahepatic ducts [16].

These distinctions in development manifest in several ways in adulthood. Recently, Sampziotis and co-workers published single cell RNA sequencing of intra-hepatic, gallbladder, and CBD BEC. The data produced demonstrated that specific genes are upregulated in primary isolated cells of each subgroup, for example *Duox2,* which was expressed more in the intrahepatic ducts [17]. Separately, Rimland and co-workers demonstrated differences in the transcriptional landscape of cultured extra- and intrahepatic duct derived BEC. They were additionally able to show that intrahepatic duct derived BEC could be induced to express hepatocyte specific markers whilst the same did not occur in extrahepatic duct derived BEC [18]. These findings demonstrate that not only are intra- and extrahepatic ducts transcriptionally distinct, but they also retain these distinctions to some degree in culture.

Finally, of the conditions that affect the biliary system (the cholangiopathies), some exclusively affect the intrahepatic ducts, some, both the intra- and extrahepatic systems and others, the extrahepatic ducts only. The reasons for the proclivity of specific conditions to affect intra-, extrahepatic, or both remains largely unclear. However, they reinforce the idea that embryologically, physiologically, anatomically, and clinically, biliary ducts are not homogeneous, and care should be taken to not consider them as such.

Figure 1.2 Schematic demonstrating the differences between intra and extrahepatic ducts and BEC

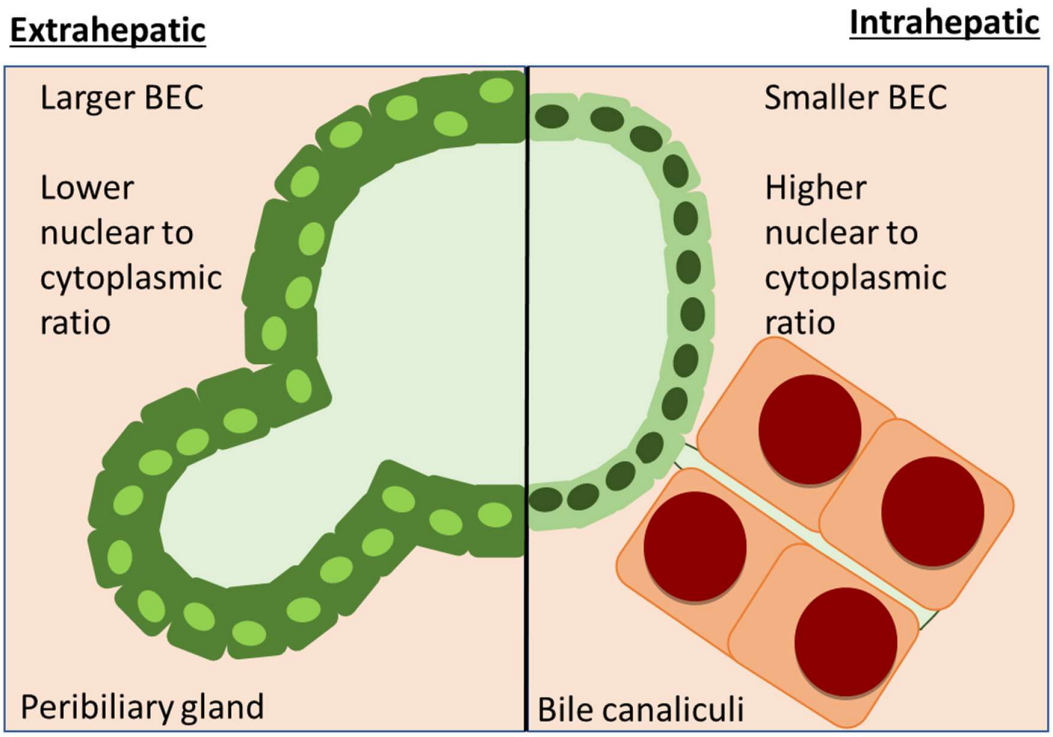

Figure 1.2 Schematic demonstrating the differences between intra and extrahepatic ducts and BEC.

Axial view of a biliary duct. Right side of the image demonstrates features of intrahepatic ducts. Orange cells represent hepatocytes with canaliculi leading into a duct.

Left side of image demonstrates features of extrahehepatic ducts with peribiliary gland.

1.3 The production and regulation of bile.

The role of hepatocytes

As noted, the smallest and most peripheral unit of the biliary tree are the bile canaliculi. Being the most peripheral, they are also the initial site of bile production, and are responsible for the majority of bile production. The canaliculi are formed by sections of the plasma membrane of neighbouring hepatocytes, with major components of bile entering the canaliculi via these hepatocytes. Bile is constituted by a mixture of substrates including, but not limited to bile acids, pigments, cholesterol, phospholipids, and electrolytes. Bile acids are one of the most important constituents, contributing to bile concentration and function. Hepatocytes produce the bile acids: cholic, and to a greater extent, chenodeoxycholic acid through a cytochrome P450 dependant metabolism pathway[19]. Once produced, bile acids are subsequently conjugated with either taurine or glycine, which increases their amphipathic potential, an essential characteristic for their function. Conjugated bile acids are then transported into the bile canaliculi in an energy dependent manner through the action of biliary salt export protein (BSEP)[20]. Bile acids are the major component of micelles, spheres in which the bile acids are orientated, with the hydrophilic pole presented externally and the hydrophobic pole internally. This arrangement allows hydrophobic fats to be carried within micelles, whilst the hydrophilic exterior of the micelles allows them to remain stable in an aqueous solution. Following delivery of bile into the gut, micelles can be absorbed by villi in the small intestine, allowing the absorption of fats and fat-soluble materials from the intestinal lumen [21], which otherwise would not be possible.

Bile acids are reabsorbed in the terminal ileum of the small bowel through the action of the apical sodium dependent bile transporter (ASBT)[22]. They are then returned into the blood through the reabsorption in the ileum, which is drained by the superior mesenteric vein, a tributary of the portal vein. The liver receives portal vein blood, and hepatocytes can reabsorb bile acids through the sodium taurocholate co-transporting polypeptide (NTCP), and organic anion transporters (OATP)[23]. In this way, most bile acids reabsorbed in the bowel are returned to the biliary system, an arrangement known as the enterohepatic circulation. A minority of bile acids are subjected to deconjugation by the microbiota of the bowel forming deoxycholate (DCA), ursodeoxycholate (UDCA) and lithocholate (LCA), which are more hydrophilic. The hydrophilic properties of UDCA have led to their use as a medical treatment for biliary diseases

with the intent to increase flow in the biliary system, in conditions where normal flow has been restricted[24].

In addition to bile acid transport, hepatocytes also express the multi drug resistant protein 2 (MDR2) in mice or (MDR3) in humans, which allows Phosphatidylcholine (PC) to become available in the biliary canaliculi[25]. PC are essential for the production and stability of micelles. In this way, they protect the BEC from the harmful hydrophobic effects of bile acids, by packaging them in micelles and reducing the concentration of free bile acids. The importance of the MDR2/3 receptor, and therefore of PC to bile has been underlined by the fact that both MDR2 deletion in the mouse [25] and MDR3 mutations in humans lead to biliary damage[26]. Furthermore, it provides evidence of the requirement of BEC to be protected from Bile acids to prevent the development of biliary injury.

Cholesterol also plays a role in micelle formation and is also secreted by hepatocytes into the bile canaliculi through the action of ATP-binding cassette transporter (ABCG) [27].

Bile pigments are also present in bile and are responsible for the characteristic yellow colour. They are biproducts of the physiological breakdown of red blood cells. The haemoglobin in red blood cells is released following their death, the haem from the haemoglobin is oxidated to form biliverdin within the spleen, and the reticuloendothelial system[28]. Biliverdin is reduced to form unconjugated bilirubin, which is hydrophobic and carried in the blood by albumin. The liver uptakes unconjugated bilirubin, conjugating it through the action of Uridine diphosphate glucose (UDP) glucuronosyltransferase 1, producing a hydrophilic molecule, which can be excreted into the bile, and subsequently into the bowel. To prevent reabsorption of bilirubin, the gut microbiome deconjugates them to stercobilinogen causing them to be excreted in the faeces[29]. The lack of excretion of bilirubin leads to accumulation of yellow pigment in the blood and subsequently other parts of the body including the skin, manifesting as the clinical sign of jaundice. Although jaundice commonly occurs in patients with biliary system dysfunction caused by obstruction of the normal pathway to excrete bilirubin; this finding is by no means specific. Excess destruction of red blood cells, and dysfunction of hepatic conjugation of bilirubin are further causes of jaundice.

The role of BEC

The passage of large molecules from hepatocytes into the biliary canaliculi increases the luminal osmolarity attracting water, causing bile to move out of the canaliculi into the ducts lined by BEC, creating flow [21]. Once bile reaches the biliary ducts via the canals of Hering, the composition of the bile can be altered by BEC in response to local and/or distant stimulants. BEC express a primary cilia which extend into the ductal lumen and detect changes in flow as well as bile composition[30]. Polycystin 1 and 2 are expressed on primary cilia, on movement of the cilia secondary to bile flow these proteins allow the entrance of calcium into the BEC which leads to increased levels of cAMP, leading to inhibition of growth signalling[31]. The lack of polycystin as seen in polycystic liver disease leads to failure of this pathway and the development of multiple intrahepatic cysts, thought to be secondary to excessive BEC proliferation.

Kinesin-like proteins 3a (KIF3a) is a further important ciliary protein which is involved in the assembly and maintenance of cilia. In a murine model with *Kif3a* knockout specifically in bile ducts, and biliary injury induced by thioacetamide (TAA), cystic lesions develop in the liver. This indicates that BEC without cilia have increased proliferative potential, which may be in response to the loss of normal signalling provided by biliary flow [32].

Cilia also express chemo sensing proteins such as P2Y12 which responds to the detection of nucleic acids, adenosine diphosphate (ADP) or adenosine triphosphate (ATP) by increasing intracellular calcium, resulting in increased secretion of electrolytes and therefore water into the biliary lumen. In a similar vein, osmo-sensors such as transient receptor potential cation 4 (TRPV4) respond to hypertonicity in the biliary lumen by increasing intracellular calcium [33, 34].

In terms of distal stimuli, there are several hormones which may influence the function of BEC. Secretin (SCT) is a small molecule which is secreted by duodenal S cells in response to the detection of gastric acid in the duodenum. Secretin receptor (SCTR) is expressed in the pancreas[35] and the biliary tree[36], in response to SCT, SCTR enacts changes in the cell via cyclic adenosine monophosphate (cAMP) signalling [37]. This leads to increased expression of anion transporters on the apical membrane such as Anion exchange protein 2 (AE2), Aquaporin-1 (AQP1) and Cystic fibrosis

transmembrane conductance regulator (CFTR) [38-40]. AE2 exchanges Chloride ions from the bile for bicarbonate from BEC leading to the production contributing the bicarbonate umbrella [41]. The umbrella is particularly important in smaller ducts which have limited capacity for producing protective mucus [42].

CFTR permits chloride ions to exit BEC and enter the bile. The presence of intraluminal chloride ions allows them to be available for exchange for bicarbonate through AE2, therefore CFTR is also essential to the maintainance of the bicarbonate umbrella. The net gain of intraluminal ions also leads to increased osmolality, attracting water, which leads to increased bile volume and contributes to biliary flow[43]. In this way bile is produced and flow is increased in response to food entering the duodenum to deliver phospholipids and bile salts required for the digestion of fat-, and fat-soluble vitamins to the gut[44].

The parasympathetic arm of the autonomic nervous system through the action of acetylcholine (ACH) is also able to affect BEC function through the muscarinic receptor (M3). In response to this stimulus intracellular cAMP is released representing an alternate pathway to increase the expression of AE2 and CFTR and increase biliary flow[45, 46]. The parasympathetic system can be activated through eating, in this way in times of rest the body can divert resources to producing more bile and increasing biliary flow aiding digestion.

Somatostatin, and Gastrin have opposing effects to SCT and acetylcholine enacted through somatostatin receptor 2 (SSTR2), and glucagon like peptide receptor 1 (GLP1R) respectively[47-49]. These hormones are important for slowing the production of bile in times outside of feeding[8].

Summary

The production of bile can be clearly compartmentalised into the initial production by hepatocytes and the refinement by BEC. The different functions of hepatocytes and BEC necessitates that they harbour a distinct complement of plasma membrane proteins to support these functions, as described in this section. Some of the distinguishing features of BEC and hepatocytes have already been defined such as BEC expression of epithelial cell adhesion molecule (EpCAM) [50] and keratin 19 (KRT19) [51]

and hepatocyte expression of asialoglycoprotein receptor (ASGPR) [52, 53]. Despite this, a comprehensive analysis of the protein compliments of hepatic and biliary plasma membrane proteins remains to be performed, which may identify novel proteins which help to characterise hepatocytes and BEC.

The complexity of bile in terms of its constituents, the transporters required to moderate its composition and the regulators of its production, mean that there is a high potential for pathology to develop within the biliary system. This fact has been exploited in the production of models of biliary injury as described later in this chapter.

The cholangiopathies, the group of conditions whose pathology primarily affect the biliary system, reflect the complexity of bile production in their diverse aetiology and clinical features.

Figure 1.3 Schematic displaying the major plasma membrane receptors of hepatocytes and BEC involved in the production of bile.

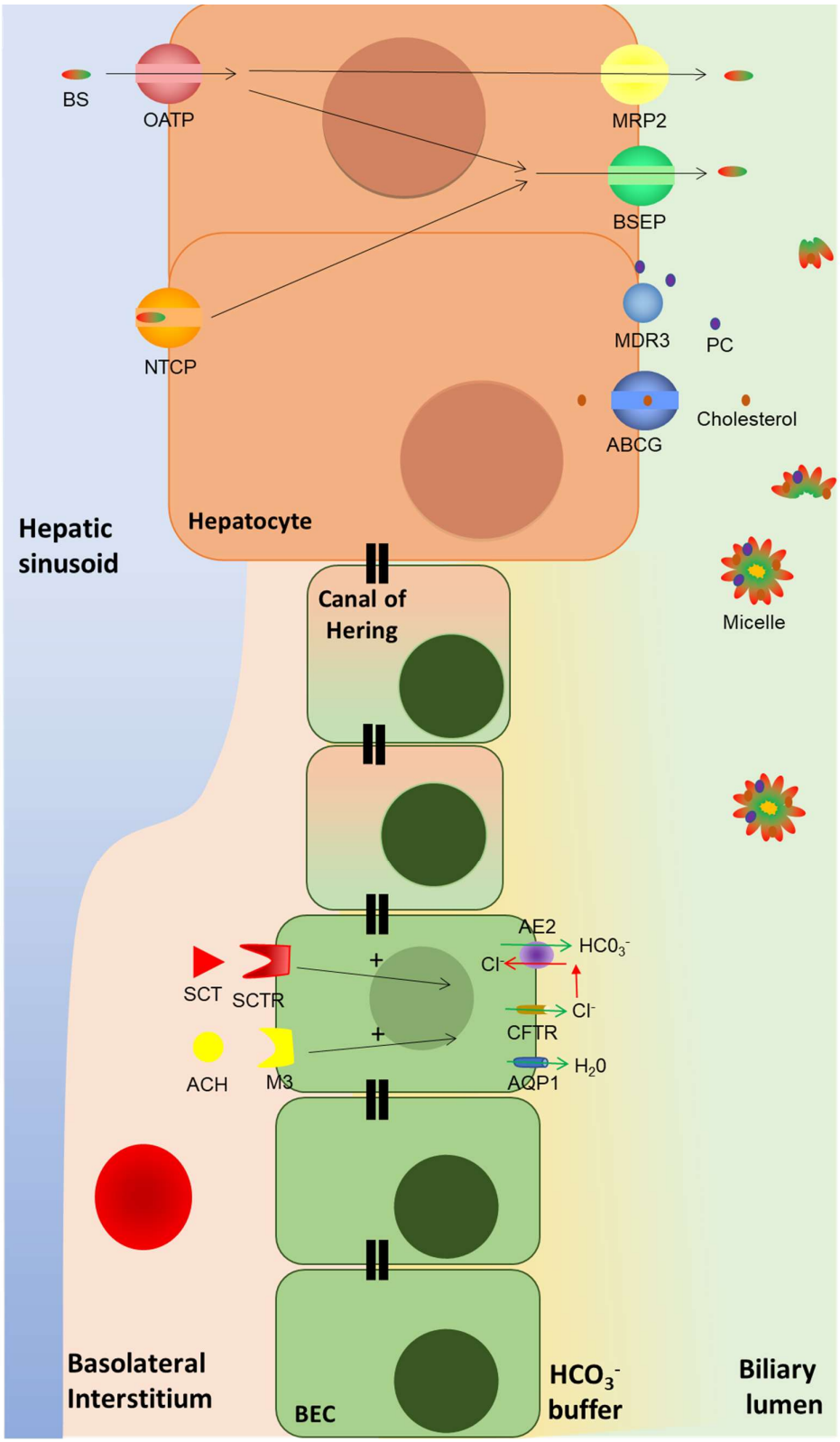

Figure 1.3 Schematic displaying the major plasma membrane receptors of hepatocytes and BEC involved in the production of bile.

Luminal aspect is shown on the right side of the figure the basolateral side on the left side.

1.4 The cholangiopathies

Although individually rare, the cholangiopathies, when considered as a whole, present a significant health burden. Cholangiopathies account for approximately 70% of all paediatric hepatic transplants[54] and between one sixth and one third of adult cases[55, 56].

The cholangiopathies are varied in terms of their demographics, anatomical distribution, and underlying aetiology. In spite of this, there are pathological and clinical features which may occur in any of the cholangiopathies including ductular reaction, fibrosis, ductopenia, inflammation, cholestasis and bowel dysfunction.

Pathological features of the cholangiopathies.

The ductular reaction is characterised by the expansion of the BEC population, associated with infiltration of inflammatory, mesenchymal, and endothelial cells adjacent to the ducts[57]. There is also an increase in deposition of the associated extracellular matrix[58]. Whilst commonly seen in the cholangiopathies, the ductular reaction is not specific, occurring in many chronic liver diseases including Non-alcoholic fatty liver disease (NAFLD) [59], Alcoholic hepatitis[60] , Hepatitis C [61].

It remains unclear whether the expansion of cells seen in the ductular reaction represents the formation or new biliary ducts or simply a discordant group of cells which do not serve any physiological purpose. It is generally believed that the ductular reaction occurs as an attempt at regeneration, however it is not specific to the cholangiopathies and occurs in chronic hepatocellular predominant injuries. Whilst appearances suggest regeneration, the presence of ductular reaction is often seen as a negative prognostic indicator[62, 63], which may indicate it as a marker of late disease, or a final attempt at regeneration in a failing liver.

Fibrosis and the ductular reaction are intimately linked, the deposition of extracellular matrix seen in the ductular reaction, is likely to contribute to the development of fibrotic changes. Although fibrosis is nigh on ubiquitously present in the cholangiopathies and in many other chronic inflammatory diseases both in the liver and in other organs, the pattern of deposition is variable. Obliterative fibrosis of ducts occurs primarily in primary sclerosing cholangitis (PSC)[64], whilst granulomatous cholangitis occurs in primary biliary cholangitis (PBC)[65]. The importance of fibrosis in the course of disease cannot be understated, the deposition of extracellular matrix leads to a progressive increase in the vascular resistance of the liver[66]. To compensate for this the pressure in the portal vein increases (the hepatic artery is less affected due to its higher internal pressure), which may progress to reversal of vascular flow or thrombosis in the portal vein[67]. Secondly, functional parenchyma is progressively replaced with non-functional fibrotic tissue which leads to reduced hepatic function and ultimately hepatic failure.

Response to biliary injury can result in ductal proliferation as in the ductular reaction, conversely loss of ducts may also occur, so called ductopenia[68].The reasons why this dichotomy should exist are unclear, however one hypothesis is an imbalance in two opposing responses to disease; proliferation to replace damaged or malfunctioning cells and apoptosis to remove cells before the damaging process of necrosis occurs. The mechanisms by which ductopenia, ductular reaction or both are induced as part of the response to biliary disease remain to be elucidated.

Inflammation is a hallmark of chronic disease and an important feature in all the cholangiopathies; however, some conditions have specific inflammatory features. In the most common forms of cholangiopathy namely PSC and PBC, lymphocytes are often seen in large numbers in the inflammatory infiltrate, however in acute forms of cholangiopathy neutrophils may be more plentiful. Antibody producing plasma cells are most seen as part of the inflammatory infiltrate of PBC[69].

Fibrosis and ductopenia lead to prevention of bile leaving the liver, known as cholestasis. Cholestasis results in increased pressure within the ducts, which is transmitted to the tight junction which hold together BEC and form a barrier between the biliary lumen and the hepatic parenchyma [70]. Eventually these junctions become leaky, exposing the hepatic parenchyma to bile which may result in parenchymal injury.

In recent times the relationship between biliary disease and senescence has become apparent, senescence occurs in the ducts in several biliary diseases[71-73]. Senescence occurs in damaged cells or as a normal process in aging, in the former case it is thought to represent a method of preventing damaged cells from attempting to proliferate[74]. The influence of senescence on the pathogenesis of the cholangiopathies is likely to be complex, including reduced capacity for regeneration, increased cellular apoptosis and the spread of senescence into adjacent cell populations through a combination of paracrine and direct cellular interactions[75]. The spread of senescence to local and neighbouring cells is a phenomenon that can turn a protective mechanism into a pathogenic one, the basis of the recently postulated threshold effect, as more cells develop senescence it increases the rate and extent of spread of senescence in the tissue, at a certain point this spread will outgrow the immune system's capacity to remove senescent cells[76]. Once this threshold has been crossed the spread of senescence will grow exponentially across the affected tissue and lead to reduced function in the organ. The importance of senescence in the prognosis of the cholangiopathies has already been demonstrated, in 2021 Cazzagon and co-workers demonstrated the association between senescence and poor outcome in patients with PSC assessed using immunohistochemistry of P16 and P21[77].

As depicted in section 1.3 the function of the bowel is highly dependent on the function of the biliary system and vice versa. It is unsurprising therefore that biliary disease and bowel disease occur together on a not infrequent basis. Some examples of bowel conditions commonly associated with biliary pathology include Crohn's disease, ulcerative colitis, and ascariasis or round worm.

Specific examples of cholangiopathies:

Primary Biliary cholangitis (PBC)

PBC is a rare condition with an annual incidence of 2.6 per 100,000, however its chronic clinical course means that the prevalence is significantly higher [78]. Females are affected in a ratio of 4:1 and it most commonly occurs in the 4^{th} to 6^{th} decades of life. Although PBC often runs an indolent course, patients may progress to develop hepatic failure.

The current prevailing hypothesis for the development of PBC is chronic injury to the ducts mediated by autoimmune T cell activity [79], leading to loss of BEC, and

destruction of the intrahepatic ducts [69, 80, 81]. As ducts are progressively damaged, cholestasis ensues leading to chronic inflammation, BEC senescence and progressive fibrosis. Another important feature of disease is the exclusive injury to the intrahepatic ducts with sparing of the extrahepatic ducts and gallbladder, the reason for this remains unclear.

Another important feature in the pathogenesis of PBC is thought to be ineffective transport of bicarbonate and development of the protective bicarbonate umbrella. In particular, the AE2 transporter has been shown to be downregulated in PBC[82]. This finding has indicated that the pathogenesis of PBC is likely at least in part to be secondary to failures in the normal BEC protective mechanisms against bile acids.

The diagnosis of PBC requires the presence of several features of disease; a combination of at least 2 of the following: raised serum alkaline phosphatase, presence of anti-mitochondrial antibody (AMA) and liver histology interlobular duct destruction. Whilst raised AMA is a sensitive marker of PBC, it is still not clear what the role these antibodies have in the pathogenesis of disease.

Ursodeoxycholic acid (UDCA) is currently recommended as a treatment for PBC, however there remains limited evidence for its long-term efficacy [83]. This treatment, in theory, works due to the hydrophilic nature of UDCA which allows it to easily move into the biliary lumen from hepatocytes and lead to increased flow. In cases of PBC which progress to hepatic failure, Orthoptic liver transplant (OLT) offers the only curative therapy.

Primary Sclerosing cholangitis (PSC)

Although there are similarities between PSC and PBC, in terms of progressive obliterative ductal damage and the likely auto-immune underlying aetiology, there are important distinguishing features. Unlike PBC, PSC may affect both the intra- and extrahepatic ducts, although there is a recognised subtype of PSC which occurs only intrahepatically [84].

PSC predominantly occurs in males and has a strong association with an atypical form of ulcerative colitis characterised by terminal ileitis and rectal sparing [85]. The strong association between PSC and colitis has led to the hypothesis that the microbiota of

the gut has a role to play in the pathogenesis of this disease, however no clear evidence to confirm this theory has been produced to date[86].

Dysfunction of the mechanisms of production and maintainance of bile have also been implicated in the development of PSC, mutations in the CFTR gene are common in patients with PSC [87, 88]. This has subsequently been associated with reduced excretion of Chloride ions into the lumen and the protective mucus layer, increasing the risk of injury.

As with PBC there are no effective medical therapies for PSC, in cases of PSC which progress to hepatic failure OLT offers the only cure.

Cystic Fibrosis

Cystic Fibrosis (CF) is a multiorgan condition which is caused by genetic mutations of CFTR. Within the liver CFTR is thought to be expressed on the apical aspect of BEC and as discussed in previous sections has a significant role in regulation of bile flow [38]. When dysfunction of CFTR occurs, bile is thought to become more viscous leading to cholestasis and damage to both the intra and extrahepatic biliary ducts which in turn leads to hepatic parenchyma damage.

CFTR is expressed in the lungs, pancreas, gut, reproductive system as well as the biliary system and CF may cause chronic damage in any of these organs. Patients with CFTR normally suffer from pulmonary dysfunction primarily, often resulting in respiratory failure in early adulthood, however new treatments and increasing numbers of lung transplantation has thankfully allowed the life expectancy of patients with CF to increase considerably in recent decades[89]. As a result of this, aspects of this condition which have a more gradual onset are becoming more common, such as cholangiopathy.

At present the biliary system is affected in around 25-40% of cases of cystic fibrosis[90]. Of the patients who develop cholangiopathy associated with CF, between 5-10% will eventually develop hepatic failure, however this is likely to increase as lung treatments for cystic fibrosis continue to improve.

Congenital biliary atresia

Congenital biliary atresia is a rare condition affecting around 1 in 18,000 births, characterised by a focal obstructing stricture in the extrahepatic biliary tree. Extrahepatic

biliary obstruction leads to cholestasis and intrahepatic fibrosis[91]. Clinical symptoms commence shortly after birth with persistent neonatal jaundice. Whilst early surgical intervention with hepatoportoenterostomy may alleviate jaundice, 60% of children with this condition develop hepatic failure despite surgery and require OLT[92].

The underlying pathogenesis for this condition remains unclear, however the disease can be grouped into cases which are associated with syndromes, so called syndromic biliary atresia (SBA) and those that occur in isolation, isolated biliary atresia (IBA). SBA is associated with other congenital abnormalities and therefore considered to be a disorder of development. Certain genetic abnormalities have been implicated, for example, the polycystic kidney disease 2 like 1 protein (PKD2L1) gene which is also associated with renal and splenic abnormalities[93].

Caroli's disease

Caroli's disease is characterised by multi-focal dilatations in the intrahepatic bile ducts and is also known as type V choledochal cyst disease. The underlying cause is thought to be related to primary cilia dysfunction; however, no definitive genetic cause has been identified at present. The intrahepatic duct dilation seen in this condition leads to biliary stagnation and recurrent infectious cholangitis. Some patients will go on to develop secondary biliary fibrosis and eventual hepatic failure [94].

Alagille syndrome

Alagille syndrome causes neonatal jaundice secondary to a congenital paucity of intrahepatic bile ducts, representing an embryological failure of development of the intrahepatic ducts. Jagged 1 (*Jag1)* and Neurogenic locus notch homolog protein (*Notch)* mutations have been implicated in more than 90% of cases[95, 96]. The fact that Alagille syndrome affects the intrahepatic ducts almost exclusively is a further indicator of the distinct embryology of the intra and extrahepatic ducts.

Between 15 and 20% of patients with Alagille syndrome develop hepatic failure requiring OLT[97].

Ischaemic cholangiopathy

Ischaemic cholangiopathy describes the development of strictures in the biliary system secondary to reduced blood supply, most commonly occurring following OLT[98]. In

the context of OLT, ischaemic cholangiopathy occurs more commonly in patients who receive donation after circulatory death (DCD) livers as opposed to donation after brain death (DBD) [99]. Out with OLT, ischaemic cholangiopathy may also occur; following trans-arterial chemo-embolisation (TACE), in conditions which induce vasculitis in the hepatic arterioles as in Acquired immune deficiency syndrome (AIDS) related cholangiopathy, or conditions which reduce blood flow through the hepatic artery, as is seen in Rendu-Osler-Weber syndrome[100].

In recent times it has become clear that there are changes within the plasma membrane of cells which occur during the disease process. De Jong and co-workers demonstrated reduced SCTR expression in samples of liver taken from patients who had developed hepatic failure following OLT from either non-anastomotic strictures or hepatic artery thrombosis[98].

The maintainance of the bicarbonate umbrella is an energy dependent process, therefore BEC may be susceptible to ischaemic insults due to compromise of this normal protective mechanism against the harmful effects of bile acids[41].

DCD livers are being used increasingly in the UK and elsewhere as the demand for OLT continues to rise, which will likely increase the incidence of ischaemic cholangiopathy in future years [101].

Progressive familial intrahepatic biliary stasis

Progressive familial intrahepatic biliary stasis represents a group of hereditary conditions which are characterised by progressive cholestasis, normally presenting in childhood. Although the pattern of disease in these rare conditions is predominantly biliary, they are most caused by alteration in function of hepatocyte transmembrane ion transporters. There are a 4 commonly described subtypes which are each associated with different specific genetic abnormalities, which code for bile canaliculi proteins.

Type I is caused by loss of function mutations in the ATPase Phospholipid Transporting 8B1 gene (*Atp8b1)* which codes for a phospholipid flipase, found on the canalicular membrane of hepatocytes[102]. Phospholipid flipases are essential for maintaining phospholipid asymmetry in the plasma membrane; in the case of ATP8B1 moving phosphatidylserine (PS) from the luminal aspect to the intracellular aspect of the plasma membrane[103]. PS in the biliary aspect of the plasma membrane presents

an area of relative sensitivity to the detergent effects of bile acid. Inability to translocate these vulnerable areas following malfunction of ATP8B1 may therefore lead to biliary injury.

Type II is caused by deficiencies in the ATP-binding cassette subfamily B member 11 (ABCB11*)* which is a bile salt pump found in the canalicular aspect of hepatocytes[104, 105]. Type III is caused by deficiencies in the MDR3. Finally tight junction protein 2 (TJP2) defects may also lead to progressive familial intrahepatic biliary stasis[26].

Summary

The cholangiopathies are a diverse group of conditions, which are characterised by injury to the biliary ducts, leading to loss of the normal regulation, and flow of bile. Given the importance of transmembrane receptors and transporters in biliary homeostasis, it is not surprising that changes in the expression of proteins such as CFTR, AE2 and SCTR have been noted in many of these diseases. Changes in plasma membrane protein expression can be implicated in the pathogenesis of the cholangiopathies, but also may occur as a consequence of the disease process. In both cases the plasma membrane could present attractive candidates for targeted therapies in the cholangiopathies.

The pursuit of therapies for the cholangiopathies is furthered by the fact that they may progress to cause hepatic failure in which the function of the liver is reduced to the point of no longer supporting normal homeostasis. There are no effective medical therapies for the cholangiopathies at present, in cases of hepatic failure OLT is the only cure. Unfortunately, there are limited livers available for transplant and demand significantly outweighs supply. In addition, there is also a significant risk of complication associated with transplantation[106, 107]. Even in success, recurrence in the most common cholangiopathies PSC and PBC, is estimated to be as high as 25%[108] and 35%[109] respectively. Alternative therapies to transplant are therefore of interest, cell therapy is one such alternative which has shown promise.

1.5 Pre-clinical models of Biliary disease.

To study the pathogenesis of the cholangiopathies in the laboratory setting, several preclinical models have been developed. These models may be useful to greater or lesser degrees for modelling treatments for these diseases, including cell therapies.

Anatomical models exist, which include bile duct ligation (BDL)[110], and hepatic artery deprivation [111, 112]. The BDL model is most closely related to biliary atresia and causes features of cholangiopathy including ductal reaction and fibrosis. Whilst this model can be helpful for studying the natural history of the cholangiopathies, it may be less effective as a model for cell therapy given the iatrogenic, permanent nature of the closure of the bile duct which is likely impossible to treat through any method other than removal of the suture or ligature used to close the duct. In addition, it is an invasive surgery which normally may only be carried out in mice of a certain age and size, whilst biliary atresia in humans is most commonly present from birth. As a more general model of cholangiopathy it is limited by the fact that it causes a solitary extrahepatic biliary stricture which may be a rare presentation of PSC but is not commonly a feature in the other forms of cholangiopathy.

Traditionally mouse and rats have been used as BDL models, more recently Vistejnova and co-workers reported on a porcine model of repeated biliary obstruction through the placement of a catheter in the CBD. The balloon associated with this catheter was periodically inflated and deflated, following this, pigs were subjected to a left hepatectomy [113]. This is a complex clinical model which aims to replicate patients who have secondary biliary cirrhosis who also require a partial hepatectomy, this is most likely to occur in patients with an obstructing biliary tumour, or cholangiopathy.

Deprivation of the hepatic artery has been employed to specifically induce injury in the biliary system, since the biliary system is supplied specifically by the hepatic artery as mentioned previously. This model has been described primarily in rats and may be difficult to replicate in smaller rodent models such as the mouse due to the size of the hepatic artery[111]. This model is most likely to be an effective model of ischaemic cholangiopathy.

Injury inducing diets have also been used to produce models of cholangiopathy. The 3,5-diethoxycarbonyl-1,4-dihydrocollidine (DDC) diet causes increased production of porphyrins through the induction of δ-aminolaevulinate (ALA) synthetase, the rate

limiting step of producing ALA from Succinyl CoA and glycine[114]. ALA is metabolised to produce porphobilinogen, the excess porphobilinogen is eventually metabolised to Heme, the breakdown of which produces bile pigments. Excess bile pigments are secreted into the bile, changing the composition of the bile, leading to plugging and cholestasis resulting in a biliary predominant injury. It has also been noted that intestinal involvement is often present in DDC diet mice which further strengthens this as a model for cholangiopathy, given the association with PSC and inflammatory bowel disease seen in humans[85, 115, 116].

TAA causes liver injury because of the production of its metabolite thioacetamide-S-oxide, a free radical. This then covalently binds to macromolecules in hepatocytes which leads to necrosis, particularly in the periportal region. Prolonged exposure to TAA induces malignancy, serving as a model for cholangiocarcinoma[117].

Carbon tetrachloride (CCl_4) is a further compound which can induce hepatic injury, Cytochrome P450 Family 2 Subfamily E Member 1(CYP2E1) system which leads to predominately hepatocellular damage but also to a degree of periportal injury[118]. The nonspecific pattern of injury in CCl4 is one weakness of this technique for modelling cholangiopathies. In addition, there are several off-target effects including CNS depression, and kidney injury.

Second mitochondria-derived activator of caspase (SMAC) mimetics have also been used to induce biliary injury through either systemic instillation or through injection directly into the biliary system. These drugs work by reducing the Cellular inhibitor of apoptosis proteins (cIAP1 and cIAP2) leading to apoptosis in the bile ducts resulting in a sclerosing cholangitis phenotype [119].

Genetic models have also been used to mimic the cholangiopathies in mice. *Mdr2* mutations, which is the murine counterpart of *Mdr3* as discussed above, have been implicated in the development of type III progressive familial intrahepatic biliary stasis in humans. Both the murine and human versions of this protein, facilitate the availability of phosphatidylcholine to the biliary canaliculi. The knockout of this gene leads to absence of phosphatidylcholine within the bile, reducing the stability of micelles. *Mdr2*-/- mice have been shown to develop progressive biliary fibrosis[25].

Further genetic models exist including a *Cftr*-/- model which causes biliary damage for the same reasons that cholangiopathy is seen in patients with cystic fibrosis[120].

Ae2 knockout has also been used which leads to bile duct destruction, portal infiltration and cholangiopathy secondary to the depletion of the bicarbonate umbrella [121]. These models further demonstrate the importance of plasma membrane receptors and transporters in the development of cholangiopathies.

Genetic models of cholangiopathy have also been developed in zebrafish, for example, in 2022 Zhao and co-workers reported a zebrafish model of Alagille syndrome induced by mutations in *Jag1b* and *2b* [122]. The use of fish models for the cell therapies is limited however given the challenges in transplanting cells into these animals.

The junctions which connect BEC together are integral to normal function, in particular the separation of bile from the hepatic parenchyma. This fact was exploited by Nakagawa and co-workers in 2014 presenting a murine model with knockout of E-cadherin which developed periductal fibrosis and in some cases malignancy[123].

Whilst many of these models have specific features of certain cholangiopathies they often lack or have not been investigated for ductular senescence, a key feature in the many of the cholangiopathies. Ferreira-Gonzalez and co-workers in 2018 published on the *Krt19 Mdm2*$^{flox/flox}$ model which allowed the floxing of double minute homologue 2 (*Mdm2*) specifically in *Krt19* expressing cells through the production of cre. Mdm2 is a negative regulator of P53 and therefore when this has been floxed it allows accumulation of P53 which subsequently causes p21 accumulation and senescence. This model when combined with DDC diet demonstrates biliary centric injury in the liver[75].

The *Krt19 Mdm2*$^{flox/flox}$ model has since been crossed with an interleukin 2 (*Il2rg)* and recombination activating gene 2 (*Rag2)* knockout line leading to immunocompromise. This line is then permissible to human cell transplantation [124] and a useful model for investigating the effects of cell therapy on the cholangiopathies.

1.6 Cell therapy for cholangiopathies

At a fundamental level cell therapies have one of two aims, either to replace lost cells, which could be termed parenchymal replacement; or to alter the environment of an organ or target, which could be referred to as environmental modification.

Several methods of parenchymal replacement have already translated into clinical practice, for example, pancreatic islet transplantation[125] for type I diabetes mellitus.

In these cases, patients receive pancreatic islet transplantation which contain beta cells that produce insulin to replace the host beta cells, which are destroyed as part of the disease process. Bone marrow transplants have also been successful in replacing the hematopoietic cell compliment which is wiped out following chemotherapy in patients with leukaemia[126]. Transplanted hematopoietic stem cells have the potential to produce any of the terminally differentiated cells found in normal blood. Both examples target the replacement of a specific group of cells, with a transplanted cell ready to act as a direct replacement.

Cell therapies whose aim is environmental modification have not translated into clinical practice to such a degree as their parenchymal replacement counterparts to date. Various cell types including mesenchymal cells[113, 127, 128] and macrophages[129] have been used across different parts of the anatomy to slow or stop a disease process and facilitate innate regeneration. As alluded to, the environmental modification strategy necessitates that the target tissue has the capacity for regeneration when the niche is modified appropriately. Additionally, there must be enough viable native cells present to enact this regeneration once the environment has become favourable to repair.

In the cholangiopathies, both schools of thought could merit support. From the parenchymal replacement perspective, ductopenia occurs in many of the cholangiopathies, the lack of ducts limits the normal flow of bile and may perpetuate injury in the ducts and initiate hepatocellular injury. The added impact of senescence means that the resident BEC are unable to effectively replace the BEC which are lost through the process of injury. For these reasons, the delivery of healthy BEC could provide the liver the material required to rebuild the biliary tree. Advocates of environmental modification may argue that following limited injury BEC can regenerate and repair, therefore the addition of alternatively activated M2 macrophages could stop the ongoing chronic inflammation associated with the cholangiopathies and allow native BEC the opportunity to repair the biliary tree as is the case in most minor isolated insults. In addition, as discussed in section 1.4, senescence is now known to play a significant role in the progression of the most common cholangiopathies, therefore, cell therapies

that could modulate the spread of senescence in the cholangiopathies would be attractive in theory.

The natural history of the cholangiopathies is an important consideration, when contemplating a strategy for cell therapy. Regarding the most common cholangiopathies, PSC and PBC, whilst patients may progress to hepatic failure, it is not guaranteed. A retrospective study of more than 7000 patients with PSC found that 37% of patients either had OLT or died during the 30-year period assessed[130]. Similarly, in PBC 23% of almost 5000 patients included in a meta-analysis either died or underwent OLT, over a median follow period of 7.3 years[131]. Cell therapies are likely initially to be performed on patients with disease severe enough to warrant OLT as it may be unethical to offer such a therapy in patients whose disease may not result in severe morbidity or mortality. This may favour parenchymal replacement at least in initial trials as patients with severe disease are likely to have extensive biliary damage and ductopenia. This has been reflected in the research on cell therapy for the cholangiopathies to date[17, 124].

1.7 BEC for cell therapy in the cholangiopathies.

When considering which cell is best placed to replace BEC, the obvious choice would be BEC themselves, as such a like for like replacement. As described previously, BEC are a diverse population of cells, with differing transcriptional signatures between the intra- and extrahepatic compartments. Cells from both compartments could be considered for cell therapy for the cholangiopathies. Additionally, biliary progenitor cells obtained from discarded fetal tissue has been considered as a possible source for fetal BEC.

Fetal BEC

Several cases of fetal BEC transplantation have been reported in patients with chronic liver disease[132, 133]. Importantly none of these cases to date have been in the setting of cholangiopathy. Differences in mature and fetal BEC exist, particularly in the presence of tight junctions and the surrounding extracellular matrix. Khandekar et al identified differences in the supporting matrix and deficiencies in the cell-to-cell junctions in neonatal BEC[134]. The junctions between BEC are essential to preventing

the leakage of damaging bile into the hepatic parenchyma. This deficiency in an important function of fetal BEC may render them less attractive as a therapy.

Extrahepatic BEC

The differences between intra and extrahepatic ducts were explored in section 1.2. These differences raise the question as to whether extrahepatic BEC could regenerate intrahepatic BEC. Zhao and co-workers used a lineage tracing model in zebrafish to show that in a model of Alagille syndrome, new intrahepatic ducts can be regenerated from extrahepatic BEC[122]. Nevi and co-workers transplanted human extrahepatic BEC as defined by EpCAM expression into immunocompromised murine models, demonstrating engraftment in the intrahepatic biliary tree [135]. Subsequently Sampaziotis et al transplanted human gallbladder BEC, also defined by EpCAM expression, into an immunodeficient model of cholangiopathy also demonstrating engraftment. They also transplanted the same cells into explanted livers [17]. These studies collectively have demonstrated the ability of extrahepatic BEC to integrate and regenerate the intrahepatic BEC compartment and shown the potential of extrahepatic BEC as a cellular therapy for the cholangiopathies.

Returning to the work of Rimland and co-workers, in addition to their findings that extra and intrahepatic ductal BEC retain transcriptional differences in culture, they also assessed the differences between organoids grown from cells of different compartments of the extrahepatic bile ducts. Comparing pancreatic, CBD and gallbladder BEC [18], transcriptional differences were shown. Although BEC from these areas became more similar during culture, they retained some distinct features. These results indicate that the extrahepatic ducts are not a monolith, and the regenerative potential of extrahepatic biliary cells could be held in a subpopulation of cells yet to be identified.

The peribiliary glands which are small outpouchings emanating from larger ducts are thought to contain cells with high regenerative capacity which can help in replacing lost and injured BEC in the extrahepatic ducts. Carpino and co-workers in 2019 used a lineage tracing model to demonstrate that extrahepatic ducts regenerate from niches of cells in the peribiliary glands positive for Sox9 and EpCAM, following DDC diet induced injury. They also demonstrated a more extensive network of PBG in human

liver samples from patients with PSC compared with controls, with higher expression of proliferation markers[136]. Together these findings indicate that PBGs have an important role in extrahepatic biliary regeneration. Further to this it has been suggested that paucity of peribiliary glands is associated with development of ischaemic cholangiopathy[98, 137], indicating that the loss of these cell niches may result in impaired regeneration and tolerance to injury.

Whilst there is evidence to suggest PBGs contain cells with high regenerative potential, the specific signature of these cells remains to be defined.

Intrahepatic BEC

The livers capacity for regeneration has long been recognised, in the search for alternative cells to replace the lost ducts in the cholangiopathies, it is important to take note of how the native hepatic cells contribute to repair. Whilst both the hepatocyte and the BEC compartments have extensive capacity for self-regeneration, in recent times it has also become apparent that both cells have the capacity to transdifferentiate into the other in order to help repair and regenerate the other compartment under certain conditions [138, 139]. Furuyama and co-workers used *Sox9* as a marker of BEC in their *Sox9*$^{IRES\text{-}CreERT2}$; Rosa26R mouse model[140]. They found that with and without injury, the majority of new hepatocytes were derived from Sox9 expressing cells, indicating biliary origin. Subsequent studies by Tarlow, also using a Sox9 reporter model, and Malato using an AAV (adeno-associated virus) Cre delivery system to label all hepatocytes, failed to replicate these results [141, 142]. Raven et al used separate β1 integrin knockout and an AAV8 mediated p21 upregulation model both targeted to hepatocyte to investigate trans differentiation[143]. These models, combined with injury inducing diets, allowed extensive hepatocyte injury to occur with associated senescence, and the authors were able to demonstrate in both models, a significant proportion of new hepatocytes arising from a biliary origin.

Hepatocytes and BEC are not by nature migratory cells. They are also separated from the other cell compartment at varying proximities, for example, cells within the distal part of the common bile duct are many multiples of the length further away

from the hepatocyte compartment compared with those in the canals of Herring. Similarly, hepatocytes positioned at the central vein are further from the BEC compartment than those in the periportal region. With this in mind, it, seems illogical that all cells in both compartments have the capacity for trans differentiation, those cells close to the border between hepatocytes and BEC would have more utility in this ability. This argument suggests the presence of a subset of cells which can transdifferentiate, so called hepatic progenitor cells (HPC), in theory with a high capacity for regeneration.

Lineage tracing studies had helped to demonstrate the bipotentiality of BEC but were not able to define a specific HPC signature. Plasma membrane proteins including EPCAM[50], CD24[144], CD44[145], FOX1[146], CD133/PROM1[147] have been used in differing combinations to try to define a HPC. The recent surge in availability of single cell RNA sequencing (scRNAseq), has allowed several groups to attempt to identify a population of HPC based on transcriptional signature. Aizarani and co-workers produced an atlas of liver cell types by performing single cell sequencing on human livers without chronic liver disease, which had been resected[148]. They identified a population of EPCAM positive cells with intermediate expression of TROP2 which had comparatively improved colony forming ability compared with TROP2 high and low expressing populations. Conversely Pepe-Mooney reported from single cell sequencing of murine EPCAM positive cells, heterogeneity in BEC defined by the expression of YAP, however, were unable to identify a specific HPC [149]. Although scRNAseq has to date been unable to conclusively define a HPC population, it is possible that the rarity of the HPC may in part account for this. Pepe-Mooney used approximately 1500 cells in each sample, Aizarani around 1000 cells. As scRNAseq progresses, it will become possible to perform analyses on larger cell numbers increasing the power to detect rare cells which may give more conclusive results regarding the existence of the elusive HPC.

The definitive transcriptional and plasma membrane protein signatures of the HPC remain to be determined however populations of cells which exhibit behaviours in keeping with HPC have been identified. Lu et al. identified in 2015 a group of murine BEC positive for EpCAM, cluster of differentiation 24 (CD24) and cluster of

differentiation 133 (CD133) which had increased in vitro clonogenic potential compared with other BEC. These cells were dubbed as HPC. When murine HPC were transplanted into a mouse model with extensive hepatocyte injury and senescence, they were able to differentiate into both hepatocyte and BEC and engraft in the liver [150].

The Forbes lab have demonstrated improvements in imaging and biochemical markers of disease in the *Krt19^{CreER}MDM2$^{fl/fl}$Rag2$^{-/-}$IL2rg$^{-/-}$* murine model of cholangiopathy, following intra-splenic injection of human HPC [124]. Despite the improvements described in this study, limited numbers of human HPC were identified on immunohistochemistry in mice that had received transplant. Prior to progressing this cell therapy to clinical research, improvements in engraftment should be made to optimise the chance of demonstrating efficacy. This thesis will aim to improve the engraftment of human HPC in the *Krt19^{CreER}MDM2$^{fl/fl}$Rag2$^{-/-}$IL2rg$^{-/-}$* model.

1.8 Cell homing

The ability of a transplanted cell to move from the site of delivery to the target is essential to successful engraftment. Increasing the propensity of transplanted cells to arrive at the target site, therefore offers an opportunity to improve the efficacy of cell therapies. There are multiple factors which may influence a cell's success in this endeavour, which this section will discuss.

Selecting a target and a starting point

The target site will significantly impact the likelihood of a cell successfully arriving following transplantation. Cells can be delivered with more ease to a less specific target such as the liver, than a more specific, such as the biliary system. It is therefore important to select a target which will enable the transplanted cells to function more impactfully. Although there are examples of implantation of hepatocytes in sites outside of the liver[151], given the lack of endocrine functions of BEC, it is likely required that transplanted HPC arrive to the biliary system to take effect in the cholangiopathies. Hallett, Ferreira-Gonzalez and co-workers demonstrated in their work when human HPC engrafted and were identified in mice following transplant they were in close

proximity to biliary ducts. Similarly, Sampaziotis and co-workers demonstrated engraftment of BEC into biliary ducts, following infiltration directly via the biliary sytem. These results indicate that the most favourable niche for transplanted BEC are the ducts themselves or the periductal region.

Equally important to the end point of a cell homing system is the start point. Often cell therapies have depended on delivery via the vasculature, either in a peripheral vein or via a specific blood vessel[129, 152]. Cells delivered via a peripheral vein must pass through the pulmonary vasculature prior to entering the heart and subsequently the arterial system. From the heart, cells could in theory reach any artery or arteriole in the body and are therefore dependent on inherent homing mechanisms to reach the target site. Unlike immune cells, which are migratory under normal circumstances, parenchymal cells such as BEC are normally constrained by a basement membrane[153]. For this reason, peripheral delivery is likely to be inefficacious for the cholangiopathies.

Biliary delivery

There are several more specific routes for cell delivery into the biliary system, each with advantages and challenges. The biliary system may be accessed directly via the Ampulla of Vater (as in Endoscopic Retrograde Cholangiopancreatography, ERCP) however, this route of administration incurs a risk of pancreatitis[154]. Similarly, delivery via the biliary system (as in cholecystostomy or the intrahepatic ducts through percutaneous transhepatic cholangiography, PTC) is associated with bleeding[155]. All biliary routes of administration would require cells to travel contra to the normal flow of bile to fully distribute throughout the biliary tree. In patients suffering from cholangiopathies this may be more challenging still due to the presence of strictures.

The work previously discussed by Sampaziotis and co-workers administered extrahepatic BEC via the biliary system in both the murine and explanted human livers[17]. In the murine model, cells were delivered via the gallbladder whilst clamping the CBD, in explanted livers via a catheter into a peripheral bile duct. The engraftment seen within the ducts in this study demonstrate the potential for the biliary route administration but do not replicate normal biliary dynamics. In both the explanted human liver and murine models normal flow of bile from the liver to the bowel had been interrupted thus allowing BEC to flow more freely into the liver.

Hepatic artery delivery

In traditional anatomy, the hepatic artery exclusively supplies the intra and extrahepatic biliary system, as described in section 1.1. This dogma has been challenged by clinical data demonstrating the development of ischaemic cholangiopathy secondary to insufficiencies of the portal venous system, in the context of a normal hepatic artery[156]. Despite this, the hepatic artery remains an attractive route for delivering cells to the biliary tree.

Laing and co-workers reported on the transplantation of fluorescently labelled MSC into explanted human livers in 2020 [157]. They reported MSC infiltrated via the hepatic artery route permeated through the liver parenchyma whilst the portal vein route limited cells to the sinusoids.

The use of the hepatic artery is also clinically feasible. The hepatic artery is used to deliver targeted therapies for malignancy to the liver, for example during TACE [158] and selective internal radiation therapy (SIRT) [159]. Whilst these procedures are often well tolerated, there is a small risk of injuring or occluding the hepatic artery, potentially leading to devastating clinical consequences including preclusion from receiving OLT[160]. Moreover, whilst it is possible to access the hepatic artery in mice, often this results in sacrifice of the artery, which could lead to biliary damage and so confound transplant results. Additionally, the hepatic artery is thought to be less dominant in the supply of the biliary system in rodents than in humans, particularly in mice [161].

Portal vein delivery

Portal vein access is increasingly used in clinical practice, for example in islet transplantation for the treatment of recurrent hypoglycaemia in diabetes mellitus[162]. In clinical practice, the portal vein is accessed through a transhepatic approach, which may result in haemorrhage in up to 10% of cases[163].

In mouse models, portal vein injection is known to carry a significant procedure- associated mortality in mice (up to 35%) due to haemorrhage [164]. Intraparenchymal splenic injection offers an alternate method of delivering cells in murine models via the portal system due to splenic veins drainage directly into the portal vein. It is associated with a lower risk of mortality in the mouse [143, 150]. From the clinical perspective it

is important to consider that increased portal vein pressure and reversal of flow may accompany chronic liver disease[67]. In cases of flow reversal, cells injected into the portal vein would be directed towards the bowel instead of the liver, significantly limiting the ability of this route to deliver cells to the liver.

In summary, the hepatic artery, portal vein and biliary system present viable methods for delivering cells to the liver, each with their own challenges. The hepatic artery may be challenging in murine models, whilst there are doubts over the effectiveness of delivering cells against normal flow into the biliary system. Although there are some drawbacks, the portal route of administration offers a clinically relevant method for modelling cell therapies and is the most pragmatic option for murine models.

Plasma membrane adaptations

Even if cells are delivered by the most effective route, there are further challenges to overcome. Cells delivered via the vasculature must pass through an endothelium, whether that be of the hepatic sinusoids, the portal venules, or hepatic arterioles. Following this they must cross the periportal extracellular matrix and possibly the hepatic parenchyma to arrive at the biliary ducts, dependant on where they exit the vasculature, as represented in Figure 1.4. Once at the biliary ducts, as discussed previously, cells are likely required to integrate into the native biliary system. The plasma membrane has a key role in determining how cells interact with their environment and is therefore important for the movement of cells through these compartments to reach the biliary epithelium[165].

Poor engraftment is common to many cell therapies[53, 127, 166, 167]. Several techniques have already been developed to alter the proteins present on the plasma membrane of transplanted cells, most commonly in the context of MSC transplantation.

The endothelium has often been touted as an appropriate target for a cell homing strategy, as it represents the first physical barrier cells must overcome to move from the bloodstream to the target. Sarkar et al developed a biotin-streptavidin bridge, which allowed immobilisation of sialyl-Lewisx (SLex) on the plasma membrane of MSC [168]. SLex has high affinity for P-selectin, a membrane protein expressed on the surface of inflamed endothelial cells. After inducing inflammation locally in the ear

using a lipo-polysaccharide (LPS) injection, a 54% increase in localisation of modified MSC to the injected ear was observed compared with non-modified MSC[169].

More recently, Dollet and co-workers used the same SLeX streptavidin bridge technique on a MSC line of hepatic origin called Adult derived human stem/progenitor cells (ADHLSC) *in vitro*. They were not able to demonstrate improved attachment of SLeX presenting ADHLSC to cultured human umbilical vein endothelial cells compared with control [170]. They proposed this finding was secondary to blocking of plasma membrane proteins on the surface of ADHLSC. Biotinyl-N-hydroxy-succinimide (BNHS) bonded to amine groups present on the plasma membrane of ADHLSC to form the base of the biotin-streptavidin bridge. A large proportion of plasma membrane proteins contain external amine groups and so may be blocked by this interaction. This system may interfere with the inherent mechanisms ADHLSC use to interact with endothelial cells and may explain why a negative result was produced.

Ko et al developed a method of coating MSC cells in antibody against vascular cell adhesion molecule 1(VCAM-1), also expressed on the plasma membrane of endothelial cells. In a mouse model of inflammatory bowel disease they exhibited improved cellular localisation to areas of inflamed bowel [171]. Jeong and co-workers were able to incorporate hyperbranched polyglycerol with an attached ligand for VCAM-1 into the plasma membrane of MSC. Using a flow chamber to simulate an arterial environment, they demonstrated increased adherence of MSC to endothelial cells grown on the wall of the flow chamber when the VCAM-1 ligand was present [172].

The extracellular matrix has also been a target for homing mechanisms. Hyaluronic acid (HA) is an important component of the extracellular matrix, CD44 is a membrane receptor which has affinity for HA. This homing mechanism has been used to improve MSC homing. Corradetti and co-workers in 2017 exposed MSC to HA in culture leading to upregulation of CD44. They subsequently transplanted these cells into BALB/c mice with inflammation induced in an ear secondary to LPS injection. Their results indicated improved homing of the MSC exposed to HA to the inflamed ears compared with controls[173].

The methods of homing described in this section involve targeting an interaction between two proteins, one expressed on the plasma membrane of transplanted cells,

the other at the target. Migration is likely to be constituted by many interactions between proteins expressed on transplanted cells and the host tissues. With respect to this, in the quest to improve one of these interactions, care must be taken not to surrender inherent cellular homing. This is particularly true in human HPC therapy for the cholangiopathies, studies have already shown that HPC can migrate to the ducts following transplantation[17, 124] and so cells have some inherent homing capacity. The work of Dollet indicates that the biotin-streptavidin bridge method may not be desirable for the presentation of ligands on the plasma membrane of human HPC as it blocks plasma membrane proteins indiscriminately. Attachment of antibody to the plasma membrane of HPC may also result in protein blockade.

Nonetheless, the evidence for augmenting or adding a homing interaction to transplanted cells is promising, and therefore will be pursued in this thesis. In this pursuit, a protein must be identified at the target site to build a homing mechanism. When considering the ideal target for cell homing in the cholangiopathies, it would be specific and available. Ideally, the target would be specific to BEC and to injury of the BEC. Additionally, the target should be available, either excreted into the local environment or be present on the surface of BEC. Intracellular proteins are unlikely to interact with transplanted cells.

The identification of a specific protein on or in close proximity to BEC, and the presentation or upregulation of a ligand or receptor for this protein on the surface of HPC may offer a novel method for cell homing in the context of HPC transplantation. Given the importance of the plasma membrane in the development of the cholangiopathies, proteomic analysis of the plasma membrane of BEC will provide information on how BEC interact with their environment and offer targets for cell homing,

Figure 1.4 Path from the vasculature to the biliary epithelium for transplanted cells.

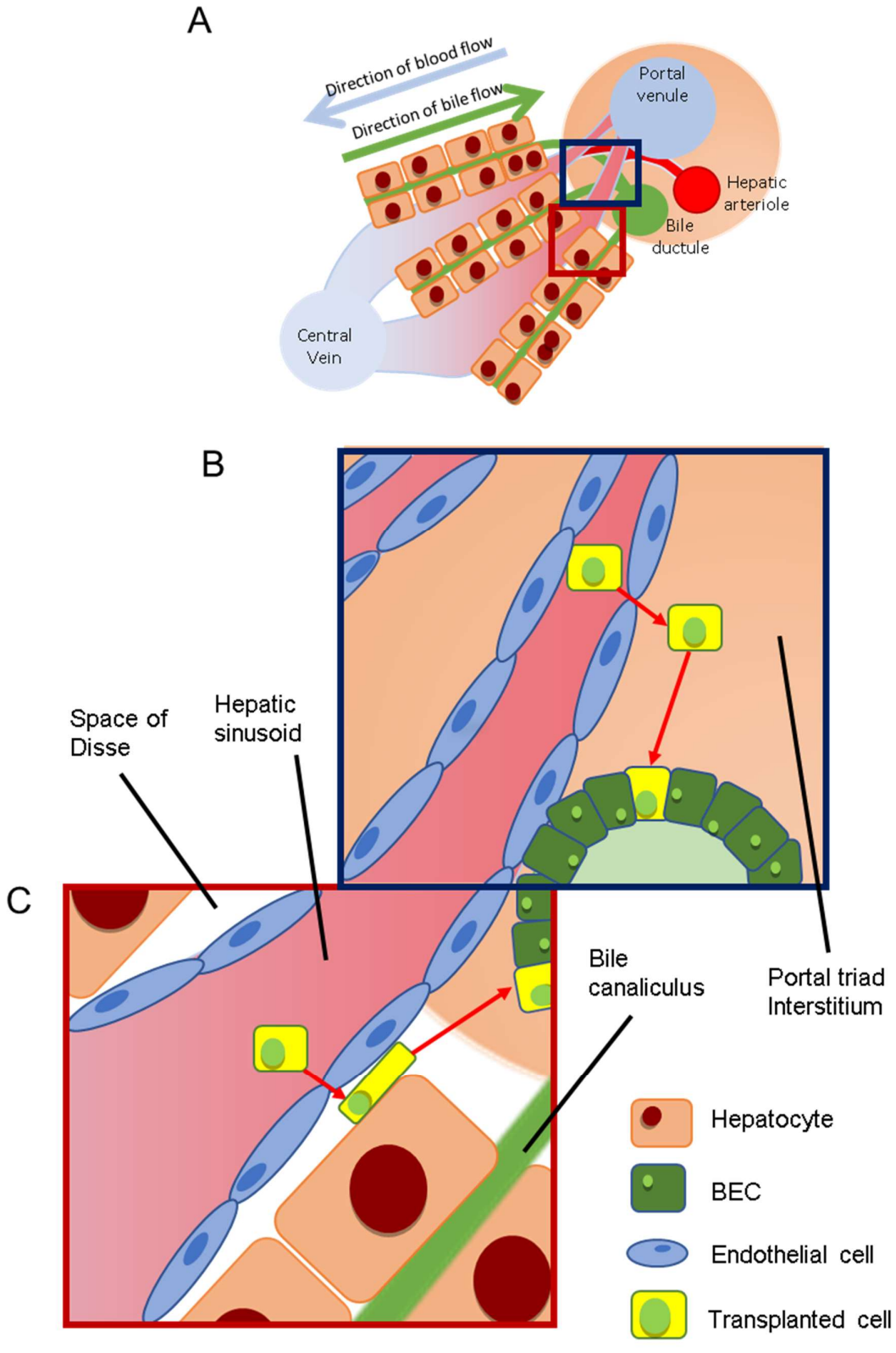

2

Figure 1.4 Path from the vasculature to the biliary epithelium for transplanted cells.

A: Arrangement of the portal triads in relation to hepatocytes, biliary canaliculi and hepatic sinusoids.

B: Theoretical route taken by transplanted cells to the biliary epithelium when exiting vessels in the portal triads.

C: Theoretical route taken by transplanted cells when exiting the hepatic sinusoids.

Red arrows indicate direction of cell migration.

1.9 Plasma membrane proteomics

The relatively low abundance of plasma membrane proteins renders their detection challenging. As such, techniques have been developed to enrich plasma membrane proteins. Differential ultracentrifugation depends on the density of the plasma membrane being different to that of other subcellular components. Differing densities cause components to pellet at varying centrifugation speeds, allowing them to be separated from each other[174]. Cells are initially lysed in a non-chemical, hypotonic buffer to allow the release of the intracellular organelles intact without separating plasma membrane proteins from the lipid bilayer. In this way the subcellular components retain their density properties. Following this, a slow centrifugation is applied to remove nuclei, non-lysed cells, and larger organelles from the lysate. High speed centrifugation is then performed to pellet the plasma membrane fraction. This technique is at risk of contamination from membranes of other cellular organelles.

Density gradient ultracentrifugation relies on the same principle as differential ultracentrifugation. In additional to serial centrifugation, a gradient of solutions of different densities are used which allow organelles to settle at interfaces between different densities according to their own density [175].

In addition to ultracentrifugation-based techniques, plasma membrane capture techniques have also been used. These techniques involve introducing non-lysed cells to a marker which can bind to proteins. By introducing the marker before lysis, only proteins exposed to the extracellular environment are tagged with the marker. Cells are subsequently lysed, and the marker is used to separate plasma membrane proteins from intracellular proteins. One example of this is using BNHS, as used by Sarkar in their previously mentioned biotin-streptavidin bridge technique. The N-hydroxy-succinimide pole of this molecule has a high propensity to react with amine groups, which are often present on plasma membrane proteins. Once this reaction has taken place a free biotin pole is left attached to plasma membrane proteins, which has a high affinity for streptavidin. Using streptavidin coated beads or columns, the tagged plasma membrane proteins can be separated from intracellular proteins, which are not bound to BNHS[176, 177]. Lectin based capture techniques use a similar model to BNHS, however they bind specifically to glycosylated proteins and therefore may bias results towards proteins with a glycosylated extracellular moiety [178].

The final method of plasma membrane proteomics is through bioinformatics. In recent years protein atlases have increased in size and new models for predicting the number of transmembrane sections of a protein have been developed [179, 180]. These advancements in techniques allow the physical isolation of plasma membrane proteins to be circumvented, although they may run the risk of missing proteins which have low abundance but may still be important as targets.

There have already been studies aiming to assess the surface proteins present in the liver [178, 181, 182], however the identification of these proteins in disease and health in different liver compartments remains to be elucidated.

In summary, there exists multiple methods of extracting data on the composition of plasma membrane proteins, each with their unique drawbacks and potential benefits. As the ability of modern mass spectroscopy technologies improve their sensitivity, it is likely that the bioinformatic method becomes the hegemon in plasma membrane proteomic analysis.

By comparing plasma membranes expressed in BEC and hepatocytes, a biliary specific plasma membrane protein can be identified. Comparing the expression of biliary specific plasma membrane proteins in biliary injury with controls will identify proteins which are upregulated in the cholangiopathies. In this way an ideal target for a cell homing system in the cholangiopathies can be identified.

1.10 SCTR as a candidate

Plasma membrane proteomics could identify a perfect target, however there may also be proteins which could act as targets which have already been described in the literature. Investigations into the physiology underlying the production and regulation of bile have uncovered several plasma membrane receptors and transporters. Some of the most obvious candidates have aspects that may preclude them from use as a target. For example, AE2, which is an important BEC membrane protein as described in section 1.3, it is also expressed on the canalicular membrane of hepatocytes[183] and therefore is not specific. As described in the subsection on PBC in section 1.4, there is evidence to suggest that AE2 is downregulated in PBC [39, 183, 184].

CFTR is also a potential target, however in certain cholangiopathies such as cystic fibrosis and PSC the receptor is dysfunctional or has reduced expression[38, 87, 88]. Such variability in the receptor may render it more challenging to target with a ligand. Additionally, both AE2 and CFTR are expressed on the apical aspect of BEC and therefore may be more difficult to access following transplantation of cells via the portal system. In contrast, SCTR is thought to be expressed on the basolateral aspect of BEC exclusively in the liver and may represent a possible target for homing.

The primary ligand for SCTR is SCT, which is produced in the duodenum and jejunum by S cells which are found in the intestinal crypts. They produce SCT in response to low pH when the gastric contents empty into the duodenum[185, 186].

The distribution of SCTR on BEC remains contentious. In 2006 Korner and co-workers reported in human liver that SCTR was present in some smaller ducts but was not in large ducts [187]. In contrast to this, Alpini and co-workers reported in rats that SCTR was expressed only on large BEC and not small, and therefore expressed more in large ducts [36]. Both groups demonstrated that SCTR was not expressed on hepatocytes.

It is also unclear how expression of SCTR changes in hepatic injury. Alpini and co-workers demonstrated an upregulation of SCTR in rats that had undergone bile duct ligation (BDL) compared with controls [37]. The *Mdr2* knockout model of cholangiopathy also demonstrates an increased expression of SCTR associated with increase of transforming growth factor beta 1 (TGF-β1) expression, an important signalling molecule in cellular senescence [188]. The *Mdr2* knockout model has also been shown to have reduced injury on administration of the SCTR receptor antagonist Sec5-27, or when mice were crossed with SCTR knockout mice, indicating that SCTR has a role in the pathogenesis of cholangiopathy [189].

More recently Kennedy and co-workers used a dominant negative, transforming growth factor beta receptor II (TGF- RII) mouse to model early stage PBC [190]. In contrast to the above-described models, they demonstrated a reduced expression of both SCTR and SCT. Following treatment with SCT they were able to demonstrate a reduction in the degree of biliary injury, indicating a possible protective role for SCTR in the development of PBC, in contrast to findings in the *Mdr2* model.

In human samples, de Jong and co-workers saw a fall in SCTR expression in human liver samples from patients with ischaemic cholangiopathy[98]. In addition, they reported that in areas of normal ducts within ischaemic cholangiopathy livers, SCTR expression was at a similar level to control livers.

The presence of SCTR specifically on BEC makes it an attractive target for cellular homing. The expression of SCTR in biliary injury should be clarified to elucidate its value as a target for cell homing in the cholangiopathies.

1.11 TFF2 as a candidate

The trefoil factors are a group of small molecules which are produced within the bile ducts. They have several functions including the protection of the biliary epithelium but also have a role in modulating cellular migration and promote healing [191].

Trefoil factor 2 (TFF2) was felt to be produced exclusively by the bile ducts, however more recently it has been suggested that these factors may also be secreted into the bile canaliculi by hepatocytes in times of hepatocellular injury[192].

In the context of biliary injury, expression in hepatocytes has not been reported to date. In 2004 Sasaki and co-workers demonstrated the presence of TFF2 in the large ducts of patients suffering from PSC and those with extrahepatic biliary obstruction and was not present in normal controls[193], indicating that TFF2 production increases in biliary injury.

The migratory function of TFF2 is felt to be mediated via its interaction with C-X-C chemokine receptor type 4 (CXCR4) [194]. The main ligand of CXCR4 is stromal cell derived factor 1 (SDF1). For this reason, TFF2 may be especially attractive as its receptor has affinity for a second small molecule involved in cell homing.

1.12 CD44 as a candidate

Originally CD44 was identified as a macrophage receptor used for homing[195]. Migration is mediated through the interaction with HA, a component of the extracellular matrix[196, 197]. This was exploited by Corradetti et al in their homing system for MSCs, as discussed in section 1.7.

He and co-workers investigated the expression of CD44 in a rat model of BDL [198]. They found a significant increase in CD44 expression assessed using quantitative polymerase chain reaction (qPCR) in BEC of rats who underwent BDL compared with controls. They demonstrated that hepatocytes did not express CD44, however, endothelial cells, Kupffer cells and Stellate cells did. Encouragingly, the highest expression was seen in BEC.

Cruickshank and co-workers investigated the expression of CD44 human liver samples from patients with biliary and hepatocellular injuries. They found low levels of CD44 expression in controls with higher biliary expression after liver injury, particularly in the cholangiopathies. They also reported no expression in hepatocytes.

The evidence provided by these studies combined depict CD44 as a near ideal target, being absent on hepatocytes, and augmented in biliary injury. The only potential obstacle would be the expression of CD44 on some non-biliary, resident hepatic cells.

Hyaluronic acid is a ligand for CD44. Coating cells in HA could improve the ability of cells to attach to and engraft in the biliary epithelium through interactions with CD44. In 2017 Nevi and co-workers coated extrahepatic human BEC in HA and transplanted cells via the spleen, into an uninjured, immunocompromised mouse model[135]. Whilst they were able to show improved engraftment compared with uncoated cells, the degree to which this is due to homing is unclear, particularly given that CD44 is thought to have low expression in uninjured BEC.

1.13 Chemokines as candidates

Cell migration is an essential process in normal physiology. Migration forms a central function of the immune system, allowing immune cells to move from the blood or tissues to areas of inflammation to enact an inflammatory response.

The chemokine- chemokine receptor axes are one important method of cellular migration used by the immune system. Several groups have attempted to utilise these axes in the name of improving homing in cell therapies. CXCR4 is a plasma membrane protein which has affinity for the chemokine SDF1, Brenner and co-workers demonstrated increased engraftment in the bone marrow of haemopoietic stem cells following upregulation of CXCR4 [199]. Similarly, Bonacini upregulated CX3

chemokine receptor 1 (CX3CR1) in T-regulatory cells and showed improved homing to plaques in the aorta due to CX3CR1's affinity for CX3CL1[200]. CXCR5 has also been upregulated in MSC, to enhance homing to inflamed murine ears compared with control MSC[201]. Recently in the liver, Xu et al overexpressed C-C chemokine receptor 2 (CCR2) in MSC cells given to mice with acute liver injury induced by TAA. Their findings suggested an increased uptake of cells in the liver in those transduced with the CCR2 GFP plasmid[202].

These studies demonstrate the potential of the chemokine- chemokine receptor axes in improving cellular homing, however there are many interactions between chemokines and their respective receptors. It would be valuable therefore, to identify chemokines which are specifically expressed by BEC in biliary injury.

In 2019 Pepe Mooney et al, in Cell Stem Cell, published single cell sequencing data comparing BEC from mice in homeostasis and those who had injury induced by two weeks of DDC diet[149]. In addition to the single cell analysis, they published, as a supplementary analysis, a bulk version of their sequencing data. The importance of this data was to demonstrate changes that occur in BEC in biliary disease however the data could also be used to identify which chemokines are produced by BEC following biliary injury. Considering only genes included in the gene ontology term chemotaxis (GO:0060326), Chemokine ligand 7 (*Ccl7*) was the most upregulated in DDC treated mice compared with controls, however within the top 10 most increased chemotaxis genes *Ccl2* had the highest overall expression. These chemokines share a common receptor in CCR2 (table 1.1).

Table 1.1 Top 10 upregulated chemokines following DDC diet in BEC

Gene	Rank	Control	DDC	Fold Change (log2)	p-value *	Receptor
Ccl7	11	0.021	32.18	-10.57	1.06E-14	CCR1,2,3,5,10[203-206]
Cxcl3	17	0.021	16.69	-9.62	5.67E-08	CXCR2[207]
Slamf9	26	0.021	13.04	-9.27	2.16E-06	Not a ligand
Ccl2	28	2.23	1319.68	-9.21	0	CCR2, 4[208, 209]
Plau	33	0.021	10.20	-8.91	3.73E-05	Not a ligand
Cx3cr1	73	0.021	4.97	-7.87	0.0070	Not a ligand
Xcl1	74	0.021	4.82	-7.83	0.0081	XCR1[210]
Ccl20	76	1.63	260.40	-7.32	2.03E-111	CCR6[211]
Adam8	79	0.30	37.99	-7.01	3.16E-17	Not a ligand
Cxcl5	82	5.35	530.11	-6.63	1.80E-219	CXCR2[207]

CCL2 has recently been implicated in the recruitment of a specific subgroup of macrophages (lipid associated macrophages (LAM)) to the periductal region in steatotic livers[212]. From a functional perspective the fact that macrophages use this ligand to migrate to the periportal space is promising, as this method of migration could be installed in human HPCs. It has also been demonstrated that senescent and inflamed ducts on PBC are more likely to express *Ccl2*[213]. In 2018 Guicciardi and co-workers found that in mice with biliary injury induced by intra-biliary injection of BV6 (a SMAC inhibitor), CCR2 knockout or pharmacological blockade led to reduced peribiliary infiltration of macrophages and reduced injury response, indicating the importance of CCL2 in migration of macrophages to the bile ducts during injury[214].

Out with the data produced by Pepe-Mooney and co-workers, the importance of CXCR2 to the migration of immune cells to sites of biliary injury has been demonstrated by Konishi and co-workers in 2019. They found a reduction in neutrophil infiltration to the biliary ducts following bile duct ligation in mice that had CXCR2 knocked out compared with those who did not, Furthermore, they demonstrated that

CXCR2 knockout reduced biliary injury [215]. In early 2022 Mohamad Zaki and co-workers published the results of their study which investigated the role of CXCL1 (a ligand for CXCR2) in extrahepatic cholangiopathies. They reported that the expression of CXCL1 was increased in their mouse model of bile duct ligation, an increase controlled by Hedgehog[216]. Rodrigo-Torres et al in 2014 provided micro-array analysis of DDC diet injured, murine BEC compared with controls, reporting in their supplementary information *Cxcl2* to be the most upregulated gene following DDC[217].

There is a relative paucity of single cell or bulk sequencing data from BEC in human cholangiopathies. There is also, therefore, limited data regarding the expression of chemokines in the cholangiopathies. Whilst it would be ideal to develop a homing system which is directly applicable to human disease, it is also important to demonstrate that conceptually developing a homing system for transplanted HPC would lead to improved engraftment. As such in this thesis has focused on data which is applicable to the *Krt19*^{CreER}*MDM2*$^{fl/fl}$*Rag2*$^{-/-}$*IL2rg*$^{-/-}$ murine model of cholangiopathy in the hope of demonstrating the potential for cell homing in human HPC.

CCL2, CXCL1, and CXCL2 have therefore been selected as potential targets for homing to BEC in biliary injury, all of which will be investigated in this thesis.

1.14 Summary

The cholangiopathies are a group of conditions which may lead to hepatic failure. The only curative therapy for patients who develop these conditions is OLT. Cell therapies offer an alternative treatment, and HPC are a promising cell type for transplantation. Initial studies have shown limited HPC engraftment in murine models. Developing a clinically translatable cell therapy requires developing a system of delivering HPC in the most efficient way to the biliary system. Several possible targets exist including SCTR, TFF2 and CD44 but require further assessment. Proteomic analysis of the plasma membrane of BEC may help to identify novel targets for cell homing. Finally, the chemokines are further possible targets which merit investigation.

Chapter 2: Hypothesis

Engraftment can be improved in a murine model of cholangiopathy by targeting specific BEC surface markers with ligands attached to the surface of transplanted human HPC.

Chapter 3: Aim

To improve engraftment of hHPCs in the *Krt19^{CreER}MDM2$^{fl/fl}$Rag2$^{-/-}$IL2rg$^{-/-}$* model of cholangiopathy.

Objective 1: To identify a target protein expressed exclusively on or in close proximity to the plasma membrane of injured BEC.

Objective 2: To present a ligand specific for the target protein in Objective 1 on the surface of hHPC.

Objective 3: To demonstrate improvement in cell engraftment of hHPC when transplanted to the *Krt19^{CreER}MDM2$^{fl/fl}$Rag2$^{-/-}$IL2rg$^{-/-}$* model.

Chapter 4: Materials and Methods

4.1 Ethics Approvals

Ethical approval for human liver tissue, which provided both control samples for immunohistochemistry and immunofluorescence and the basis to produce human HPC was obtained prior to the PhD candidate starting in the group.

Human livers which were deemed unsuitable for transplantation were collected following approval from the Lothian research and ethics committee reference number 15/SS/0218. Samples from patients with PSC and PBC were obtained from livers that had been explanted in preparation for OLT. Ethical approval for these samples was also obtained from the Lothian research and development committee, reference number 15/ES/0094.

4.2 Animal experiments

All animal experiments were carried out with ethical permission from the University of Edinburgh Welfare and Ethical Review Body and the United Kingdom home office. All animals were housed in ventilated cages under a 12-hour day/night cycle. Access to food and water was provided *ad libitum*. Mice were aged between 12 and 22 weeks for both transplant and cell isolation experiments. Where possible, an equal distribution of male and female mice was used.

For downstream immunofluorescence or immunohistochemistry, livers were washed with phosphate buffered saline (PBS) instilled via the inferior vena cava (IVC). Organs were harvested and fixed in 10% formalin for 6 hours at room temperature. The median lobe of the liver was placed on dry ice then stored at -80^{o}C, to provide tissue for RNA isolation.

C57B6/J mice were sourced from Charles River.

4.3 Tissue processing

On completion of fixation, organs were sent to the histology unit at the Queen's medical research institute at the University of Edinburgh, for embedment in paraffin. Embedded samples were cut into 4µm sections using a Leica RM 2125RT microtome and collected onto glass slide (Epredia, J1800AMNz).

4.4 Immunohistochemistry

Slides were exposed to xylene for 10 minutes followed by rehydration by passing through a gradient of decreasing concentrations of ethanol ranging from 100 to 70%. Rehydration was completed by placing slides in running tap water for 5 minutes. Heat assisted antigen retrieval was performed using Tris-EDTA pH9.0 or sodium citrate pH pH6.0 and heating in a microwave at high power. For proteinase K retrieval, slides were incubated at 37^0C in a water bath. Slides were then cooled in running tap water. When targeting intracellular proteins, 0.1% triton in PBS solution was applied for 5 minutes, for membrane permeabilization (Sigma-Aldrich, 93443).

Incubation with peroxidase and alkaline phosphatase blocker (Bloxall, Vector, SP-6000-100) for 30 minutes was performed, followed by 15 mins each avidin and biotin (Invitrogen, 00-4303), and protein block (Spring Bioscience, DPB-125) for 1 hour. Slides were washed with PBS between each of these steps but not after the application of protein block.

Primary antibodies were prepared according to table 4.1 and incubated overnight at 4^{o}C, in Antibody diluent (Invitrogen, 003218). Species specific biotinylated secondary antibodies were applied at concentrations specified in Table 4.2 for 45 minutes, followed by a streptavidin conjugated horseradish peroxidase, Vectastain (Vectar, PK-7100) for 30 minutes.

3,3'-Diaminobenzidine (DAB) (2B Scientific, SK-4103-100 or DAKO, 3468) was applied for between 30 and 120 seconds to stain sections. Counterstaining was performed using haematoxylin for 1 minute and Scott's tap water for 30 seconds. Sections were dehydrated using increasing concentrations of ethanol and xylene. Slides were mounted using Perstex.

Isotype controls were performed for each stain, using an isotype from the same species as the primary antibody was raised in, at the same concentration of the antibody of interest. Figures 4.1 and 4.2 present images of isotype controls used for immunohistochemistry in murine and human samples.

Table 4.1 List of primary antibodies used for immunohistochemistry

Target Protein	Manufacturer	Catalogue Number	Antigen retrieval (time in mins)	Dilution	Host Species
ANXAV	Abcam	ab14196	Citrate (10)	1:400	Rabbit
GFP	Abcam	ab13970	Tris EDTA (10)	1:200	Chicken
F4/80	Abcam	ab6640	Proteinase K (15)	1:100	Rat
MYH14	Cell Signaling	8189	Tris EDTA (30)	1:50	Rabbit

Table 4.2 List of secondary antibodies used for immunohistochemistry

Antibody	Manufacturer	Catalogue number	Dilution	Host Species
Anti-chicken IgG biotinylated	Vector Laboratories	BA-9010	1:400	Goat
Anti-rabbit IgG biotinylated	2BScientific	BA-1000	1:250	Goat
Anti-rat IgG biotinylated	Vector Laboratories	BA-9400-1.5	1:250	Goat

Figure 4.1 Isotype controls used for immunohistochemistry in mouse tissue.

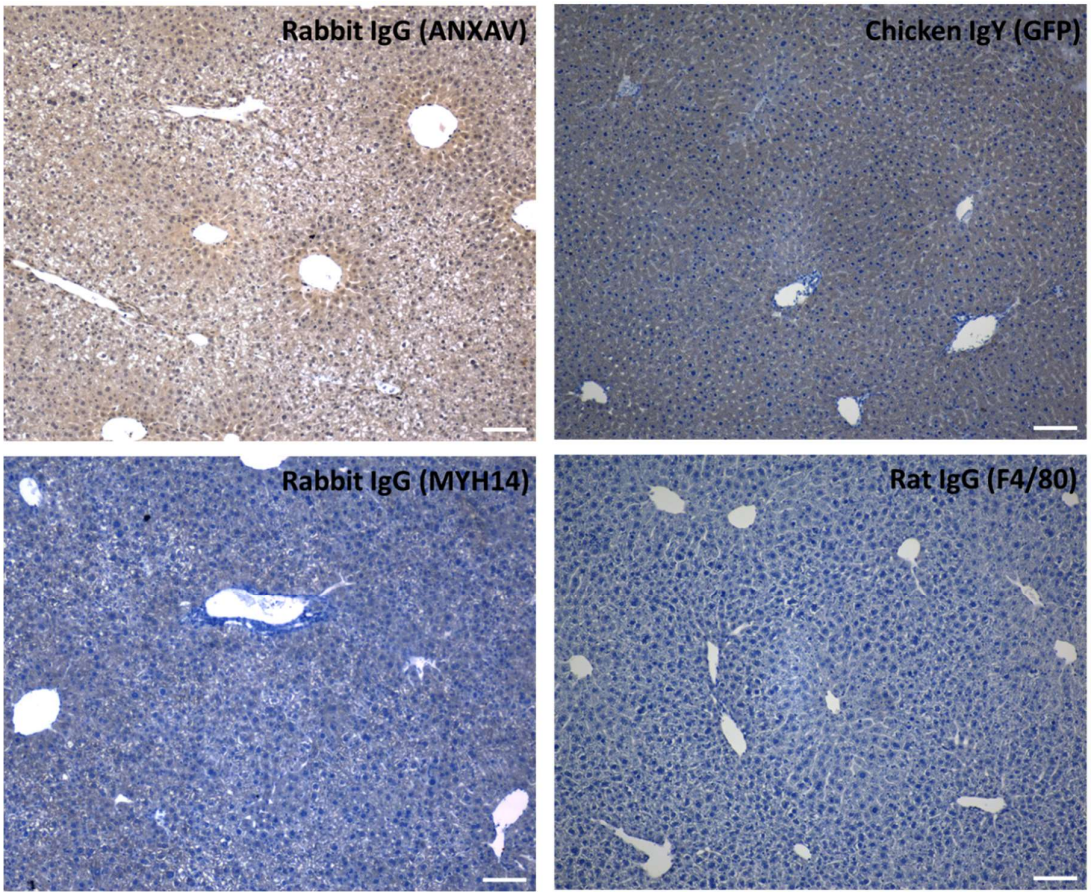

Figure 4.1: Isotype controls used for immunohistochemistry in mouse tissue.

All images taken at x10 magnification, scale bars 100μm.

Figure 4.2 Isotype controls used for immunohistochemistry in human tissue.

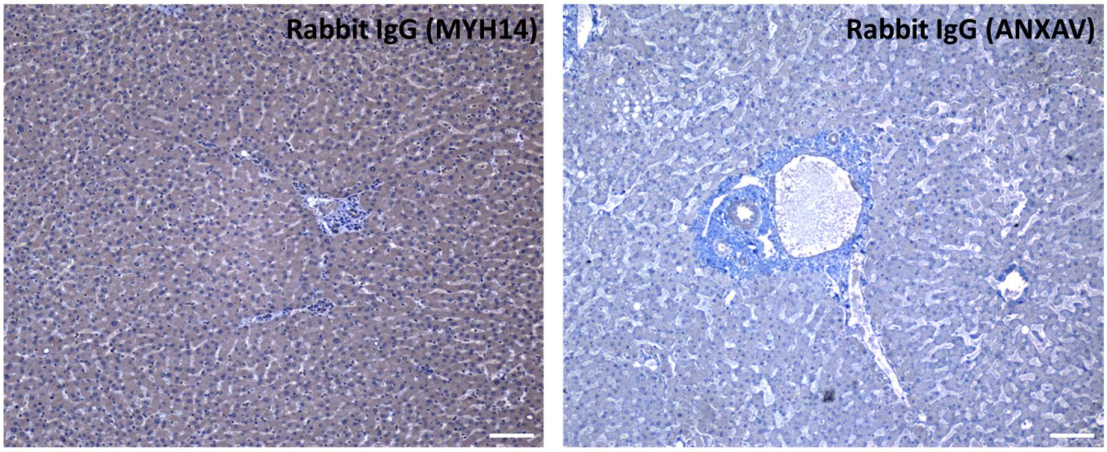

Figure 4.2: Isotype controls used for immunohistochemistry in human tissue.

All images taken at x10 magnification, scale bars 100μm.

4.5 Immunofluorescence

Slides were treated in the same way as for immunohistochemistry to the point of permeabilization. Protein block was then applied for 1 hour at room temperature. Slides were then incubated with primary antibody overnight at 4^{o}C, at concentrations shown in table 4.3. Species specific secondary antibodies with an attached fluorophore were applied at dilution of 1 in 400 for 45 minutes at room temperature. Slides were subsequently washed in 2 ml of 50% ethanol, then 70% ethanol.

1% Sudan Black was applied to slides. Following 20 minutes incubation, slides were rehydrated using 2 ml 70% then 50% ethanol. Mounting was performed using Fluoromount-G with DAPI (ThermoFisher Cat No. 00-4959-52).

Figures 4.1 and 4.2 present images of isotype controls used for immunofluorescence in murine and human samples.

Table 4.3 List of primary antibodies used for immunofluorescence

Target Protein	Manufacturer	Catalogue Number	Antigen retrieval (time in mins)	Dilution	Host Species
CD44	Abcam	ab157107	Tris EDTA (10)	1:400	Rabbit
GFP	Abcam	ab13970	Tris EDTA (10)	1:200	Chicken
KRT19	DSHB	AB_213357	Tris EDTA (10)	1:50/200	Rat
P21	Abcam	ab188224	Tris EDTA	1:200	Rabbit
SCTR	Biouss	0089R	Tris EDTA (10)	1:150	Rabbit
TFF2	Proteintech	13681-1-AP	Tris EDTA (20)	1:200	Rabbit

Table 4.4 List of primary antibodies used for immunofluorescence

Antibody	Manufacturer	Catalogue number	Dilution	Host Species
Anti-chicken IgG Fluor 488	Invitrogen	A11039	1:400	Goat
Anti-rabbit IgG Alexa Fluor 555	Invitrogen	A31572	1:400	Donkey
Anti-rat IgG Alexa Fluor 488	Invitrogen	A21208	1:400	Donkey
Anti-rat IgG Alexa Fluor 555	Invitrogen	A21434	1:400	Goat

Figure 4.3 Isotype controls for immunofluorescence in murine samples

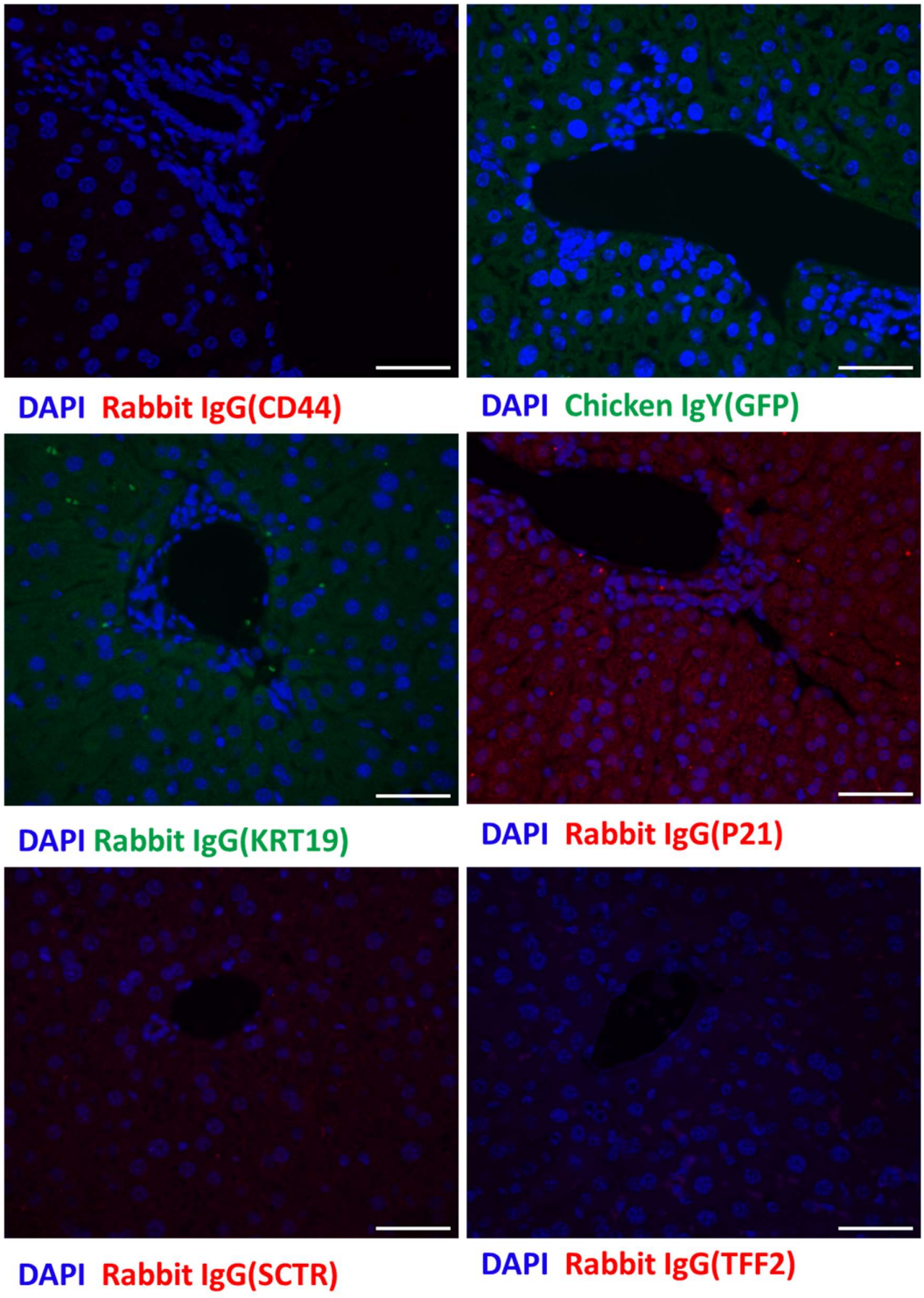

Figure 4.3: Isotype controls for immunofluorescence in murine samples

All images taken at x40 magnification error bars represent 50μm. Images in green represent the 488 channel, in red the 555 channel.

Figure 4.4 Isotype controls for immunofluorescence in human samples

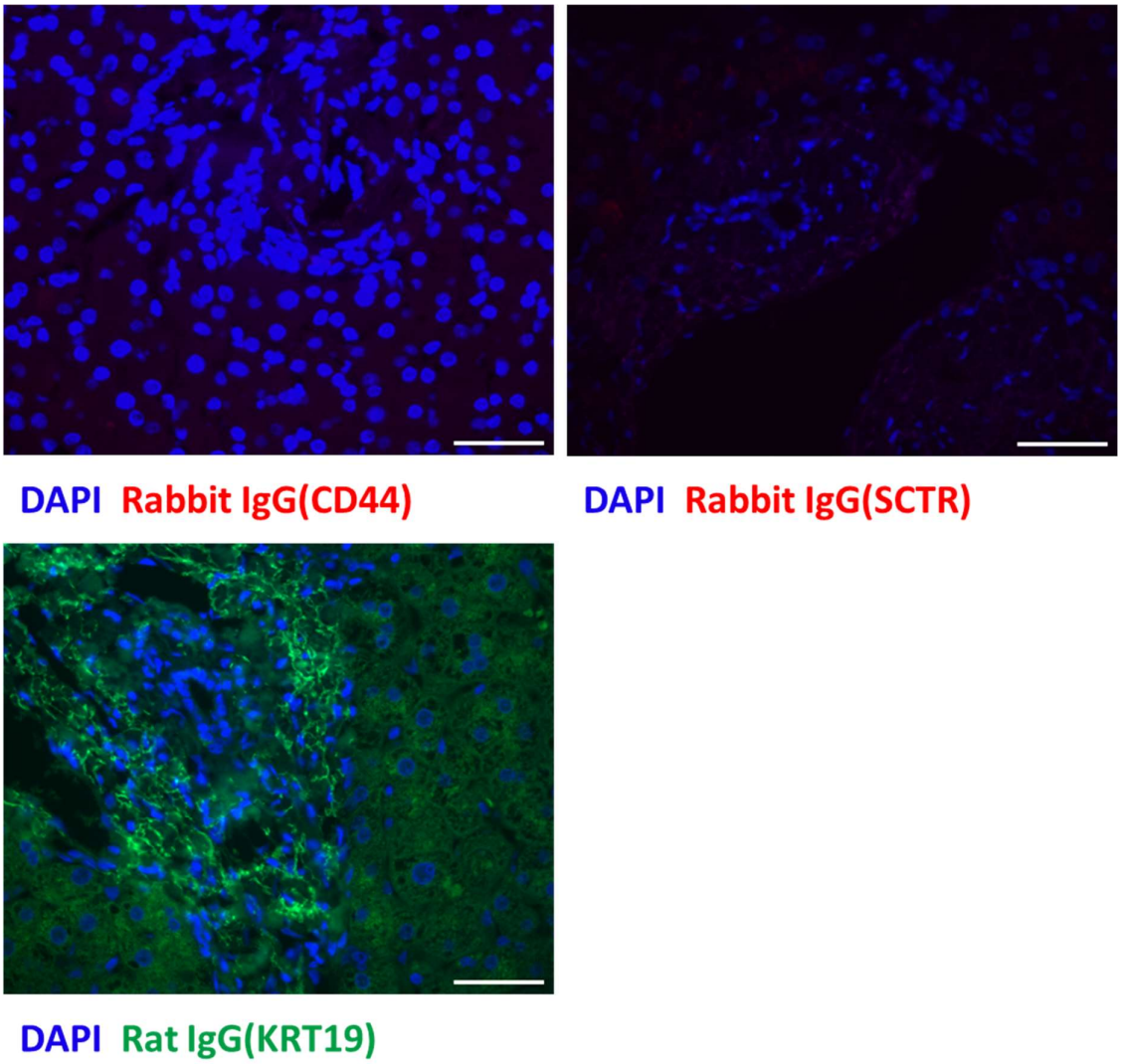

Figure 4.4: Isotype controls for immunofluorescence in human samples

All images taken at x40 magnification error bars represent 50μm. Images in green represent the 488 channel, in red the 555 channel.

4.6 Image acquisition

Images of tissue sections were taken using the Nikon eclipse e600 or the Nikon eclipse Ni microscopes, attached to a QImaging micropublisher 6 camera. For quantification blinding of slides was undertaken prior to image capturing.

When making assessment of expression of proteins in the ductal areas 10 images at 40x magnification were obtained. This primarily describes the imaging undertaken in Chapter 5 and in the assessment of distance of GFP positive cells from ductal areas in Chapter 7. Biliary ducts were identified as groups of cells positive for KRT19. A maximum of 5 images were taken on each piece of liver on the same slide.

For immunohistochemistry images, 10 images were taken at x20 magnification at random, 5 images on one piece of liver, a further 5 on a second piece of liver.

Images of cultured cells were taken using a Nikon Eclipse Ts2R microscope, with a Digital imaging systems Photometrics CoolSNAP DYNO camera.

.

4.7 Image quantification

Immunohistochemistry

Percentage of the area of expression was measured using a macro produced on ImageJ with a pre-set threshold. Images were split using the “colour deconvolution” function H and DAB setting. The DAB channel was selected for analysis. For both analysis, a threshold was set and applied to all images in an experiment. The process of analysis is demonstrated in Figure 4.5. An example macro is displayed in Appendix 4.1.

Immunofluorescence

Immunofluorescence images were analysed using either ImageJ or QuPath software. In ImageJ a standardised macro was developed which was used to initially segment the image to select areas positive for KRT19, therefore corresponding to biliary ducts. This area was called the ductal area.

To ensure the segmented areas were not artefactual, a second criteria was set: to ensure at least 20% of the selected area was positive in the DAPI channel, utilising the fact that the nuclei of BEC are more closely packed than in other areas of the liver. The expression of a protein of interest was then measured in the ductal area. 10μm

surrounding the ductal area, was also defined as the periductal areas. Finally, the tissue out with the ductal areas was analysed, and classified as the non-ductal area.

The threshold for positive staining was 2 standard deviations above the mean for the image for KRT19 expression and 3 standard deviations above the mean for expression of the protein of interest. The method for analysis is demonstrated in Figure 4.6. An example macro is displayed in Appendix 4.2.

The free to use QuPath software was used to count the numbers of individual cells positive for different markers. The software also has the inbuilt ability to measure the distance between cells. Analysis was performed using a pipeline which initially identified cells using nuclei. Following this, cells were classified as either positive or negative for specific markers. Finally, the distance of cells from the closest BEC (as defined by positive stain for KRT19) was calculated. Figure 4.7 demonstrates an example of QuPath analysis.

Figure 4.5 Example of analysis of immunohistochemistry

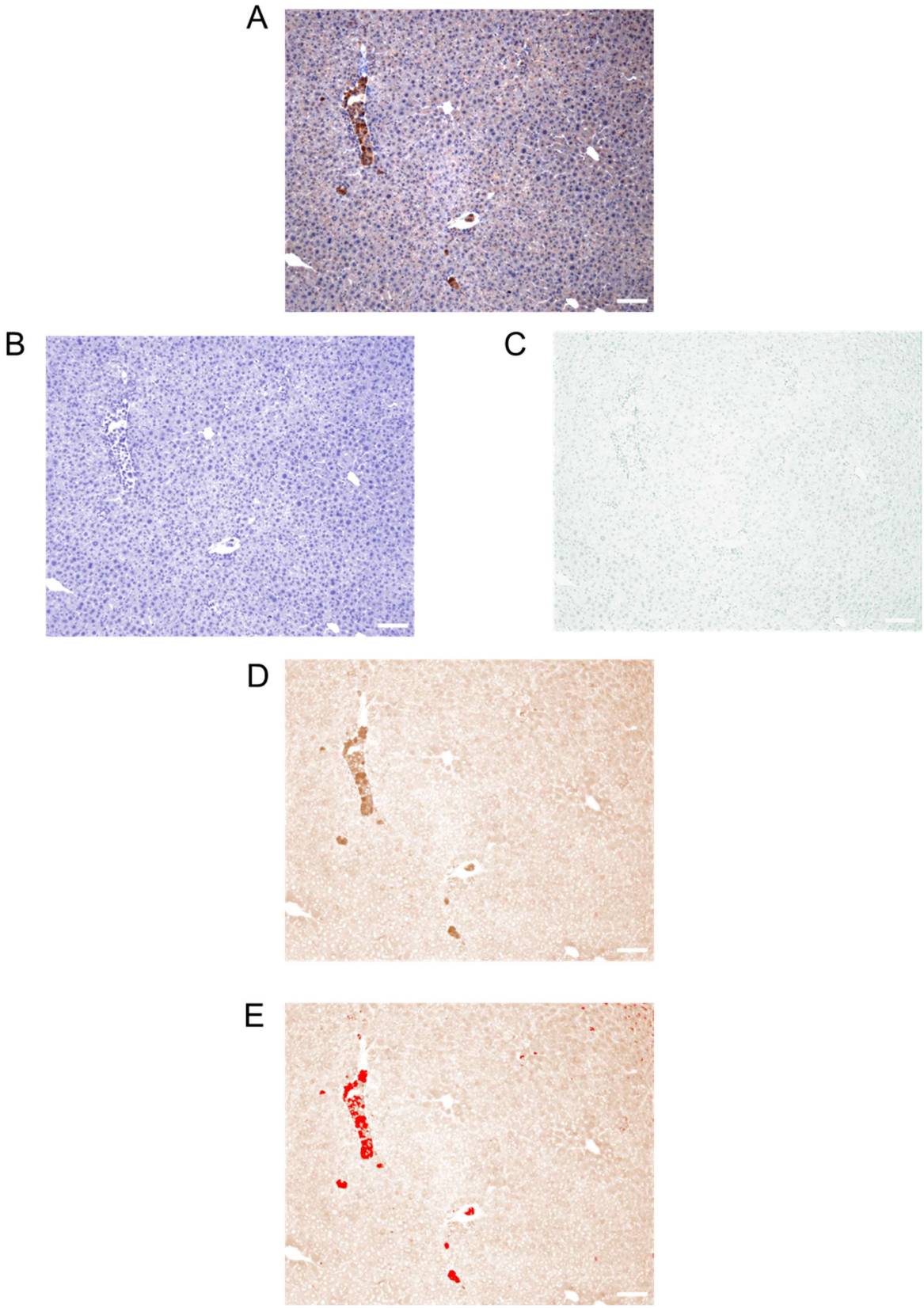

Figure 4.5 Example of analysis of immunohistochemistry.

Segmentation of a representative image taken at x20 magnification. Scale bar is 100μm

A: Original image showing example immunohistochemistry in a murine liver following transplantation of GFP positive HPC.

B: Haematoxylin image following colour deconvolution, not used in the analysis

C: Light green image following colour deconvolution, not used in the analysis

D: DAB image following colour deconvolution used for the analysis

E: Thresholding for DAB positive areas for measuring of positive area. Red indicates areas detected as positive.

Figure 4.6 Example of analysis of immunofluoresence.

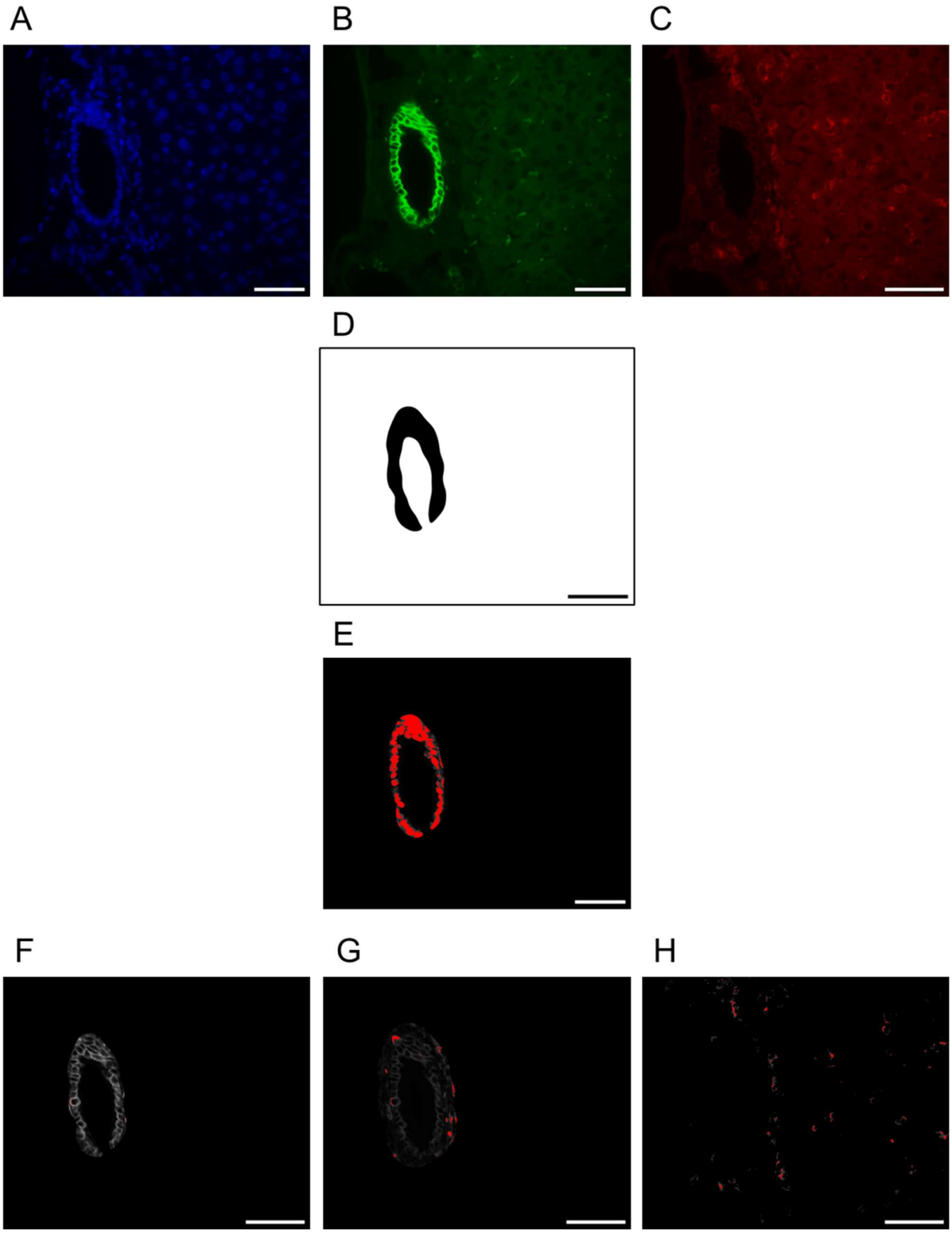

Figure 4.6: Example of analysis of immunofluoresence.

Segmentation of a representative image taken at x40 magnification. Scale bar is 50μm.

A: Image in the DAPI channel.

B: Image in the KRT19 channel.

C: Image in the CD44 channel.

D: KRT19 positive area segmentation

E: Measurement of DAPI positive area within the KRT19 segment.

F: Ductal area assessment. Analysis of CD44 positive area within the KRT19 positive segment.

G: Periductal area assessment. Analysis of CD44 positive area within the KRT19 positive segment and the 10μm surrounding.

H: Non-ductal area assessment. Analysis of CD44 positive area out with the KRT19 positive segment.

Figure 4.7 Analysis of immunofluorescence images using QuPath.

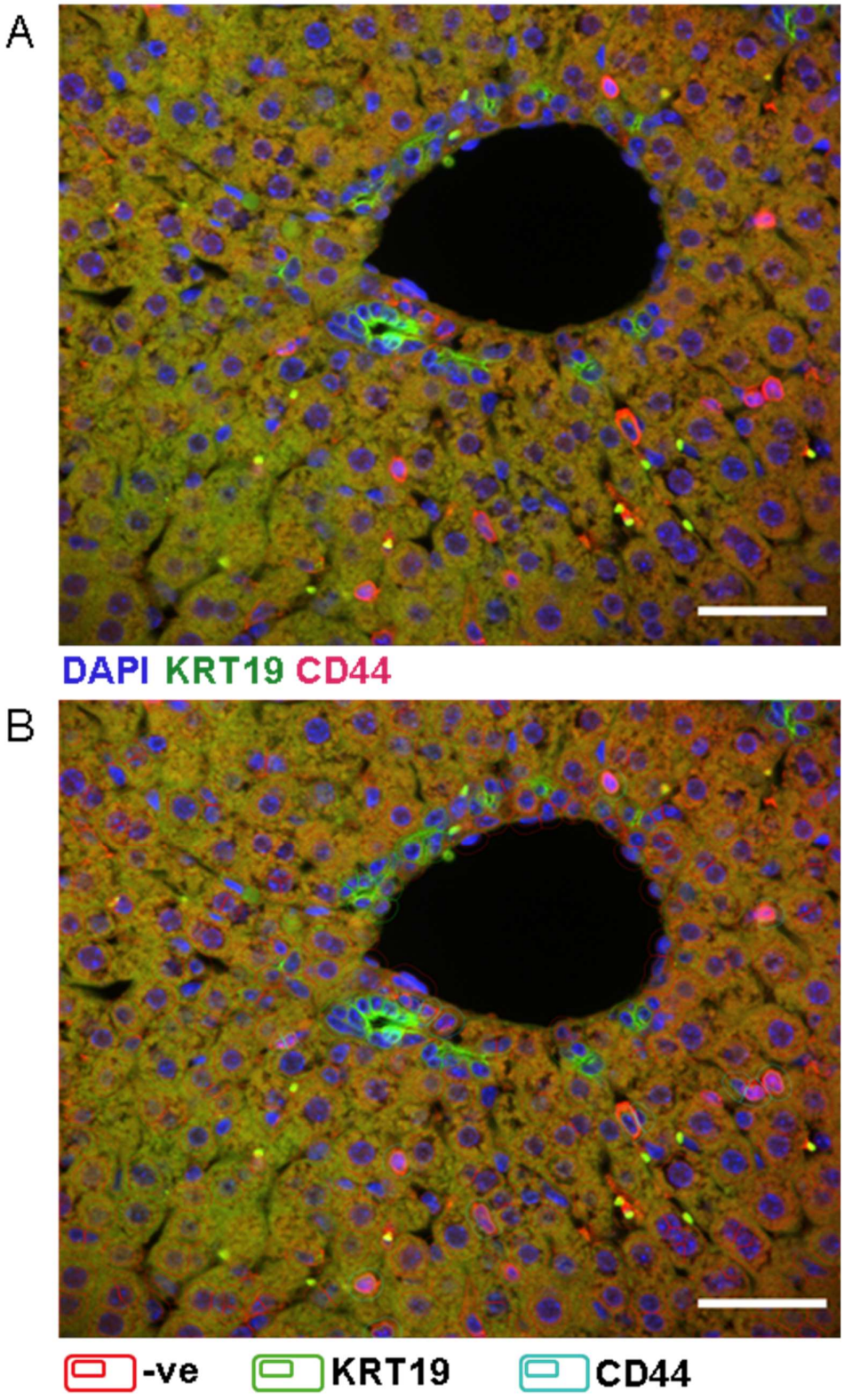

Figure 4.7: Analysis of immunofluorescence images using QuPath. Images at 40x magnification, scale bars represent 50μm.

A: Combined image containing DAPI image in blue, KRT19 in green for identification of BEC, and the stain of interest in this case CD44 in red.

B: Segmentation of image shown in Figure 4.7A. Cells were segmented based on the DAPI signal and subsequently defined as BEC when positive for KRT19. Analysis could then be made of the number of BEC also positive for CD44 and overall numbers of CD44 positive cells.

4.8 Hepatocyte isolation

Hepatocyte isolation procedures were performed under microscopic guidance. Mice were placed under terminal anaesthesia using a combination of ketamine (Pfizer) at a dose of 200mg/kg and Medetomidine (Orion Pharma) at 3mg/kg. The abdominal skin and peritoneum were opened to expose the abdominal contents. The bowels were mobilised to the right exposing the portal vein and IVC. A ligature was placed around the proximal part of the portal vein for control, then the portal vein was cannulated using a 26G cannula (BD, 381212). Via the cannula the liver was washed with Liver perfusion media (LPM) (Gibco, 17701038) at 5mls/minute using a peristaltic pump (Watson-Marlow 120). The IVC was then opened to allow blood to wash through. The chest was subsequently opened, and a ligature was placed around the superior vena cava but not tightened.

Once 20mls of LPM had passed through the vena cava, this was closed using mosquito forceps and an incision was made in the right atrium of the heart to allow blood to exit through this site. When a further 20mls of LPM had washed exited through the heart, Liver digest medium (LDM) (Gibco, 17703034) was introduced at the same rate through the pump. Once the LPM had washed out of the liver the superior vena cava was closed and 35mls of LDM was infused into the now closed system. The liver was then collected and placed in ice cold Williams E media (Gibco, 12551032) with 10% FCS, 1% penicillin/streptomycin.

To extract hepatocytes, livers were gently scraped with a 1ml pipette tip to remove the capsule and release cells. Cells were collected in Williams E media with 10% FCS and passed through a 100µm filter (Fisherbrand, 22363549) to remove any undigested tissue. The filtrate was washed and resuspended in 25mls of Williams E media without FCS. This was added to 25mls 90% percoll (Sigma, P4937) in HBSS (Gibco, 14175095) and spun at 100xg for 10mins with brake and acceleration set to 0. Dead cells and debris collect at the top of the percoll whilst live cells pellet at the bottom. Live cells were collected and washed in PBS before use for downstream applications.

4.9 Biliary Duct isolation

For the isolation of biliary ducts, mice were sacrificed using cervical dislocation. Livers were perfused with PBS via the IVC, then collected and placed in 4°C wash media

(Dulbecco's Modified Eagle's Medium high glucose [Gibco,10569-010] supplemented with 1% fetal calf serum (FCS) (Gibco 10082139) and 1% penicillin/streptomycin (Gibco 15140122)). Livers were minced lightly using scissors. The minced liver was washed in 30mls of wash media then placed in 15mls of wash media with 0.24mg/ml Collagenase (Sigma-Aldrich, C9407) and Dispase II (Life Technologies, 17105-041). After 25 minutes of incubation samples were mixed using a 10 ml pipette at 45minutes the media was replaced with 10 ml of fresh digestion media. Tissue was subsequently incubated for 45 minutes with a further mix at 25minutes. Tissue was washed with wash media at the end of digestion and resuspended in 3 ml of fresh wash media. Under microscopic guidance biliary ducts were selected using a 20 µm pipette and placed in a fresh collection tube.

Figure 4.6C demonstrates microscopic appearance of the ducts following selection with multiple non ductal cells present within the collection media. Once the ducts had been selected, they were washed in wash media and then were passed through a further round of selection under microscopic guidance. Figure 4.6D demonstrates appearances of ducts following the second round of selection with a significant reduction in the non-ductal cells in the media.

4.10 Isolation of the extrahepatic ducts and gallbladder

Extrahepatic ducts and gallbladders were collected at the same time as either duct isolation, or hepatocyte isolation. In all cases the extrahepatic ducts and gallbladder were collected in the wash media (Dulbecco's Modified Eagle's Medium high glucose supplemented with 1% FCS and 1% penicillin/streptomycin), then washed in PBS. Dissection was undertaken under the microscope to remove any excess tissue. The extrahepatic ducts were then cut into smaller pieces in preparation for protein or RNA extraction. Figure 4.6E demonstrates appearances of the extrahepatic ducts following collection with excess periductal tissue. Figure 4.6F demonstrates extrahepatic ducts following the removal of periductal tissues through blunt dissection.

Expression as assessed by qPCR of the hepatocyte marker *Albumin* and the biliary marker *Krt19* in hepatocytes, intrahepatic ducts and extrahepatic ducts are presented in Figures 4.6A and B respectively.

Figure 4.8 Intra and extrahepatic duct isolation

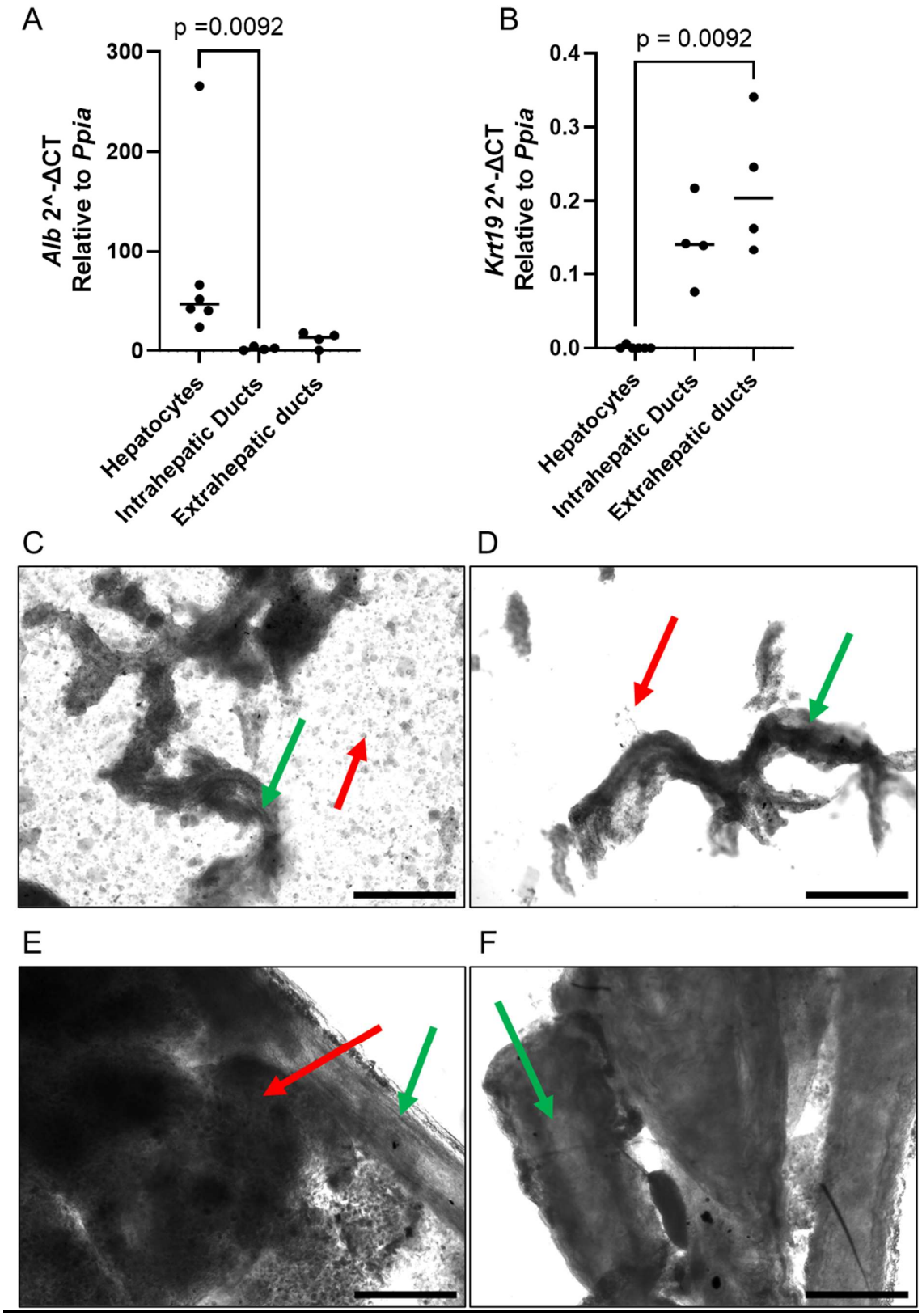

Figure 4.8: Intra and extrahepatic duct isolation

A: Quantitative PCR comparing expression of *Albumin in* liver compartments. Median expression relative to *Ppia* in hepatocytes 46.82, in intrahepatic ducts 2.10, in extrahepatic ducts 13.46. Kruskal Wallis ANOVA p=0.0004, hepatocytes vs intrahepatic ducts p=0.0092 on multiple comparison testing

B: Quantitative PCR comparing expression of *Krt19 in* liver compartments. Median expression relative to *Ppia* in hepatocytes 0.0002, in intrahepatic ducts 0.141, in extrahepatic ducts 0.204. Kruskal Wallis ANOVA p=0.0004, hepatocytes vs extrahepatic ducts p=0.0092 on multiple comparison testing

C: Example image of intrahepatic duct isolation following first round of selection. Red arrow indicates non ductal cells. Green arrow demonstrates a biliary duct.

D: Example image of intrahepatic duct isolation following second round of selection. Red arrow indicates non ductal cells. Green arrow demonstrates a biliary duct.

E: Example image of extrahepatic duct after removing from mouse. Green arrow indicates ductal tissue, red arrow indicates excess periductal tissue.

F: Example image of extrahepatic duct after removing excess tissue.

C-F: 4x magnification, all scale bars represent 500μm

4.11 Biotinylated plasma membrane isolation

This protocol was adapted from the cell surface protein isolation kit (Abcam, ab206998). All reagents were obtained from this kit aside from protease inhibitor cocktail (ThermoFisher, 78429). Hepatocytes were isolated directly from murine livers as described in section 4.5 and washed in ice-cold PBS. N-Hydroxysulfosuccinimide biotin (NHSB) powder was reconstituted in 20 ml of PBS according to instructions. 10 ml of the biotin solution was used per sample, which included all hepatocytes obtained from a single mouse.

Cells were then incubated at 4^{o}C with gentle agitation for 1 hour. Centrifugation was undertaken at 100 x g for 3 minutes at 4^{o}C. The pellet was washed in 5 ml of Tris-buffered saline (TBS), twice. At this point the cells should have NHSB attached to plasma membrane proteins but importantly the cells remain non-lysed, therefore no intracellular proteins react with NHSB.

400-500µl of lysis buffer (included in ab206998 kit) was added to cells, supplemented with protease inhibitor cocktail. Samples were incubated on ice and vortexed every 15 minutes. Centrifugation was performed at 10,000 g for 2 minutes at room temperature, to pellet debris. The supernatant was removed and added to a streptavidin bead solution (included in ab206998 kit) and incubated for 1 hour. At this point the proteins which were bound by NHSB, namely plasma membrane proteins, would become attached to the beads due to the binding of biotin and streptavidin.

Following incubation samples were spun at 800xg for 1 minute. The resulting supernatant contained non bound proteins, and therefore those which were not present in the plasma membrane, was discarded. After washing, the streptavidin beads are then incubated in 0.1M Dithiothreitol (DTT) at room temperature for 10 minutes, which allows elution of the bound proteins. Samples were centrifuged for a further 1 minute at 800xg, the resulting supernatant was collected, containing the plasma membrane protein sample.

4.12 Ultracentrifugation

Gradient ultracentrifugation (adapted from Suski et al, Nature protocols 2014)

The protocol for ultracentrifugation was adapted from Suski and co-workers protocol paper in 2014 [218]. As described in this protocol Starting buffer (SB) was made

containing 225 mM mannitol (Sigma Aldrich, 69-65-8), 75 mM sucrose (Sigma Aldrich, S0389) 30 mM Tris-HCL (Sigma-Aldrich, 1185-53-1). Once cooled to 4^0C, SB was brought to a pH7.4 using 5 mM hydrochloric acid (Fisher, 7647-01-0) and potassium hydroxide capsules (Fisher, 1310-58-3). Isolation buffer 1 (IB1) was produced by adding 0.5% bovine serum albumin (Fisher, 9048-46-8) and ethylene glycol-bis-N,N,N′,N′-tetraacetic acid (EGTA) (Sigma-Aldrich,67-42-5) to a concentration of 0.5 mM, to the SB. On the day of use isolation buffer 1 was supplemented with 1 in 100 protease inhibitor cocktails. Isolation buffer 2 (IB2) was produced by adding protease inhibitors at a concentration of 1:100 to SB. Plasma membrane resuspension buffer (PMRB) consisted of 5 mM Bis-Tris (Sigma-Aldrich, 6976-37-0), 0.2 mM EDTA (Sigma-Aldrich,6381-92-6) to bidistilled water. This solution was adjusted to pH6.0 using either potassium hydroxide or hydrochloric acid.

Following isolation as described in section 4.8 freshly isolated hepatocytes were placed in 200µl of IB1 per million cells and stored overnight at -80°C. On the following day, cells were thawed on ice and went through three pulses of homogenisation at 1500 rpm on a biospecs tissue tearor (Biospecs, 985370). Following this cell were spun at 800 g for 5 minutes at 4°C, the pellet was discarded, and the supernatant was placed in a new tube and spun again at 800xg for 5 minutes. The resulting supernatant was spun at 10,000xg for 10 minutes at 4°C, the pellet contains mitochondrial fractions and was discarded, the supernatant was placed in a new tube and spun again at 10,000xg for 10 minutes at 4°C.

The supernatant was placed in a new Eppendorf and was centrifuged at maximum speed (20,800 g) on the desk top centrifuge for 30mins at 4°C. At this point the supernatant was discarded, and the pellet was resuspended in SB. The sample underwent a second centrifugation at 20,800 g for 30minutes.

The pellet was resuspended in 1.5 ml of PMRB and layered on top of a sucrose gradient. The sucrose gradient was produced by dissolving sucrose in PMRB to 53%, 43% and 38% concentration. 9 ml of 53% sucrose solution were placed in the bottom of a thin-walled polypropylene tube from (Beckman Coulter, 326823), 12 ml 43% were placed on top, followed by 12 ml of 38%. Samples were centrifuged in an optima XPN-80 ultracentrifuge (Beckman Coulter, A95765) using a SW 32Ti swing out rotor (Beckman Coulter, 369650) at 95,000 g for 150 minutes at 4°C. The plasma membrane fraction (PM) was taken from the interface between the 53% and 43% layer. The

plasma membrane associated membrane fraction (PAM) was taken from on top of the 38% layer.

PM and PAM proteins were separately resuspended in SB and centrifuged for 10 minutes at 4000 g to remove any mitochondrial contamination. The supernatant was taken and centrifuged again at 95,000 g for 60 minutes at 4^{o}C. The resultant pellet contained the PM or PAM proteins and was resuspended in starting buffer and stored at -80 ^{o}C.

Ultracentrifugation, (adapted from Lund 2009, Journal of Proteome research 2009)

The second protocol used was described by Lund and colleagues in 2009, using method 2 [219]. Buffers were made in accordance with the description in the paper. A hypotonic buffer was produced with concentration 0.01 M Tris Base (Sigma-Aldrich, 77-86-1), 0.0015 M $MgCl_2$ (Sigma-Aldrich, 7791-18-6) and 0.01 M NaCl (Sigma-Aldrich, 7647-14-5). Lysis buffer was made with the following concentrations of substrates dissolved in bidistilled water; 255 mM sucrose, 20 mM N-2-hydroxyethylpiperazine-N-2-ethane sulfonic acid (HEPES), 1 mM EDTA. Protease inhibitor was added to both buffers before use at 1 in 100 concentrations before use.

Hepatocytes were washed in PBS before adding 1ml of Hypotonic buffer and incubating at room temperature for 5 minutes. Cells were then centrifuged and resuspended in lysis buffer 1ml per 1 million cells. Cells underwent lysis with 50 strokes from the tissue tearor at 1500rpm. Lysates were centrifuged at 20,000 g for 10 minutes to remove large organelles.

The supernatant was centrifuged at 240,000 g for 120 minutes at 4^{0}C (with acceleration set to 9 and deacceleration to 7) on a 70ti fixed angle rotor (Beckman coulter, 337922). The pellet was resuspended in IB2 described in the Suski protocol[218].

4.13 Protein quantification

Protein quantification was performed in a flat bottomed 96 well plate and read using a FLUOstar Omega microplate reader (BMG Labtech). 5 µl of concentrated protein solution was added to 250 µl of Bradford solution (Sigma-Aldrich, B6916) and incubated

for 15 minutes at room temperature. Samples were performed as duplicates. A BSA protein standard was performed with every quantification using Bovine serum albumin (BIO-RAD, 500-0007) at concentrations of 1.5, 1, 0.75, 0.5, 0.25, 0.125, 0.0625 and 0 µg/µl. Absorbance of samples compared with a linear equation calculated from the absorbance of the BSA standard.

4.14 Whole cell protein extraction

Prior to the production of protein cells or tissue were collected and stored at -80^{o}C as described in section 4.2. Up to 1 ml of Radioimmunoprecipitation assay (RIPA) buffer (Thermo-Fisher, 89900) was added to the tissue along with 1x protease inhibitor cock-tail (Thermo-Fisher, 78429). Samples were homogenised at 1500 rpm for 10 strokes for cells or until tissue was no longer visible for tissue samples. Samples were kept on ice between homogenisations. Homogenates were spun at 12,000g for 15 minutes at 4^{o}C, the supernatant containing proteins was stored at -80^{o}C.

Protein extraction for mass spectroscopy samples was performed at the proteomics service by Dr.. D. Kurian and Ms. J. Aguilar at the Roslin institute. For these experiments ducts and hepatocytes were frozen using liquid nitrogen and stored at -80^{0}C.

The following information has been kindly provided by Dr. Kurian's team. *"The samples were homogenised in an extraction buffer (5%SDS in 50mM TEAB pH 8.5) at sample to buffer ratio of 1:10, (w/v) using Precellys homogenizer (5000-2x10) in a beads ceramics vial (Precellys Lysing Kit, Tissue homogenizing CK mix). Following homogenization samples were centrifuged for 10min at 16,000g and supernatant was transferred into a clean protein low binding vial then sonicated for 10 cycles with 30 sec on and 30 sec off per cycle. (Pico Sonicator Diagenode bioruptor). After sonication samples were centrifuged (16,000g for 10min) supernatant was collected and a BCA assay performed."*

4.15 Mass spectroscopy

Mass spectroscopy was carried out in Dr. D. Kurian's laboratory in the Roslin institute, University of Edinburgh. Dr. Kurian's lab have kindly provided the following information *"The proteins samples were reduced with dithiothreitol and alkylated with*

iodoacetamide prior to tryptic digestion on S-TRAP (Protifi, USA) cartridges according to the manufactures protocol. The resulting peptides were cleaned up using C_{18} stagetips. Purified peptides were separated over a 90 minutes gradient on an Aurora-25 cm column (IonOpticks Australia) using a UltiMate RSLCnano LC System (Dionex) coupled to a timsTOF FleX mass spectrometer via a CaptiveSpray ionization source. The gradient was delivered at a flow rate of 200 nL/min and washout was performed at 500 nL/min. The column temperature was set at 50°C. For DDA-PASEF acquisition, the full scans were recorded from 100 to 1700 m/z spanning from 1.45 to 0.65 Vs/cm2 in the mobility (1/K0) dimension. Up to 10 PASEF MS/MS frames were performed on ion-mobility separated precursors, excluding singly charged ions which are fully segregated in the mobility dimension, with a threshold and target intensity of 1750 and 14,500 counts, respectively. Raw mass spectral data was processed using PEAKS Studio X-Pro Software (Bioinformatics LTD). Search was performed against Uniprot Mouse sequence database containing 20,865 entries with MS1 precursor tolerance of 20 ppm and MS2 tolerance of 0.06 Da. Fully tryptic digestion allowing one missed cleavages, fixed modification of cystine [+57.02] and oxidation of methionine and deamination of asparagine and glutamine were also specified for database search. Quantitative LFQ analysis was performed with default parameters and with optional ID transfer enabled".

4.16 Proteomic analysis

Proteomic analysis was performed using free to use R software. The limma package was employed for analysis[220]. Proteins which had not been detected in any of the analysed samples were excluded. Samples were normalised using the quantile technique, log to base 2 transformation was performed. For each analysis a weighted model was created which accounted for paired samples within the model. Figures were created using the ggplot package. The Benjamini-Hochberg method was used to account for multiple comparisons.

4.17 Western blot

Protein samples were combined with lithium dodecyl sulphate (LDS) (Thermo Fisher, NP0007) and heated to 70^{O}C for 10 minutes for denaturation. Samples were loaded into wells of either a 10 or 15 well 4-12% bis- tris gel (Invitrogen, NP0322). The

gel was placed in a running chamber with 500 ml of 3-N-morpholinopropanesulfonic acid **(**MOPS) running buffer (Thermo Fisher, NP0001) with 500µl of antioxidant (Thermo Fisher, NP0005). A combination of 3µl Magic Marker (Thermo Fisher, LC5602).5µl of Novex Sharp (Thermo Fisher, LC5800) were used as a protein standard. The gel was run for 1 hour at 200V, or until the band of protein reached the bottom of the gel. Transfer was carried out at 350 mA for 1 hour, with the cassette submerged in ice. Blocking was performed in 5% bovine serum albumin (BSA) for 1 hour at room temperature. Primary antibody incubation was performed overnight in 4^{o}C, using SCTR at 1:1000 concentration (Biouss, 0089R). After washing with 5 ml TBST 3 times for 10minutes each, the secondary antibody was applied diluted in 5% BSA for 1 hour at room temperature. A further three washes were undertaken using TBST. Following this Blots were developed using ECL substrate (Thermo Fisher, 32106).

4.18 RNA production

To produce RNA from tissue including intra and extrahepatic ducts, samples were placed in 800 µl of cold Qiazol (Qiagen, 79306) and homogenised using a biospecs tissue tearor (cat no. 985370), until no pieces were visible. 200 µl of chloroform and a further 200 µl of Qiazol were added. Samples were then incubated at room temperature for 3 minutes. 12,000 g centrifugation for 15 minutes at 4^{o}C was performed to separate RNA from proteins and cellular debris. The resulting superior most phase was removed and mixed in a 1:1 ratio with 70% ethanol.

To produce RNA from cultured cells, cells were first washed with PBS, then 350µl of cold RLT (Qiagen, 79216) was added. Lysate was collected and 350µl of 70%ethanol was added.

The Qiagen RNeasy mini kit (Qiagen, 74004) was used for isolation of RNA from both cell and tissue samples according to the instruction in the kit. Nanodrop spectrophotometer was used to establish concentrations (Thermo-Fisher).

4.19 Quantitative PCR

cDNA was produced using the Quantitect kit (Qiagen, 205311). Real time-qPCR was performed on a LightCycler 480 II (Roche). cDNA was diluted 1 in 8 in sterile RNAse

and DNAse free water (Invitrogen, 10977-015). Sybr green (Applied Biosystems, 4385616) was used as a fluorescent dye.

All primers were purchased from Qiagen and have been detailed in Table 4.5. All samples were run in triplicates. If any of the three values was greater than 1 CT value from the other two replicates, it was removed from subsequent analysis. Samples were run with peptidylprolyl isomerase A (*Ppia)* and Glyceraldehyde 3-phosphate dehydrogenase (*Gapdh)* as housekeeper genes, the housekeeper with the lowest intrasample variation was used. This meant in tissue samples *Ppia* was used as the internal control, for murine HPC samples *Gapdh*. Data was presented as either 2^-ΔCT, or 2^-ΔΔCT in presence of a control group.

Table 4.5 List of primers used.

Primer	Manufacturer	Catalogue number
Alb	Qiagen	QT00115570
Casp3	Qiagen	QT00260169
Casp8	Qiagen	QT00171437
Ccl2	Qiagen	QT00167832
Cdkn1α	Qiagen	QT00137053
Cxcl1	Qiagen	QT00115647
Cxcl2	Qiagen	QT00113253
Gapdh	Qiagen	QT01658692
Emr-1 (F4/80)	Qiagen	QT00099617
IL1-β	Qiagen	QT01048355
Krt19	Qiagen	QT00156667
Ppia	Qiagen	QT00247709
Sctr	Qiagen	QT01066646
Trp53	Qiagen	QT00101906

4.20 *Krt19Cre^{ER}Mdm2 $^{fl/fl}$ Rag2$^{-/-}$ Il2rg$^{-/-}$* model

Krt19Cre^{ER}Mdm2 $^{fl/fl}$ Rag2$^{-/-}$ Il2rg$^{-/-}$-mice were used to induced BEC-specific senescence. This mouse model was originally produced by Dr. John Hallett [124]. This line was bred on a background of C57B6/J and produced from crossing *Rag2$^{-/-}$IL2rg$^{-/-}$* and *Krt19^{CreER}MDM2$^{fl/fl}$* mice. In the *Krt19^{CreER}MDM2$^{fl/fl}$* model an oestrogen receptor is bound to a Cre transgene and then inserted into the *Krt19* gene locus which is expressed in all BEC. On administration of the selective oestrogen receptor modulator tamoxifen, Cre-recombinase production occurs in all *Krt19* expressing cells, including BEC. In this mouse the *Mdm2* gene is flanked by two loxP sequences and, upon

inbduction, is cleaved due to the action of Cre recombinase. *Mdm2* is a key negative regulator of *p53*, therefore *p53* accumulates in BEC upon induction[75]. *p53* induces the production of *p21*, which in turn leads to an irreversible cell cycle arrest and cellular senescence.

Rag2 is an essential gene in lymphocyte maturity, therefore knockout compromises adaptive immunity[221]. *IL2rg* deletion leads to deficient NK cell function and reduction in the production of several cytokines The combination of *Rag2* and *IL2rg* knockout leads to a significant immunocompromised response (lacking B, T and NK cells) and makes this model permissible to xenograft [222].

Genotyping: Mouse genotyping was carried out for Cre recombinase and *Mdm2* flox through PCR analysis (Transnetyx, Tennessee, USA) from ear notch samples.

Induction of the model: Tamoxifen (Sigma-Aldrich, T5648) was dissolved in sunflower oil (Sigma-Aldrich, S5007) to a concentration of 20mg/ml. This solution was kept at -20^{o}C until the day of use and was resuspended using a combination of sonication and heating. Mice were given three doses of tamoxifen on alternate days (Mondays, Wednesdays, and Fridays) at 180mg/kg via oral gavage. Mice were weighed daily during the experimental period and doses were calculated based on same day weights. Control mice were given 200 µl of sunflower oil only (Figure 4.1a).

24 hours following the final dose of tamoxifen, 0.1% DDC diet was commenced (Special Diets Services, 824943). Mice were removed from experiments if their weight fell by more than 20% for at least 48hours or if they displayed signs of suffering beyond a moderate level, as per recommendation of University of Edinburgh veterinary services.

Mice were culled using a combination of two Schedule 1 techniques, in accordance with UK Home office guidance. Blood was collected via the IVC. The liver was perfused with 10mls of PBS via the IVC, the portal vein was then opened to allow transhepatic flow.

4.21 CCl_4 model

Paraffin blocks of liver tissue from mice who had received 12 weeks of CCl_4 diet were kindly given by Dr. P. Starkey-Lewis. As described in section 1.5 the CCl_4 model leads to mixed intrahepatic and biliary injury and has been used as a model of NAFLD[223].

4.22 MCD model

Paraffin blocks of liver tissue from mice who had received 15 days of (Methionine and choline deficient) MCD diet with or without senescence induced in hepatocytes using an AAV8 virus were kindly given by Dr. N. Aleksieva. MCD diet is known to induce fat accumulation in the hepatocytes[224]. When combined with induction of AAV8.TBG.p21 adenovirus, senescence is induced in hepatocytes leading to increased fibrosis and ductular reaction (unpublished data, Dr. N. Aleksieva).

4,23 The ischaemia reperfusion injury (IRI) model

Ischaemia reperfusion has been used to model the process of liver transplantation [225, 226]. For this study Dr. S. Ferreira-Gonazalez performed the surgeries assisted by the present PhD candidate. Prior to surgery mice were dosed with 0.1 mg/kg Buprenorphine. Lacrilube (Allergan) was applied to the eyes to prevent drying. Mice were anaesthetised using isofluorine at 3%**,** subsequently reduced to 1.5% once adequate anaesthetic depth had been achieved. Under sterile conditions, a midline laparotomy was performed. The liver was mobilised inferiorly with gentle pressure on the chest. A clamp was applied to the vascular pedicle supplying the median and left lateral lobes of liver (Figure 4.7B), the affected lobes are seen to turn pale at this point indicating ischaemia. The clamp remained in place for 30 minutes and was subsequently released to allow reperfusion to occur. 500 µl of sterile PBS was given into the peritoneum. Repair of the midline incision was performed using vicryl 6.0 suture for the abdominal muscle and adam skin clips for the skin.

In cases of IRI followed by intrasplenic injection in the same procedure, injection was performed immediately following release of the clamp. The viscera were returned to the abdomen, the spleen was mobilised into the midline. Injection was performed using a 30G needle. Surgicel (Ethicon 1903GB) and pressure were used for haemostasis. After achieving haemostasis the spleen was returned to the left flank and closure performed as described above.

Ischaemia reperfusion was combined with the *Krt19Cre^{ER}Mdm2 $^{fl/fl}$ Rag2$^{-/-}$ Il2rg$^{-/-}$* model. Mice were given three doses of tamoxifen at 180 mg/kg or oil as previously

described. Following this induction, a further dose was given on day 24, 7 days prior to surgery to maintain a senescent response (Figure 4.2A). On day 31 ischaemia reperfusion was performed. Mice were culled 2 days after surgery.

Senescence in the biliary ducts was demonstratable on immunofluorescence as shown in Figure 4.7C which compares the number of BEC positive for p21 in mice who underwent IRI who did and did not receive tamoxifen induction. Representative images are presented in Figure 4.7D.

Figure 4.9 The *Krt19CreERMDM2fox/flox RAG2-/- Il2RG-/-* IRI model.

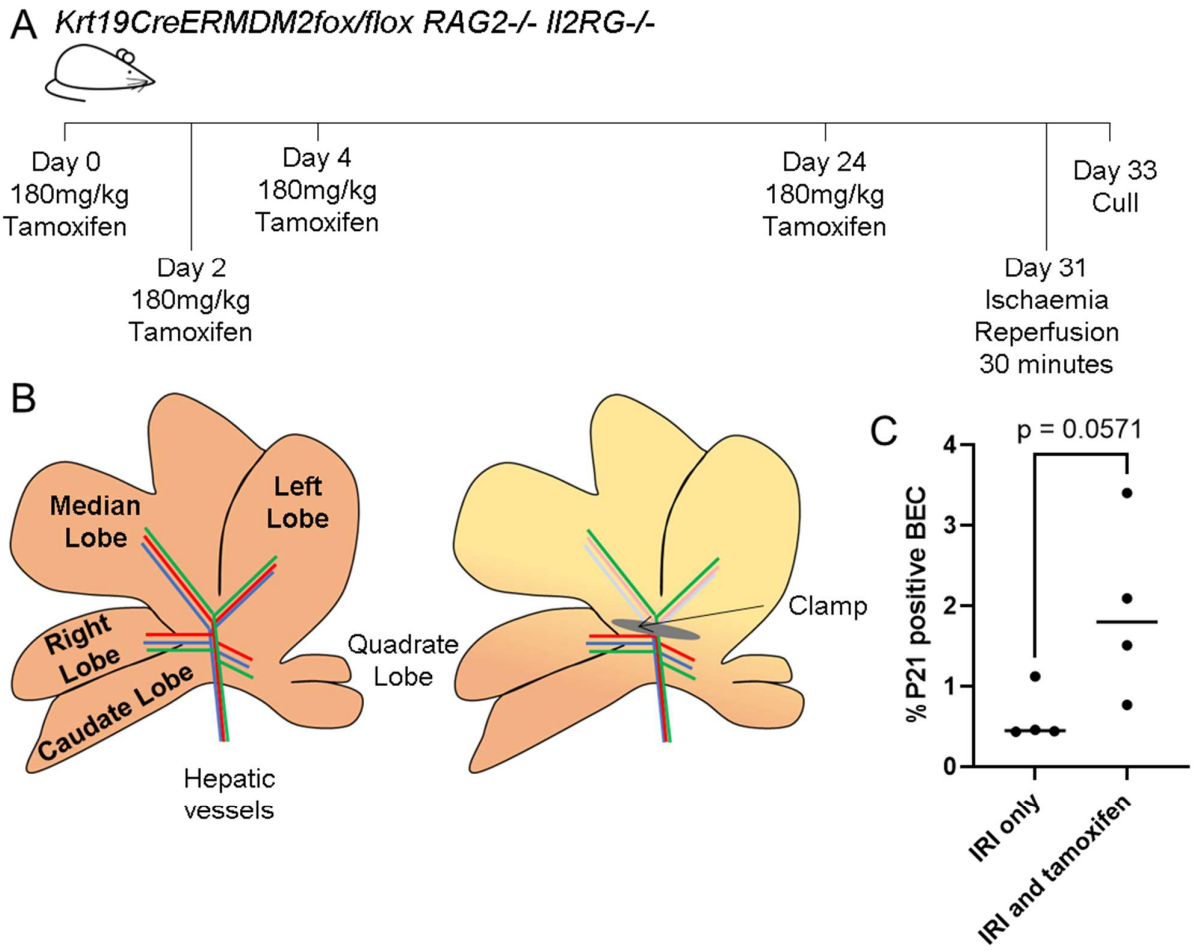

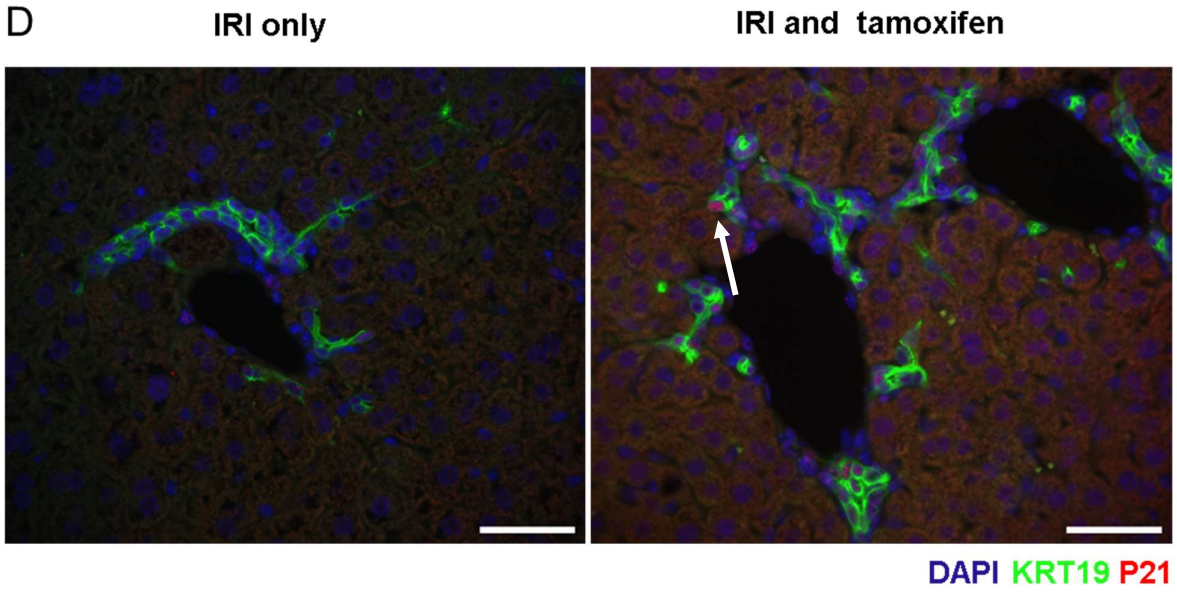

Figure 4.9: The *Krt19CreERMDM2fox/flox RAG2-/- Il2RG-/-* IRI model.

A: Schematic for the model.

B: Schematic demonstrating the surgical procedure.

C: Quantification of P21 expression in BEC as defined by KR19 expression. Mean percentage P21 positive BEC in mice that received only IRI 0.453%, in mice that received IRI and tamoxifen 1.802%. Mann Whitney test p=0.0571.

D: Example images of P21 expression in BEC. Images taken at 40x magnification; scale bars represent 50μm. White arrow indicates a P21 positive BEC.

4.24 Transplant procedures

For transplantation experiments, anaesthesia was induced using 3-4% inhaled isoflurane, and maintained between 1 and 2% during the surgery. The site of surgery was cleaned using an alcohol-based sterilisation fluid. Lacrilube was applied to the eyes to prevent them drying during the surgery. Either bupenephorine 0.1 mg/kg or carprofen 20 mg/kg was administered to mice prior to surgery. At the end of the procedure mice were given 500μl of subcutaneous saline for hydration and were recovered in a warmed cage.

Intrasplenic injections were performed by opening the skin and muscular layer in the left flank. The spleen was mobilised and externalised before cells were injected into the lower pole via a 30G needle. Surgicel (Ethicon 1903GB) and pressure were used for haemostasis. The spleen was then returned to the abdomen and the muscle and skin were closed in two layers using vicryl 6.0 suture for the abdominal muscle and adam skin clips for the skin.

Portal vein injections were performed using microscopic guidance via a midline incision. The bowel was externalised and kept within a dampened swab. The portal vein was visualised and cannulated with a 26G cannula. Cells were injected through this route, after 15 minutes the liver was washed through with PBS. Portal vein injections have only been performed under terminal anaesthetic in this thesis.

4.25 Cell culture murine samples

Cell culture was performed under sterile conditions within a laminar flow cabinet. Instruments and culture apparatus were cleaned with 70% ethanol prior to use.

Human and murine HPC had previously been isolated. Murine HPC were produced by Dr. Wei-Yu Lu and human cells by Dr Sofia Ferreira-Gonzalez, Dr John Hallett and Ms Janet T Man, and kept as a biobank in liquid nitrogen. Murine HPC were isolated as described in Lu et al Nature cell biology 2015[150]. Human HPC isolation has been described by Hallett and Ferreira-Gonzalez in 2022[124]. Briefly, livers were digested as specified in the respective studies to produce a non-parenchymal cell population. This population underwent fluorescence activated cell sorting (FACs), to exclude CD45, CD31 and Ter119 positive cells then to select cells expressing EpCAM, CD24 and CD133. Isolated HPC were cultured as specified in the proceeding paragraphs according to species.

For storage, HPC had been suspended in cell banker (Amsbio 11892),and cooled gradually to -80°C using a Mr Frosty Freezing container (Nalgene C1562). Once cooled, HPC were transferred to liquid nitrogen for storage.

Murine HPC were cultured on flat bottom cell culture plates with either 12 or 24 wells (Corning, #3526). Prior to plating wells were coated in 1 mg/ml rat tail collagen (Sigma-Aldrick, C3867) and incubated for at least one hour. Cells were grown in media consisting of William's E media, 10% FCS and 1% penicillin/streptomycin along with additional factors as described by Lu in 2015 [150]. Passaging was performed by washing cells in sterile PBS then incubating with Accutase solution (Sigma-Aldrich, A6964) for 7 minutes at 37^0C. Cells were washed in media and centrifuged at 200 g for 7 minutes, resuspended in media and plated. Cells were passaged routinely following one week of culturing, media was changed once in the intervening time.

Peroxide (Sigma-Aldrich, 31642) or etoposide (Stratech, A1971) were added to a concentration of 1 mM and 1 µM respectively and added to cells on day 6 and day 7 of culture respectively, with the intention of inducing senescence and apoptosis. Etoposide was stored at a concentration of 20 µm in DMSO.

5 µl of sterile PBS or Dimethyl-sulphoxide (VWR chemicals, 23500.260) were added to wells to act as controls for peroxide and etoposide respectively.

In preparation for flow cytometry or cell transplantation, cells were lifted for passage and subsequently filtered using a 100 µm filter for transplants and 40 µm for flow cytometry or FACs.

4.26 Cell culture human organoids.

Human HPC were grown in 20µl Matrigel (Corning 356234) spheroids on suspension culture plates (Greiner Bio-one, 665 102). The media for expansion of these cells was Advanced Dulbecco's Modified Eagle Medium (Adv. DMEM) (Gibco, 12634-010) supplemented with 1% penicillin/streptomycin, 1% Glutamate, with further factors as described by Hallett and Ferreira-Gonzalez [124]. Cells were passaged on a weekly basis, with a single change of media in the intervening time.

In preparation for transplantation, flow cytometry, or FACs, HPC were moved into suspension. Briefly, media was removed, and wells were washed twice with cold PE (PBS supplemented with 0.5mM EDTA (Sigma-Aldrich, E7889)) without disrupting the Matrigel domes. Dispase (Stemcell, 07913) was diluted to a working concentration of 1 U/ml. 2 ml of the working concentration were added per well of a 12 well plate. Following 30 minutes incubation at 37^0C, cells were disrupted using a 1ml pipette, then incubated for a further 30 minutes. 4 ml of cold PE were added per well and the solution was centrifuged at 400 g for 5 minutes. 2 ml per well of 7x TryplE was added to the pellet and incubated at 37^0C for 10 minutes. Cells were washed in DMEM and filtered through a 40 µm filter for FACs or flow cytometry and a 100 µm filter for transplants.

4.27 Virus production

Stable competent *Escherichia Coli* (E. coli) (New England Biolabs C304H) was used for initial growth of plasmids. 20ng of plasmid were added to the E.coli and incubated on ice for 30 minutes. The E. coli was subsequently placed at 42^0C for 30 seconds. The bacteria were then diluted in 250µl of Luria Broth base (Centre for regenerative medicine, University of Edinburgh) and spread across an agarose plate (Centre for regenerative medicine, University of Edinburgh) with 1:1000 ampicillin (Sigma-Aldrich A9518). After 72 hours incubation at 37^0C colonies of bacteria were selected and placed in 500ml of fresh Luria Broth base for 24 hours.

The bacterial media was then collected, and plasmids were extracted using the DNA plasmid Maxi prep (Qiagen, 12163).

The base for GFP virus was the pLenti *Gfp* which uses a CMV promotor (Addgene, 658-5). The red fluorescent protein (RFP) virus was a similar construct containing dsred2 (Addgene, 109377)

The *Cxcr2* and Atypical chemokine receptor 2 (*Ackr2)* lentivirus was produced Dr. Pamela Brown at the MRC centre for Reproductive health, University of Edinburgh. In both cases the gene constructs were placed between the cytomegalovirus (CMV) promotor and the *Gfp* constructs. A P2A sequence was placed between the *Ackr2* or *Cxcr2* and the *Gfp* constructs. Human variant NM_001168298 was used for the *Cxcr2* construct (Origene, RC229936). Human *Ackr2* gene construct was provided kindly by the laboratory of Professor G. Graham of The University of Glasgow.

Figure 4.10 *Cxcr2 Gfp* plasmid construct

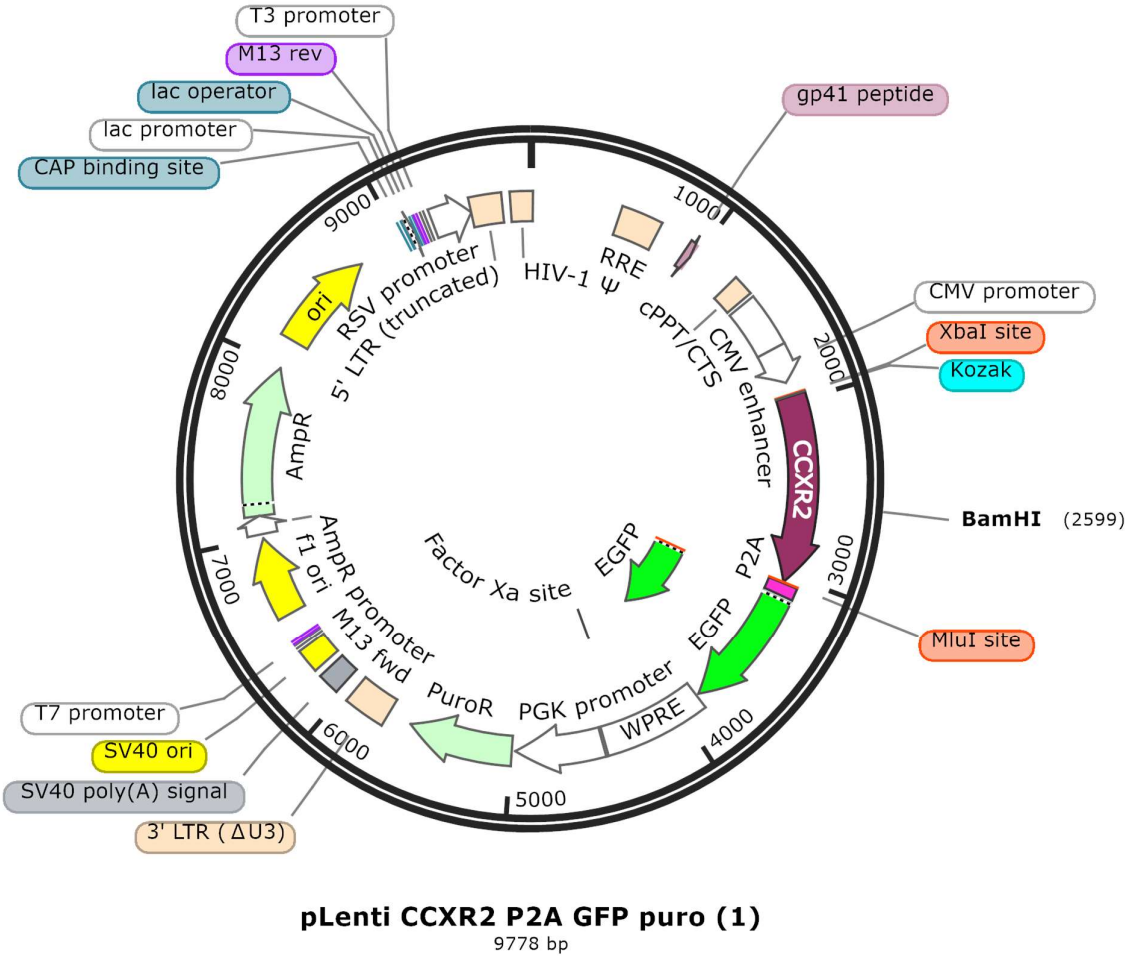

Figure 4.10 *Cxcr2 Gfp* plasmid construct

Plasmid map provided by Dr. Pamela Brown produced on snapgene software, detailing the *Cxcr2 Gfp* construct.

4.28 Virus isolation

For production of virus 4.5 x 10^6 Human embryonic kidney 293T (HEK 293T) cells were plated in T75 flasks (Corning, 431464) in Glasgow Modified Eagle Medium (GMEM) culture media (Gibco, 11710-035) supplemented with 10% FCS, 1% penicillin/streptomycin and 1% glutamate. 24 hours later 11.25ug of the base plasmid (GFP or RFP as described above), 8.4315ug of pD8.91 plasmid (Kind gift from the laboratory of Dr. Gilbert Fruhworth, King's College London) and 2.8125 ug of pVSV-G plasmid (Kind gift from the laboratory of Dr. Gilbert Fruhworth, King's College London) were diluted in 1.5mls GMEM. Finally, 67.5µl of polyethylenimine (PEI) (Fisher scientific, 11460630) of concentration 1 µg/ µl was added to the plasmid mixture, then incubated at room temperature for 15 minutes. The mixture of PEI and viral plasmids were then diluted to make 6mls, replacing the media previously in the T75. 48 hours later the media was collected and passed through a 0.45 µm filter (Fisherbrand, 15216869).

To concentrate the virus Speedy Lentivirus purification solution was used (ABM, LV999). The media containing virus following filtration was added to the purification solution in a ratio of 9:1. The solution was mixed and centrifuged at 5000 g for 10 minutes at 4^0C. The pellet was then resuspended to the desired concentration and stored in Adv DMEM media at -80^0C.

The CXCR2 and ACKR2 viruses were produced by Dr. Pamela Brown at the MRC centre for Reproductive health, University of Edinburgh. pSPAX2 (Addgene,12260) was used as a packaging vector and pLP/VSVg (Originally obtained from Invitrogen, long standing within Dr. Brown's lab) as an envelope vector.

4.29 Transduction

Murine HPC transduction was performed by adding concentrated virus supernatant to cells following passage.

Human HPC were transduced in the following manner: media was removed from the culture well, then 1 ml of TryplE 1x for each well of a 12 well plate was added directly on to the Matrigel spheres[227]. The spheres were disrupted with a pipette and the solution was collected. The wells were then washed with 1 ml TryplE 1x, this wash

was also collected. The solution was incubated in a water bath for 10 minutes at 37^0C, then disrupted further with a 1ml pipette. Cells were washed in Adv DMEM media, then resuspended in the appropriate volume of Matrigel (53.3 µl per intended well in a 12 well plate) in addition to half that volume of virus along with polybrene to a concentration of 8 µg/ml (Sigma-Aldrich, TR-1003-G). The solution was incubated at 37^0C for 30 minutes, before being plated as previously described.

4.30 Flow cytometry

CXCR2 selection was performed by incubating cells with PerCP CXCR2 antibody (BioLegend, 320718) at a concentration of 5 µl per 1 million cells, for 30 minutes on ice. For selection of ACKR2, cells were incubated with CCL22 ligand associated with Alexa Fluorophore 647 (Almac, CAF-04), kindly gifted by Professor Gerard Graham, The University of Glasgow. CCL22 is a ligand for ACKR2, therefore expression of AF647 by cells exposed to CCL22 demonstrates both presence and function of ACKR2 [228]. CCL22 ligand was made up in the appropriate media according to the cell type and added at 100 µl of 25 nM solution per 250,000 cells. Incubation was performed for 30minutes at 37^OC. After incubation cells were washed in media.

Negative and single stain controls were used for each experiment. FACs was performed by Dr. F. Rossi and the flow cytometry team at the Centre of Regenerative medicine, University of Edinburgh. FACS Aria III Fusion (BD biosciences) and FACS Aria II Fusion (BD biosciences) were used for FACS. Flow cytometry was performed on a Fortessa Flow cytometer (BD biosciences), with either 4 or 5 lasers.

4.31 Blood biochemistry

Following collection blood was incubated overnight at 4^0C, to allow coagulation. Centrifugation at 1500 g was performed for 5 minutes at 4^0C, the supernatant was then centrifuged a further time at 14000 g for 5 minutes at 4^0C. The resulting supernatant represented blood serum and was stored at -20^0C. Serum biochemistry analysis was performed by Dr. Forbes Howie and Ms. Kirsten Wilson at the Queen's medical research institute at the University of Edinburgh. Alanine aminotransferase (ALT), Aspartate Aminotransferase (AST), total bilirubin, Glutamate dehydrogenase (GLDH),

Alkaline phosphatase (ALP) and albumin were analysed using kits from Alpha laboratories.

4.32 Statistical analysis

Genomic and proteomic bulk analyses were performed using R. Further details are provided in section 4.16. All other statistical tests were performed using GraphPad software. n represents the number of biological replicates unless explicitly stated. Data with n number less than 5 nonparametric testing was performed and median was presented in associated graphs[229]. In groups of larger than 5 the D'Agostino test of normality was performed, based on the outcome either parametric or non-parametric testing. When parametric tests were used data was presented as means +/- standard deviation. Genomic and proteomic studies used parametric testing.

Two-tailed unpaired Student's t-test in for two groups and one way ANOVA were used in groups of greater than two, when using parametric testing. Multiple comparison testing was performed using Tukey's test.

Mann-Whitney testing for two groups and Kruskal Wallace in groups of greater than two, was used for non-parametric testing. Multiple comparison testing was performed using Dunn's multiple comparisons. n refers to biological replicates unless specified otherwise. The number of technical replicates is defined in figure legends.

Multiple comparisons were performed comparing all conditions to all other conditions except when there was a clear control group. Specific details are found in the figure legends.

R^2 were calculated using simple linear regression. Strong associations were defined as $R^2>0.8$ or <-0.8 for the purposes of this thesis.

Appendix 4.1: Example immunohistochemistry macro from Fiji

```
1
2
3  setBatchMode(false);
4  inDir=getDirectory("getdir");
5  myList=getFileList(inDir);
6
7  for (j = 0 ; j < myList.length ; j++ ){
8      path=inDir+myList[j];   //path to each file
9      open(path);
10     FileName=File.nameWithoutExtension;
11     ImageID=File.name;
12     print("Processing "+ImageID);
13 run("RGB Color");
14 selectWindow(ImageID);
15 close();
16 selectWindow(ImageID +" (RGB)");
17 run("Colour Deconvolution", "vectors=[H DAB]");
18 selectWindow(ImageID +" (RGB)-(Colour_1)");
19 close();
20 selectWindow(ImageID +" (RGB)-(Colour_3)");
21 close();
22 selectWindow(ImageID +" (RGB)");
23 close();
24 selectWindow(ImageID +" (RGB)-(Colour_2)");
25 run("Set Scale...","distance=4.407 known=1 pixel=1 unit=um");
26 setAutoThreshold();
27 getThreshold(min,max);
28 setThreshold(min,50);
29 run("Measure");
30 selectWindow("Colour Deconvolution");
31 close();
32 selectWindow(ImageID +" (RGB)-(Colour_2)");
33 close();}
34
35
```

Appendix 4.2: Example immunofluoresence macro from Fiji part A

```
setBatchMode(true);
Dir1=getDirectory("Choose from directory");
dir2=getDirectory("directory");
Dir3=getDirectory("Choose from directory");
myList=getFileList(Dir1);
myList2=getFileList(dir2);
myList3=getFileList(Dir3);

for (j = 0 ; j < myList.length ; j++ ){
    path=Dir1+myList[j];
    path2=dir2+myList2[j];
    path3=Dir3+myList3[j];
    open(path);
    FileName=File.nameWithoutExtension;
    ImageID=File.name;
    print("Processing "+ImageID);
    run("Set Scale...","distance=8.8286 known=1 unit=um global");
open(path2);
FileName=File.nameWithoutExtension;
ImageID2=File.name;
open(path3);
run("Set Scale...","distance=8.8286 known=1 unit=um global");
FileName=File.nameWithoutExtension;
ImageID3=File.name;
run("Set Scale...","distance=8.8286 known=1 unit=um global");
selectWindow(ImageID);
run("Duplicate...", " ");
rename("Mask" + ImageID);
run("Set Scale...","distance=8.8286 known=1 unit=um");
run("Subtract Background...", "rolling=20 sliding");
run("Gaussian Blur...", "sigma=40");
setAutoThreshold();
getThreshold(min,max);
getStatistics(area, mean, min, max, std, histogram);
meanID=mean;
stdID=std;
setThreshold(meanID + stdID*2,max);
run("Convert to Mask");
run("Analyze Particles...", "size=160-Infinity display include summarize add in_situ");
ROIS=(roiManager("count"));

if (roiManager("count")>0) ;{
                for (i=0; i<ROIS;i++){
                 selectWindow(ImageID3);
                 run("Duplicate...",ImageID3);
                 rename("DAPI" + ImageID3);
                 selectWindow(ImageID2);
                 run("Duplicate...",ImageID2);
                 rename("Interest" + ImageID2);
                 imageCalculator("Subtract...","DAPI" + ImageID3,"Interest" + ImageID2);
                 selectWindow("DAPI" + ImageID3);
                 run("Subtract Background...", "rolling=20 sliding");
                 run("Set Scale...","distance=8.8286 known=1 unit=um global");
```

Appendix 4.2: Example immunofluoresence macro from Fiji part B

```
                roiManager("select", i);
                run("Clear Outside");
                setAutoThreshold();
                getThreshold(min,max);
                setThreshold(2000,max);
                run("Measure");
                close("DAPI" + ImageID3);
                close("Interest" + ImageID2);
                DAPIA=getResult("%Area",nResults-1);
                if(DAPIA>20){;
                selectWindow(ImageID2);
                run("Duplicate...",ImageID2);
                rename("PeriDuct" + ImageID2);
                selectWindow(ImageID2);
                run("Duplicate...",ImageID2);
                rename("Duct" + ImageID2);
                selectWindow("Duct" + ImageID2);
                run("Subtract Background...", "rolling=20 sliding");
                run("Set Scale...","distance=8.8286 known=1 unit=um global");
                getStatistics(area, mean, min, max, std, histogram);
                meanID2=mean;
                stdID2=std;
                roiManager("select", i);
                run("Clear Outside");
                setAutoThreshold();
                getThreshold(min,max);
                setThreshold(meanID2 + stdID2*3,max);
                run("Measure");
                selectWindow("PeriDuct" + ImageID2);
                run("Subtract Background...", "rolling=20 sliding");
                run("Set Scale...","distance=8.8286 known=1 unit=um global");
                roiManager("select", i);
                run("Enlarge...", "enlarge=10");
                run("Clear Outside");
                run("Measure");
                selectWindow("PeriDuct" + ImageID2);
                rename("PeriDuctB" + ImageID2);
                setAutoThreshold();
                getThreshold(min,max);
                setThreshold(meanID2 + stdID2*3,max);
                run("Measure");
                close("Duct" + ImageID2);
                close("PeriDuctB" + ImageID2);}
                else{;
                                }
                                }
}
    selectWindow(ImageID2);
    run("Subtract Background...", "rolling=20 sliding");
    run("Set Scale...","distance=8.8286 known=1 unit=um global");
    getStatistics(area, mean, min, max, std, histogram);
    meanID2=mean;
```

Appendix 4.2: Example immunofluoresence macro from Fiji part C

```
105     getStatistics(area, mean, min, max, std, histogram);
106     meanID2=mean;
107     stdID2=std;
108     imageCalculator("Subtract create",ImageID2,ImageID);
109     run("Subtract Background...", "rolling=20 sliding");
110     rename("NonDuct" + ImageID2);
111     run("Set Scale...","distance=8.8286 known=1 unit=um global");
112     setAutoThreshold();
113     setThreshold(meanID2 + stdID2*3,max);
114     run("Measure");
115 
116 close(ImageID);
117 close(ImageID2);
118 close("NonDuct" + ImageID2);
119 roiManager("Deselect");
120 roiManager("reset");}
```

Chapter 5: Identifying specific plasma membrane proteins for cholangiopathy

5.1 Introduction

Central to the development of a mechanism for cell homing is the need to identify an axis involving a ligand and a receptor. The ligand should be expressed specifically at the target homing site, for the purposes of this study, biliary ducts. Additionally, the ligand should have higher expression at the sites of injury. The ideal ligand would be specific. It is also essential that the ligand is accessible for interacting with the receptor and therefore transplanted cells. The ligand therefore could be an excreted protein or one that is externally [199, 230] presented on the plasma membrane of cells at the target site [169, 170, 231].

The overall aim of this study is to improve HPC engraftment in the *Krt19Cre^{ER}Mdm2$^{fl/fl}$ Rag2$^{-/-}$ Il2rg$^{-/-}$* mice, therefore in this chapter the presence of a ligand expressed specifically in the ducts in this model will be pursued.

From the literature six proteins were identified which were either plasma membrane proteins, SCTR and CD44, or excreted by the cell, TFF2, CCL2, CXCL1, and CXCL2, the rationale behind these selections has been described in detail in the introduction, sections 1.9, 1.10 and 1.11. Broadly, in this thesis, the plasma membrane proteins have been assessed by immunofluorescence and excreted proteins by gene expression. The selection of these techniques was based on the following logic. Excreted proteins will be present not only in the cell of origin but also in the extracellular matrix and beyond [232]. Immunofluorescence in the context of excreted proteins may demonstrate staining in sites other than the source cell, and therefore could mask the specific production of a ligand. qPCR reports on the level of mRNA expression at a particular timepoint. As mRNA expression is the step prior to protein translation this was therefore considered the optimal alternative to immunofluorescence as it precedes any potential extracellular protein secretion.

The primary and foremost aim of this chapter is to identify a duct specific and injury upregulated protein, however there are some additional accompanying considerations. Whilst the core of this thesis works with a murine model of cholangiopathy, the overarching intention is to make HPC cell therapy more viable as a clinical therapy. Therefore, it was also beneficial to assess the expression of the potential ligands in human samples where possible, to understand the translational potential of any findings in the murine model.

Candidate ligands would preferentially be present in damaged ducts, where relevant and possible these were also assessed in other murine disease models, donated by current and former members of the Forbes laboratory. This has been further detailed in the methods section, sections 4.20 and 4.21.

To further assess these ligands an *in vitro* model of cholangiopathy was developed, injuring a murine line of BEC with either peroxide [233] or etoposide[234, 235]. These agents induce senescence and cellular injury, replicating the *Krt19Cre^{ER}Mdm2$^{fl/fl}$ Rag2$^{-/-}$ Il2rg$^{-/-}$* model.

5.2 SCTR is specific to the bile ducts within the liver.

SCTR is thought to be exclusively expressed in BEC within the liver, however it was necessary to confirm this in the *Krt19Cre^{ER}Mdm2 $^{fl/fl}$ Rag2$^{-/-}$ Il2rg$^{-/-}$,* particularly given the fact that the line has been genetically modified.

Figure 5.1 presents evidence for the expression of SCTR being specific to the ducts and BEC in the uninjured *Krt19Cre^{ER}Mdm2$^{fl/fl}$ Rag2$^{-/-}$ Il2rg$^{-/-}$* model, using three independent methods. Figure 5.1A displays a western blot showing a faint band present at 50kDa in protein obtained from intrahepatic ducts compared with hepatocytes. There are multiple further bands demonstrated in the western blot primarily around the 30,40 and 60kDa levels. If more mice could have been spared for isolation of protein, a further western blot could have been performed to improve the confidence in this result including an isotype control to assess for nonspecific binding of the primary antibody, and a control containing no primary antibody to assess for nonspecific secondary antibody binding. Additionally, a positive control using recombinant SCTR would have given more confidence that the 50kDa band was indeed SCTR.

Figure 5.1B shows significantly higher gene expression of *Sctr* in isolated intrahepatic ducts compared with hepatocytes. Finally, the results of a comparison between the ductal, periductal and non-ductal regions expression of SCTR as measured by immunofluorescence in mice that received only oral oil is presented by Figure 5.1C, showing significantly higher expression in the ductal region compared with the non-ductal areas. A representative example of the analysed images is shown in the

control sample of Figure 5.2E. The method for analysis has been described in section 4.7 and graphically displayed in Figure 4.6.

These results collectively indicate that SCTR is specific to BEC in the *Krt19Cre^{ER}Mdm2 $^{fl/fl}$ Rag2$^{-/-}$ Il2rg$^{-/-}$* model.

Figure 5.1 Secretin receptor is specifically expressed in the bile ducts within the liver.

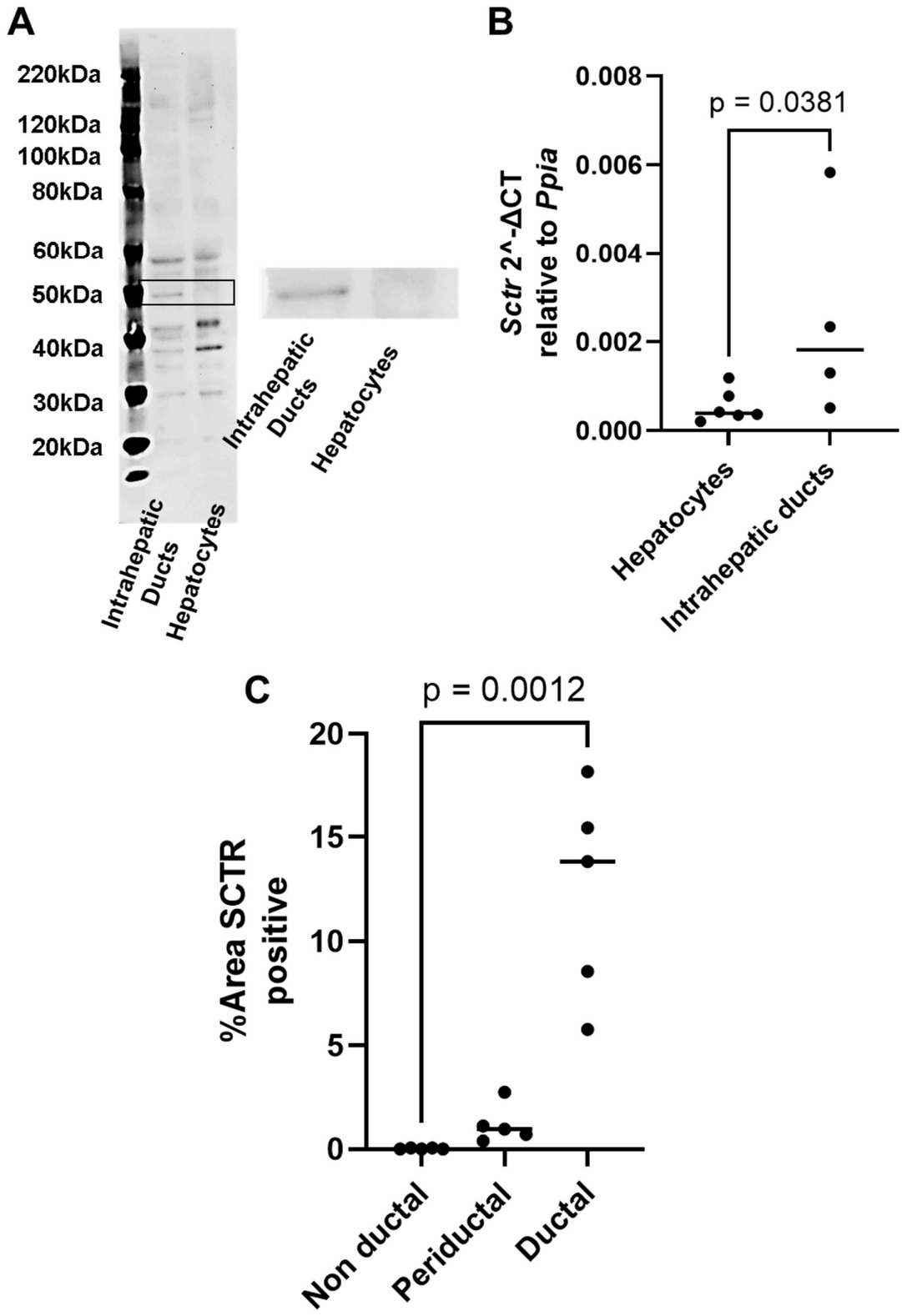

Figure 5.1; Secretin receptor is specifically expressed in the bile ducts within the liver.

Each dot represents a data obtained from a single mouse. Horizontal lines represent median.

A: Western blot comparing in expression of SCTR in protein extracted from biliary ducts and from extracted hepatocytes. Inset shows focused image of blot at the 50kDa level, expected site for SCTR. Contrast enhancements have been applied to whole image for clarity.

B: Comparison of SCTR gene expression in isolated intrahepatic ducts and hepatocytes from the uninduced *Krt19^{CreER}MDM2$^{fl/fl}$Rag2$^{-/-}$IL2rg$^{-/-}$* model. SCTR expression relative to PPIA. for ducts and hepatocytes respectively n=4-6 as shown. Median duct expression relative to PPIA, in hepatocytes 0.0004, in intrahepatic ducts 0.002. Mann-Whitney test p=0.0381.

C: Comparison of the expression of SCTR assessed by immunofluorescence in the *Krt19^{CreER}MDM2$^{fl/fl}$Rag2$^{-/-}$IL2rg$^{-/-}$* model, treated with oral oil only, n=5. Median % area SCTR positive in the ductal area was 13.83%, 0.9525% in the periductal region, and 0.01107 in the non-ductal. Kruskal Wallis ANOVA p<0.0001. Ductal vs non-ductal expression on Dunn's multiple comparison p=0.0012.

5.3 SCTR expression in the ducts is not increased in murine biliary specific injury models but may be increased in hepatocellular injury models.

Confirming the specificity of SCTR to BEC in the liver, it was then necessary to assess the change in %area of SCTR following injury in the ductal areas, using immunofluorescence.

Liver tissue from mice with IRI injury described in section 4.19 was examined for SCTR %area compared, with *Krt19Cre^{ER}Mdm2 $^{fl/fl}$ Rag2$^{-/-}$ Il2rg$^{-/-}$* mice treated with oil only, senescence induced by tamoxifen only or IRI only. There was significant heterogeneity in ductal SCTR %area between the groups in the IRI injury model however there was no significant difference between mean expression (Dunn's multiple comparison test), Figure 5.2A.

SCTR was also assessed in the *Krt19Cre^{ER}Mdm2 $^{fl/fl}$ Rag2$^{-/-}$ Il2rg$^{-/-}$* induced as described in 4.18, the CCl_4 (section 4.20) and MCD (section 4.21). No significant differences were identified between the %area of SCTR in any of the other three models investigated (Figures 5.2B-5.2D). There were trends towards higher expression in the CCl_4 and MCD models. Overall appearances suggest that SCTR is increased in hepatocellular injury models, but not so in biliary specific injuries, however the results obtained in this thesis were not statistically significant.

Representative images of immunofluorescence micrographs of the injury models investigated are shown in Figure 5.2E demonstrating colocalization of SCTR with KRT19 staining in all the models, and no evidence of extra biliary expression of SCTR. As indicated in Figure 5.1 SCTR is biliary specific, however this study finds no evidence that it has increased expression in hepatic injury.

Figure 5.2 SCTR ductal expression across different injury models.

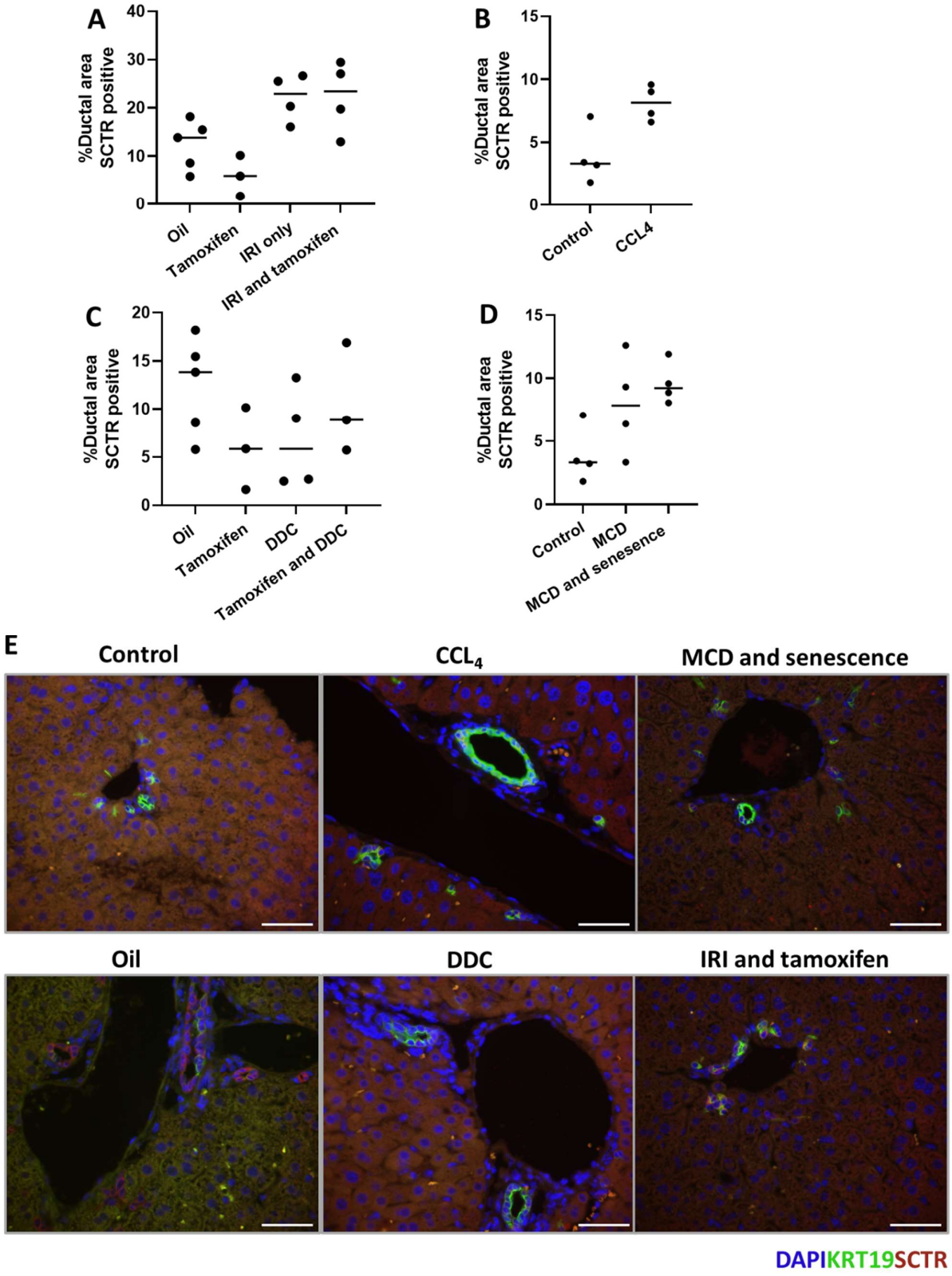

Figure 5.2; SCTR ductal expression across different injury models.

A-D demonstrate median expression of SCTR within areas defined as ducts by KRT19 expression on immunofluorescence. Each individual point on the graphs represents data from a single animal. Horizontal lines represent medians (shown in brackets in legend). n=3-5 as shown.

A: Comparison of SCTR expression in ducts of *Krt19Cre^{ER}Mdm2 $^{fl/fl}$ Rag2$^{-/-}$ Il2rg$^{-/-}$* mice which have received; oral gavage of oil (13.82%), oral gavage tamoxifen (5.85%), oral gavage of oil and DDC diet (5.85%), or oral gavage tamoxifen and DDC diet (8.85%). Kruskal Wallace ANOVA p=0.4346.

B: Comparison of SCTR expression in ducts of C57B6 mice who received 12 weeks CCL diet (8.16%) compared with controls (3.318%). Mann Whitney U test p=0.0571.

C: Comparison of SCTR expression in ducts of *Krt19Cre^{ER}Mdm2 $^{fl/fl}$ Rag2$^{-/-}$ Il2rg$^{-/-}$* mice who received oral gavage of oil (13.82%), oral gavage tamoxifen (5.85%), IRI injury only (22.92%), or oral gavage tamoxifen followed by ischaemia reperfusion injury (23.41%). Kruskal Wallace ANOVA p=0.0077 no significant differences on Dunn's multiple comparison comparing oil and other conditions.

D: Comparison of SCTR expression in ducts of C57/BL6J mice treated with AAV8.p21 and MCD diet (9.221%), MCD diet only (7.84%) and naïve controls (3.318%). Kruskal Wallace ANOVA p=0.465.

E: Representative images of DAPI, KRT19 and SCTR across the injury models tested. All scale bars represent 50μm.

5.4 SCTR expression is not specific to the ducts in human biliary injury.

The expression of SCTR was also assessed in human disease as shown in Figure 5.3.

Figure 5.3A demonstrates the % area of ductal regions positive for SCTR in PSC, PBC and control liver samples. There was no evidence of increased expression in either PSC or PBC, at the liver hilum or in the peripheral liver, compared with control samples. However, significant variability was identified between the groups, on Dunn's multiple comparison there was a significant reduction in the area expression of SCTR in the ducts of patients with PSC compared with controls.

There was no difference identified between the %area of non-ductal areas positive for SCTR between PSC, PBC and controls. Despite this and in contrast to appearances seen in the mouse, SCTR expression did not colocalise as closely with KRT19 expression, as seen in the representative images shown in Figure 5.3C. This is most clearly demonstrated in the image of hilar liver tissue from PBC in which multiple cells which do not express KRT19 shown in green, are positive for SCTR in red.

Overall, this section has shown that there was a significant reduction in ductal expression of PSC compared with control sample, using immunofluorescence. Additionally, appearances indicate that SCTR may not be specific to BEC within the liver of humans. For these reasons it would not represent an appropriate ligand for cell homing.

Figure 5.3 SCTR expression is not increased in human cholangiopathies.

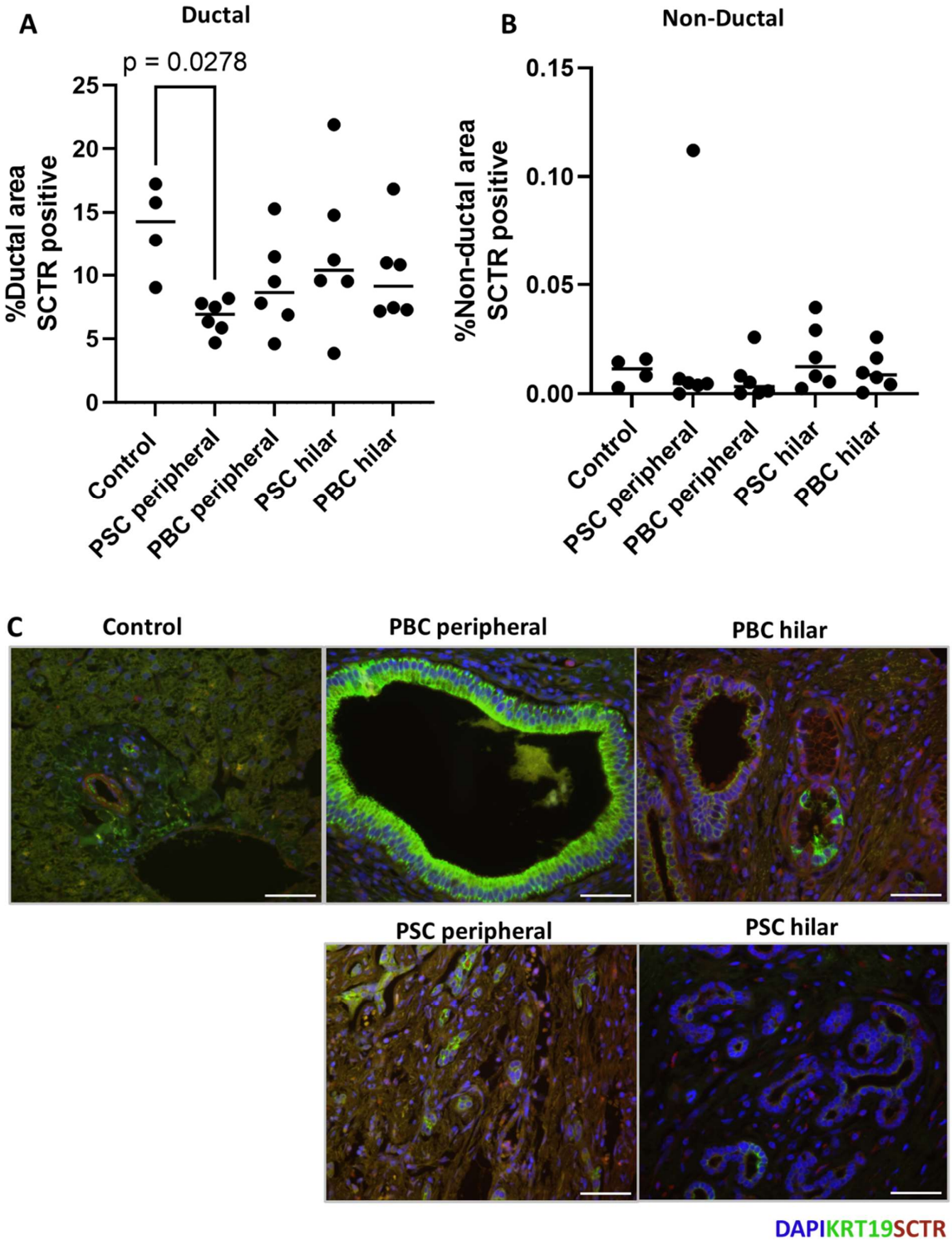

Figure 5.3; SCTR ductal expression in human liver samples.

Each individual point on the graphs represents a single patient. Horizontal lines represent median % Area SCTR positive (reported in brackets for each group below).

A: Comparison of SCTR ductal expression in control, PBC and PSC samples. Results show expression of SCTR within areas defined as ducts based on KRT19 immunofluorescence. Control livers median %ductal area SCTR positive (14.26%), peripheral PSC (6.918%), peripheral PBC (8.638%), hilar PSC (10.39%) and hilar PBC (9.131%). Kruskal Wallace ANOVA p=0.079. Dunn's multiple comparison was performed, with controls compared to each other group. Control vs PSC peripheral p=-.0278, no other significant differences.

B: Comparison of SCTR expression outside ductal regions in control, PBC and PSC samples. Median expression of SCTR within non-ductal areas defined as KRT19 negative regions by immunofluorescence. Control livers (0.0011%), peripheral PSC (0.0049%), peripheral PBC (0.0033%), hilar PSC (0.012%) and hilar PBC (0.0086%). Kruskal Wallace ANOVA showed no significant differences between groups p=0.463.

C: Representative images of DAPI, KRT19 and SCTR across control, PSC and PBC samples. All scale bars represent 50μm.

5.5 CD44 is not specific to the biliary ducts in murine liver

The second candidate assessed for ductal specificity was CD44. To assess the specificity of CD44 to the ducts in the liver and potential changes in expression following biliary injury, immunofluorescence was employed. Initially the *Krt19Cre^{ER}Mdm2 $^{fl/fl}$ Rag2$^{-/-}$ Il2rg$^{-/-}$* model was investigated.

Figure 5.4A presents the ductal expression of CD44, with ducts defined as areas positive for KRT19. There was no clear evidence of increased CD44 expression in this model. There was also no change in the periductal expression across injury in this model, Figure 5.4B.

In the non-ductal areas, there was significant heterogeneity between groups, and higher expression in mice that received both DDC diet and tamoxifen induction compared with oil only Figure 5.4C. As can be seen in the images provided in Figure 5.4D single cells positive for CD44 were interspersed within the hepatic parenchyma or in the periductal areas, and this was more prominent in mice that had received DDC diet. Jointly these results showed that expression was not limited to the BEC, additionally increased expression was seen primarily out with the ducts following biliary injury.

Figure 5.4 CD44 is not specific to the biliary ducts in murine liver.

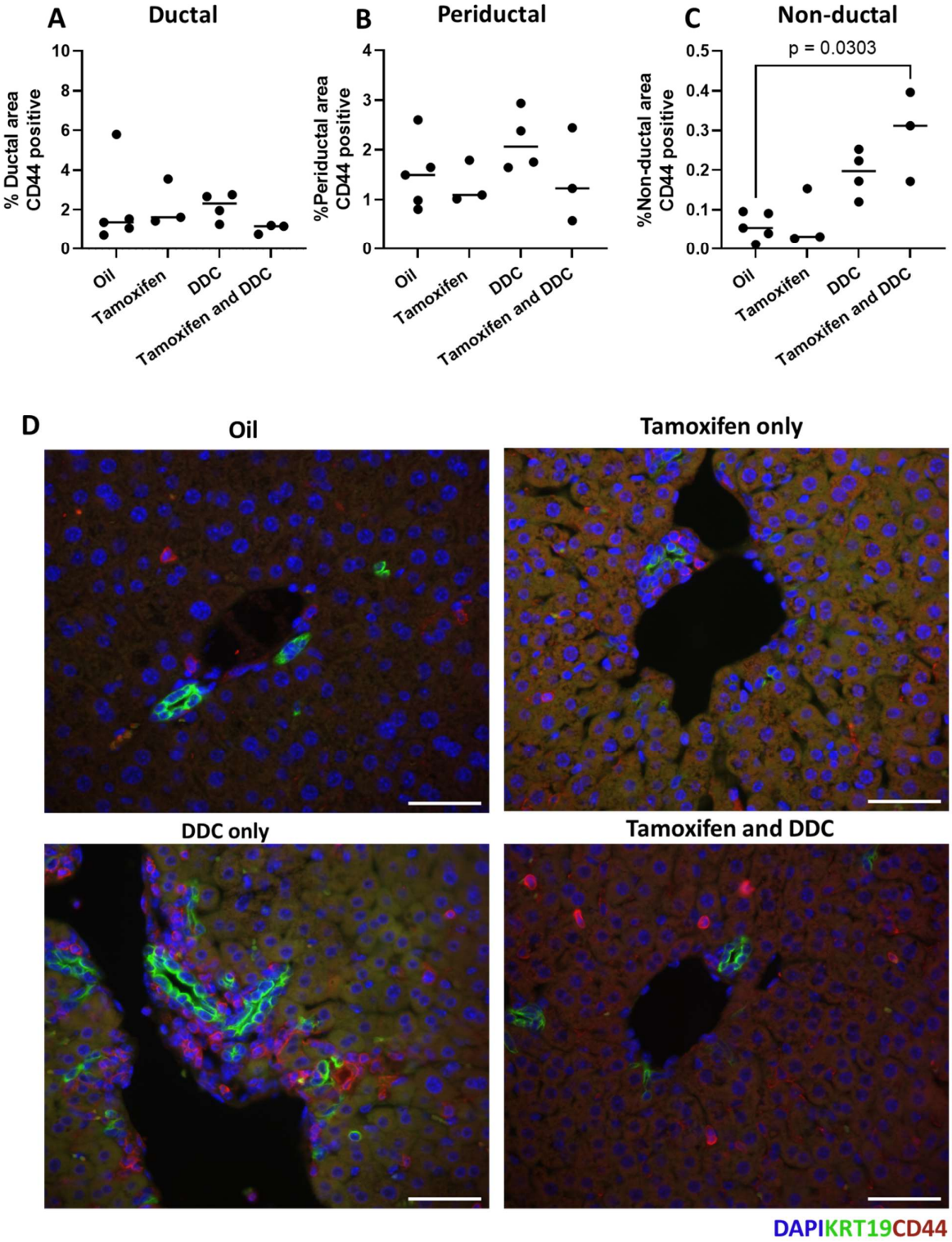

Figure 5.4 CD44 ductal expression in murine liver samples.

Each individual point on the graphs represents a single animal. Horizontal lines represent medians. n=3-5

A: Comparison of CD44 ductal expression in the *Krt19Cre^{ER}Mdm2 $^{fl/fl}$ Rag2$^{-/-}$.* Median expression of CD44 within areas defined as ducts by KRT19 expression on immunofluorescence. Mice induced with oil only median ductal %Area CD44 positive 1.362%, in mice given three doses of tamoxifen 1.616%, in mice given oil and DDC diet 2.308%, and mice given DDC and tamoxifen 1.161%. Kruskal Wallace ANOVA p=0.440.

B: Comparison of CD44 periductal expression in the *Krt19Cre^{ER}Mdm2 $^{fl/fl}$ Rag2$^{-/-}$*. Median expression of CD44 adjacent to areas defined as ducts by KRT19 expression on immunofluorescence. Mice induced with oil only median ductal %Area CD44 positive 1.495%, in mice given three doses of tamoxifen 1.096%, in mice given oil and DDC diet 2.066%, and in mice given DDC and tamoxifen 1.226%. Kruskal Wallace ANOVA p=0.140.

C: Comparison of CD44 non-ductal expression in the *Krt19Cre^{ER}Mdm2 $^{fl/fl}$ Rag2$^{-/-}$*. Median expression of CD44 adjacent to areas defined as ducts by KRT19 expression on immunofluorescence. Mice induced with oil only median ductal %Area CD44 positive 0.054%, in mice given three doses of tamoxifen 0.031%, in mice given oil and DDC diet 0.197%, and in mice given DDC and tamoxifen 0.312%. Kruskal Wallace ANOVA p=0.003. Dunn's multiple comparison was performed, with oil compared to each other group. Oil vs tamoxifen and DDC p=0.03, no other significant differences.

D: Representative images of DAPI, KRT19 and CD44 across samples. All scale bars represent 50μm.

5.6 CD44 positive cells are not found closer to the ducts in injury compared with controls.

Whilst CD44 was demonstrated not to be a specific BEC protein, it was of intrigue that there was higher expression of CD44 in mice with biliary injury compared with controls in the non-ductal compartments. Image analysis as shown in Figure 5.4 suggested an infiltration or proliferation of CD44 positive cells. To corroborate these results, a count of CD44 positive cells was performed on QuPath. To investigate this further, the proximity of CD44 positive cells to ducts was assessed, to determine whether they may be homing to the ducts following injury. This was also carried out using QuPath, by calculating the distance between CD44 positive cells and the nearest KRT19 positive cell [236].

In support of the findings depicted in Figure 5.4C, there was a greater proportion of CD44 positive cells identified in mice who received DDC and tamoxifen compared with mice that received only oil, Figure 5.5A. Of note no cells double positive for KRT19 and CD44 were identified in any group, likely reflecting low expression of CD44 in BEC in the mouse.

There was no difference between injury groups in terms of mean distance of CD44 positive cells to the closest KRT19 positive cell, Figure 5.5B. This may suggest that the increase in CD44 positive cells in the liver is secondary to clonal expansion as opposed to migration of a cell population into the liver.

Figure 5.5 CD44 positive cells do not localise to the ducts following biliary injury

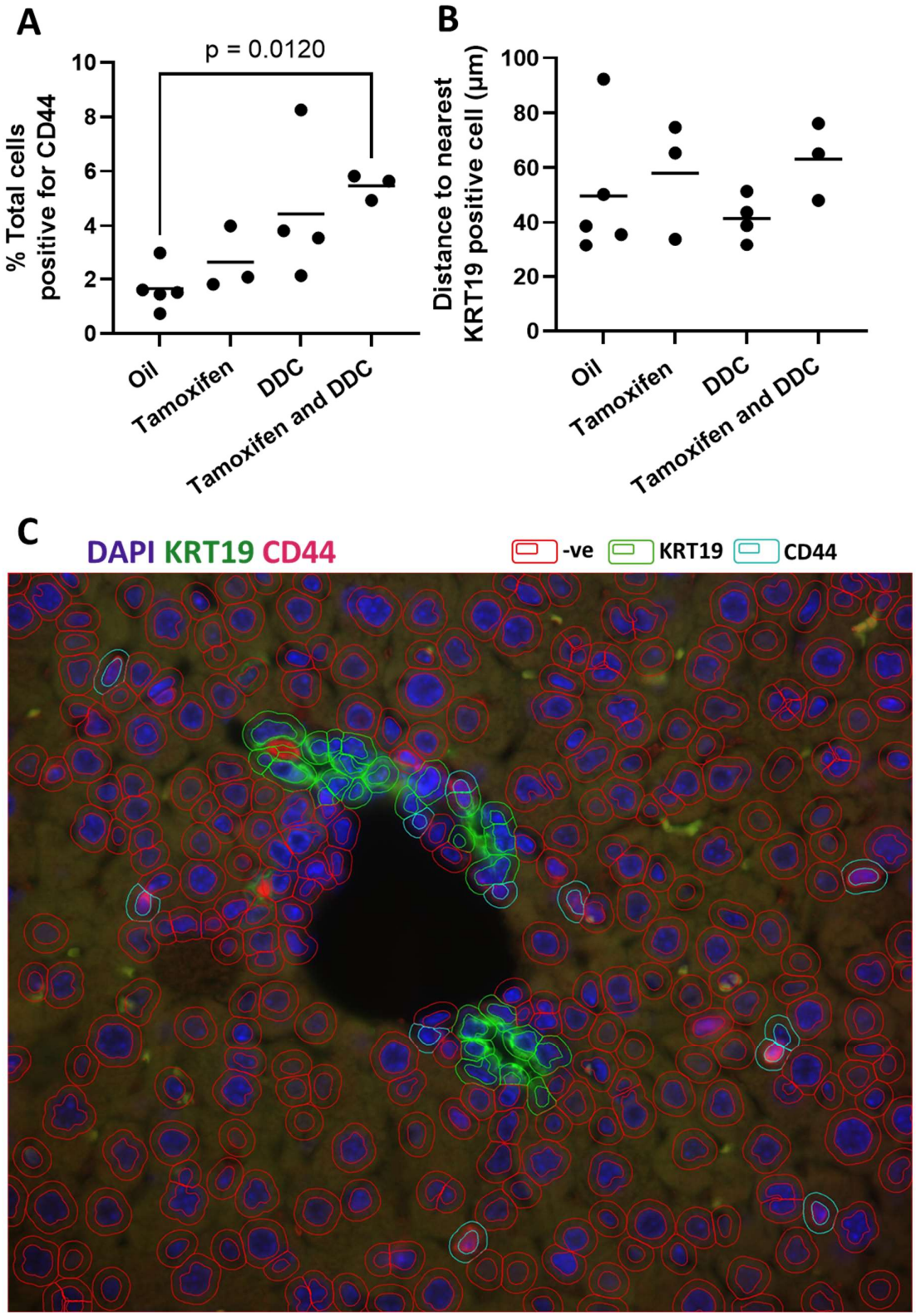

Figure 5.5 CD44 positive cells do not localise to the ducts following biliary injury.

Each dot represents a single mouse. Horizontal lines represent median shown in brackets. N=3-5 as shown

A: Percentage of total cells from 10 images in each of the conditions positive for CD44. Median CD44 percentage positive for mice that received oil only (1.52%), those that received tamoxifen (2.08%), DDC diet only (3.68%) and both tamoxifen and DDC (5.65%). Kruskall Wallis ANOVA test p=0.0053, Dunn's multiple comparison Oil vs tamoxifen p=0.012.

B: Mean distance in μm of CD44 positive cells to nearest KRT19 positive cell. Median, mean distance from CD44 cells to nearest KRT19 positive cell in mice who received oil only 38.68μm, in mice who received tamoxifen 65.38μm, in mice who received DDC only 41.29μm and in mice who received both tamoxifen and DDC 65.11μm. Kruskall Wallace ANOVA test p=0.4948.

C: Representative image of the designation of cells as KRT19 and CD44 positive on QuPath.

5.7 CD44 is not specific to the ducts in human liver.

Figure 5.5 demonstrated that in the *Krt19Cre^{ER}Mdm2 $^{fl/fl}$ Rag2$^{-/-}$ Il2rg$^{-/-}$* murine injury model, increased expression of CD44 was primarily seen out with the ducts. The increased number of CD44 positive cells warranted further investigation. Therefore, CD44 expression was assessed by immunofluorescence with relation to KRT19 cells in human tissue to determine if similar outcomes are seen in humans.

Figure 5.6 demonstrates the expression of CD44 in control human samples and, from patients with PSC and PBC. Figure 5.6A shows the ductal expression of CD44, with no change in expression across the groups investigated shown, in agreement with findings in the mouse model.

Figure 5.6B demonstrates the expression of CD44 in the periductal area. Control samples had significantly higher periductal expression compared with peripheral PSC samples. There were no further significant differences between the groups investigated.

Figure 5.6C demonstrates the non-ductal expression of CD44 in human samples with higher expression in the control livers compared with PSC peripheral samples, and PBC peripheral samples.

Figure 5.6D presents representative images of samples, reflecting the higher expression CD44 in the non-ductal tissues of controls, in direct contrast to the results in the mouse where higher expression was associated with injury. As seen in the murine samples presented in Figures 5.4D and 5.5C the CD44 positive cells appear as single cells and are found in the periductal area and interspersed between the hepatic parenchyma. Overall, the findings in Figure 5.6 suggest that CD44 is not specific to ducts in human liver as in murine tissue. In neither human nor murine tissues was CD44 expression identified as being higher in bile ducts following injury, indicating it would not be an appropriate target for homing.

Figure 5.6 CD44 expression is not increased in the ducts in human liver

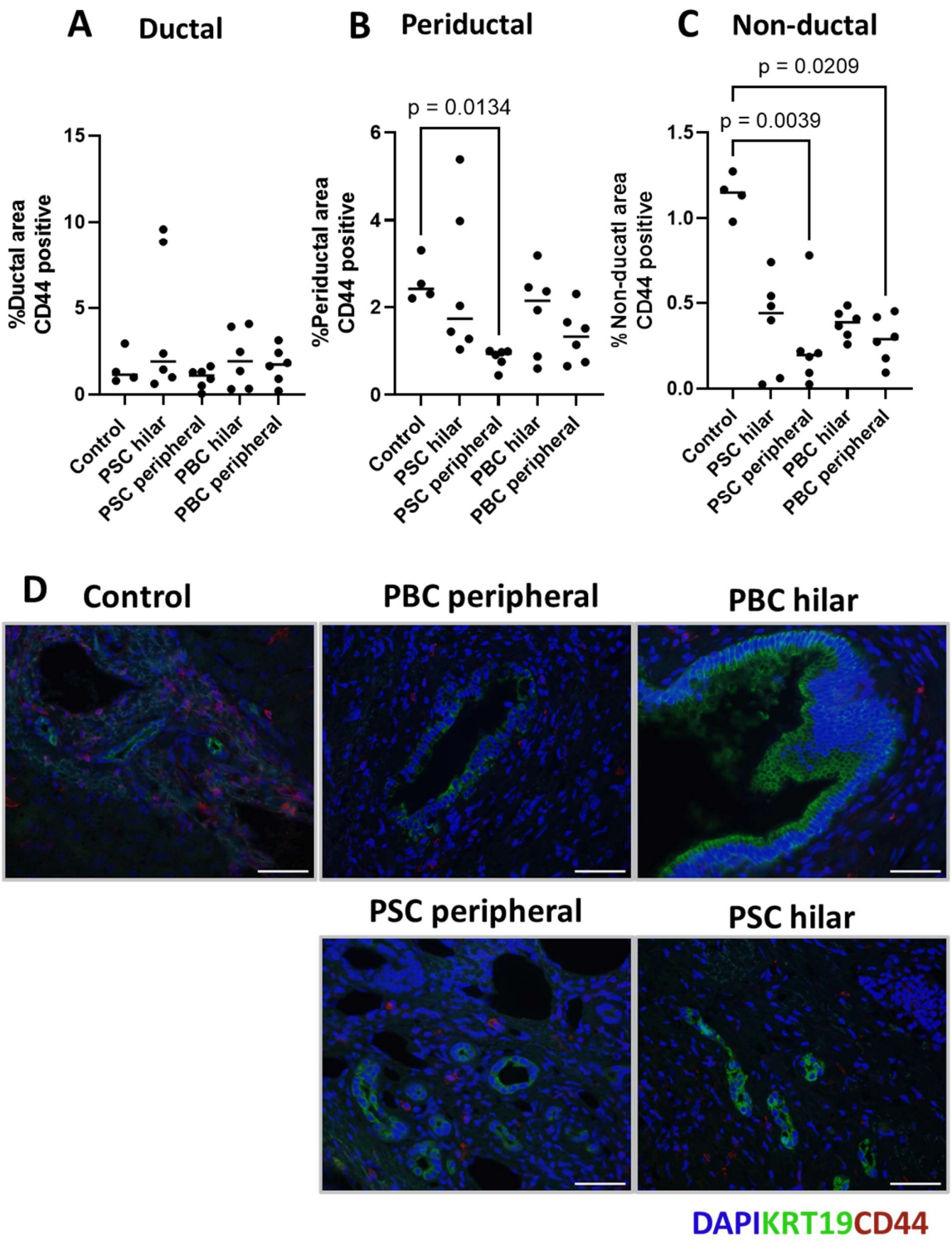

Figure 5.6 CD44 expression is not increased in the ducts in human liver.

Each dot represents a single human liver. Horizontal lines represent median. N=4-6 as shown

A: Comparison of CD44 ductal expression in human tissue. Median expression of CD44 within areas defined as ducts by KRT19 expression on immunofluorescence. Control liver %Area CD44 positive 1.144%, in hilar PSC 1.907%, in peripheral PSC 1.092% in hilar PBC 1.916%, and in peripheral PBC 1.737%. Kruskal Wallace ANOVA p=0.4656.

B: Comparison of CD44nonductal expression in human tissue. Median expression of CD44 within areas outwith the ducts defined by KRT19 expression on immunofluorescence. Control liver %Area CD44 positive 2.416%, in hilar PSC 1.737%, in peripheral PSC 0.9409% in hilar PBC 2.147%, and in peripheral PBC 1.329%. Kruskal Wallace ANOVA p=0.0244. Dunn's multiple comparison was performed, with control compared to each other group. Control vs PSC peripheral p=0.0134, no other significant differences.

C: Comparison of CD44periductal expression in human tissue. Median expression of CD44 within areas adjacent to the ducts defined by KRT19 expression on immunofluorescence. Control liver %Area CD44 positive 1.150%, in hilar PSC 0.4407%, in peripheral PSC 0.1957% in hilar PBC 0.3864%, and in peripheral PBC 0.2883%. Kruskal Wallace ANOVA p=0.0174. Dunn's multiple comparison was performed, with oil compared to each other group. Control vs PSC peripheral p=0.0039, control vs PBC peripheral p=0.021, no other significant associations.

D: Representative image of the designation of cells as KRT19 and CD44 positive on QuPath, all scale bars represent 50μm.

5.8 TFF2 is not specific to the ducts in murine liver and expression is not increased in injury.

TFF2 was also considered as a possible candidate based on the literature available. Figure 5.7 presents the expression of TFF2 in mouse models of liver injury.

There was no evidence of increased expression of TFF2 in the ducts in any of the injury models investigated, Figures 5.7A-D. On the contrary, in the *Krt19Cre^{ER}Mdm2 $^{fl/fl}$ Rag2$^{-/-}$ Il2rg$^{-/-}$* there was reduced expression in mice who had received DDC, and tamoxifen compared with those who only received oil.

On close inspection, as demonstrated in Figure 5.7E, there were areas of canalicular expression of TFF2 in most of the models.

These findings in combination indicate that TFF2 would not be a good ligand for homing due to both a lack of specificity and a lack of increased expression in injury. Despite TFF2 representing an excreted protein, it was elected not to investigate this candidate further due to the clear results produced from immunofluorescence.

Figure 5.7 TFF2 is not specific to the ducts in mouse liver nor is ductal expression increased in injury.

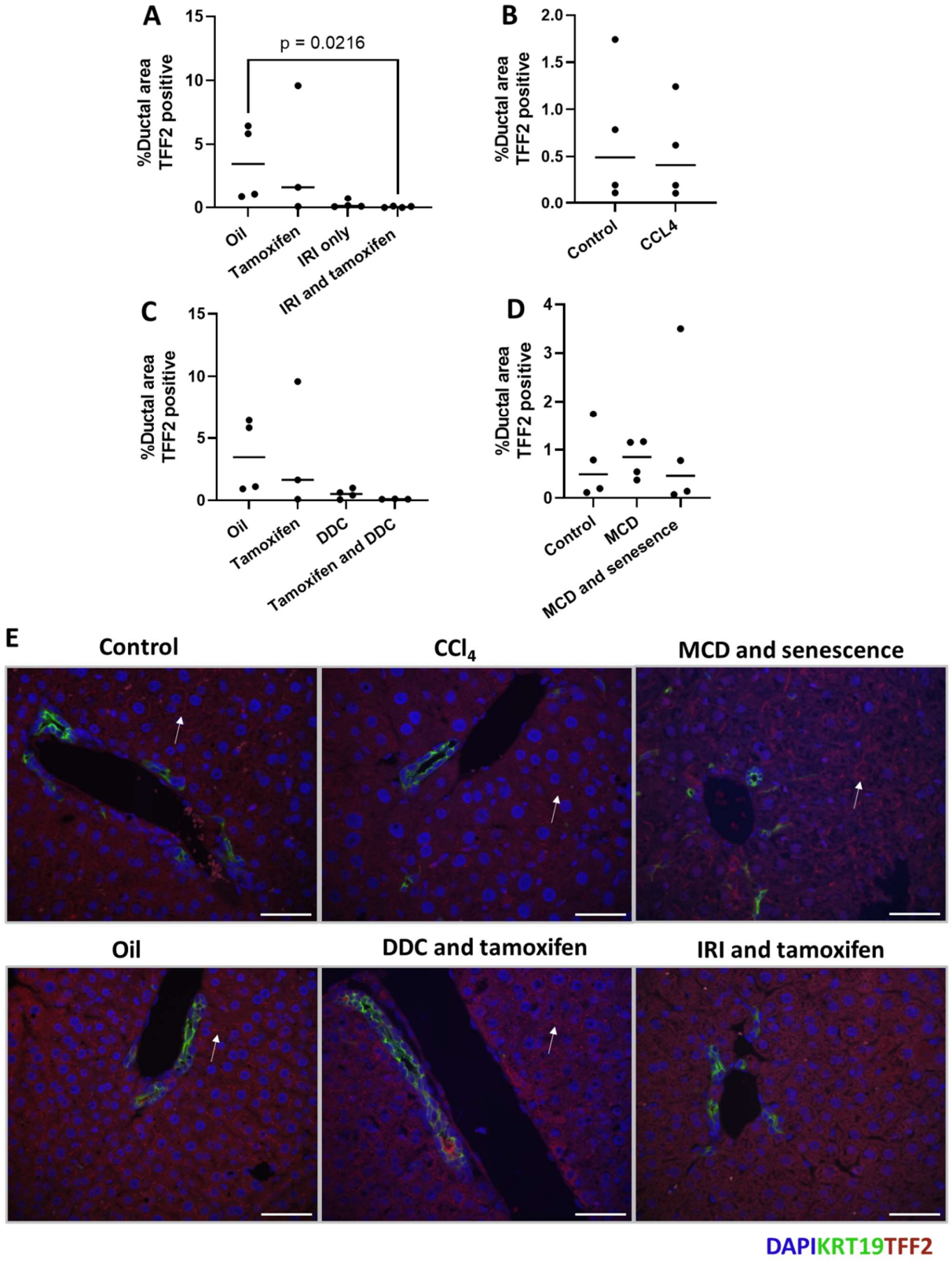

Figure 5.7 TFF2 is not specific to the ducts in mouse liver nor is ductal expression increased in injury.

A-D demonstrate mean expression of TFF2 within areas defined as ducts by KRT19 expression on immunofluorescence. Each individual point on the graphs represents a single animal. Horizontal lines represent medians shown in brackets.

A: Comparison of median TFF2 expression in ducts of *Krt19Cre^{ER}Mdm2 $^{fl/fl}$ Rag2$^{-/-}$ Il2rg$^{-/-}$* mice who have received: oral gavage of oil (3.468%), oral gavage tamoxifen (1.641%), oral gavage of oil and DDC diet (0.521%), or oral gavage tamoxifen and DDC diet (0.0973%). Kruskal Wallace ANOVA p=0.0888.

B) Comparison of TFF2 expression in ducts of C57/BL6J mice who received 12 weeks CCL_4 induced liver injury median ductal TFF2 expression (0.407%), compared with controls (0.490%). Mann Whitney U test p=0.6857.

C) Comparison of median TFF2 expression in ducts of *Krt19Cre^{ER}Mdm2 $^{fl/fl}$ Rag2$^{-/-}$ Il2rg$^{-/-}$* mice who have received: oral gavage of oil 3.468%, oral gavage tamoxifen 1.641%, IRI only 0.1337%, IRI and tamoxifen induction 0.0461%. Kruskal Wallace ANOVA p=0.0131. Dunn's multiple comparison was performed, with oil compared to each other group. Oil and IRI and tamoxifen p=0.022, no other significant differences.

D) Comparison of TFF2 expression in ducts of C57/BL6J mice treated with AAV8.p21 and MCD diet median ductal TFF2 expression (0.458%), MCD diet only (0.845%) and controls (0.490%). Kruskal Wallace ANOVA p=0.8151.

E) Representative images of DAPI, KRT19 and TFF2 across the injury models tested. All scale bars represent 50μm. White arrows point out areas of canalicular expression.

5.9 CXCL2 is specific to the intrahepatic ducts.

In addition to the three proteins investigated in the previous sections, the chemokines CCL2, CXCL1 and CXCL2 were investigated as candidate ligands, upregulation in biliary ducts in biliary injury.

Biliary ducts were isolated from the *Krt19Cre^{ER}Mdm2 $^{fl/fl}$ Rag2$^{-/-}$ Il2rg$^{-/-}$* model in injured mice (induced by tamoxifen and DDC) and in control mice (no induction). Extrahepatic ducts from injured and control mice were also isolated, as were hepatocytes. Hepatocytes did not undergo the usual percoll centrifugation isolation step, to preserve cells associated with the hepatocyte compartment that may be producing chemokines but may not necessarily be hepatocytes. Total RNA was extracted from each of these isolated cell compartments and mRNA expression of the chemokine candidates was examined by qPCR.

Results showed no significant difference regarding expression of *Ccl2* in injured and uninjured mice across the different cellular compartments analysed, Figure 5.8A. *Cxcl1* showed significantly higher expression in the intrahepatic ducts compared with the extrahepatic ducts in control samples, Figure 5.8B, but no other significant associations were identified. In both injured and uninjured intrahepatic ducts higher expression of *Cxcl2* was found compared with uninjured hepatocyte samples.

Overall, these findings indicate that CXCL2 may be an attractive ligand for cell homing, due to the it's specificity to intrahepatic biliary ducts and potential upregulation in injury. CXCL2 has a known receptor in CXCR2 (Table 1.1) which may simplify the installation of a homing mechanism in HPC for this ligand.

Figure 5.8 Assessment of chemokines in RNA extracted from the *Krt19Cre^{ER}Mdm2 $^{fl/fl}$ Rag2$^{-/-}$* model

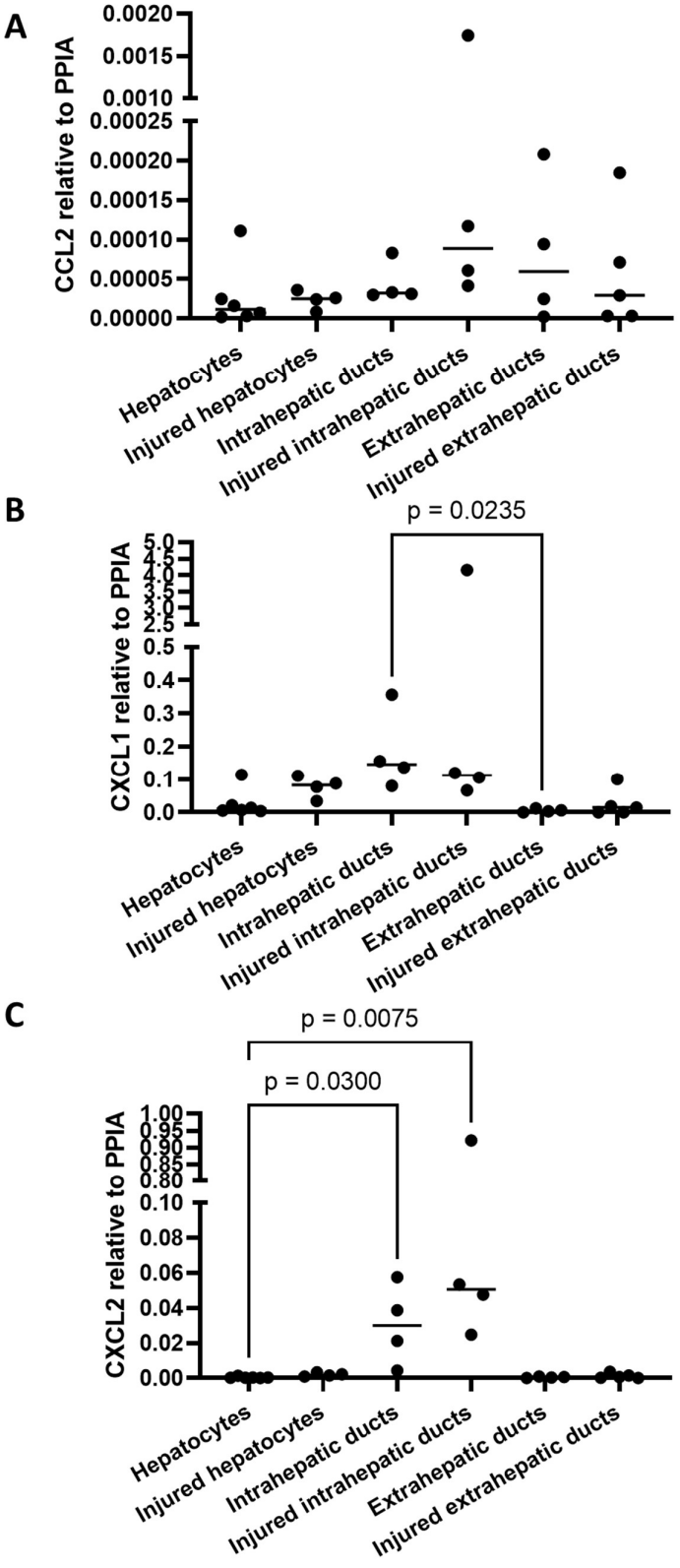

Figure 5.8: Assessment of chemokines in RNA extracted from the *Krt19Cre^{ER}Mdm2 $^{fl/fl}$ Rag2$^{-/-}$ Il2rg$^{-/-}$* model

Injured mice received three doses of tamoxifen and 48 hours of DDC diet, control mice had no induction. Each dot represents an individual mouse, n=4-6 as presented.

A: qPCR of *Ccl2* relative to PPIA 2^(-ΔT). Median in; uninjured hepatocytes 0.00001, injured hepatocytes 0.00002, in intrahepatic ducts 0.00003, injured intrahepatic ducts 0.00009, extrahepatic ducts 0.00006 and injured extrahepatic ducts 0.00003. Kruskall Wallace ANOVA p=0.1799

B: qPCR of *Cxcl1* relative to PPIA 2^(-ΔT). Median in; uninjured hepatocytes 0.011, injured hepatocytes 0.082, in intrahepatic ducts 0.146, injured intrahepatic ducts 0.113, extrahepatic ducts 0.005 and injured extrahepatic ducts 0.015. Kruskall Wallace ANOVA p=0.005, significant difference between uninjured intra and extrahepatic ducts on Dunn's multiple comparison testing.

C: qPCR of *Cxcl2* relative to PPIA 2^(-ΔT). Median in; uninjured hepatocytes 0.0002, injured hepatocytes 0.002, in intrahepatic ducts 0.03, injured intrahepatic ducts 0.051, extrahepatic ducts 0.0005 and injured extrahepatic ducts 0.0006. Kruskall Wallace ANOVA p=0.0014. Significantly higher expression of *Cxcl2* relative to *Ppia* in intrahepatic ducts compared with hepatocytes p=0.03 and injured intrahepatic ducts compared with hepatocytes p=0.0075 on Dunn's multiple comparison testing.

5.10 Development of a model of biliary injury *in vitro*

To complement *in vivo* analyses of ligand expression in injury models, an *in vitro* model of biliary injury was developed using a line of murine BEC, further described in the methods, section 4.22. 2000 cells were seeded on a collagen coated plate and left to culture for a further 4 days. Following this, cells were injured by treatment with etoposide on day 4 or peroxide on day 5 post-seeding. The treatment date for peroxide was adjusted following recuperation of low yields of RNA after Peroxide induction experiments. The peroxide and etoposide models of *in vitro* injury have been displayed graphically in Figures 5.10A and 5.11A respectively.

Both models of injury led to increased cell size by Day 7 (24 hours prior to collection of RNA) Figures 5.10C and Figures 5.11C, with fewer surviving cells apparent in the etoposide model, Figure 5.11C.

To assess the suitability of these *in vitro* systems to model biliary injury, and specifically complement the *Krt19Cre^{ER}Mdm2$^{fl/fl}$ Rag2$^{-/-}$ Il2rg$^{-/-}$* model expression of the genes *Cdkn1a* (*p21*) and *Trp53* (*p53*) was analysed, as both genes are induced in the mouse model. To evaluate apoptosis induction *Casp3* expression was assessed. As shown in Figure 5.12A *Casp3* expression was increased significantly in cells that received peroxide. There was also higher expression of *Cdkn1a* in peroxide compared with controls which was not the case in the etoposide model, Figure 5.12B. No significant increase in *p53* expression was seen in either of the *in vitro* models.

Due to the more reliable induction of *p21* and apoptosis in the peroxide model, this model was selected for further assessment of expression of the chemokines *Ccl2*, *Cxcl1*, *Cxcl2* given the varying evidence for their upregulation in biliary injury in the mouse (as shown in Figure 5.8).

Figure 5.9 Peroxide injury induction of murine BEC in culture

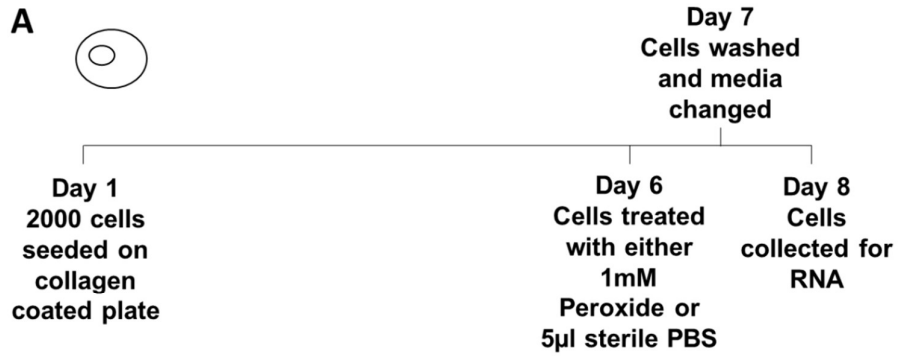

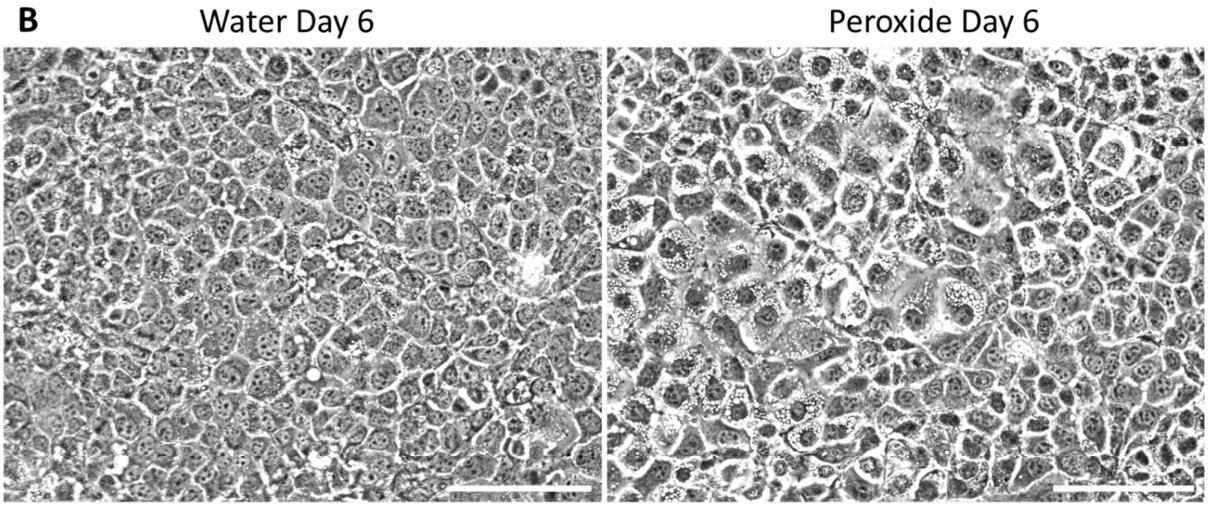

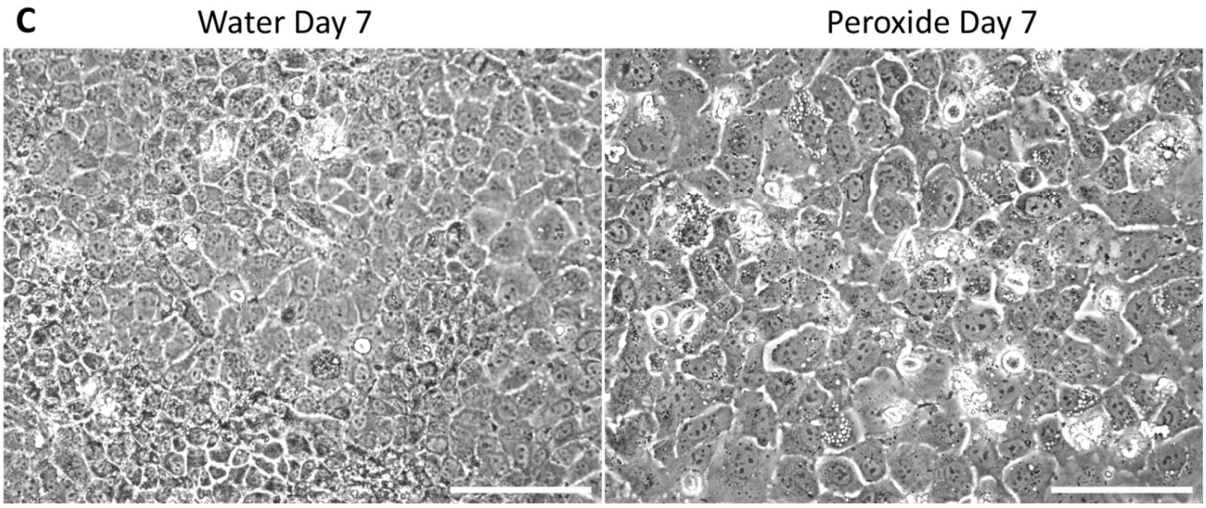

Figure 5.9 Peroxide injury induction of murine BEC in culture.

All images taken at x20 magnification; scale bar represents 100μm.

A: Schematic of the experimental plan

B: Images on day 6 following plating of 2000 cells in a single well of a 12 well plate, before treatment.

C: Images on day 7, one day following washing cells after 24 hours of treatment with either 1mM Peroxide or 5μl of sterile PBS.

Figure 5.10 Etoposide injury induction of murine BEC in culture.

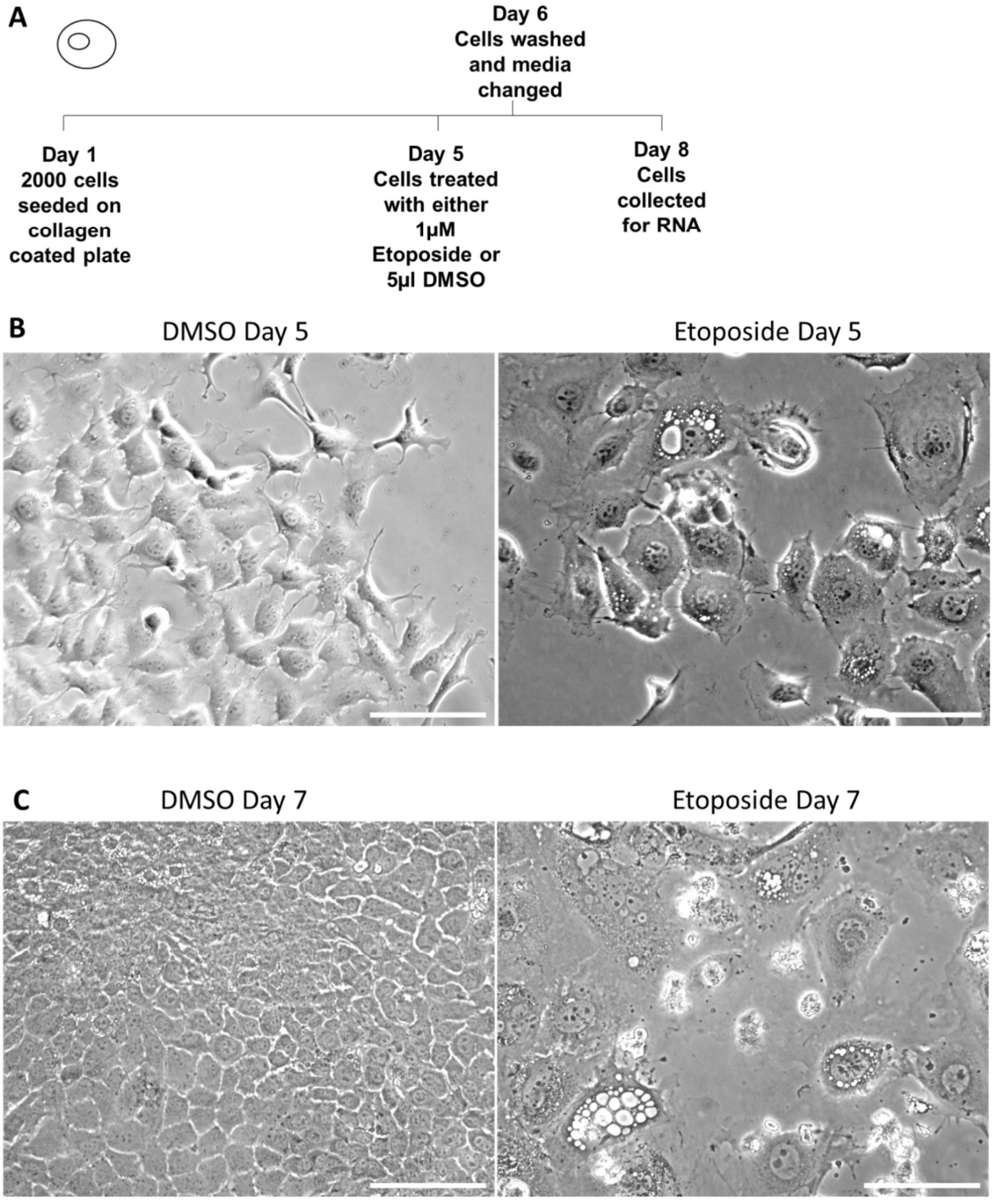

Figure 5.10 Etoposide injury induction of murine BEC in culture.

All images taken at x20 magnification; scale bar represents 100μm. Brightness in these images has been altered.

A: Schematic of the experimental plan

B: Images on day 5 following plating of 2000 cells in a single well of a 12 well plate, before treatment.

C: Images on day 7 one day following washing cells after 24 hours of treatment with either 1μM etoposide or 5μl of DMSO.

Figure 5.11 Assessment of senescence and apoptosis in *in vitro* murine BEC injury models.

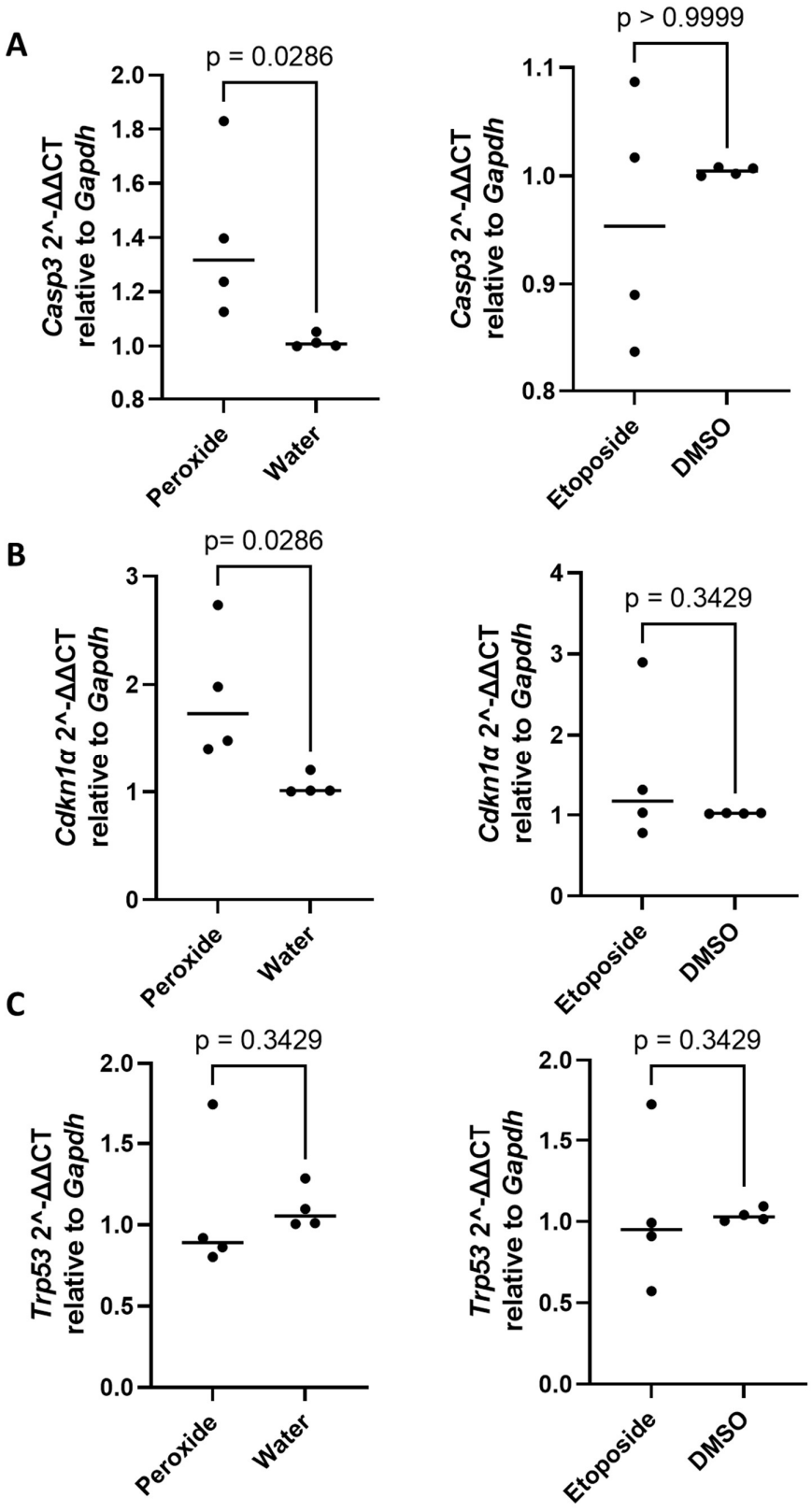

Figure 5.11: Assessment of senescence, and apoptosis in *in vitro* murine BEC injury models.

Each dot represents an individual experiment of 3 wells of a 12 well plate. Horizontal lines represent median. (n=4 as shown)

A: qPCR of Casp3 in cells treated with peroxide, water, etoposide, or DMSO. Mean fold change of Peroxide vs water 1.317 p= 0.029 using Mann-Whitney test. Median fold change of Etoposide vs DMSO 0.958, p<0.999 using Mann-Whitney test.

B: qPCR of *Cdkn1α* in cells treated with peroxide, water, etoposide or DMSO. Mean fold change of Peroxide vs water 1.73, p=0.029 using Mann Whitney test. Mean fold change of Etoposide vs DMSO 1.174, p=0.343 using Mann-Whitney test.

C: qPCR of *Trp53* in cells treated with peroxide, water, etoposide or DMSO. Mean fold change of Peroxide vs water 0.891, p=0.343 using Mann Whitney test. Mean fold change of Etoposide vs DMSO 0.951, p=0.343 using Mann-Whitney test.

5.11 The expression of chemokine ligands in cell model of BEC injury

Having established an *in vitro* model of cholangiopathy, gene expression of the candidates identified from the preceding sections (namely CCL2, CXCL1 and CXCL2) were assessed using qPCR.

As shown in Figure 5.13 none of the candidates were significantly upregulated in the Peroxide model of cell injury.

In addition to assessing changes in expression of these candidate genes in response to peroxide, their expression with respect to apoptosis and senescence genes was examined, given the changes in expression shown in Figure 5.12. Associations between senescence or apoptosis and the candidate chemokines may indicate that cells undergoing this process have higher expression of the candidates. This could be attractive for a homing system as transplanted cells would be inclined towards apoptotic or senescent cells, which are likely to represent areas of significant injury.

To this end, comparisons were made between the candidates and *Casp3* or *Casp8*, to assess apoptosis[237, 238].The candidates were also compared with *p21* or *p53* to assess senescence[239, 240].

Results showed *Ccl2* expression was not strongly associated with markers of apoptosis, Figure 5.14A and D. Strong positive associations were identified between the level of *Cxcl1* expression and *Casp3* and *Casp8* expression in both injured cells and controls, Figure 5.14B and E. *Cxcl2* expression in cells that had received peroxide was strongly positively associated with *Casp3* expression and to a greater degree *Casp8* expression; in cells that had received water only *Casp8* expression was strongly associated with *Cxcl2* expression Figures 5.14C and F.

Comparing expression of markers of senescence with the three candidates no strong associations were identified with *p21,* Figures 5.15A-C. *p53* expression was strongly negatively associated with *Ccl2* in control but not injured cells 5.15D.

Overall, these results suggest that whilst the peroxide model of BEC injury does not induce increased expression of the candidate chemokines, higher expression of *Cxcl1* and *Cxcl2* is associated with apoptotic markers in murine BEC. This finding could be beneficial for targeting areas of apoptotic cells and therefore injury.

Figure 5.12 Assessment of *Ccl2*, *Cxcl1* and *Cxcl2* expression by qPCR in peroxide injury model.

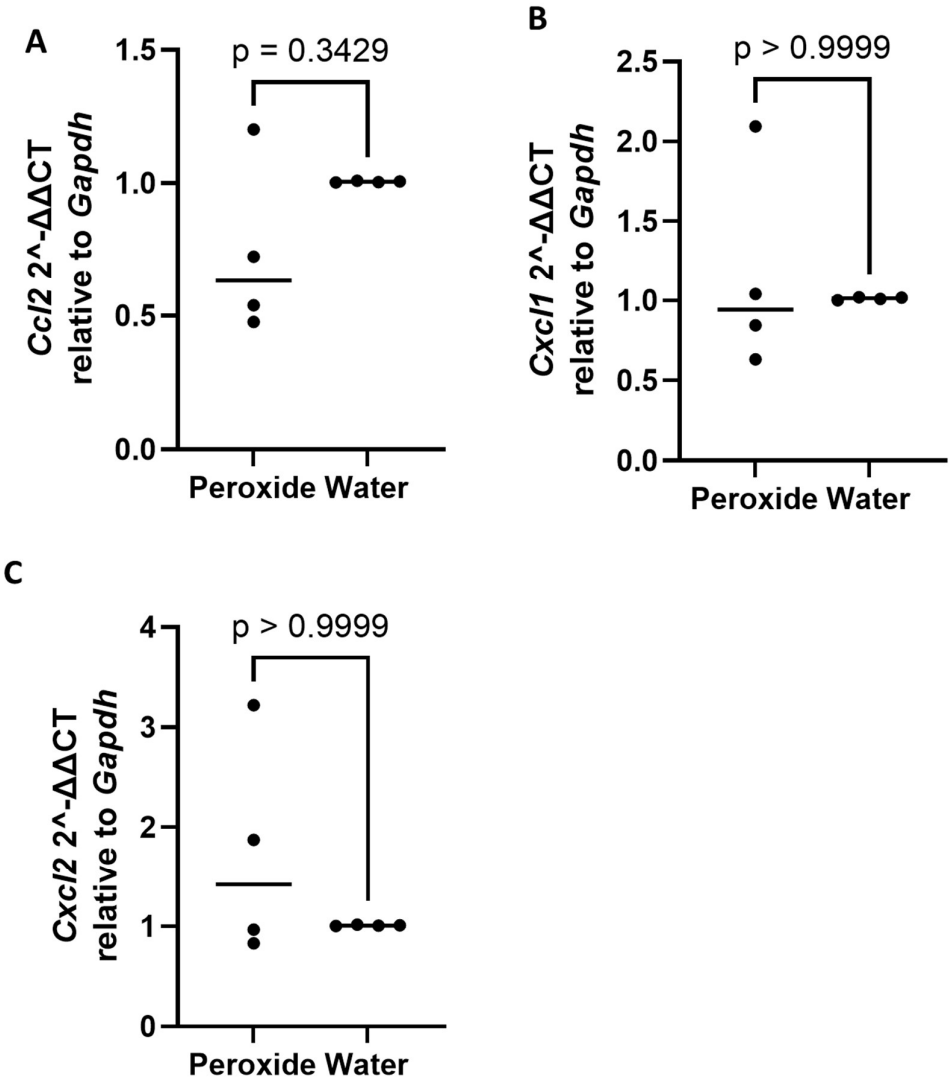

Figure 5.12: Assessment of *Ccl2*, *Cxcl1* and *Cxcl2* expression by qPCR in peroxide injury model.

Each dot represents an individual experiment containing 3 wells of a 12 well plate. Horizontal lines represent median. n=4

A: qPCR of *Ccl2* in cells treated with peroxide or water. Median fold change of Peroxide vs water 0.632 p= 0.343 using Mann-Whitney test.

B: qPCR of *Cxcl1* in cells treated with peroxide or water. Median fold change of Peroxide vs water 0.943 p>0.999 using Mann-Whitney test.

C: qPCR of *Cxcl2* in cells treated with peroxide or water. Median fold change of Peroxide vs water 1.422 p>0.999 using Mann-Whitney test.

Figure 5.13 Association between markers of apoptosis and selected chemo-kines using qPCR.

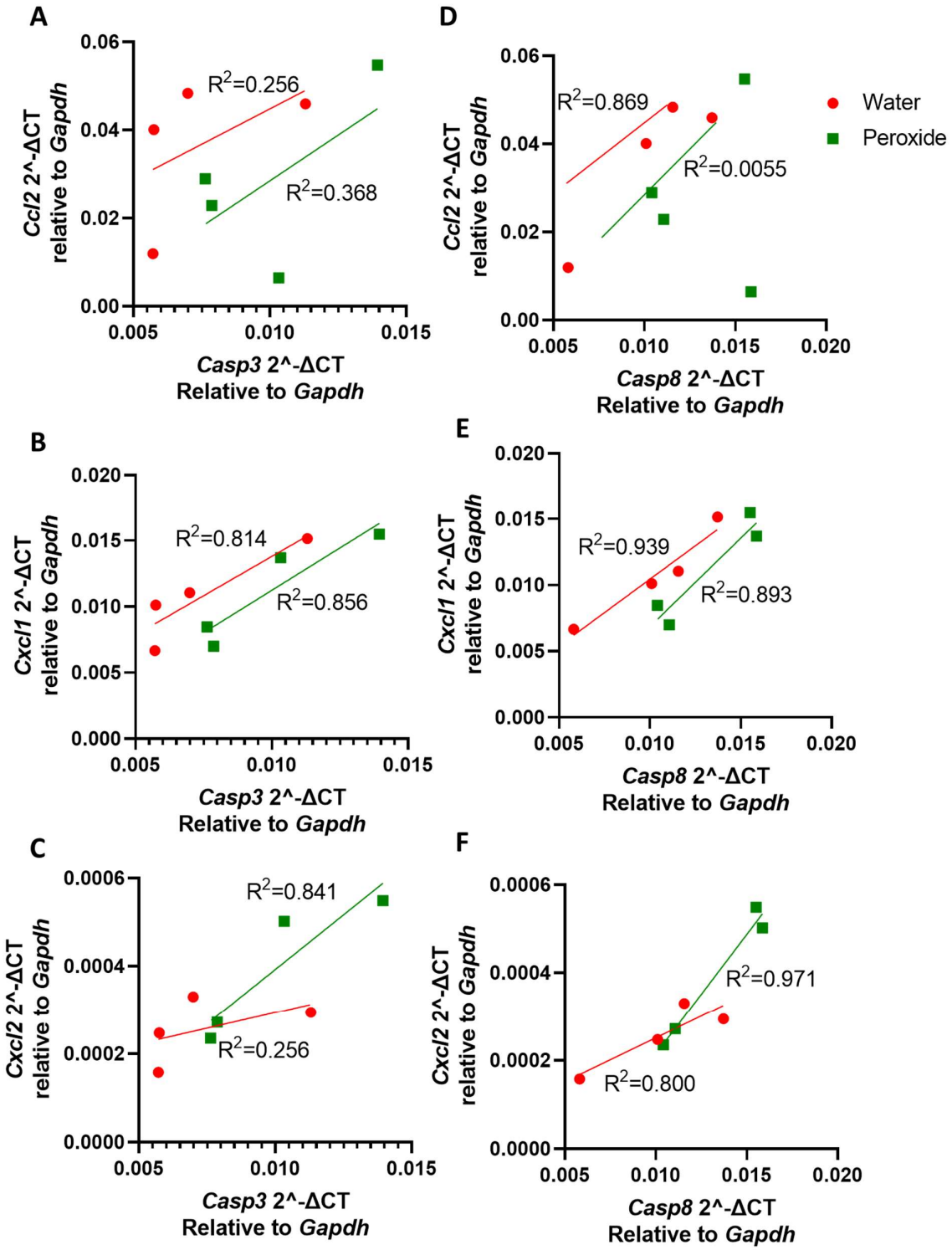

Figure 5.13: Association between markers of apoptosis and selected chemokines using qPCR.

Each dot represents an individual experiment containing 3 wells of a 12 well plate. Lines represent results of simple linear regression. Samples that received peroxide are shown in green, samples that received water (controls) shown in red. R^2 as shown.

A: XY plot comparing *Ccl2* relative to *Gapdh* and *Casp3* relative to *Gapdh.* Association in water samples R^2 =0.256, in peroxide samples 0.368.

B: XY plot comparing *Cxcl1* relative to *Gapdh* and *Casp3* relative to *Gapdh.* Association in water samples R^2 =0.814, in peroxide samples 0.856.

C: XY plot comparing *Cxcl2* relative to *Gapdh* and *Casp3* relative to *Gapdh.* Association in water samples R^2 =0.256, in peroxide samples 0.841.

D: XY plot comparing *Ccl2* relative to *Gapdh* and *Casp8* relative to *Gapdh.* Association in water samples R^2 =0.869, in peroxide samples 0.0055.

E: XY plot comparing *Cxcl1* relative to *Gapdh* and *Casp8* relative to *Gapdh.* Association in water samples R^2 =0.939, in peroxide samples 0.893.

F: XY plot comparing *Cxcl2* relative to *Gapdh* and *Casp8* relative to *Gapdh.* Association in water samples R^2 =0.800, in peroxide samples 0.971.

Figure 5.14 Assessment of senescence, and apoptosis in murine BEC.

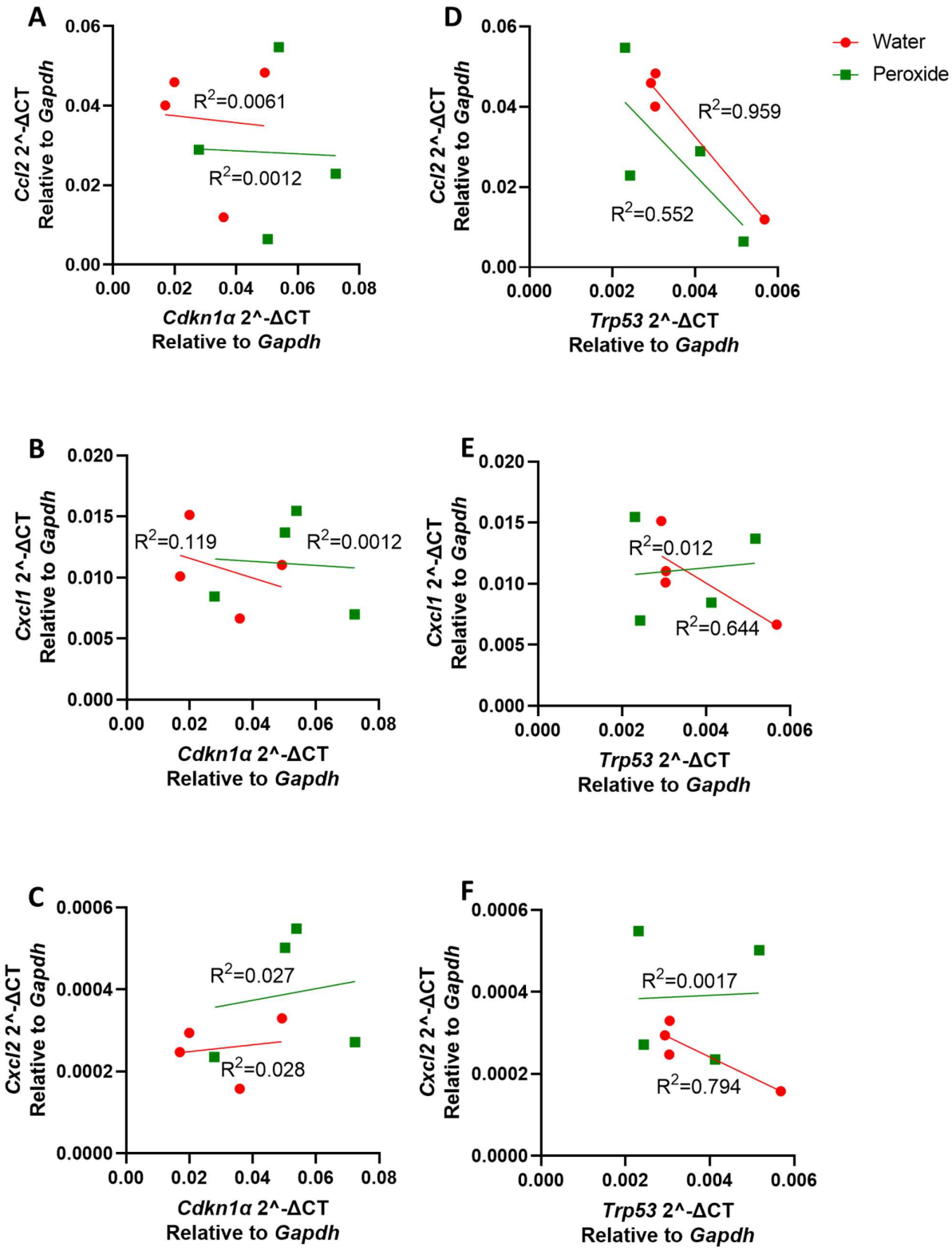

Figure 5.14: Association between markers of senescence and selected chemokines using qPCR.

Each dot represents an individual experiment containing 3 wells of a 12 well plate. Lines represent results of simple linear regression. Samples that received peroxide are shown in green, samples that received water (controls) shown in red. R^2 as shown.

A: XY plot comparing *Ccl2* relative to *Gapdh* and *Cdkn1*α relative to *Gapdh.* Association in water samples R^2 =0.0061, in peroxide samples 0.0012.

B: XY plot comparing *Cxcl1* relative to *Gapdh* and *Cdkn1*α relative to *Gapdh.* Association in water samples R^2 =0.119, in peroxide samples 0.0012.

C: XY plot comparing *Cxcl2* relative to *Gapdh* and *Cdkn1*α relative to *Gapdh.* Association in water samples R^2 =0.028, in peroxide samples 0.027.

D: XY plot comparing *Ccl2* relative to *Gapdh* and *Trp53* relative to *Gapdh.* Association in water samples R^2 =0.959, in peroxide samples 0.552.

E: XY plot comparing *Cxcl1* relative to *Gapdh* and *Trp53* relative to *Gapdh.* Association in water samples R^2 =0.644, in peroxide samples 0.012.

F: XY plot comparing *Cxcl2* relative to *Gapdh* and *Trp53* relative to *Gapdh.* Association in water samples R^2 =0.794, in peroxide samples 0.0017.

5.12 Previously published data regarding the change of expression biliary targets in injury

Previously published data may also be relevant to the assessment of change in expression of the investigated targets described in this chapter.

Rodrigo-Torres and co-workers presented microarray data in 2014 in Hepatology investigating the role of BEC in replenishing injured hepatocytes in multiple dietary injury models[217]. To isolate BEC, the Hnf1βCreER^{Yfp} mouse model, was used, selecting for cells with yellow fluorescent protein (YFP) expression using FACS [217]. As part of their research this group produced micro-array data using mice that had received DDC or CDE diet, in addition to controls. Finally, they also performed micro-array analysis on YFP negative cells, representing cells which survived the digestion and filtration steps they described, but were not selected by FACs. This population has been described as non-parenchymal cells (NPC) for the purposes of this study. It is important to note that this population is unlikely to contain hepatocytes.

This data was re-analysed to assess the expression of the six assessed targets namely *Sctr*, *Tff2*, *Cd44*, *Ccl2*, *Cxcl1*, and *Cxcl2*, using the limma package on R software. The results of this are presented in Figure 5.15. The *Cxcl2* gene was the most upregulated gene when comparing BEC from mice treated with DDC diet to controls, and mice that received CDE diet, Figures 5.15A and B. Despite this, neither of these comparisons demonstrated a statistically significant difference in *Cxcl2* expression. When comparing with the NPC, control mice had significantly lower expression of *Cxcl2.* This was no longer the case when comparing BEC from mice treated with DDC diet and the NPC population, Figures 5.15C and D. The other 5 potential targets have also been considered in this analysis. *Sctr* and *Tff2* had significantly higher expression in BEC in both controls and mice that received DDC diet compared with NPC population.

Figure 5.15 Analysis dataset GSE51389, using R software.

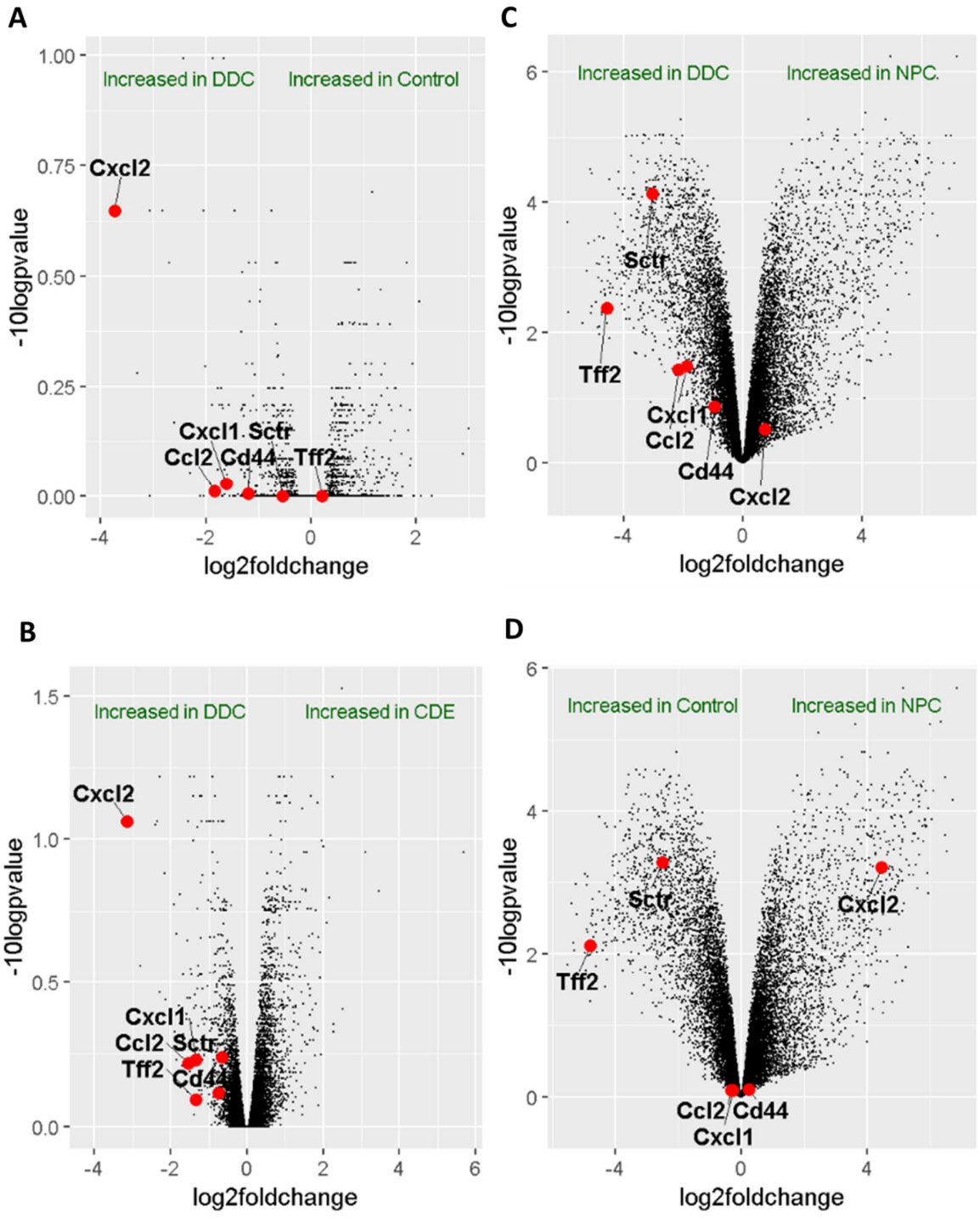

Figure 5.15 Analysis dataset GSE51389, using R software.

Comparisons are made between four groups,

BEC from mice who received DDC diet (n=3), mice who received CDE diet (n=3), or controls (n=2). NPC sample was also obtained from control mice (n=3). All plots compare –log10pvalue on the y axis and log2foldchange on the x axis. The six genes of interest are annotated, and dots are in red. Each black dot represents an individual gene.

A: Comparison between mice who received DDC and controls.

B: Comparison between mice who received DDC and CDE.

C: Comparison between mice who received DDC and NPC.

D: Comparison between mice who received controls and NPC.

NPC = Non-parenchymal cells.

5.13 Discussion

The fundamental assumption underlying this section of work is that the optimal way to develop a homing mechanism to facilitate the migration of transplanted HPCs to biliary ducts would be through the identification of a ligand specific to BEC, which ideally is also upregulated in response to injury. As such, in this chapter candidate ligands identified from the literature were examined for ductal and biliary injury specificity.

The first half of this chapter uses immunofluorescence to assess the expression of the proteins SCTR, CD44 and TFF2 in the biliary ducts, across a range of murine injury models. The second half of this chapter pertains to the assessment of three chemokines as potential candidates for homing. In contrast to the first section, given that chemokines are excreted from cells, qPCR was chosen as the method of assessment.

Sample/study limitations

Before discussing the results in detail there are some important caveats which should be noted, these are outlined alongside the mitigations that were made to compensate for these limitations where possible. The tissue samples from the models analysed were collected by different researchers at different times, as such it is acknowledged that there may be some inherent variability between samples. One key example of this is the heterogeneity in fixation time which was kept at 6 hours for samples collected for the mice used for the duration of this thesis. Unfortunately, the fixation time for historical samples was not available and may have been different. Additionally, as is a common limitation for animal studies, particularly using genetically modified strains, the ages of mice could not be matched between all the different groups studied. Finally, the *Krt19Cre^{ER}Mdm2 $^{fl/fl}$ Rag2$^{-/-}$ Il2rg$^{-/-}$* model is an immunocompromised strain, whilst the CCL_4 and MCD diet models used immunocompetent mice.

To mitigate against these possible confounding agents, a separate control group of mice was added to compare with the immunocompetent mice. Additionally, the algorithms used to assess expression by immunofluorescence analysis were based on the background expression of each individual image, thus reducing the risk of a

group of mice with higher or lower background brightness immunofluorescence skewing the results. Changes in background could occur due to changes in the efficacy of the antibody or staining process due to changes in fixation periods, for example. The only data which did not use this individual image background expression threshold approach was produced by QuPath analysis, in which identification of KRT19 and CD44 positive cells was automated by following QuPath training. QuPath analysis has been described in more detail in section 4.7. This analysis was limited to assessing CD44 expression in the *Krt19Cre^{ER}Mdm2 $^{fl/fl}$ Rag2$^{-/-}$ Il2rg$^{-/-}$* model, Figure 5.6.

The extrahepatic ducts are an important part of the biliary tree and are frequently affected in cholangiopathies. There are reports of performing immunohistochemistry in the extrahepatic ducts [136]. This was not possible for the analysis of SCTR, CD44 and TFF2 expression, due to reliance on previously obtained samples where extrahepatic ducts had not been collected. During the experiments assessing chemokine expression, the extrahepatic ducts were included. Extraction of intra and extrahepatic ducts were performed as described in Sections 4.9 and 4.10.

The human control samples used in this study were sourced from livers which had been rejected for transplantation. These livers are often placed on ice for a varying number of hours before being processed and chunks being fixed in formalin. In contrast livers which were obtained from patients with PSC and PBC were explanted livers and are likely to have been placed directly into a fixation medium. As was the case for murine samples, there may be differences therefore in fixation time between the groups. To reduce the impact of this variability control livers were selected on the basis of being donated from DBD donors, as it has been well described that DCD donor livers are more associated with biliary complications [99, 241]. Additionally, livers with low time on ice were selected, to minimise the influence of this.

There are limitations to the use of immunofluorescence in determining changes in expression of proteins. Whilst accurate spatial information is provided with regards to the expression pattern of assessed proteins, immunofluorescence is generally described as being semi-quantitative. The expression of proteins does not reliably correlate to the fluorescence signal returned from the tissue[242]. The %area ductal expression has been used as a semi-quantitative means of determining changes in expression in this chapter with the knowledge that the proteomic analysis described in

chapter 6 would be performed. Alternate methods of analysis would include RNA in situ hybridisation, and spatial transcriptiomics, however both of these methods would assess RNA expression, which may not reflect the expression at the protein level of the targets assessed. Enzyme-linked immunosorbent assay (ELISA) of protein isolated from ducts may have been an alternative or complimentary method to provide a more quantitative assessment of the expression of targets in ducts however given that mass spectrometry was to be performed the added value of this was felt to be limited.

Finally, it was challenging to identify a reliable antibody to the three chemokine candidates identified from the literature. Indeed, an antibody to *Ccl2* exists, but did not yield any clear staining in the *Krt19Cre^{ER}Mdm2 $^{fl/fl}$ Rag2$^{-/-}$* model. This result was felt to be due to technical limitations in the tissue samples available, given the exceptionally high expression of *Ccl2* reported in RNA sequencing analysis of mice treated with DDC diet in a previous study[149]. Therefore, it was elected to depend mainly on qPCR results for the assessment of the chemokine targets.

Plasma membrane candidate outcomes

The first candidate investigated was SCTR. As outlined in section 1.3 SCTR plays an important role in the regulation of bile flow. There is also somewhat conflicting evidence regarding the expression of SCTR in biliary injury [98, 187, 190]. The results presented in this chapter indicate that SCTR is specifically expressed in the BEC in mice (Figure 5.1). Although this result was largely expected based on its functional role and previous literature[37, 243], it confirmed that use of immunocompromised murine models does not influence the expression of SCTR. In both murine and human liver injury, expression of SCTR did not change significantly (Figure 5.2 and Figure 5.3), for this reason it was not considered to be an optimum target. In human samples there appeared to be areas of expression out with the ducts. This has not been reported previously and could be technical, but for the purposes of this study it also makes SCTR a less attractive ligand for targeting. *Sctr* was not within the detectable limits on qPCR in the *in vitro* model of biliary injury and therefore could not be assessed.

CD44 was the next candidate assessed. It has previously been used as a marker of BEC, particularly for the illusive hepatic progenitor cell[198, 244]. Previously it was

suggested that CD44 was not present in hepatocytes, but was in BEC and other resident hepatic cells[198]. It became clear that increased expression of CD44 was seen in the non-ductal but not clearly in the ductal areas in the *Krt19Cre^{ER}Mdm2 $^{fl/fl}$ Rag2$^{-/-}$* model (Figure 5.4). In contrast to previous work, increases in expression of CD44 were primarily seen in cells out with the ducts and not in the BEC themselves[198]. For this reason, it was not deemed necessary to assess CD44 in other murine injury models. It was also noted however that an infiltration of CD44 positive cells was seen in the hepatic parenchyma following biliary injury. CD44 is a receptor for HA, which is an important component of the extracellular matrix. Through this interaction it has been suggested that cell migration is facilitated[245, 246] . This raised the possibility that the increased presence of CD44 positive cells (Figure 5.4), represents a cell population which were migrating to the ducts following injury. To assess this hypothesis an algorithm was developed using QuPath software. This allowed the assessment of the distance of CD44 positive cells to the closest KRT19 positive cell, representing a BEC[236]. There was no evidence that CD44 positive cells found in injured mice were closer to ducts than in non-injured mice, Figure 5.5. Whilst the inverse of this finding would not have conclusively demonstrated that CD44 is important for migration to the biliary ducts, it may have highlighted a subpopulation of cells that were developing adjacent to or migrating to the ducts. It may have been possible then to extract these cells using flow cytometry and investigate their phenotype to identify their plasma membrane complement and identify receptors that are essential for migration to the biliary ducts.

In human tissue, CD44 had significantly higher expression in the periductal and non-ductal areas of control samples than PSC samples taken from the peripheral liver (Figure 5.6). This result was in complete contrast to the findings in the mouse model (Figure 5.4 and Figure 5.5). The reasons for this discrepancy remain unclear, however it may be due to differences in chronicity of the mouse and human disease. Particularly, differences in the degree of fibrosis may exist between species and therefore the extracellular matrix, which may lead to changes in the ability of cells to infiltrate and migrate into these tissues. Ultimately CD44 was not an appropriate target primarily due to increased expression out with the ducts. Using CD44 as a target for a homing system would likely result in homing to sites other than the ducts.

TFF2 was also assessed by immunofluorescence and was shown to be non-specific for the biliary ducts, also being expressed in the bile canaliculi (Figure 5.7). This rendered it an unattractive target and so was not investigated further. Previous studies have indicated that canalicular expression of TFF2 occurs in hepatocellular injury [192], this data indicates for the first time TFF2 may also be produced by hepatocytes in homeostasis and in biliary injury.

Chemokine candidate outcomes

Chemokines are small molecules integral in the process of chemotaxis, particularly of immune cells. In the biliary tree CXCL1, CXCL2 and CCL2 have been implicated in the migration of cells, in particular *Ccl2* gene expression has been shown to increase significantly in BEC following biliary injury[149].

In this chapter, different cellular compartments were extracted to assess the expression of these chemokine candidates. I elected not to perform a percoll spin on the hepatocyte compartment, a step which is ordinarily included in hepatocyte isolation protocols to enhance population purity, section 1.8. Omitting this spin intended to retain cells which are interspersed within the hepatic parenchyma that may locally contribute to the production of these candidate chemokines. The impact of this protocol modification has been further assessed in the supplementary Figure S5.1, which compares the expression of genes in paired samples of hepatocytes that did and did not undergo percoll centrifugation. The results demonstrate that both *Krt19* and *Cxcl2* were consistently lower following percoll centrifugation, and these genes were closely associated. These results could indicate that there are a population of cells expressing *Krt19* which also express *Cxcl2* which are being removed following percoll centrifugation, in the liver the most likely explanation for this is contamination through ductal cells. Thus, it was a more conservative option not to perform a percoll centrifugation on hepatocytes, making the findings that CXCL2 a specific target more robust.

The results presented in this chapter have demonstrated that *Cxcl2* is highly specific to the ducts (Figure 5.8C). Whilst a significant increase in the expression of *Cxcl2* was not identified in the tissue samples, nor in the *in vitro* model, an association between the expression of *Cxcl2* and markers of apoptosis (rather than senescence) was identified (Figure 5.13). The importance of this for a cell homing mechanism is

that cells, in theory, would be most attracted to dying cells, which is likely to be desirable as they can replenish areas in which BEC are being lost.

Given that CXCL1 and CXCL2 are primarily neutrophil attractants[247, 248], it is not unexpected that apoptotic cells would produce more of these proteins to ensure that phagocytic neutrophils can localise to BEC in anticipation of removing debris following the death of the cell[249, 250].

Ccl2, *Cxcl1* and *Cxcl2* have all been associated with the senescence associated secretory pathway (SASP), therefore the lack of associations identified between these chemokines and markers of senescence was surprising [251]. This could be due to the time frame investigated, given that injury was initiated 24 hours before collection of the sample.

There are limitations to the value of these results as RNA analysis of senescence and apoptosis are known to be less reliable in detecting cellular apoptosis and senescence than proteomic analysis. Ideally the chemokines, markers of apoptosis and senescence would be measured and compared on the proteomic level[252, 253].

There is a wealth of data now available, which is of relevance to the candidates investigated in this chapter. The work of Pepe-Mooney and co-workers has been discussed in the introduction, section 1.12 [149], with the work of Rodrigo-Torres and co-workers re-analysed in section 5.12[217]. Although no statistically significant change in expression was identified in BEC extracted from mice who had received DDC diet compared with controls *Cxcl2*. This was also the case comparing DDC diet BEC to CDE diet BEC. These results provide further evidence of higher expression specifically following biliary injury and not following hepatocellular injury induced by CDE.

Taken together the results of this chapter have demonstrated that *Cxcl2* is a specific marker in the duct using qPCR. Although not statistically significant, there was higher expression of *Cxcl2* in injured intrahepatic ducts than non-injured in the *Krt19Cre^{ER}Mdm2 $^{fl/fl}$ Rag2$^{-/-}$ Il2rg$^{-/-}$* model. Further to this, data from Rodrigo-Torres and co-workers have shown that *Cxcl2* is the most upregulated gene in mice who receive DDC diet[217]. Finally, there is a strong association between *Cxcl2* and markers of apoptosis in murine BEC *in vitro*. All these factors make Cxcl2 the most attractive ligand for exploiting an enhanced homing mechanism, therefore this candidate

was selected to progress with. This is described further in Chapter 7 with the production of a line of human HPCs which express CXCR2.

5.14 Conclusion

CXCL2 is specifically expressed within the bile ducts in the liver and genetic expression is upregulated in biliary injury.

Supplementary Figure S5.1 Comparison of gene expression in hepatocytes which did and did not undergo percoll centrifugation.

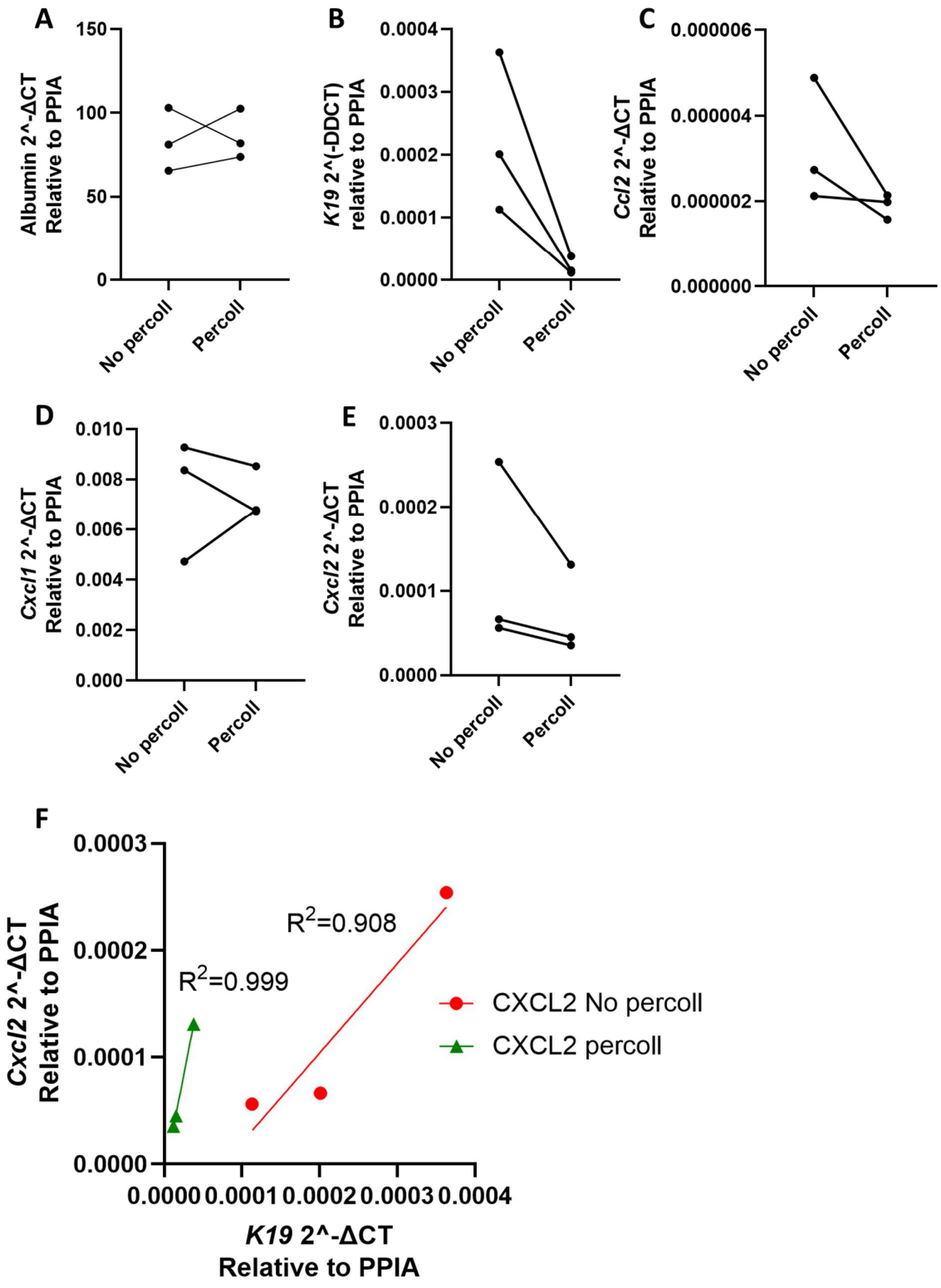

Supplementary Figure S5.1 Comparison of gene expression in hepatocytes which did and did not undergo percoll centrifugation.

Each represents a biological replicate. Figures A-E lines indicate paired samples, coming from the same mouse. In Figure F lines indicate line of best fit through linear regression. R^2 as shown.

A: Comparison of expression of *Alb* relative to *Ppia* in hepatocytes that did and did not undergo percoll centrifugation.

B: Comparison of expression of *Krt19* relative to *Ppia* in hepatocytes that did and did not undergo percoll centrifugation.

C: Comparison of expression of *Ccl2* relative to *Ppia* in hepatocytes that did and did not undergo percoll centrifugation.

D: Comparison of expression of *Cxcl1* relative to *Ppia* in hepatocytes that did and did not undergo percoll centrifugation.

E: Comparison of expression of *Cxcl2* relative to *Ppia* in hepatocytes that did and did not undergo percoll centrifugation.

F: XY plot comparing *Krt19* and *Cxcl2* expression relative to *Ppia,* in hepatocytes which did and did not undergo percoll centrifugation

Chapter 6: Discovery approach

6.1 Introduction:

The interaction between a cell and its external environment is significantly influenced by the cell's plasma membrane, and more specifically, the proteins present within the plasma membrane. For this reason, the extraction and identification of plasma membrane proteins has been of interest to a range of researchers. Insights into the plasma membrane composition of specific cell populations may help to characterise that cell population. From a clinical perspective, detection of plasma membrane proteins up-regulated in disease may allow the production of targeted drug or cellular therapies.

In the context of cell therapy for the cholangiopathies, it would be of interest to identify plasma membrane proteins which are specific to BEC and upregulated in injury. Such a protein could be exploited for cell homing, as described in the introduction.

There have been rapid advances in genomic analysis methods in recent years; RNA sequencing at single cell resolution is now widely available. This level of precision has not been replicated in the proteomic field to date. In the study of plasma membrane proteins, the limitation in protein detection is compounded by the fact that plasma membrane proteins constitute a small proportion of total cellular proteins, estimated 9-13%[177].

Given the disparity in the detection ability between genomic and proteomic techniques, it would be tempting to use genomic data as a surrogate for proteomic analysis. Whilst the concept of translation of mRNA to polypeptide chains at the ribosome creates a theoretically linear relationship between the production of mRNA and the production of peptides, this does not manifest in practice[254]. Proteins are degraded at differing rates, some proteins are excreted from the cell, whilst others remain; these processes contribute to the true cellular abundance of a protein, in addition to, and independent of the translation process[255].

Both proteomic and genomic analyses assess the level of their respective units at a specific point in time. This introduces a further layer of inaccuracy in the use of genomic analysis when used as a surrogate for proteomic analysis, as states of gene expression may be transient or persistent, having varied effects on the final abundance of a protein[256].

In the past 40 years, several methods of plasma membrane isolation for proteomic analysis have been developed. The inherent differences in density and solubility of

subcellular compartments have been exploited by differential and density gradient centrifugation. Membrane proteins are embedded in a phospholipid bilayer and therefore, are less dense than proteins in other cellular compartments, for example, in the cytoplasm[218].

Targeting ubiquitous or common features of the extracellular component of plasma membrane proteins, such as terminal amine groups which are often external in plasma membrane proteins, have allowed the development of capture techniques in which plasma membrane proteins are tagged with a compound prior to cell lysis, and subsequently separated from non-plasma membrane proteins using the tag.

The challenge implicit in the isolation of plasma membrane proteins is the isolation of adequate levels of protein for analysis. This problem is deepened by the fact that BEC make up approximately 5% of the cellular population of the liver.

The aim of this chapter is to identify proteins specifically expressed on the plasma membrane of BECs during biliary injury. To meet this aim, protein was extracted from the ductal and hepatocellular compartments of the liver in the *Krt19^{CreER}MDM2$^{fl/fl}$Rag2$^{-/-}$IL2rg$^{-/-}$* model in biliary injury and in normal controls, comparing the results to identify the desired proteins.

6.2 Gradient ultracentrifugation and differential centrifugation techniques do not adequately enrich plasma membrane proteins.

To extract plasma membrane proteins, three methods were employed: biotinylation performed using a kit purchased from Abcam, gradient ultracentrifugation as described by Suski and co-workers in 2014 [218] and differential ultracentrifugation as described by Lund et al in 2009 [219]. The gradient ultracentrifugation technique permitted the extraction of plasma membrane proteins (PM) and additionally plasma membrane associated membranes (PAM).

Initially experiments were undertaken using primary isolated hepatocytes from wild type mice. Figure 6.1A displays the mass of protein obtained from all the hepatocytes from a single murine liver using different techniques. The biotinylation technique requires isolated hepatocytes to go through Percoll centrifugation to remove any dead cells as described in section 4.8 on hepatocyte isolation, as dying cells with permeable membranes would allow biotin to enter the cells and bind to non-membrane proteins.

Conversely, as gradient ultracentrifugation and differential ultracentrifugation depend on differences in density between subcellular compartments, there is no necessity to exclude dying cells and therefore a Percoll spin was not performed. For this reason, significantly more hepatocytes from a single liver were available for the gradient ultracentrifugation and ultracentrifugation techniques compared with biotinylation. This may in part explain the lower protein yield produced using the biotinylation technique as demonstrated in Figure 6.1A. Figure 6.1B adds weight to this notion by showing protein produced per hepatocyte to be greater in the biotinylation technique than the gradient ultracentrifugation technique although less than with differential ultracentrifugation.

To assess the effectiveness of the different techniques in isolating plasma membrane proteins, qualitative mass spectroscopy was performed. Samples were sent as two separate batches to the mass spectroscopy facility: initially, one ultracentrifugation and one gradient plasma membrane sample (U1 and PM1 respectively), followed by a whole cell lysate sample and replicates of the first samples (W, U2 and PM2). Unfortunately, enough protein could not be produced to perform mass spectroscopy using the biotinylation technique.

The efficiency of isolating plasma membrane proteins across the techniques was assessed by comparing identified proteins with the Gene Ontology (GO) term plasma membrane (GO:0005885) and the predictor of transmembrane helices, TMHMM [257], Figures 6.1C and 6.1D respectively. There was a trend towards higher proportion of plasma membrane proteins obtained from the gradient ultracentrifugation compared with whole protein and differential ultracentrifugation according to both GO term and TMHMM comparisons.

Within the limits of low experimental replicates, the overall number of plasma membrane proteins did not appear to be different between techniques according to the plasma membrane GO terms, as reflected by Figure 6.1E.

Whilst there was no evidence of increased yields of plasma membrane proteins, it was also important to define the similarities between the proteins detected by each technique. 46 of the 1738 proteins were identified in all five samples. There was limited agreement between replicates using both techniques: of the 1062 proteins identified

on ultracentrifugation, only 228 were shared between samples and only 98 of the 892 proteins identified by gradient ultracentrifugation were shared between samples.

There was also limited agreement between techniques and replicates when considering plasma membrane proteins only. Figure 6.1F demonstrates the distribution of identified plasma membrane proteins across the gradient ultracentrifugation samples and the whole cell lysate control. 52 plasma membrane proteins were detected only in the whole cell lysate sample. There was also poor agreement between replicates with 16 of the 182 plasma membrane proteins identified by gradient ultracentrifugation being shared between samples.

Similarly, 41 plasma membrane proteins were identified in the whole cell protein sample which were not identified in the two-ultracentrifugation sample. 37 plasma membrane proteins were detected in both ultracentrifugation of the 192 plasma membrane proteins identified across both samples.

The methods of plasma membrane extraction yielded masses of proteins as shown in figure 6.1A and B. Gradient ultracentrifugation provided a higher proportion of plasma membrane proteins but not a higher quantity of plasma membrane proteins compared to whole cell lysate and ultracentrifugation. Finally, as shown in figures 6.1F and G several proteins were only detected in whole cell lysate.

Figure 6.6.1 Comparison of biotinylation, gradient ultracentrifugation and ultra-centrifugation techniques.

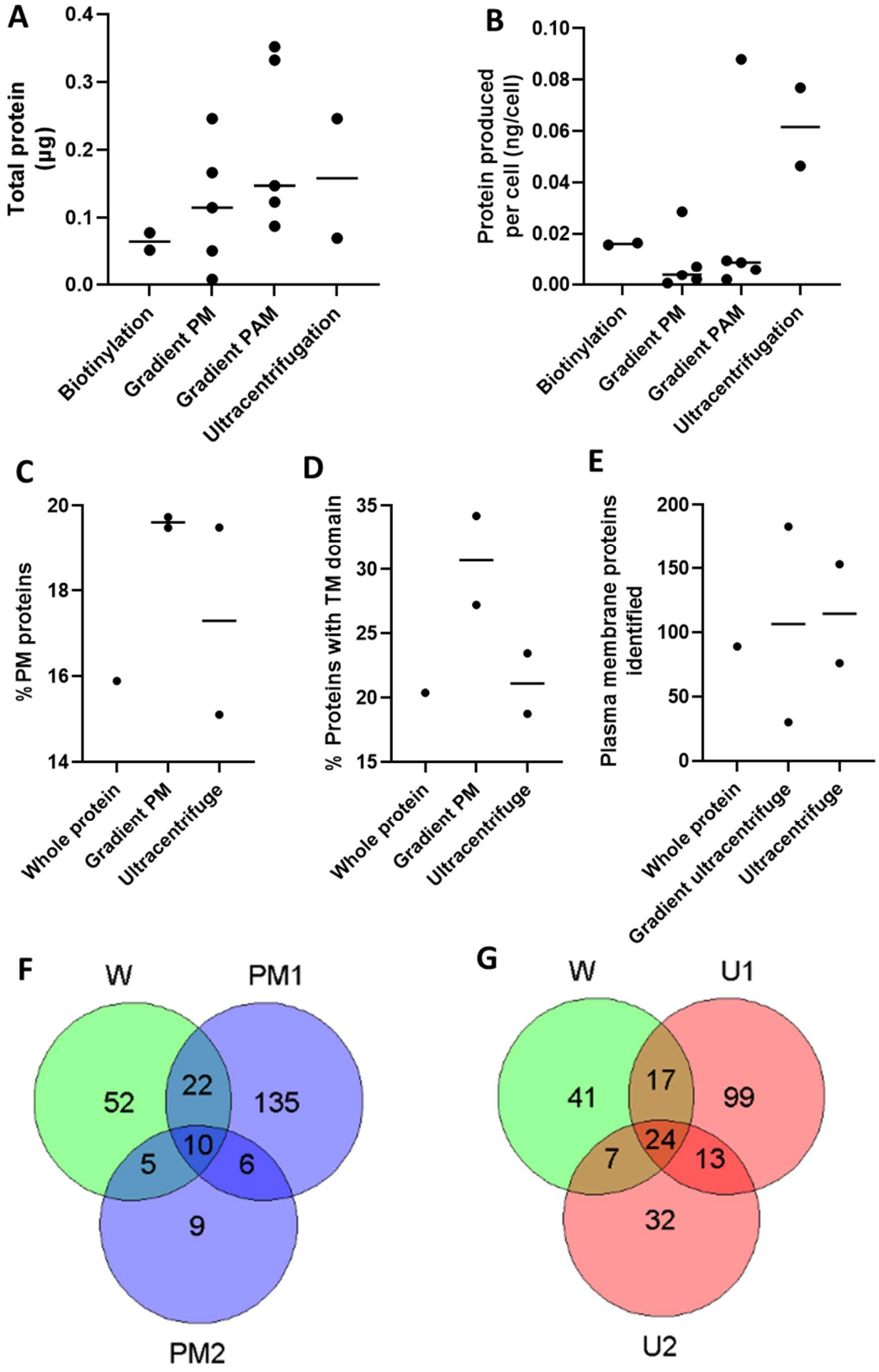

Figure 6.1; Comparison of biotinylation, gradient ultracentrifugation and ultracentrifugation techniques.

Figures 6.1A-E each dot represents protein obtained from all hepatocytes from a single mouse. Horizontal lines represent medians.

A: Total protein produced from hepatocytes obtained from a single wild type mouse. n=2-5 mice. Median protein mass obtained from; Biotinylation 0.065µg, Gradient PM 0.115 µg, Gradient PAM 0.147µg and Ultracentrifugation 0.158µg.

B: Protein obtained per hepatocyte from wild type mice using different techniques, n=2-5 as shown. Median protein per cell obtained from; Biotinylation 0.016ng, Gradient PM 0.004ng, Gradient PAM 0.009ng and Ultracentrifugation 0.062ng.

C: Percentage of identified proteins which are plasma membrane proteins on qualitative mass spectroscopy. n=1-2 as shown. Whole cell lysate 15.89%, gradient PM median 19.61%, ultracentrifugation median 17.30%.

D: Percentage of identified proteins with at least one transmembrane component as defined by TMHMM. n=1-2 as shown. Whole cell lysate 20.39%, gradient PM median 30.71%, ultracentrifugation median 21.10%.

E. Total number of plasma membrane proteins identified. Whole cell lysate 89, ultracentrifugation medina 114.5, gradient PM median 116.5.

F. Venn diagram demonstrating the number of proteins in each of the 5 samples sent to mass spectroscopy.

G. Venn diagram demonstrating the number of plasma membrane proteins in each of the 5 samples sent to mass spectroscopy.

Gradient PM= plasma membrane proteins obtained from the gradient technique, Gradient PAM = plasma membrane associated membranes proteins, PM1= Gradient PM sample 1, PM2 = Gradient PM sample 2, U1 = Ultracentrifugation sample 1, U2=Ultracentrifugation sample 2

6.3 Adequate protein for mass spectroscopy can be extracted from biliary duct isolation and hepatocyte isolation.

Concluding that in the context of a murine model, practicable biochemical methods of plasma membrane extraction such as biotin capture, gradient ultracentrifugation, and ultracentrifugation, do not reliably enrich the plasma membrane compliment of extracted proteins, it was elected to use a bioinformatics-based approach for the identification of plasma membrane proteins. Additionally, the knowledge that biochemical plasma membrane extraction methods were not identifying some of the proteins identified in whole cell lysate, suggested that these techniques could introduce bias into the study.

The *Krt19Cre^{ER}Mdm2$^{fl/fl}$Rag2$^{-/-}$ Il2rg$^{-/-}$* model induced by three doses of tamoxifen followed by 48 hours of DDC diet was used for mass spectroscopy experiments. Hepatocytes, intrahepatic ducts, and extrahepatic ducts were obtained from mice following induction of injury (injured) and in controls (uninjured). Figure 6.2 demonstrates the mass of protein extracted from each of these samples. All concentrations obtained were deemed adequate for mass spectroscopy. This allowed 6 experimental conditions to be studied: hepatocytes, intrahepatic, and extrahepatic ducts from injured and uninjured mice. Three replicates were obtained from each of the conditions described.

Figure 6.6.2 Concentrations of protein obtained from samples.

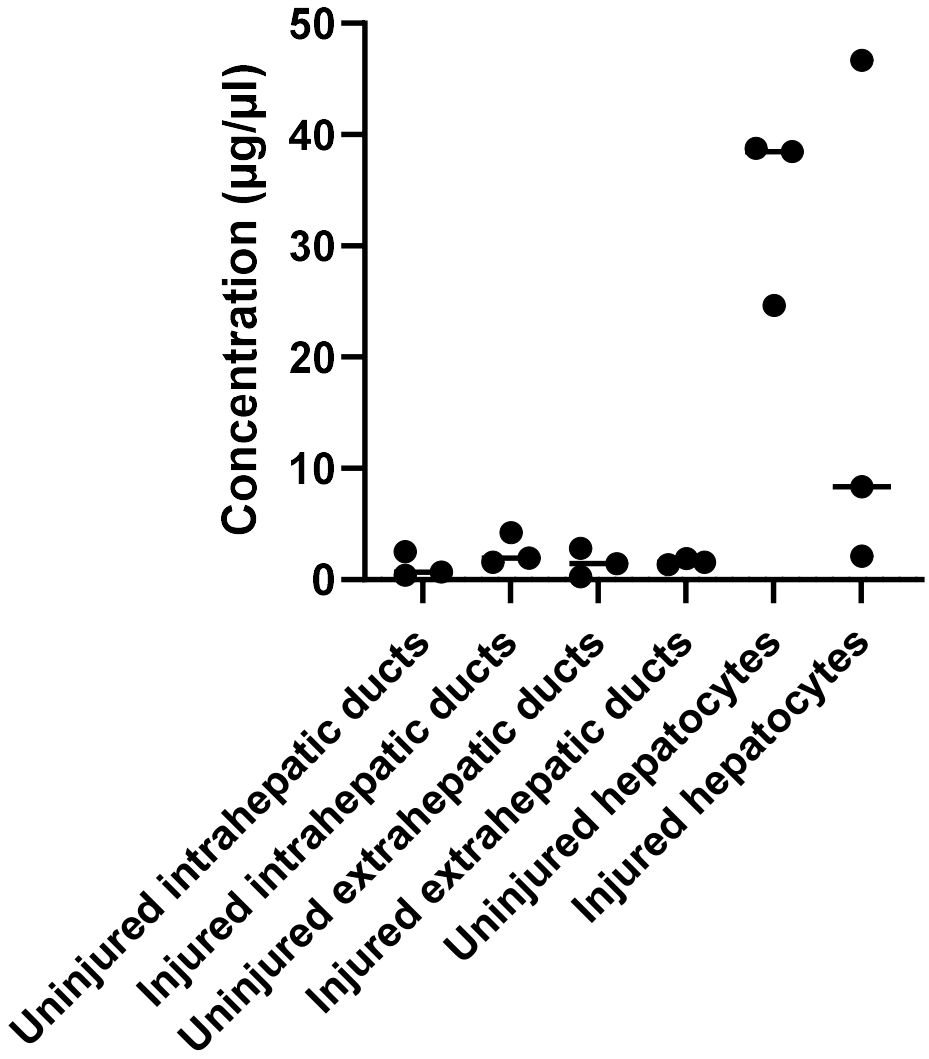

Figure 6.2: Concentrations of protein obtained from samples.

Dots represent a biological replicate; horizontal lines represent medians. n=3 as shown.

Median concentration from; uninjured intrahepatic ducts 0.706, injured intrahepatic ducts 1.937, uninjured extrahepatic ducts 1.437, injured extrahepatic ducts 1.560, uninjured hepatocytes 38.46 and Injured hepatocytes 8.360.

6.4 Transformation of proteomic samples using log function and normalisation

In total, 4509 proteins were identified between the intra and extrahepatic biliary duct samples, whilst 3358 proteins were identified in the hepatocyte samples. There were 2844 proteins which were detected in at least one sample of each of the 6 studied conditions.

Proteins not identified in every individual sample were excluded, leaving a total of 1902 proteins.

Log2 transformation was performed on protein abundance to account for the inherent heteroscedasticity within samples, thereby reducing the disparity in variance in the most compared with the least abundant proteins detected. Figure 6.3A plots standard deviation and mean for each individual protein detected in each condition outlined above prior to log transformation. The blue line demonstrates the best fit using linear modelling (geom_smooth() function in R) for the data points, showing trend towards increasing standard deviation as mean abundance increases. Figure 6.3B shows the same data following log2 transformation, demonstrating an amelioration of the trend towards higher variance in more abundant proteins.

Following transformation, normalisation was performed using the quantile technique contained in the limma R/Bioconductor package [220, 258]. Figure 6.4A demonstrates the variability in the abundance of proteins across samples prior to normalisation, particularly within the ductal samples. As shown in Figure 6.4B, this resolves post normalisation.

Figure 6.6.3 Log transformation of protein samples

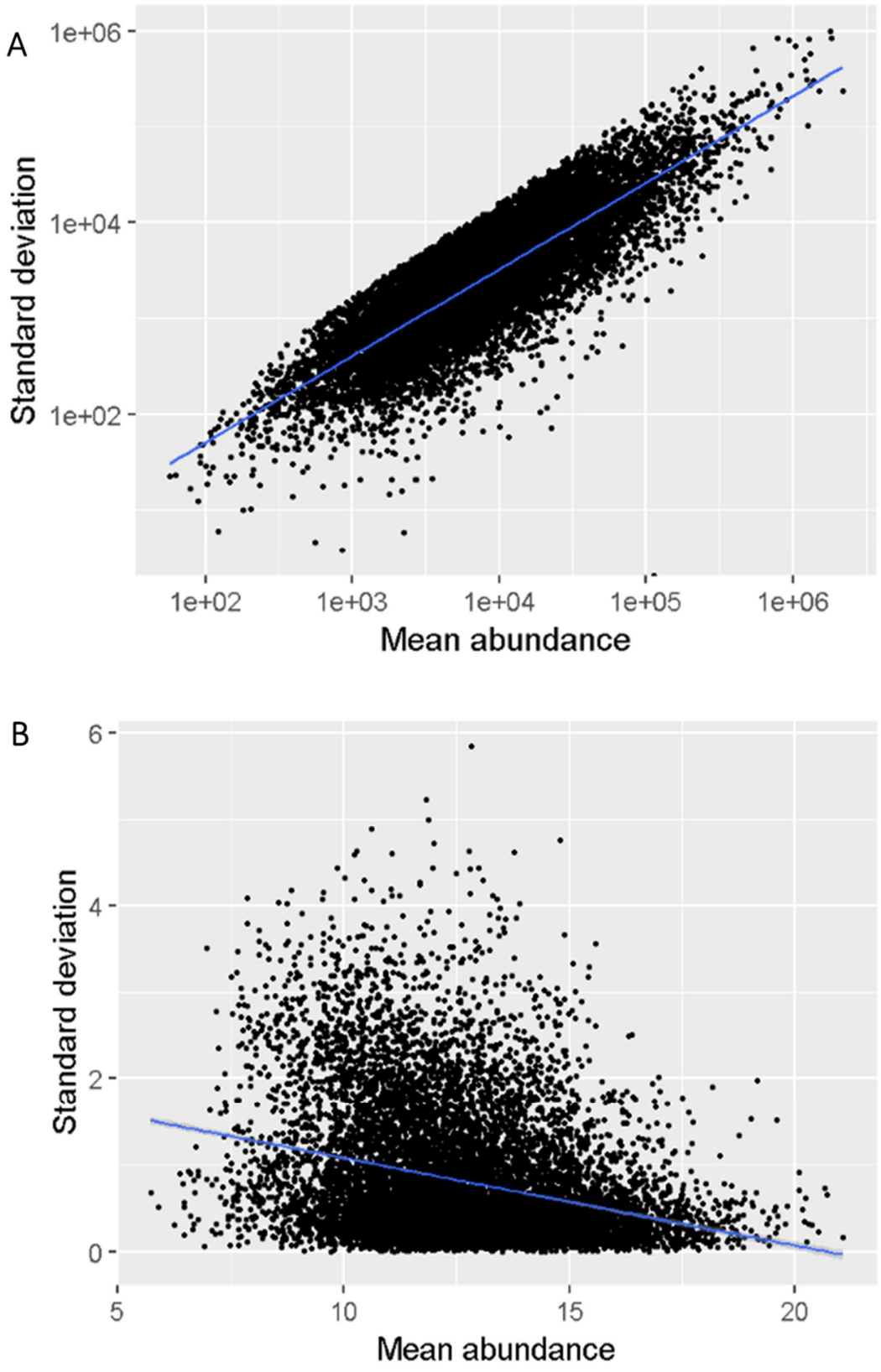

Figure 6.3: Log transformation of protein samples.

Each dot represents the mean abundance and standard deviation of a protein in a group of samples. Samples were grouped as follows; Uninjured intrahepatic ducts, injured intrahepatic ducts, uninjured extrahepatic ducts, injured extrahepatic ducts, uninjured hepatocytes, injured hepatocytes.

A: Samples prior to log transformation. The blue line represents best fit. X and Y axes are log scale.

B: Samples following log transformation. The blue line represents best fit.

Figure 6.6.4 Normalisation of protein samples.

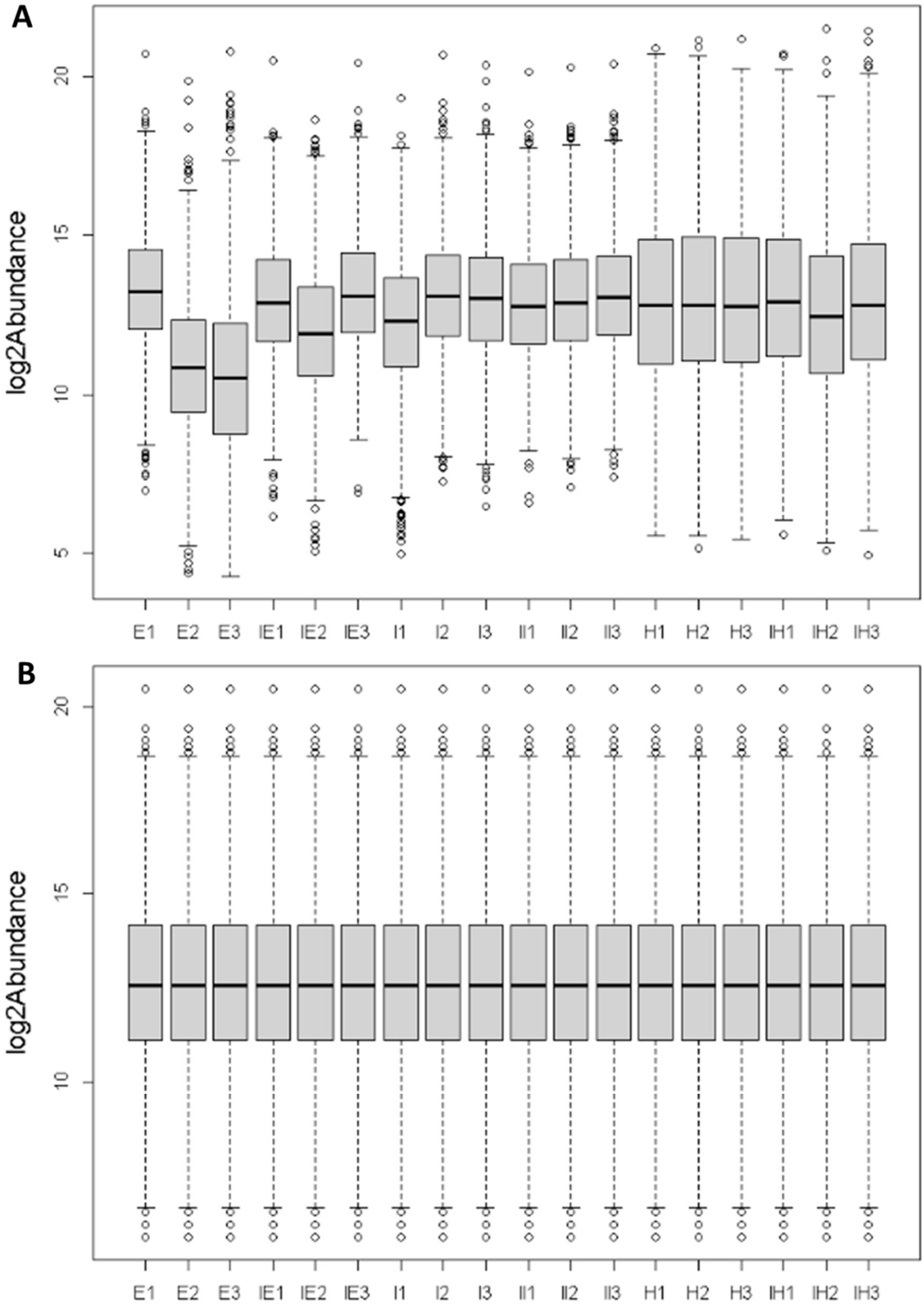

Figure 6.4: Normalisation of protein samples.

Each bar represents all the detected proteins in a single mass spectroscopy sample.

A: Samples prior to normalisation

B: Samples following normalisation

E= Extrahepatic ducts

IE= Injured extrahepatic ducts

I= Intrahepatic ducts

II= Injured intrahepatic ducts

H= Hepatocytes

IH = Injured hepatocytes

6.5 Principal component and unbiased clustering analysis of protein samples obtained.

To assess the variability within groups, unbiased hierarchal clustering was performed as shown in Figure 6.5A. In addition, a principal component analysis (PCA) was performed (Figure 6.5B).

On unbiased clustering five of the six intrahepatic duct samples cluster together with the uninjured intrahepatic duct sample 1 an outlier shown, I1. Within this cluster of five the injured and uninjured samples form subclusters, indicating reproducibility in the intrahepatic samples and a signature for injury.

All six hepatocyte samples formed a separate cluster, indicating a separate hepatocyte signature was identified. Within this cluster, two of the three injured hepatocyte samples form a cluster with injured hepatocyte sample 1 (IH1), joining a subcluster with the uninjured hepatocytes.

Extrahepatic duct samples showed less clear clustering, indicating a less clearly defined proteomic signature.

Similar findings are seen on the principal component analysis diagram shown in figure 6.5B. Principal component 1 is plotted on the x-axis and accounts for a much larger amount of the variance at 69%. Whilst there is significant inter-sample variation between both injured and uninjured extrahepatic ducts, and in uninjured intrahepatic ducts on the x-axis, there is also a trend for injured samples to be on the left of the graph with control samples on the right. This holds true for both hepatocyte and duct samples.

Clear separation is shown between the hepatocyte samples and the intra and extrahepatic duct samples primarily on the y-axis. The y-axis plots principal component 2, which accounts for only 16% of the total variance in the experiment, however.

One key influencer on appearances in both components of Figure 6.5B is the experimental design, which is a mixture of paired and unpaired samples. Injured extrahepatic and intrahepatic duct samples and uninjured intrahepatic and extrahepatic duct samples were obtained from the same mice. This complication will be addressed in the next section. Figure 6.5A illustrates the experimental design. Mice 1 through 6 had both intra and extrahepatic ducts extracted and have been shown in grey scale. Mice

who had hepatocytes isolated had no tissue taken, were therefore not paired and have been displayed in black.

Figure 6.6.5 Unbiased clustering of hepatocyte and biliary duct samples

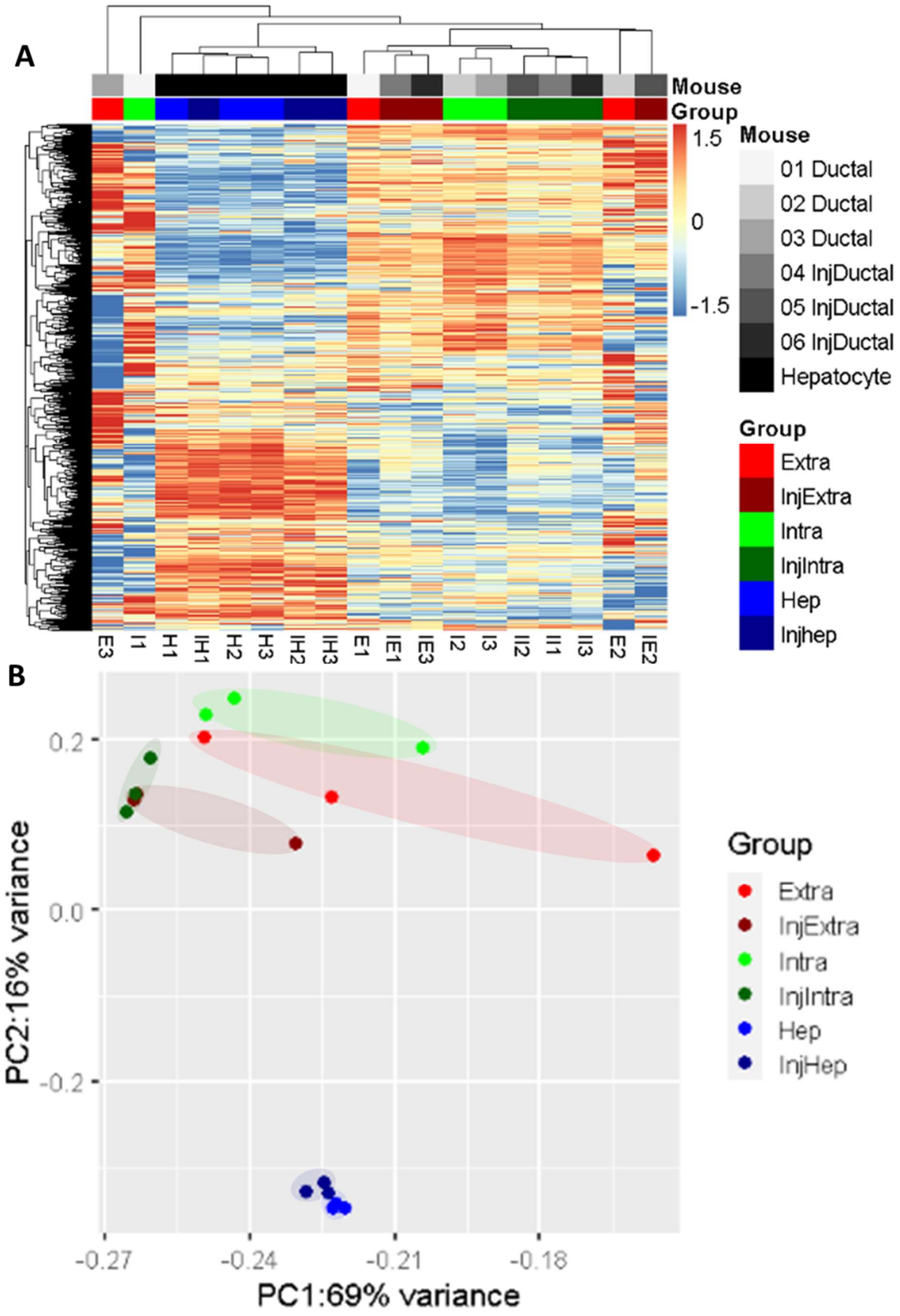

Figure 6.5: Unbiased clustering of hepatocyte and biliary duct samples

A: Heatmap demonstrating all proteins detected in hepatocyte and biliary samples. Colours represent normalised log2 abundance.

B: PCA plot of samples demonstrating clustering pattern.

Ductal = Intra and extrahepatic ducts extracted
InjDuctal= Injured intra and extrahepatic ducts extracted
Hepatocytes= Hepatocytes only extracted

Extra= Extrahepatic ducts
InjExtra= Injured extrahepatic ducts
Intra= Intrahepatic ducts
InjIntra= Injured intrahepatic ducts
Hep= Hepatocytes
InjHep = Injured hepatocytes

6.6 Identification of proteins significantly more abundant in intra or extrahepatic duct samples than in hepatocytes.

1902 proteins were detected to be present in all samples under all conditions. The abundance of these proteins was compared between samples and conditions to identify those which were specific to biliary ducts and upregulated in injury.

As mentioned in section 6.5, with the aim of reducing the number of mice used, injured extrahepatic and intrahepatic ducts were obtained from the same mice. This was also the case for uninjured intrahepatic and extrahepatic ducts. Thus, the experimental contained both paired and unpaired samples. This necessitated the production of a model which could account for correlation between paired samples. To this end, the limma function “duplicateCorrelation()” was employed to calculate the correlation between samples obtained from the same mouse. The correlation coefficient in this model was -0.0288 which was considered as low [259]. Nonetheless this correlation was accounted for in the model using the lmfitfunction().

Using the 1902 proteins which were detected in all samples in all conditions, a model was created using the limma() package in R.

Using the ebayes function, which calculates log-odds and t-statistics, comparisons were made between each of the samples under each condition[220]. Subsequently, I selected proteins significantly (adjusted p value<0.05 and fold change greater than 2) more abundant in injured extrahepatic ducts compared with injured hepatocytes (Figure 6.6A), and significantly more abundant in injured intrahepatic ducts compared with injured hepatocytes (Figure 6.7A).

Figure 6.6B displays a heatmap comparing expression across all samples in the 296 proteins identified as significantly upregulated in injured extrahepatic ducts. As portrayed in the figure, there are proteins which appear to have higher expression in injured intrahepatic ducts compared to injured and uninjured hepatocytes.

When injured intrahepatic ducts were compared with injured hepatocytes, 325 proteins were significantly upregulated in intrahepatic ducts, as shown in Figure 6.7B. The heatmap indicates the majority of these proteins also appear to have higher expression in the extrahepatic ducts.

In total, 240 proteins were significantly more abundant in injured extrahepatic and intrahepatic ducts compared with injured hepatocytes. The BEC marker KRT19 was identified amongst this list of proteins, which was reassuring.

Figure 6.6.6 Selection of proteins upregulated in injured extrahepatic ducts compared with injured hepatocytes

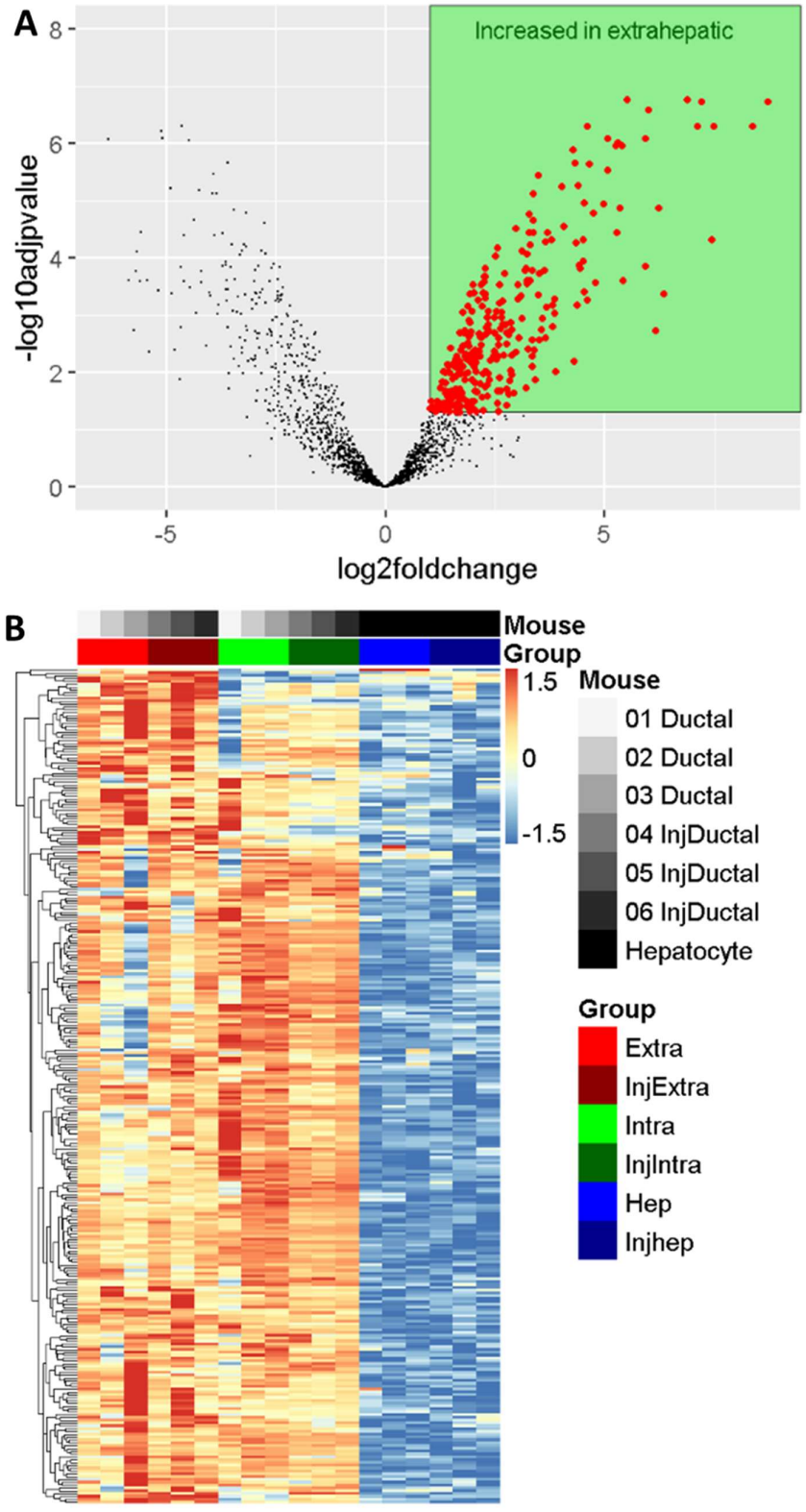

Figure 6.6: Selection of proteins upregulated in injured extrahepatic ducts compared with injured hepatocytes

A: Volcano plot comparing –log10pvalue (y axis) and log2 fold change (x axis). Proteins which an adjusted p-value>0.05 and a fold change greater than 2 are contained within the green box. 296 proteins in total were identified.

B: Heatmap demonstrating the relative normalised abundance of proteins contained within the green box in Figure 6.6A. Each row represents a single protein; each column represents a single sample from a single mouse.

Ductal = Intra and extrahepatic ducts extracted
InjDuctal= Injured intra and extrahepatic ducts extracted
Hepatocytes= Hepatocytes only extracted

Extra= Extrahepatic ducts
InjExtra= Injured extrahepatic ducts
Intra= Intrahepatic ducts
InjIntra= Injured intrahepatic ducts
Hep= Hepatocytes
Injhep= Injured hepatocytes

Figure 6.6.7 Selection of proteins upregulated in injured intrahepatic ducts compared with injured hepatocytes

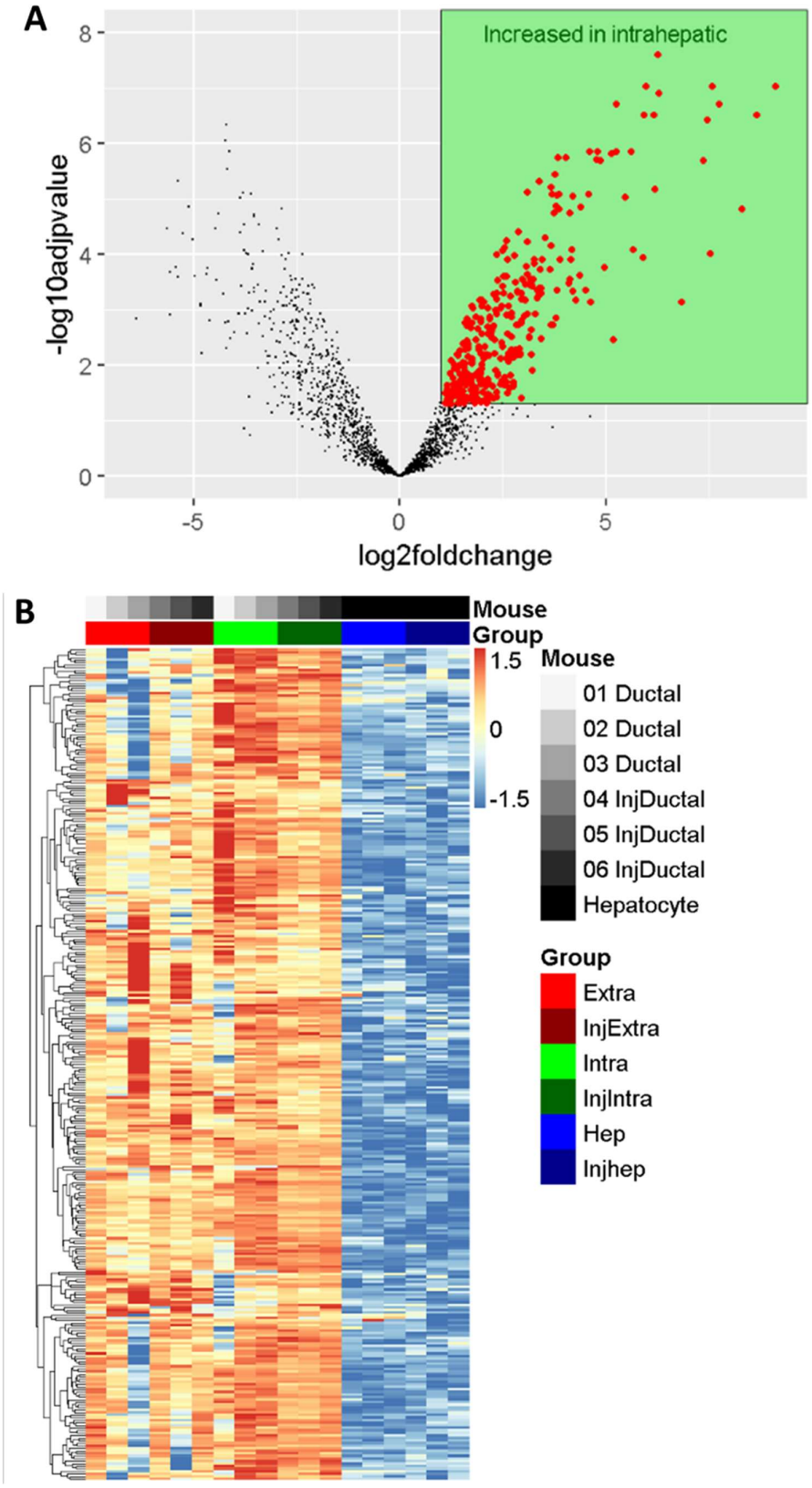

Figure 6.7: Comparison of protein abundance in injured hepatocytes and injured intrahepatic ducts.

A: Volcano plot comparing –log10pvalue (y axis) and log2 fold change (x axis). Proteins which an adjusted p-value>0.05 and a fold change greater than 2 are contained within the green box. 325 proteins identified in total.

B: Heatmap demonstrating the relative normalised abundance of proteins containing within the green box in Figure 6.7A. Each row represents a single protein; each column represents a single sample from a single mouse.

Ductal = Intra and extrahepatic ducts extracted
InjDuctal= Injured intra and extrahepatic ducts extracted
Hepatocytes= Hepatocytes only extracted

Extra= Extrahepatic ducts
InjExtra= Injured extrahepatic ducts
Intra= Intrahepatic ducts
InjIntra= Injured intrahepatic ducts
Hep= Hepatocytes
Injhep= Injured hepatocytes

6.7 Identification of proteins upregulated in injury.

As indicated in the introduction, the ideal target for homing would be one which is upregulated in injury, based on the assumption that transplanted cells can be most effective at sites of disease. Therefore, the 240 proteins identified as upregulated in both injured intra-, and extrahepatic ducts compared with injured hepatocytes were compared with control intra- and extrahepatic ducts to assess for upregulation in injury. This was done by creating a new model using the limma function, as described in section 6.6 using the same framework described in section 6.6, but with the inclusion of the 240 identified proteins only. The correlation between paired samples remained low at -0.051.

The volcano plot in Figure 6.8A shows that only one protein, TPM1, was significantly upregulated in injured extrahepatic ducts compared with uninjured extrahepatic ducts. Figure 6.8B demonstrates the log2 transformed, normalised abundance of TPM1 across all the studied samples. Whilst there is increased abundance of the protein in injured extrahepatic ducts compared with uninjured extrahepatic ducts, this is not the case for intrahepatic ducts, in which there is a non-significant decrease in abundance.

A further volcano plot in figure 6.9A shows the same analysis comparing injured intrahepatic ducts with uninjured intrahepatic duct. A further solitary protein was identified, non-muscle myosin IIc (MYH14). As shown in figure 6.9B there is increased abundance of MYH14 in injury in both intra and extrahepatic duct compartments. This makes MYH14 an attractive and potentially important candidate.

Figure 6.6.8 Comparison of protein abundance in non-injured extrahepatic ducts and injured extrahepatic ducts.

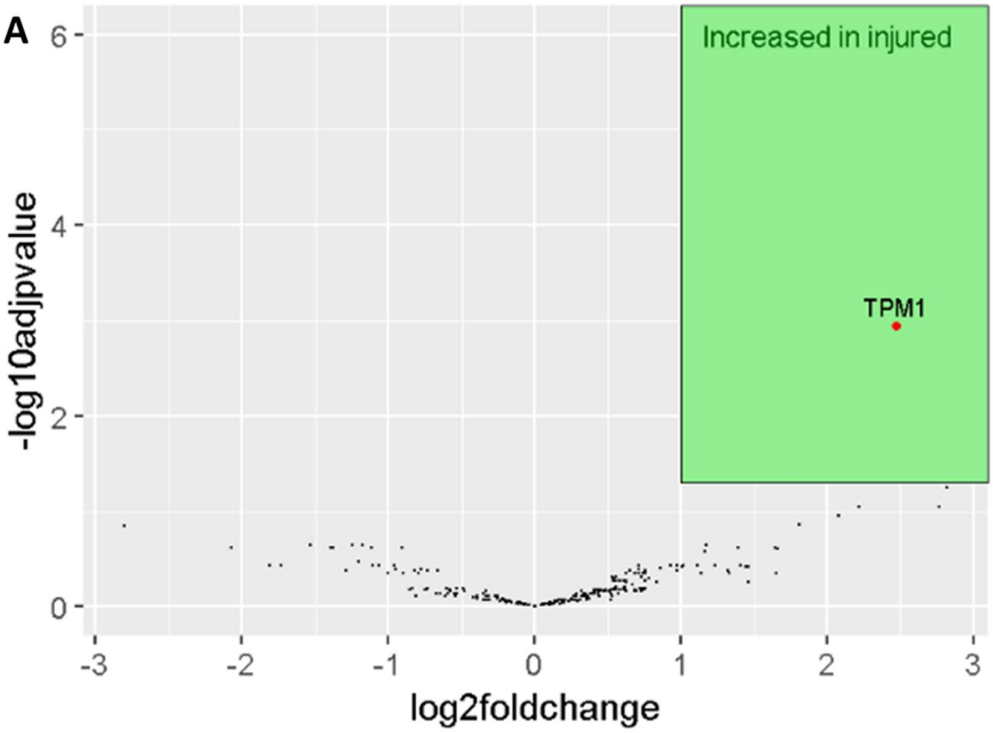

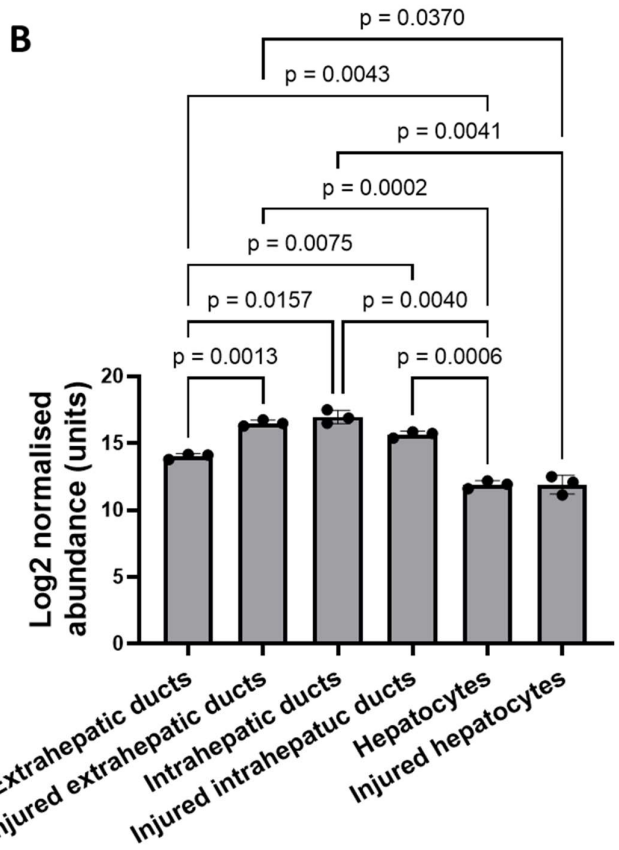

Figure 6.8: Comparison of protein abundance in non-injured extrahepatic ducts and injured extrahepatic ducts (n=3).

A: Volcano plot comparing –log10pvalue (y axis) and log2 fold change (x axis). Proteins which an adjusted p-value>0.05 and a fold change greater than 2 are contained in the green box. Tropomyosin alpha-1 chain (TPM1) was identified as the only protein which was upregulated in injured extrahepatic ducts, log2fold change 2.473, adjusted p value 0.0013.

B: Individual dot plot of TPM1 across investigated tissues and conditions. Bars represent mean, error bars represent standard deviation. Individual points represent protein abundance in a single mouse. Uninjured extrahepatic duct mean log normalised abundance 14.036 +/- 0.208 standard deviation, injured extrahepatic ducts mean 16.510 +/- 0.232, uninjured intrahepatic ducts 16.971 +/- 0.496, injured intrahepatic ducts 15.664 +/- 0.246, uninjured hepatocytes 11.917 +/- 0.298, and injured hepatocytes 11.911 +/- 0.698. Brown-Forsythe ANOVA $p<0.0001$, significant individual comparisons as shown.

Figure 6.6.9 Comparison of protein abundance in non-injured intrahepatic ducts and injured intrahepatic ducts.

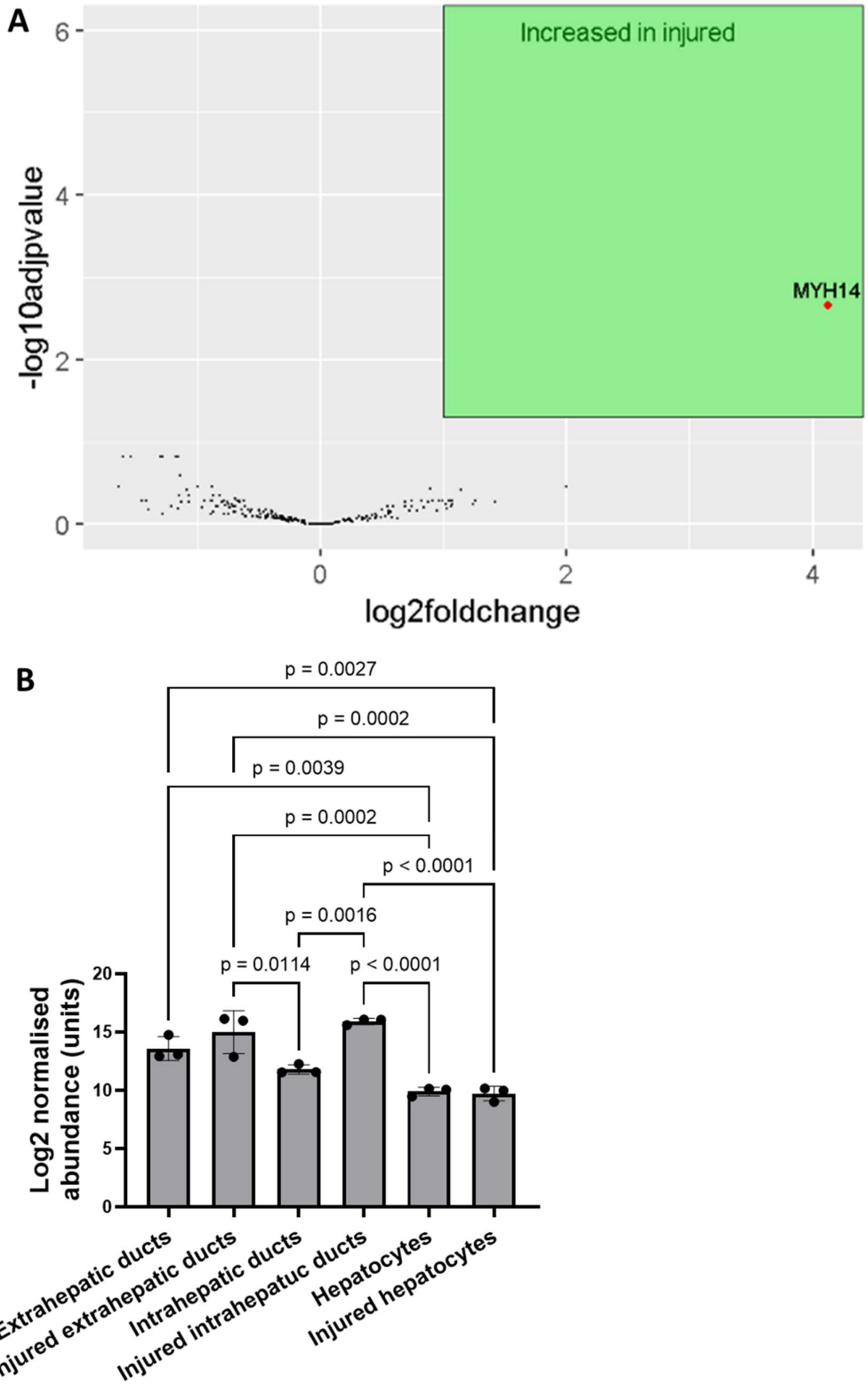

Figure 6.9: Comparison of protein abundance in non-injured intrahepatic ducts and injured intrahepatic ducts (n=3).

A: Volcano plot comparing –log10pvalue (y axis) and log2 fold change (x axis). Proteins which an adjusted p-value>0.05 and a fold change greater than 2 are contained in the green box. MYH14 was identified as the only proteins which was upregulated in injured intrahepatic ducts log2fold change 4.116, adjusted p value 0.0022.

B: Individual dot plot of MYH14 across investigated tissues and conditions. Bars represent mean, error bars represent standard deviation. Individual points represent protein abundance in a single mouse. Uninjured extrahepatic duct mean log normalised abundance 13.6 +/- 1.018 standard deviation, injured extrahepatic ducts mean 15.006 +/- 1.832, uninjured intrahepatic ducts 11.805 +/- 0.401, injured intrahepatic ducts 15.921 +/- 0.278, uninjured hepatocytes 9.909 +/- 0.361, and injured hepatocytes 9.729 +/- 0.624. Brown-Forsythe ANOVA $p<0.0001$, significant individual comparisons as shown.

6.8 Assessment of proteins only identified in ductal samples.

In addition to the 2844 proteins which were identified in all samples, there were a further 1665 proteins which were only detected in bile duct samples. Once proteins that were not detected in all samples were removed from the analysis, 582 proteins remained.

The same code was employed using R software, and data underwent log2 transformation followed by normalisation using the quantile method, with similar results to those shown in figure 6.3 and 6.4.

Figure 6.10A demonstrates unbiased clustering analysis of the proteins only detected in bile ducts. As was the case in the previous analysis, there is more clear clustering of the intrahepatic ducts compared with extrahepatic duct samples, both in injured and uninjured mice.

Supporting information is added by the PCA plot in figure 6.10B. In the top left corner of the plot, the injured intrahepatic ducts cluster closely together. The remaining samples are more widely dispersed. However, there is separation of intrahepatic and extrahepatic ductal samples on the y-axis, which represents principal component 2. However, this accounts for very little of the variance in the dataset at 2.9%. It is also notable that the Injured samples appear for the most part to the left of the respective uninjured samples, as was the case in figure 6.5B. This pattern would be accounted for by principal component 1, which accounts for 72% of variance and is plotted on the x-axis. The importance of this is again to demonstrate that the injury appears to have a significant impact on the dataset. We can be more confident of this observation in light of the low correlation observed between paired samples.

Figure 6.6.10 Unbiased cluster of biliary duct samples

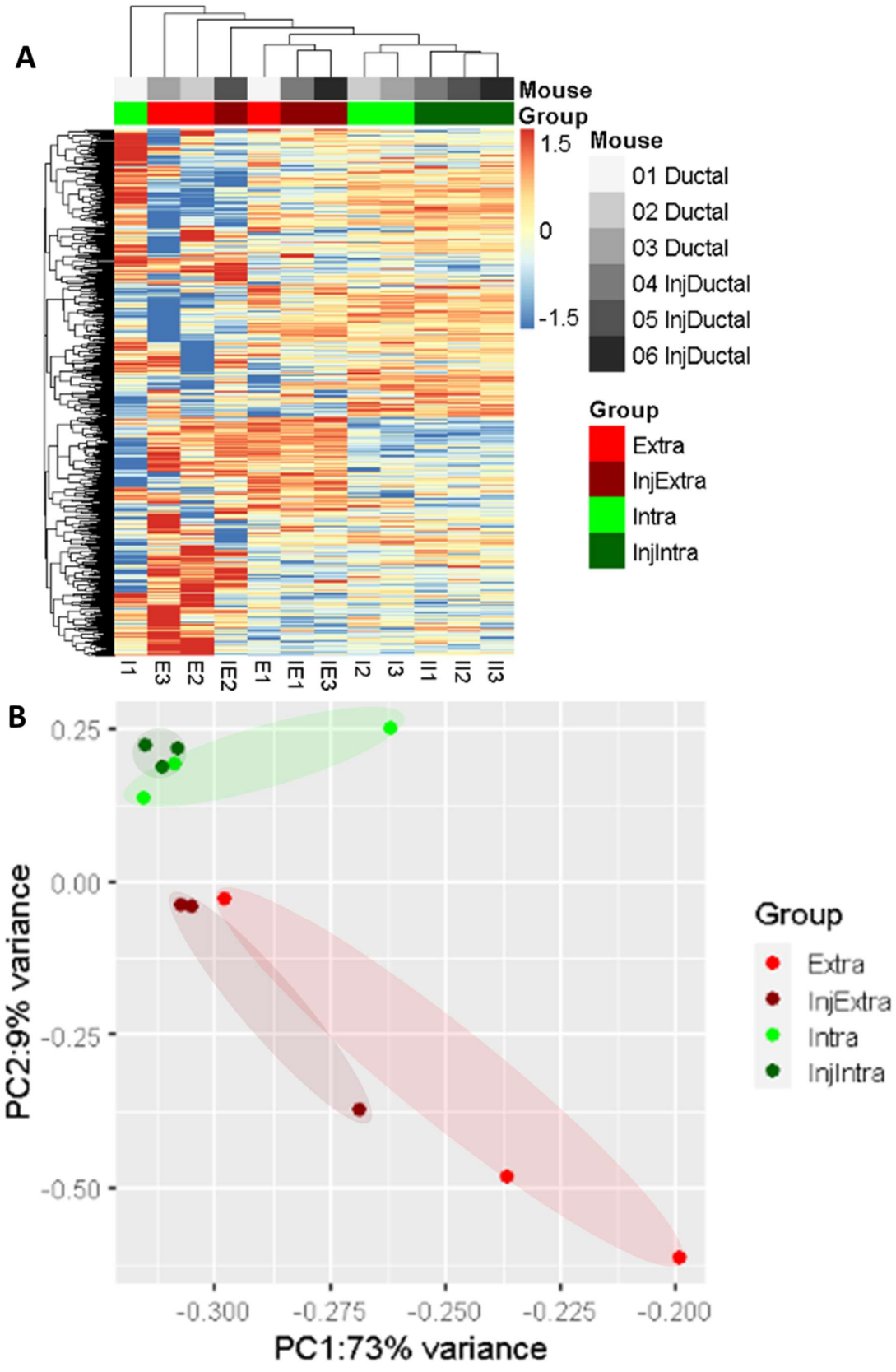

Figure 6.10: Unbiased cluster of biliary duct samples

A: Heatmap demonstrating all proteins detected in biliary but not hepatocyte samples. Colours represent normalised log2abundance.

B: PCA plot of samples demonstrating clustering pattern.

Ductal = Intra and extrahepatic ducts extracted
InjDuctal= Injured intra and extrahepatic ducts extracted
Extra= Extrahepatic ducts
InjExtra= Injured extrahepatic ducts
Intra= Intrahepatic ducts
InjIntra= Injured intrahepatic ducts

6.9 Identification of proteins upregulated in injury only found in biliary samples.

A further model was created using the limma software provided by R, again accounting for the mixed paired and independent samples contained within the model, as in the previous two models the correlation remained low at 0.0036. Proteins were defined as significant when they had both adjusted p value <0.05 and log2 fold change greater than 1

Figure 6.11A shows proteins significantly upregulated in injury in the extrahepatic ducts compared with uninjured extrahepatic ducts, namely Zinc finger protein 830 (ZNF830), TPM2, Phosphoglucomutase-like protein 5 (PGM5) and Leiomodin 1 (LMOD1). All these proteins met the criteria of mean log2 fold change of greater than 1 and therefore more than twice as abundant in the injury compared with uninjured samples in addition to an adjusted p value of less than 0.05. Figure 6.11B demonstrates a heatmap of the log2 normalised abundance of protein across of all of the samples. There is no clear increase in abundance in any of these proteins in injured intrahepatic ducts, columns 7 to 9, compared with uninjured, columns 10 to 12.

The volcano plot in figure 6.12 displays all the proteins in this comparative analysis, adjusted p value on the y-axis and log2foldchange on the x-axis. None of the proteins in this analysis met the criteria for inclusion of having an adjusted p value of less than 0.05 and a fold change of greater than 1.

Figure 6.6.11 Comparison of protein abundance in uninjured extrahepatic ducts and injured extrahepatic ducts

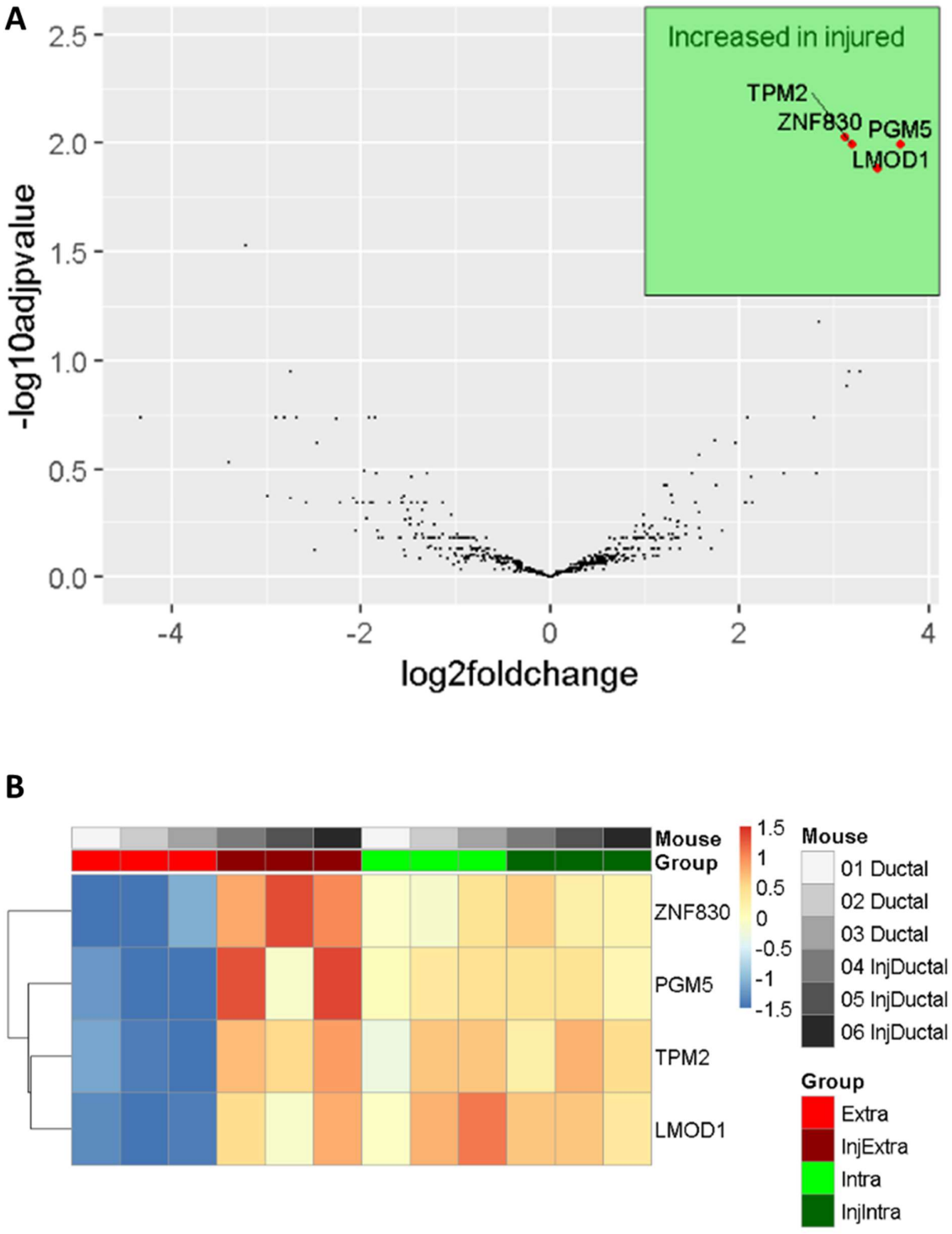

Figure 6.11: Comparison of protein abundance in non injured intrahepatic ducts and injured intrahepatic ducts

A: Volcano plot comparing –log10pvalue (y axis) and log2 fold change (x axis). Proteins with an adjusted p-value>0.05 and a log2 fold change greater than 1 are placed within the green box in the top left corner of the figure namely, ZNF830, PGM5, TPM2, and LMOD1. ZNF830 log2fold change 3.1097, adjusted p value 0.0094. PGM5 log2fold change 3.7024, adjusted p value 0.0101. TPM2 log2fold change 3.1872, adjusted p value 0.0101. LMOD1 log2fold change 3.4477, adjusted p value 0.0131.

B: Heatmap depicting the mean log normalised values from each sample across the upregulated proteins identified in Figure 6.9A, n=3.

Figure 6.6.12 Comparison of protein abundance in non injured intrahepatic ducts and injured intrahepatic ducts

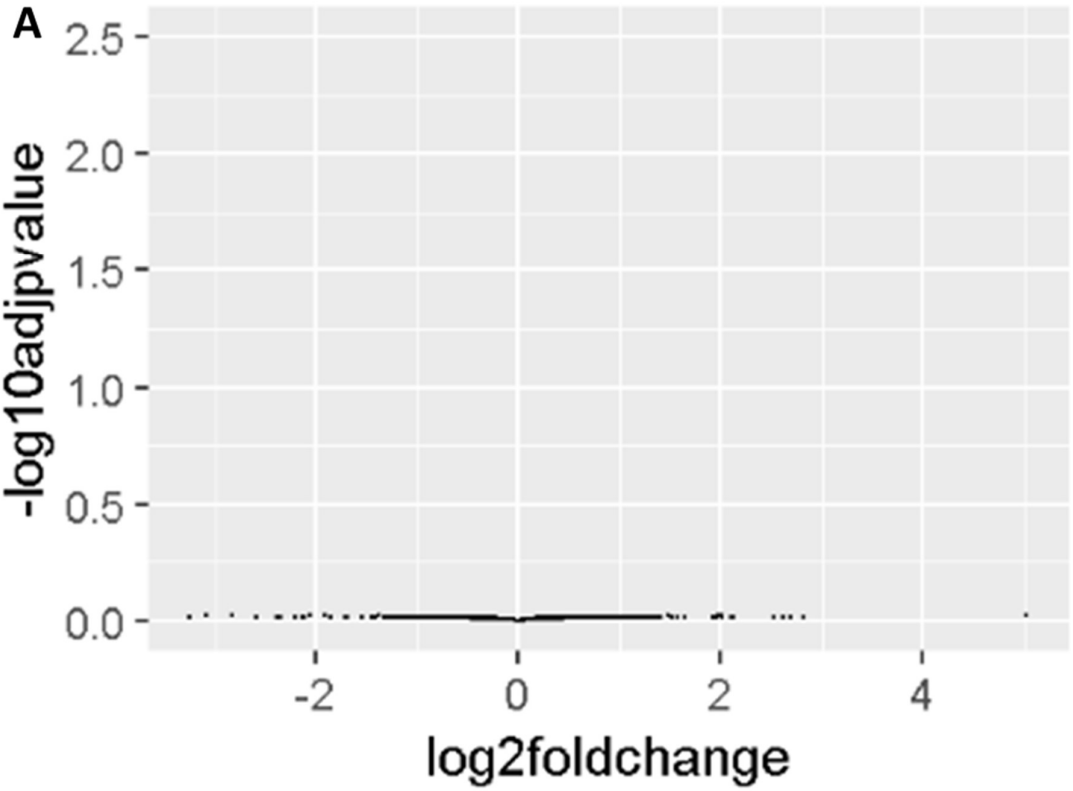

Figure 6.12: Comparison of protein abundance in non injured intrahepatic ducts and injured intrahepatic ducts

A: Volcano plot comparing –log10pvalue (y axis) and log2 fold change (x axis). No proteins had an adjusted p-value>0.05 and a fold change greater than 2 as shown by empty green box in the top left of the figure.

6.10 Identification of protein targets.

Having established a list of protein targets in the previous sections, it was necessary to assess whether any proteins were significantly upregulated in injury in both ductal compartments.

Figure 6.13A demonstrates the protein abundance and fold change in both intra- and extrahepatic ducts following injury. MYH14 was upregulated in both intra- and extrahepatic ducts. However, the other identified proteins were only upregulated in the extrahepatic ducts.

None of the proteins displayed in Figure 6.13A were plasma membrane proteins as defined by the plasma membrane GO term (GO:0005885). As described in chapter 5 the chemokines are also of interest as possible targets for cell homing. None of the displayed proteins were present within the gene ontology term cell chemotaxis (GO:0060326).

To assess interactions between the identified candidates, an overrepresentation analysis using GO terms was performed using the Panther engine[260], as displayed in Figure 6.13B. GO terms were considered only when false discovery rate (FDR) was <0.05. Additionally, if the identified candidates accounted for less than 1% of the genes associated with a GO term, this term was not considered. GO terms in which the proteins shown in Figure 6.13A accounted for less than 1% of the listed genes within the GO term were excluded, to improve the specificity of the analysis. The GO biological process with the lowest FDR was “actomyosin structure organisation”; the GO cellular component with the lowest FDR was “myofilament”. The only significant GO molecular function term identified was “actin filament binding”. All the terms listed in table 6.13B were associated with muscle fibre development or contractility.

Figure 6.6.13 Analysis of identified candidates

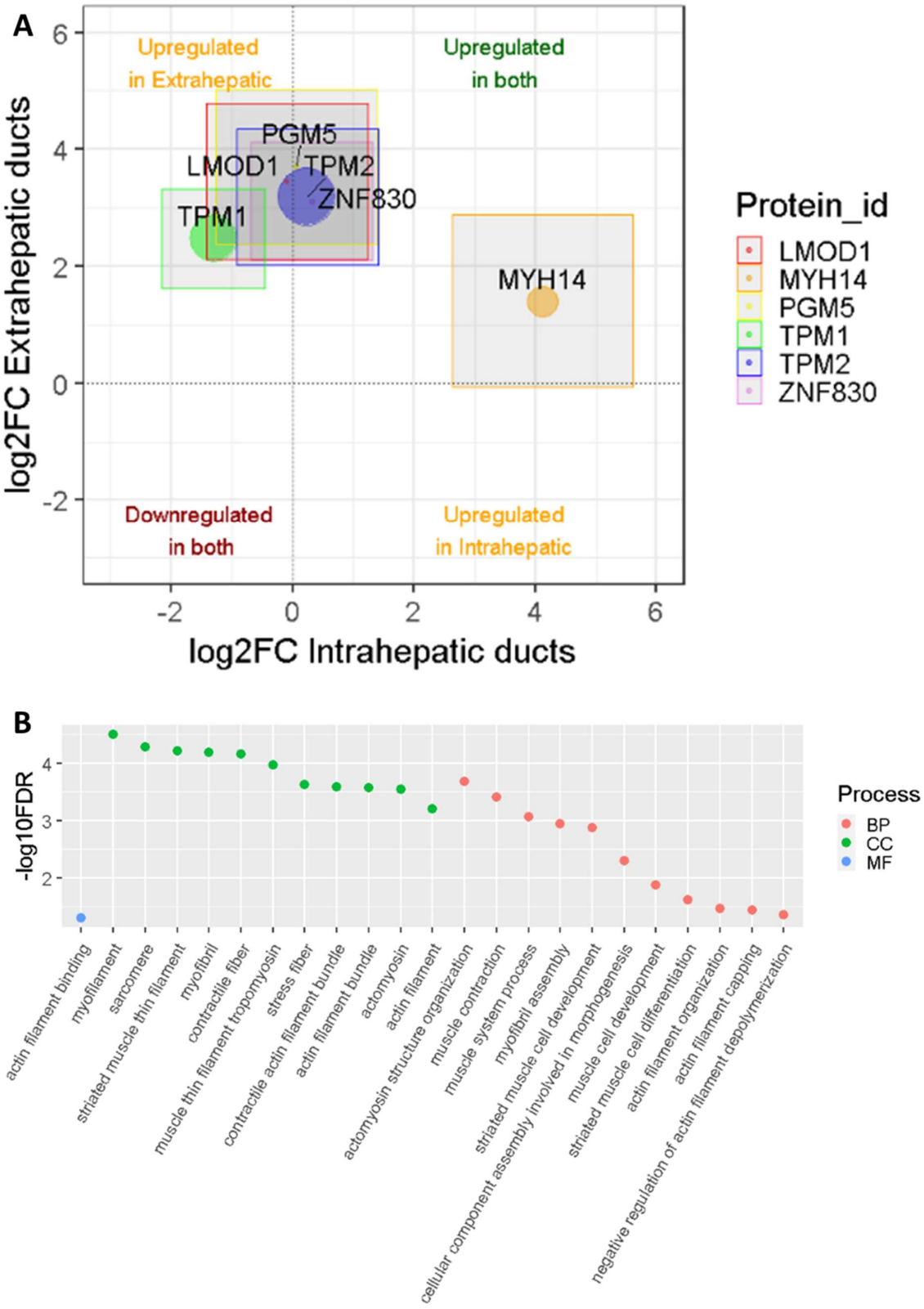

Figure 6.13: Analysis of identified candidates

A) Comparison of fold change in identified candidates in extra- and intrahepatic duct samples. Dot size is directly proportional to normalized mean abundance in injured extra- and intrahepatic ducts, rectangle represents two-dimensional 95% confidence intervals.

LMOD1 mean normalized abundance 5,590.18, intrahepatic duct log2 fold change in injury -0.0984 (95% confidence interval -1.4309 to 1.2339), extrahepatic duct log2 fold change in injury 3.4477 (95% confidence interval 2.1153 to 4.7800).

MYH14 mean normalized abundance 45,817.244, intrahepatic duct 4.1162 (95% confidence interval 2.6356 to 5.5968), extrahepatic duct 1.4069 (95% confidence interval -0.0737 to 2.8875).

PGM5 mean normalized abundance 8529.011, intrahepatic duct 0.0662 (95% confidence interval -1.2632 to 1.3955), extrahepatic duct 3.7024 (95% confidence interval 2.3731 to 5.0318).

TPM1 mean normalized abundance 69,621.870, intrahepatic duct -1.3071 (95% confidence interval -2.1577 to -0.4565), extrahepatic duct 2.4740 (95% confidence interval 1.6234 to 3.3246).

TPM2 mean normalized abundance 85,990.456, intrahepatic duct 0.2442 (95% confidence interval -0.9187 to 1.4071), extrahepatic duct 3.1872 (95% confidence interval 2.2043 to 4.3501).

ZNF830 mean normalized abundance 7123.723, intrahepatic duct 0.3124 (95% confidence interval -0.6958 to 1.3205), extrahepatic duct 3.1097 (95% confidence interval 2.1016 to 4.1179).

B) Gene enrichment analysis conducted on the six proteins outlined above. GOterms plotted on x-axis, -log10 false discovery rate on the y axis. BP= biological process, CC= Cellular component, MF = Molecular function process.

6.11 MYH14 is localised to the ducts in mouse and human tissue.

Inherent in the duct isolation technique is the possibility that identified proteins could be originating from BEC, or other cells contained within the ductal tracts such as endothelial and immune cells. For this reason and to confirm the lack of expression in the hepatocyte compartment of the liver, immunohistochemistry was undertaken. This section presents the preliminary results of this investigation, using a single sample for each condition.

Figure 6.14 demonstrates the specific expression of MYH14 to BECs. In all mice assessed, including the *Krt19^{CreER}MDM2$^{fl/fl}$Rag2$^{-/-}$IL2rg$^{-/-}$* model both injured and not, MYH14 was demonstrated to be specifically expressed in the bile ducts. No expression was detected in the extra-ductal tissues.

Figures 6.15 and 6.16 contain images from human samples of control livers, and cases of PSC and PBC. Figure 6.15 focuses on the ductal compartment mirroring the images shown in the mice models with expression in the BEC across all injuries. The images also appear to localise expression to the apical aspect of BEC.

Figure 6.16 focuses on hepatocellular expression of MYH14. In both PBC and the control sample, no expression was identified in the hepatocellular compartment. However, in the PSC section, canalicular expression was identified as shown in bottom right image of the figure.

Figure 6.6.14 Expression of MYH14 in different murine disease states

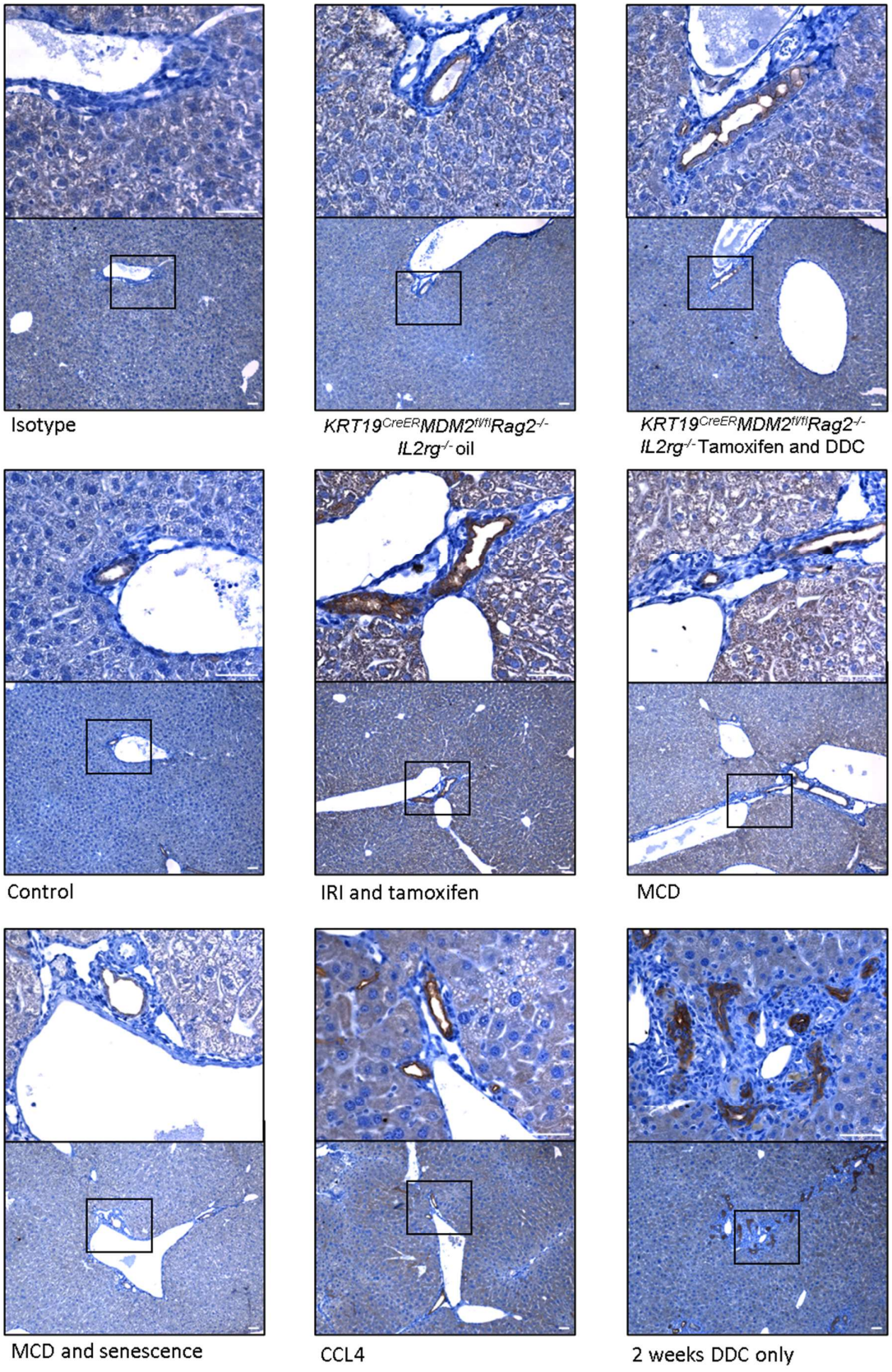

Figure 6.14: Expression of MYH14 in different murine disease states

All scale bars represent 50μm. Representative images of DAB immunohistochemistry of MYH14 across different injury models in mouse. Superior images are 40x magnification, inferior images 10x.

All mice bred on a C57BL/6 background are the same as the models described in Chapter 5.

2 weeks DDC diet C57BL/6 were a kind gift from Dr. S. Ferreira-Gonzalez.

(n=1)

Figure 6.6.15 Expression of MYH14 in human tissue

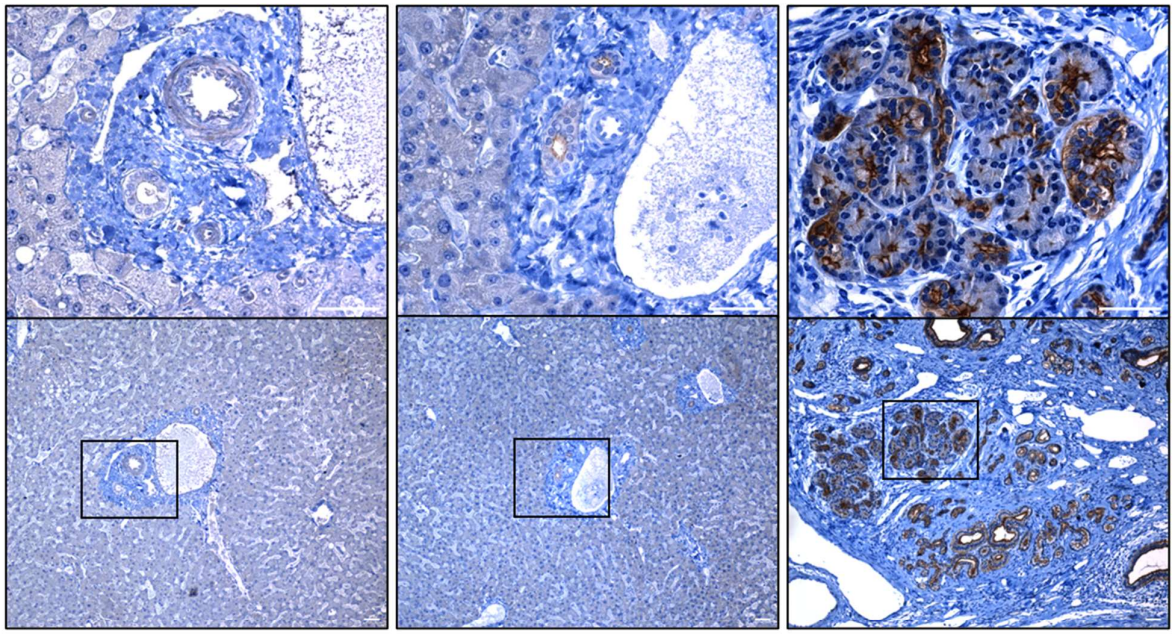

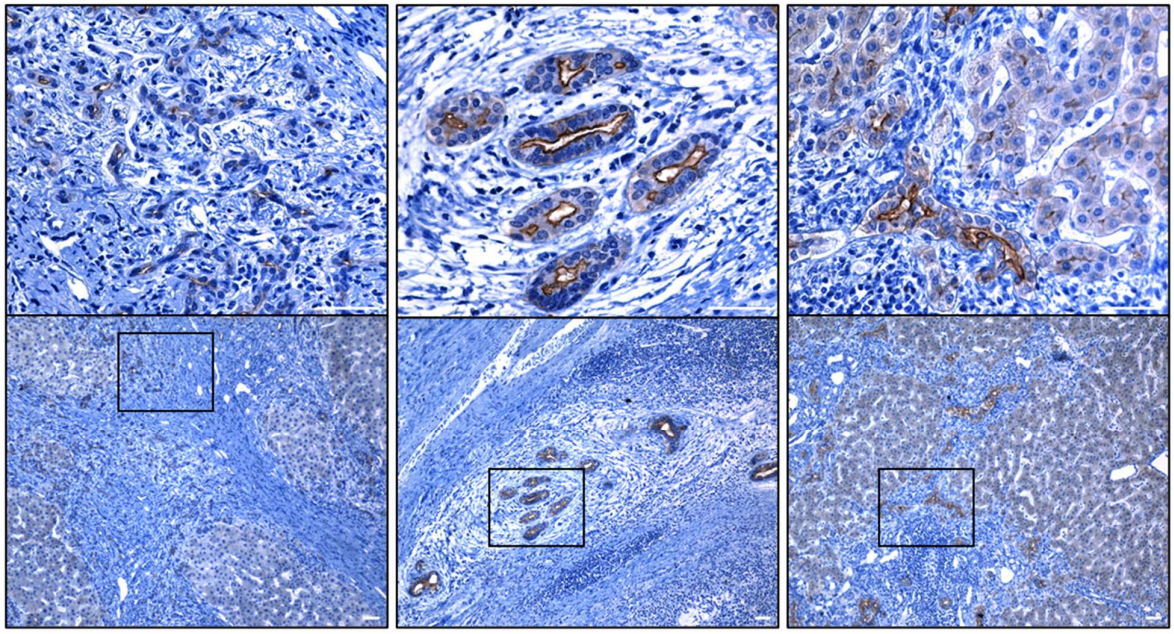

Figure 6.15: Expression of MYH14 in human tissue

All scale bars represent 50μm. Representative images of DAB immunohistochemistry of MYH14 across different human samples. Superior images are 40x magnification, inferior images 10x.

(n=1)

Figure 6.6.16 Expression of MYH14 in human hepatocytes

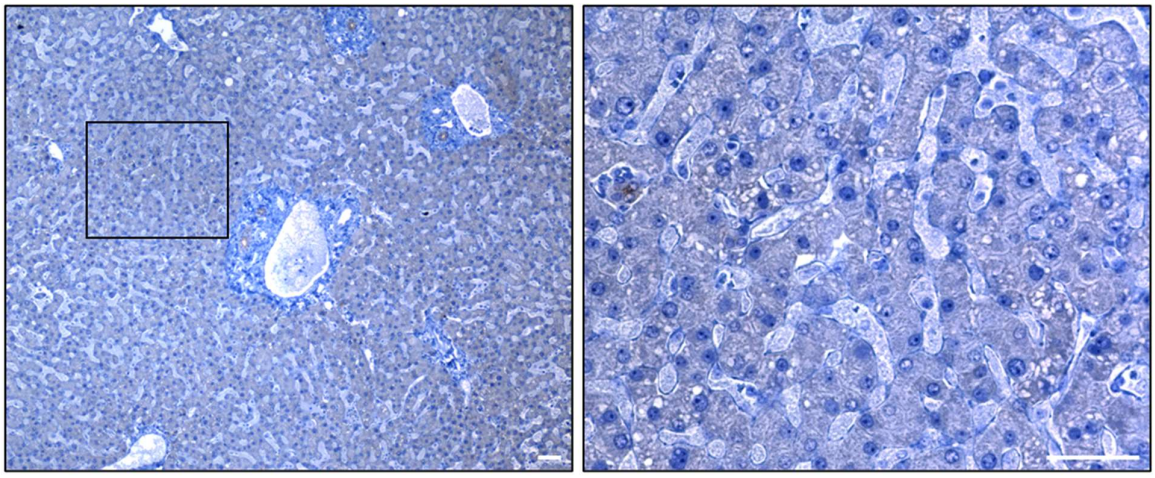

Control

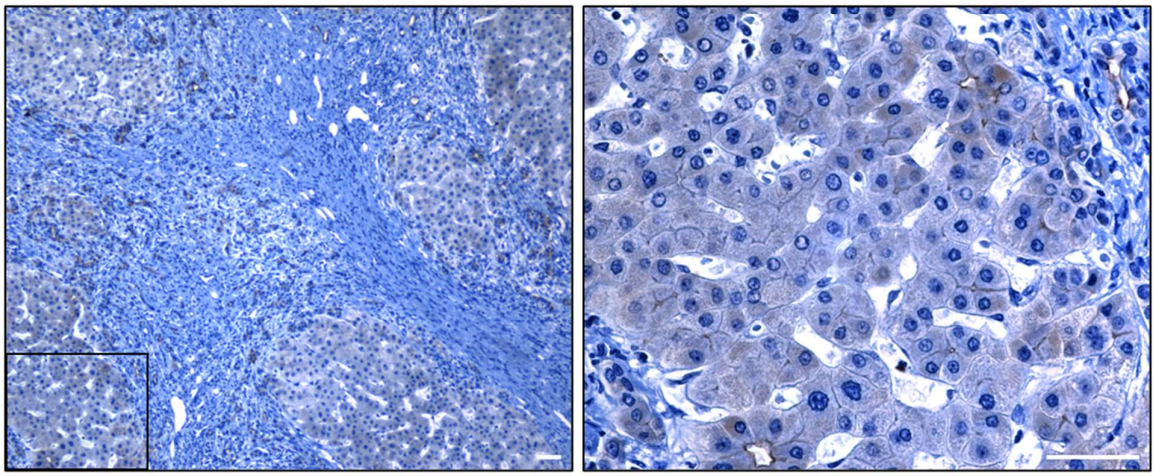

Peripheral PBC

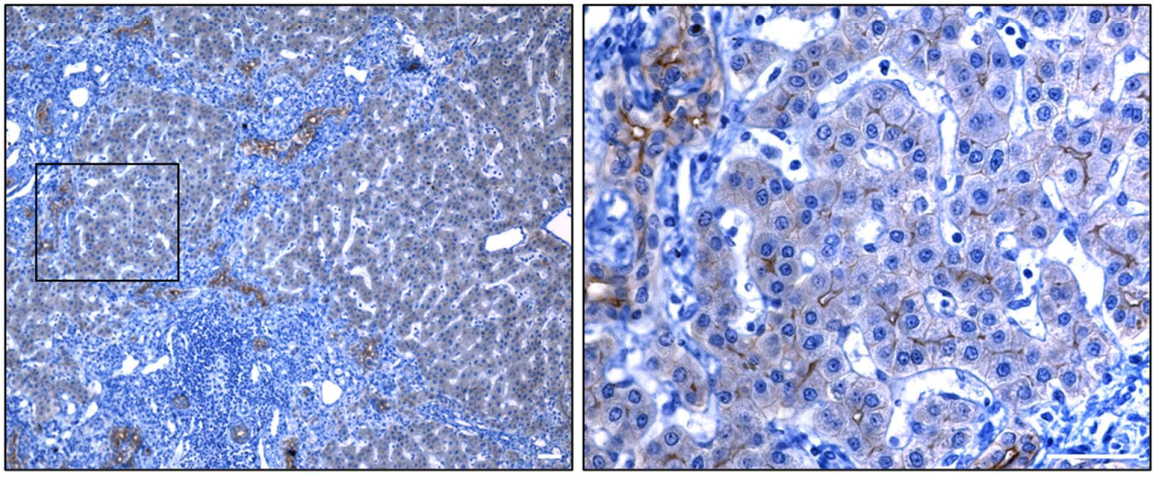

Peripheral PSC

Figure 6.16: Expression of MYH14 in human hepatocytes

All scale bars represent 50μm. Representative images of DAB immunohistochemistry of MYH14 across different human samples. Left sided images are 40x magnification, right sided images 10x.

(n=1)

6.12 Analysis of the most abundant proteins which are specific to BEC,

Whilst an ideal target would be upregulated in injury to attract cells to areas of injury, highly abundant proteins may also be useful in acting as a target for cell homing.

As such, a reanalysis was performed to assess the most abundant proteins detected in injured intrahepatic and extrahepatic ducts respectively. Figure 6.17A shows the ten most abundant proteins in injured intrahepatic ducts, those of which are plasma membrane proteins are in red. The most abundant plasma membrane protein was vimentin, with Annexin V representing the second most abundant.

Figure 6.17B shows the ten most abundant proteins in injured extrahepatic ducts. The most abundant plasma membrane protein was vimentin with Annexin II being the second most abundant.

Whilst vimentin was the most abundant plasma membrane protein, this was removed as a candidate here for two reasons. Firstly, the expression of vimentin has already been characterised in biliary disease[261, 262]. Secondly, while intracellular vimentin is known to be attached to the plasma membrane, it does not have a transmembrane component and therefore nor an external component. This would make it a challenging target for a cell homing mechanism[263, 264].

The second most abundant plasma membrane protein detected in intrahepatic proteins was Annexin V and this was also the eighth most abundant protein in the extrahepatic ducts. The next section aims to localise Annexin V expression in the liver of both human and murine samples in both injury and disease.

Figure 6.6.17 Most abundant proteins identified in injured intra and extrahepatic duct samples

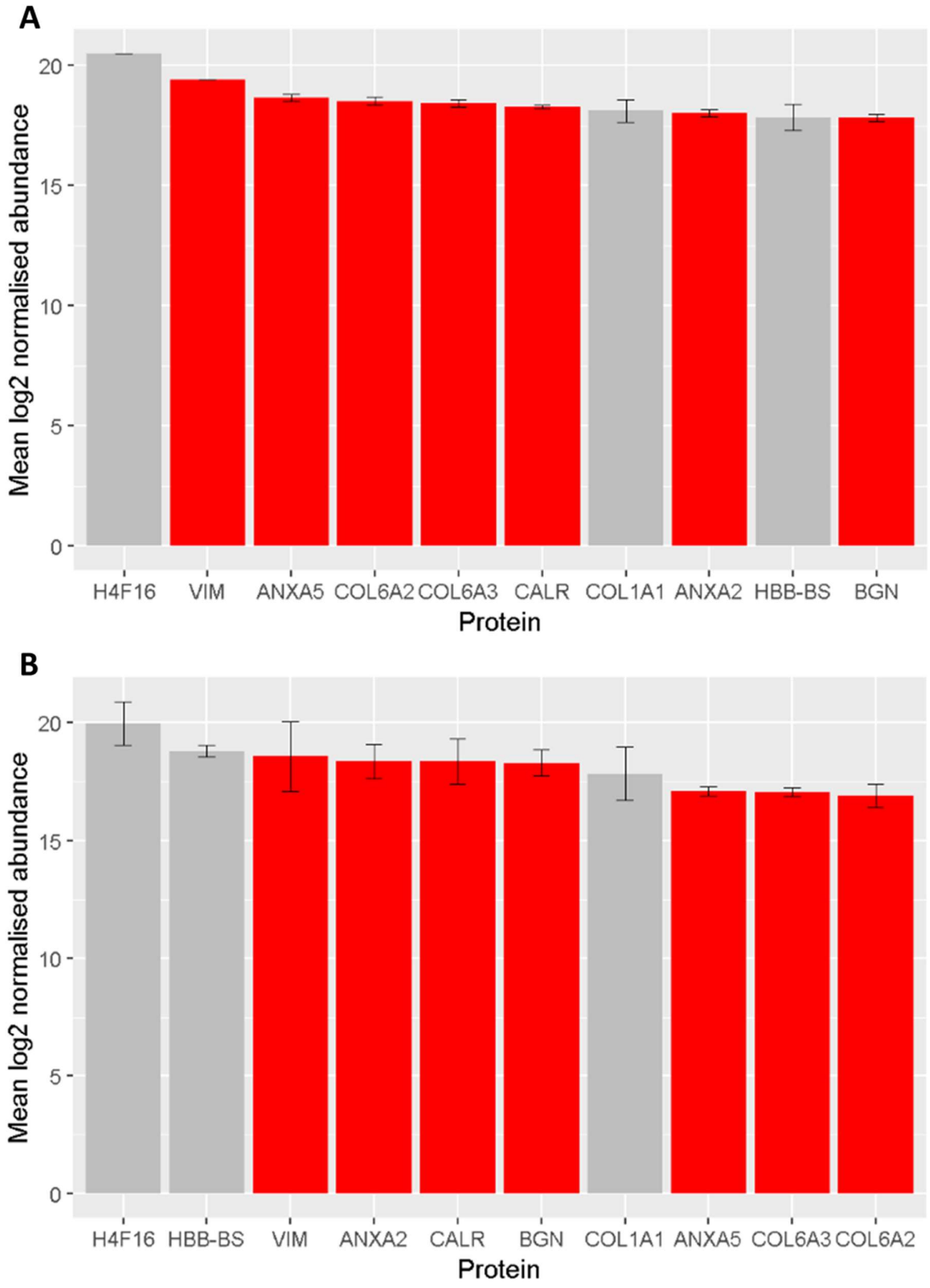

Figure 6.17: Most abundant proteins identified in injured intra and extrahepatic duct samples.

Each bar represents the mean log2 transformed, normalized abundance of a protein (n=3). Error bars represent standard deviation. Red bars represent plasma membrane proteins.

A: The ten most abundant proteins identified in injured intrahepatic ducts.

B: The ten most abundant proteins identified in injured extrahepatic ducts.

6.13 Localisation of Annexin V to BEC within murine and human liver.

Figure 6.18 demonstrates the expression and location of Annexin V in the liver, with restricted expression in BEC as shown in each of the images displayed. Subjectively there appears to be less expression in the chronic biliary model (2 weeks of DDC diet). There was no clear pattern of expression at the subcellular level.

There were areas of suspected endothelial expression, as shown in the image of mouse given MCD diet. There were also some areas of non-specific extraductal expression, which are highlighted using green arrows.

Figure 6.19 displays representative images from human samples from controls (samples from livers rejected for transplantation) and patients with PSC or PBC. As seen in the mouse model, expression is restricted to the biliary compartment. In the immunohistochemistry performed, there was apparent lower expression in PSC than in the control sample.

Figure 6.6.18 Expression of Annexin V in different murine disease states

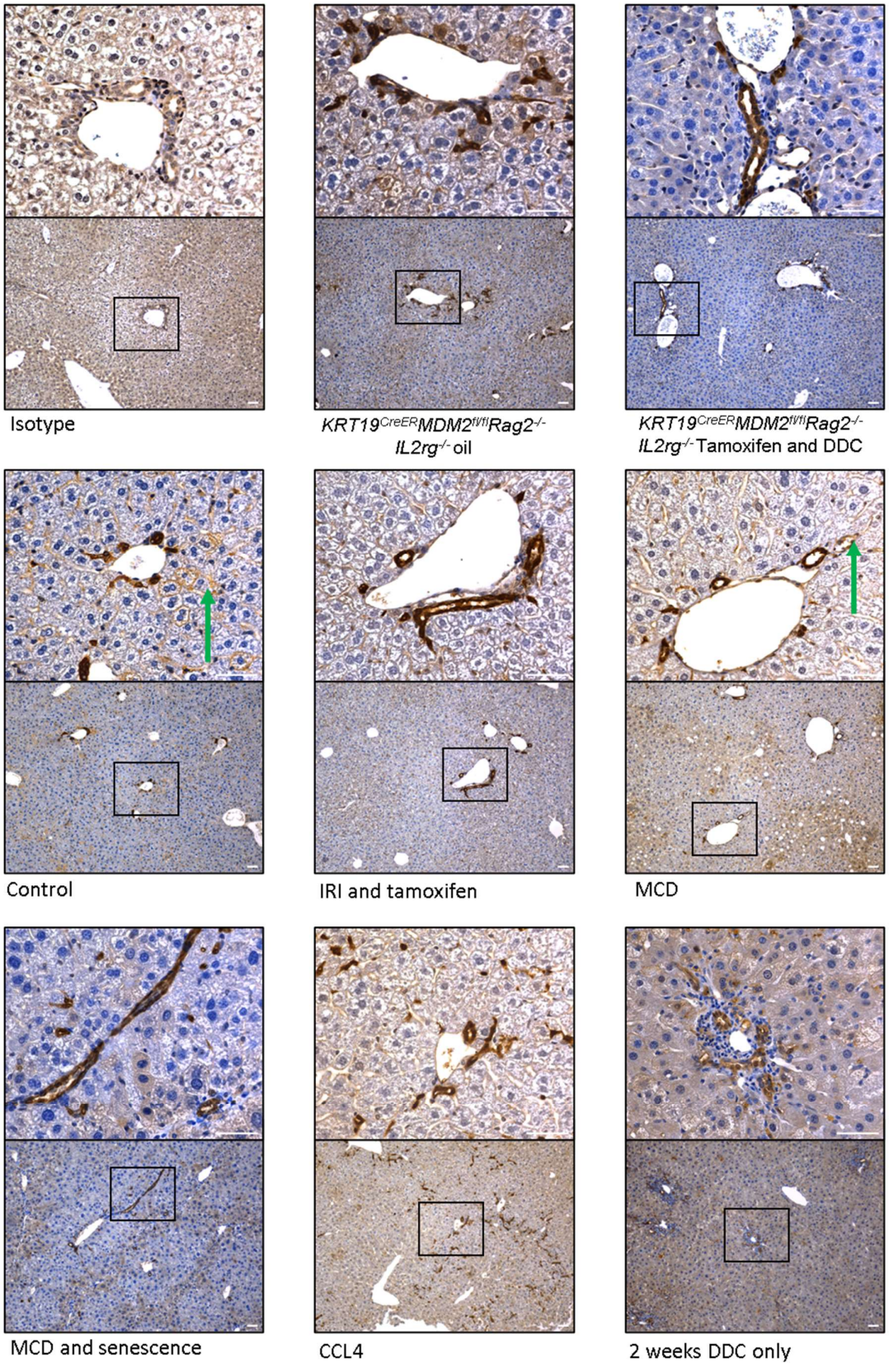

Figure 6.18: Expression of Annexin V in different murine disease states

All scale bars represent 50μm. Representative images of DAB immunohistochemistry of Annexin V across different liver injury models in mouse. Superior images are 40x magnification, inferior images 10x.

All mice bred on a C57BL/6 background and are the same as models described in Chapter 5.

Red arrow indicates suspected endothelial expression, green arrows indicate areas of non specific extra-ductal expression.

Figure 6.6.19 Expression of Annexin V in different human biliary disease

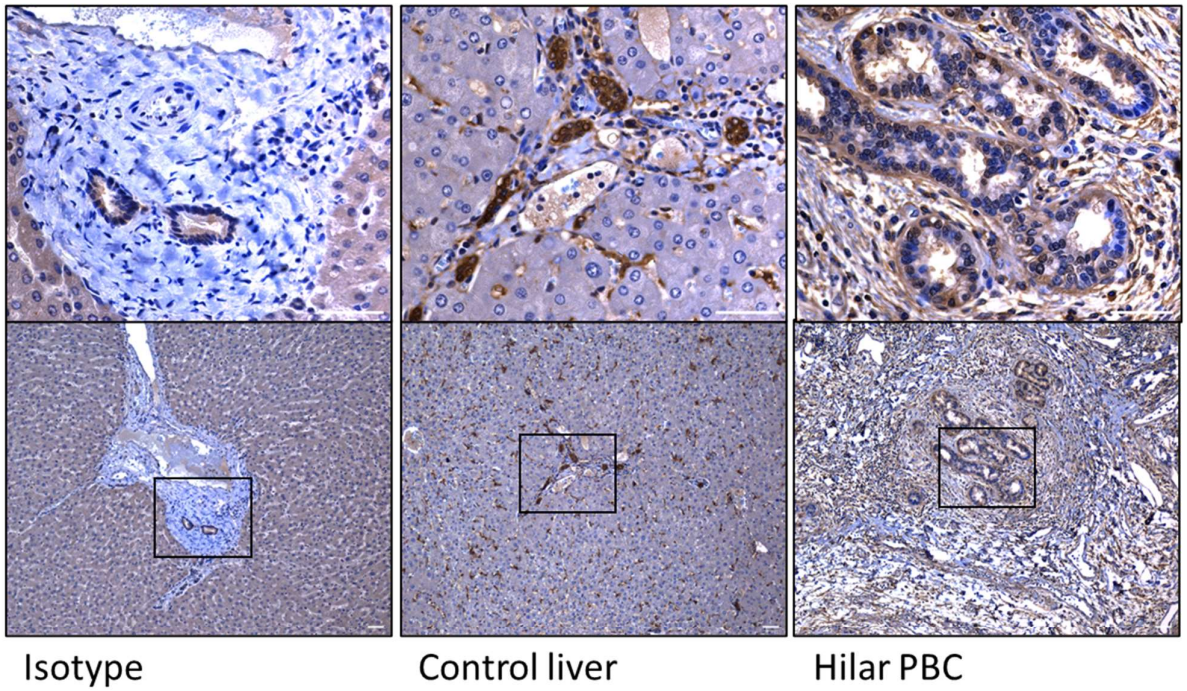

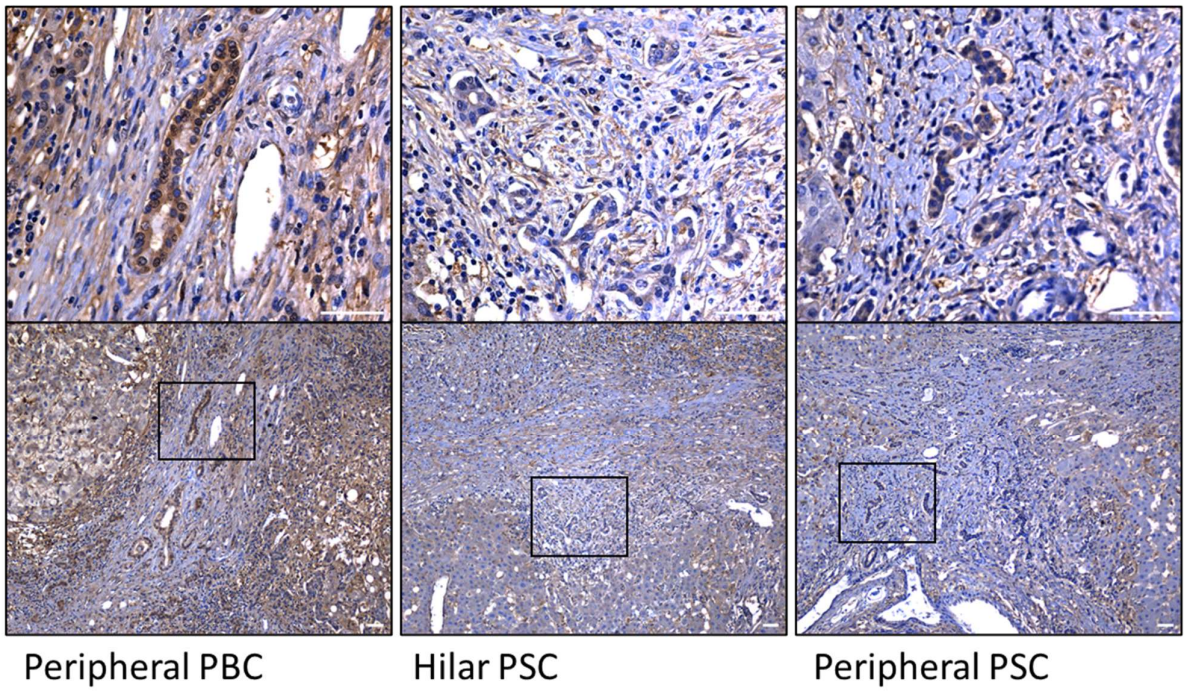

Figure 6.19: Expression of Annexin V in human tissue

All scale bars represent 50μm. Representative images of DAB immunohistochemistry of Annexin V across different samples in human. Superior images are 40x magnification, inferior images 10x.

6.14 Discussion

The specific detection of plasma membrane proteins can be challenging, given the low abundance of these proteins and the inherent difficulties in isolating them. This study compared 3 methods of extraction of plasma membrane proteins finding each of them to have individual challenges and merits. Theoretically, a biotin capture technique should be an efficient and specific method of selecting plasma membrane proteins, however, an adequate mass of protein could not be extracted for mass spectroscopy with the technology available at the time of performing these experiments. Other capture techniques could have been trialled, for example, glycosylation capture. The likelihood that this would have been successful given the difficulties with the biotinylation technique would ostensibly be slim. Additionally, it should be noted that capture techniques introduce an inherent bias, as they require proteins to have certain characteristics, for example an exposed amine group in the case of biotinylation or be a glycoprotein for glycogen capture. A key challenge of using a capture technique is the necessity that cells should be kept alive when exposed to the capturing agent; if this is not observed, the capturing agent can enter the cell and bind to other intracellular structures, creating contamination. This stipulation becomes more challenging when trying to extract protein from a finite cell population such as BEC. As mass spectroscopy becomes more sensitive it will also make the assessment of the plasma membrane protein compliment of primary cells more feasible and at that point these experiments could be revisited.

The study was carried out on cells which had been isolated from tissues, as opposed to those in culture. Culturing cells could have allowed larger yields of proteins to be obtained, however, this was not undertaken for two reasons. Firstly, cell culture represents clonal expansion of a subgroup of isolated cells and therefore may favour subgroups of a cellular population, as some cells fail in culture conditions and others thrive. Whilst this fact may not pose a problem when investigating specific cell functions, it is unlikely to give an accurate representation of the original type at a proteomic level. For example, it is possible that a subgroup of cells expressing a specific protein may thrive in culture, leading to the over detection of that protein in the final analysis. Secondly, it is challenging to culture hepatocytes, which effectively removes cell culture as a solution to low yields of protein.

Another option would have been to pool hepatocytes and ducts from multiple mice to give adequate protein. It was elected not to pursue this, due to concerns that inter-sample variability may create problems in the analysis, the heterogeneity in the bile duct samples demonstrated in the PCA plots featured in the chapter vindicate this decision to a degree (Figures 6.5B, and 6.10B).

Techniques using ultracentrifugation depend on differential density within the plasma membrane and other sub cellular structures. They run the risk of contamination with other organelles, particularly other membranes, as these may share some of the same properties as the plasma membrane. The relatively low density of the plasma membrane compared with other subcellular compartments is dependent on the phospholipids bilayer which constitutes much of the structure. If this is disrupted, the plasma membrane proteins will no longer be separable based on density. For this reason, lysis of the cell must be performed in a way that damages the plasma membrane without destroying it, preventing the use of chemical lysis buffers. The most efficient forms of cell lysis therefore cannot be used. Inefficiencies of cell lysis led to an increase in the numbers of cells required for isolation or lower protein yields.

Specifically considering gradient ultracentrifugation, the technical aspects can be challenging, and proteins must be extracted manually between layers of fluids of different density, in this thesis, layers of sucrose solution. The extraction is dependent on the ability of the operator to identify proteins between layers and to extract those efficiently. These technical challenges limit the reproducibility of the technique and possibly the efficiency of the technique in extracting proteins. Despite this, figure 6.1 demonstrates that this was the most effective method in extracting plasma membrane proteins in hepatocytes, in terms of what was recovered from a single murine liver.

This method appeared effective in extracting plasma membrane proteins with up to 34% from the entire sample representing plasma membrane proteins. Unfortunately, 10% of all proteins identified in the investigation of plasma membrane isolation techniques were exclusively detected in the control sample. Assuming that proteins identified in the whole protein sample are the most abundant plasma membrane proteins, the gradient technique is failing to detect some of the most abundant plasma membrane proteins, indicating inherent bias in the technique. This left a choice between selecting a technique with an unknown bias for selecting a subgroup of plasma membrane proteins in gradient ultracentrifugation or one with a more defined bias, in whole

tissue or cell lysis. The selection of the latter likely limited the detection of lowly abundant plasma membrane proteins. However, in theory, the abundance of a protein is likely to influence the efficacy of using a protein as a target for cell homing: more abundant proteins are more available and so increase the chance of cells reaching and interacting with their intended target.

Secondly the decision to use duct isolation, and not isolate single cells using FACS may also have influenced the results. Duct isolation leads to the analysis of not only BEC but also cells and tissues associated with the ductal structure. For this reason, protein from the BEC cells is in effect diluted and therefore the detection of lowly abundant proteins is likely limited. As discussed in section 6.3, the limitation of this technique may also represent a benefit, the detection of proteins within the ductal structure but not directly expressed by BEC could represent important targets for homing to the bile ducts even though they are not present on the BEC themselves.

For the identification of a specifically expressed protein on injured ducts, R software was used along with the limma package[258]. One of the largest benefits of using this package was the ability to account for a mixed model of both paired and unpaired samples. In all the models created using this package, there was low correlation between the paired samples, namely extrahepatic and intrahepatic ducts which came from the same mice in injury and in uninjured samples. This result alone indicates that there is a difference in the proteomic signature from intrahepatic and extrahepatic biliary ducts. The assessment of the extrahepatic biliary tree is at present under investigation in preclinical research of cholangiopathies with many major studies only considering intrahepatic ducts.

To exclude proteins which are present in hepatocytes, primary isolated hepatocytes were used as a comparator. Comparisons between cell suspensions as was the case for hepatocytes and tissue, intra and extrahepatic ducts, may be challenging however the only alternative would be using whole pieces of liver, as it is not possible to separate the biliary ducts from the hepatocytes without digestion. It should be noted that this may influence the results of the experiments undertaken, for example through the increased detection of basement membrane proteins, as for the ductal samples these remain intact, whilst hepatocytes are freed from the basement membrane in the process of digestion.

Despite these uncertainties surrounding the ductal isolation method, the results of this chapter have justified the means, making possible the identification of a biliary specific protein which was upregulated in injury, MYH14, and a further specific target such as Annexin V. The legitimisation of this technique for certain applications is important, as it requires significantly less technology than the FACS sorting of EpCAM positive cells[149]. This in turn will allow a more widespread investigation of cholangiopathies, which ultimately will allow more rapid progress to occur in the field. An important area for future research would be to make a direct comparison between ductal isolation and EpCAM sorted cells to assess what biases are inherent in each of these techniques.

Normalisation of mass spectroscopy datasets aims to take account of a number of unknown biases inherent to the prospect of detecting proteins and measuring abundance[265]. There are several possible methods for normalisation, however in this study the quantile method of normalisation was selected due to the high variability between sample abundance as shown in Figure 6.4A. The selection of the quantile method of normalisation should be discussed as it has significant implications particularly for the analysis of the most abundant proteins (section 6.12). Quantile normalisation is a stringent method with the mean of the highest ranked protein from each sample becoming the value for the highest protein in all the samples. For this reason, if there was an exceptionally abundant protein in the ductal samples this could be tempered significantly by low expression in the hepatocyte samples, and less importantly for the purposes of this analysis vice versa. Other forms of normalisation would have been possible, such as median normalisation which transforms data to make the median the same between groups. Median normalisation (referred to as scale in the normalizeBetweenArrays() function in R software) has a lesser impact on the most least abundant proteins in a sample therefore could be less impactful when countering batch effect. Following the presented analysis, a further analysis was performed using the median method. Using this technique MYH14 remained significantly upregulated in intrahepatic ducts per the criteria stipulated of having a fold change of greater than 2 and adjusted p value of 0.05.

Proteins which were not detected in every sample were excluded from the downstream analysis. The reason for this was to increase the confidence of detection, an alternative would be to impute values based on the values obtained in other samples. Given the low sample size in each group, imputation was felt likely to introduce a significant

degree of bias and therefore filtering was selected. In total 39 proteins which were in all three samples of at least one of the ductal conditions (injured or uninjured, extra or intra) but not in all hepatocyte samples were present. These proteins were ultimately excluded since they were in some of the hepatocyte samples and therefore were likely present at some level in these tissues. As there was missing data, a comparison between ductal and hepatocyte expression could not be made for these proteins. A higher number of samples may have given more confidence regarding the true expression of these proteins and allowed for their inclusion in the main analysis.

Similarly, it could have been possible to filter proteins based on the number of unique peptides identified for each protein, using the percentage coverage of proteins by unique peptides or a combination of both. The benefit of this would have been to increase the confidence in detected proteins and to reduce the number of proteins in the analysis and therefore increase the likelihood of detecting an association. The reason that this was not pursued was the potential that this would negatively bias proteins which are made up of fewer numbers of peptides.

The process of identification of a protein specifically expressed on BEC commenced by identifying proteins that were significantly upregulated in both intrahepatic and extrahepatic ducts compared with hepatocytes in injury, yielding 240 proteins in total. In a parallel analysis, the proteins which had only been detected in ductal samples were also investigated. The benefit of this method of analysis would be a more focused group of proteins present within the final analysis, thus less comparisons and a less severe adjustment to the p value when accounting for multiple comparisons. The threshold of less than 0.05 adjusted p value and greater than 1 log2FC could have been altered. It was necessary to select a cut off and this was felt to be a scientifically relevant level and so was adopted.

Ultimately only 6 proteins were identified as being specific and upregulated in injury in either the intra or extrahepatic ducts. It was expected that more candidates would be identified and there are several possible reasons why the candidate yield was so low. As discussed, 39 proteins could have potentially been included that were present in at least three of the ductal samples but not all the hepatocyte samples, this group may have included viable candidates. The low sample numbers are likely to have contributed to the detection of proteins as statistical power was reduced. The other possible consideration would be the severity of biliary injury and the length of DDC diet.

Unfortunately, the *Krt19Cre^{ER}Mdm2 $^{fl/fl}$ Rag2$^{-/-}$ Il2rg$^{-/-}$* is not able to reliably tolerate longer periods of DDC diet.

MYH14 was identified as a protein which was upregulated in injured intrahepatic biliary ducts. The specific expression of MYH14 in BEC was demonstrated in multiple murine models and in human samples. In PSC there was also canalicular expression within the hepatocytes, indicating at a subcellular level expression of MYH14 is likely to be present at the apical aspect of BEC. Whilst proteomic quantification was possible in murine samples, only fixed paraffin slides were available with regards to human samples, therefore proteomic quantification could not be performed. Semi-quantitative analysis of immunohistochemistry could be performed either through scoring of ductal expression or through percentage of biliary ducts positive for MYH14 to validate the results found in mouse, in human. Additionally, if it became possible in the future to obtain fresh samples of liver from patients with PSC and PBC, isolation of ducts and hepatocytes could be performed to perform proteomic analysis as has been done on murine samples in this chapter.

The function of MYH14 is thought to relate to cellular contraction and cellular morphology[266]. Given the mechanism of injury produced by the DDC diet discussed in the introduction, this is not unexpected; contraction of cells to increase intra-ductular pressure in order to expel debris which accumulates within the duct following DDC diet[114]. As shown in Figure 6.13B, overenrichment analysis using GOterms indicated that the hits identified were related either to the production of muscle fibres or to cellular contraction, which further reflects the response of BEC to ductal obstruction.

It was of interest that in PSC sample there was expression of MYH14 in the hepatocyte canaliculi. This could suggest that hepatocytes also contribute to improving bile flow in chronic obstructive cholangiopathy. Accepting this it can be considered whether this adaptation is beneficial or detrimental, whether the expression of MYH14 allows improvement of flow in an injured biliary system or if it contributes to damage through increasing the intraductal pressure. It would be of interest to investigate whether canalicular expression of MYH14 is associated with prognosis at a clinical level to aid the prognostication of patients with PSC.

Finally, MYH14 is not a plasma membrane protein, but is a form of non-muscle myosin II. For these reasons, despite a higher expression in injury, MYH14 would not be an ideal candidate as a target for cellular homing.

The most abundant proteins identified in intrahepatic ducts which were also significantly more abundant than in hepatocyte samples were Histone 4f4, Vimentin and Annexin V. Histone 4f4 is not a plasma membrane protein whilst both vimentin and Annexin V are. As noted in the results section, Vimentin is thought to be predominately intracellular, although can also be excreted into the extracellular matrix.

Annexin V was highly expressed in BEC on immunohistochemistry with no expression in hepatocytes or other liver cells; this was true across all the murine and human injuries.

Annexin V was shown to be highly expressed in BEC compared with hepatocytes and other cells in the liver. There appeared to be expression within the endothelial cells of the liver and with further areas of non-specific extra-ductal staining on immunohistochemistry. This could make Annexin V a less attractive target for cell homing; however, this would require corroboration with more biological replicates. More importantly, the present data demonstrated no increase in abundance of Annexin V following biliary injury on mass spectroscopy. Additionally, according to the data presented by Pepe-Mooney and co-workers in 2019 a fold change of -0.92 was identified when comparing control mice and those that had received two weeks DDC diet. This change in expression was found to be statistically significant and therefore indicates that Annexin V expression may indeed decrease following biliary injury [15]. For these reasons Annexin V is not felt to be an appropriate target for cell homing.

Our data contrasts with that of Katayanagi and co-workers, in which Annexin V was mostly expressed in the intrahepatic ducts[267]. Although the extrahepatic duct abundance was less in than intrahepatic in the present study, Annexin V remained the eighth most abundant protein detected in injured extrahepatic ducts as figure 6.17B demonstrates.

Annexin V was not the only highly expressed member of the Annexin family identified in this dataset. Annexins II, III, IV, VI and XIII were all detected in the 822 proteins which were either identified exclusively in biliary ducts or upregulated in the intra- and

extrahepatic ducts compared with hepatocytes. Annexin II was also in the top 10 most abundant proteins both in injured intra- and extrahepatic ducts.

The Annexins are a group of proteins which either directly bind to calcium or bind to phospholipids in a calcium dependent manner [268]. There is limited knowledge at present of their function and expression in the biliary system. In biliary atresia, Annexin II has been shown to be upregulated. Nuerzhati and co-workers in 2019 demonstrated that knocking down Annexin II led to decreased cell proliferation and cell cycle arrest, indicating that Annexin II may have a role in regeneration[269]. Annexin IV has been implicated in gallbladder cancer as a negative prognostic marker. In addition, knock-down of Annexin IV in gallbladder cancer cell lines has led to increased apoptosis and reduced cell growth[270]. Increased Annexin X has been associated with poor prognosis in cholangiocarcinoma [271], suggesting that Annexin X is promoting proliferation and growth in cholangiocarcinoma. Annexin XI has been shown to be specific to BEC in the context of the liver. Tolenaars and co-workers have demonstrated Annexin XI colocalization with the chloride channel ANO1 which is expressed on the apical membrane of BEC[272]. It has also been shown that Annexin 11 is targeted by auto-antibodies in IG4 related liver disease[273]. These observations in combination indicate that the Annexins may promote proliferation in BEC.

The function of Annexin V in the ducts remains unclear. The observation that Annexin V appeared less clearly expressed in PBC and PSC, could be an interesting line for further investigation; it is possible that reduced Annexin V could reflect a reduction in the capacity of BEC to regenerate in these chronic cholangiopathies.

A further interesting line of investigation would be to assess the effects of Annexin V knockout on cell growth in biliary organoids, which may indicate if Annexin V is important for cellular proliferation.

At a biochemical level, Annexin V could be acting in several ways. Annexin V has a high affinity for the phospholipid phosphatidylserine (PS). Under normal circumstances, PS is in the internal aspect of the plasma membrane's lipid bilayer, however in cellular apoptosis PS translocate to the outer aspect of the plasma membrane[274, 275]. Annexin V may then bind to PS identifying cells which are in the process of apoptosis. The same process is also seen in biology as Annexin V has been shown to protect endothelial cells which following damage express PS externally. PS can also

interact with the coagulation cascade and can lead to clot formation and ultimately vascular damage[276]. It is possible that Annexin V is forming a protective coat over the plasma membrane of BEC to prevent damage from the detergent effects of bile. This hypothesis could also be tested in vitro, by exposing wild type BEC and BEC with Annexin V knocked out to bile and comparing injury responses.

Annexin V has also been implicated in the trafficking of CFTR to the plasma membrane[277]. Dysfunction in CFTR lead to cholangiopathies, as outlined in the introduction. It is possible that the observed reduction in Annexin V may lead to a reduction in membrane CFTR in BEC and contribute to injury in the cholangiopathies.

6.15 Conclusion:

Whilst no target for a cell homing mechanism to BEC could be identified in this proteomic analysis, a novel biliary specific protein MYH14 was found to be both biliary specific and had increased expression in biliary injury.

Chapter 7: Improving cell therapy for the cholangiopathies in vivo

7.1 Introduction

The aim of all preclinical cell therapies is ultimately to progress to the clinic. The cost and competition for funding in clinical research means that novel therapies which are often themselves expensive have limited opportunities to prove evidence of efficacy[278]. A negative clinical trial could result in reduced subsequent interest. Therefore, it is important to optimize therapies prior to embarking on clinical studies, to ensure a therapy has the best possible chance of demonstrating efficacy.

Several decisions must be considered before embarking on clinical research such as the dose range, the method of administration and the frequency of treatment. In contrast to drug therapy, cell therapy has several further considerations which could significantly impact the efficacy and side effect profile. These include how cells are isolated, the suspension the cells are held in, if cells are cultured prior to therapy and whether any of a multitude of modifications should be made to the cells. In a similar vein to combination drug therapy, cells can also be administered in association with drugs or other cells. It is important to collect evidence to inform these decisions as best as possible prior to embarking into the clinical sphere.

When considering methods for optimisation of a cell therapy, it is important to understand the process a cell must undergo following administration. They must evade the host immune system, migrate from the delivery site to the target and finally engraft at the target site. In addition, there are likely a multitude of, at present, unknown factors which influence the success of a cell following transplantation. As an example, in recent years the influence of shear stresses on transplanted cells, are being increasing investigated as a possible reason for poor engraft[279, 280].

The most recent evidence of human HPC in the treatment of cholangiopathy comes from Hallett, Ferreira-Gonzalez and co-workers published in cell stem cell in 2022 [124], in which cells were transplanted into the *Krt19Cre^{ER}Mdm2 $^{fl/fl}$ Rag2$^{-/-}$ Il2rg$^{-/-}$* model of cholangiopathy via the spleen. When human HPC were identified, they were found near the biliary ducts. The results of this study and others [17] indicate that at least some HPC have the capacity to make the journey from delivery to engraftment. This evidence invites the interrogation of individual aspects of HPC migration and engraftment, to determine where improvements can be made. Contrastingly if cells had not been identified following transplantation there would be

no evidence that HPC could achieve engraftment under any circumstances, and it may have been futile to investigate the process of HPC migration and engraftment.

Cell homing is the central theme of this research thesis. BEC are not known to migrate under normal circumstances[153], however immune cells may migrate towards the biliary ducts[57, 281, 282] following injury. These systems of immune cell migration have been used in the past to improve on cell migration to the liver, for example the work of Xu and colleagues in upregulating CCR2 expression in MSCs, increasing migration to the liver [202], whilst Du and co-workers demonstrated improved migration to the liver following overexpression of CXCR4 also in MSCs[283].

A prerequisite for improving on an aspect of the cell homing process is that there is space for an improvement to be made. For example, if transplanted cells already express CXCR4 highly, it may not be useful to attempt to further increase the expression of this receptor.

The preceding two chapters identified CXCL2 as a possible candidate for cell homing. This has been supported by previous studies which indicate CXCL2 to be integral to the process of neutrophil migration to the biliary ducts during biliary injury[215]. The focus of this chapter is developing human HPC which express CXCR2 and comparing their ability to migrate to the ducts with control HPC.

This chapter attempts to use the increased expression of CXCL2 in injured BEC to improve homing of human HPC in the *Krt19Cre^{ER}Mdm2 $^{fl/fl}$ Rag2$^{-/-}$ Il2rg$^{-/-}$* model.

7.2 Human HPC do not express chemokine receptors at the gene level.

Before increasing the expression of CXCR2 in human HPCs, it was first necessary to assess the baseline expression level.

Included in the work of Hallett, Ferreira-Gonzalez and co-workers was RNA bulk sequencing data of human HPCs [124]. This data has been reanalysed using the deSeQ package in R to assess the expression of chemokine receptors in human HPC [284]. Data was normalised and is presented as normalised reads.

All the detected chemokine receptors, including *Cxcr2* had very low numbers of normalised reads as shown in figure 7.1, mean normalised read 2.0 +/-4.6 standard deviation. For comparison the mean normalised reads +/- standard deviation of biliary markers *Krt19*, *Epcam*, *Cftr* and *Sctr* were 26298.8 +/- 7388.9, 4551.7 +/- 971.2, 9097.0 +/- 6551.2 and 94.7 +/- 69.4 respectively. This demonstrates that *Cxcr2* has low genetic expression in human HPC. It was therefore felt that increasing the expression of *Cxcr2* in human HPC could influence the ability of these cells to home to the biliary ducts.

Figure 7.7.1 Expression of chemokine receptor genes in bulk sequencing data.

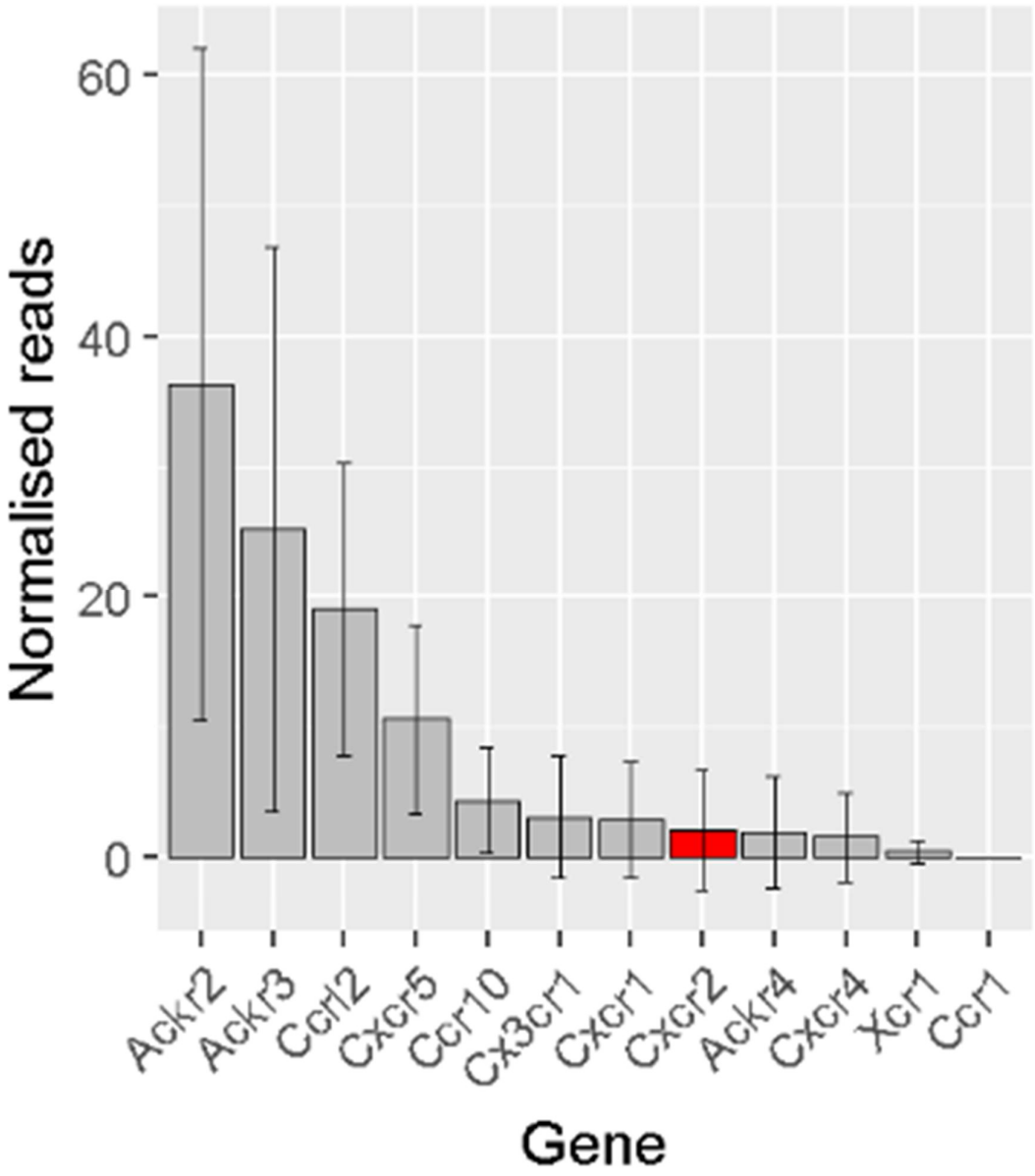

Figure 7.1. Expression of chemokine receptor gene in bulk sequencing data. (n=5)

Bars indicate mean expression, error bars standard deviation. Red bar indicates *Cxcr2.*

7.3 Transduction of human HPC with CXCR2-GFP lentivirus

To produce human HPC which express CXCR2, lentiviral transduction was employed as described in the methods section, using a virus produced by Dr. Pamela Brown at the University of Edinburgh. The gene construct for human CXCR2 was inserted into a GFP lentivirus vector, on the same promotor as GFP, upstream.

Following transduction, cells were selected using an antibody for CXCR2 bound to PerCP and on GFP expression. Due to poor transduction efficiencies sorting was performed twice. As a control, GFP positive cells were also produced using the same lentivirus without the addition of CXCR2.

An example of the gating technique is shown in figure 7.2A. The selection of cells is shown using side scatter (SSC)-A and forward scatter (FSC)-A, single cells were then separated from doublets using FSC-A and FSC-H. Live cells were identified using DAPI. GFP or double positive (CXCR2-GFP) HPCs were sorted as shown in Figure 7.2B and C.

Following sorting, cells were collected in Matrigel and grown as described in the methods. Figure 7.2D demonstrates appearances of control, GFP and CXCR2-GFP organoids demonstrating no change in the appearance of organoids following transduction. However, CXCR2-GFP organoids subjectively grew more slowly than GFP organoids.

Whilst it has been demonstrated that in HPC there is low genetic expression of CXCR2, this was also assessed at a proteomic level using flow cytometry. Figure 7.3 displays comparison between HPC, GFP and CXCR2-GFP HPC. After staining with CXCR2 antibody there was a clear shift in the population of CXCR2-GFP transduced HPCs as expected. As shown in Figure 7.3A and B when HPC and GFP HPC are incubated with the CXCR2 antibody no shift in the expression of the associated fluorophore peidinin chlorophyll (PerCP) was demonstrated.

Figure 7.7.2 Production of GFP and GFP CXCR2 human HPC

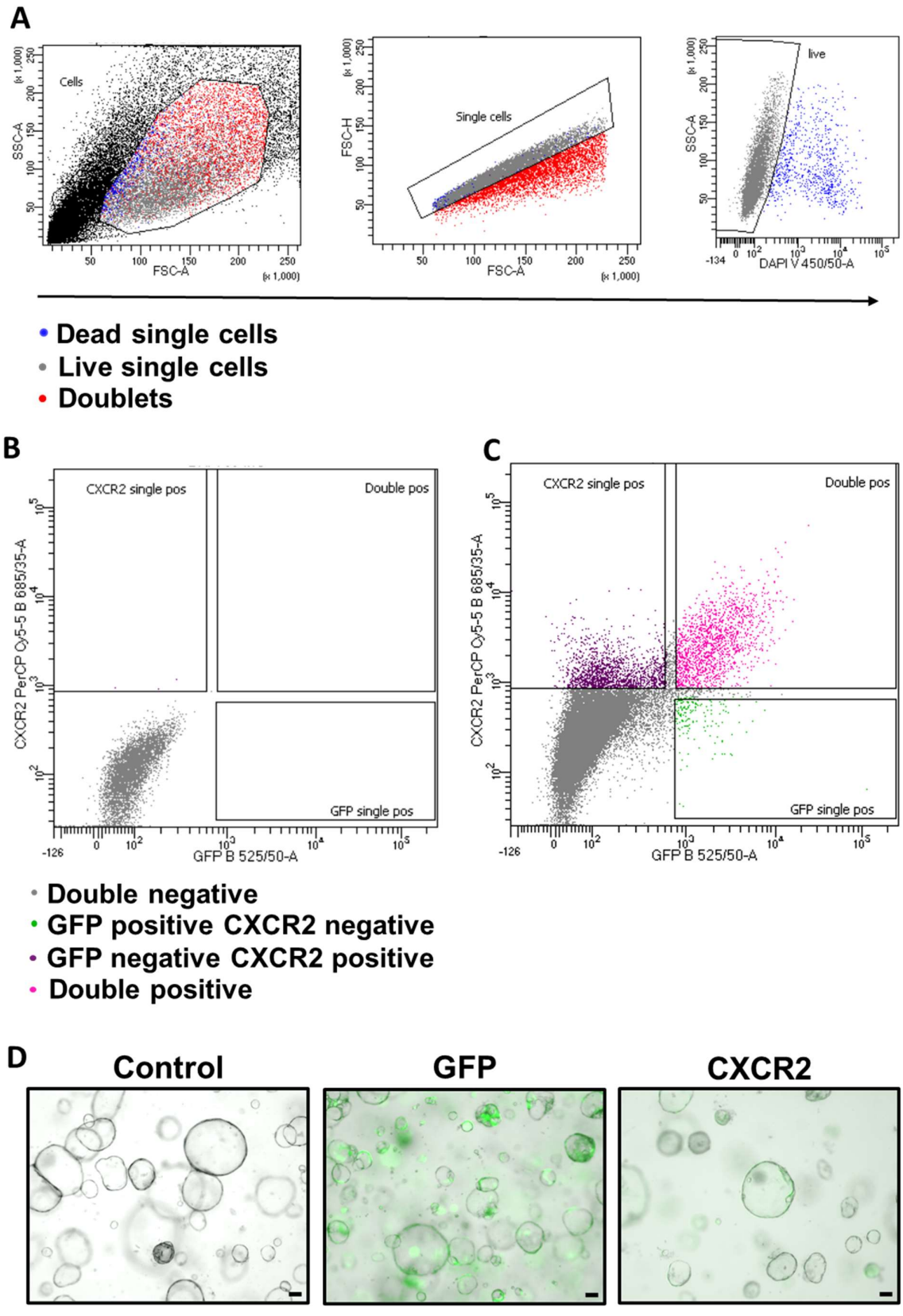

Figure 7.2: Production of GFP and GFP CXCR2 human HPC

A: Gating strategy for selection of live single cells, arrow indicates direction of selection. From left to right, selection of cells using SSC-A and FSC-A, singlets using FSC-A and FSC-H. and selection of live cells using DAPI SSC-A

B: Selection of GFP or CXCR2 positive cells using GFP and PerCP. Example of a negative control.

C: Selection of GFP or CXCR2 positive cells using GFP and PerCP. Example of a positive sample.

D: Images of control HPC, GFP transduced cells and CXCR2-GFP transduced HPC. GFP in green. Scale bars represent 100μm.

Figure 7.7.3 CXCR2 is not expressed in HPC at the proteomic level

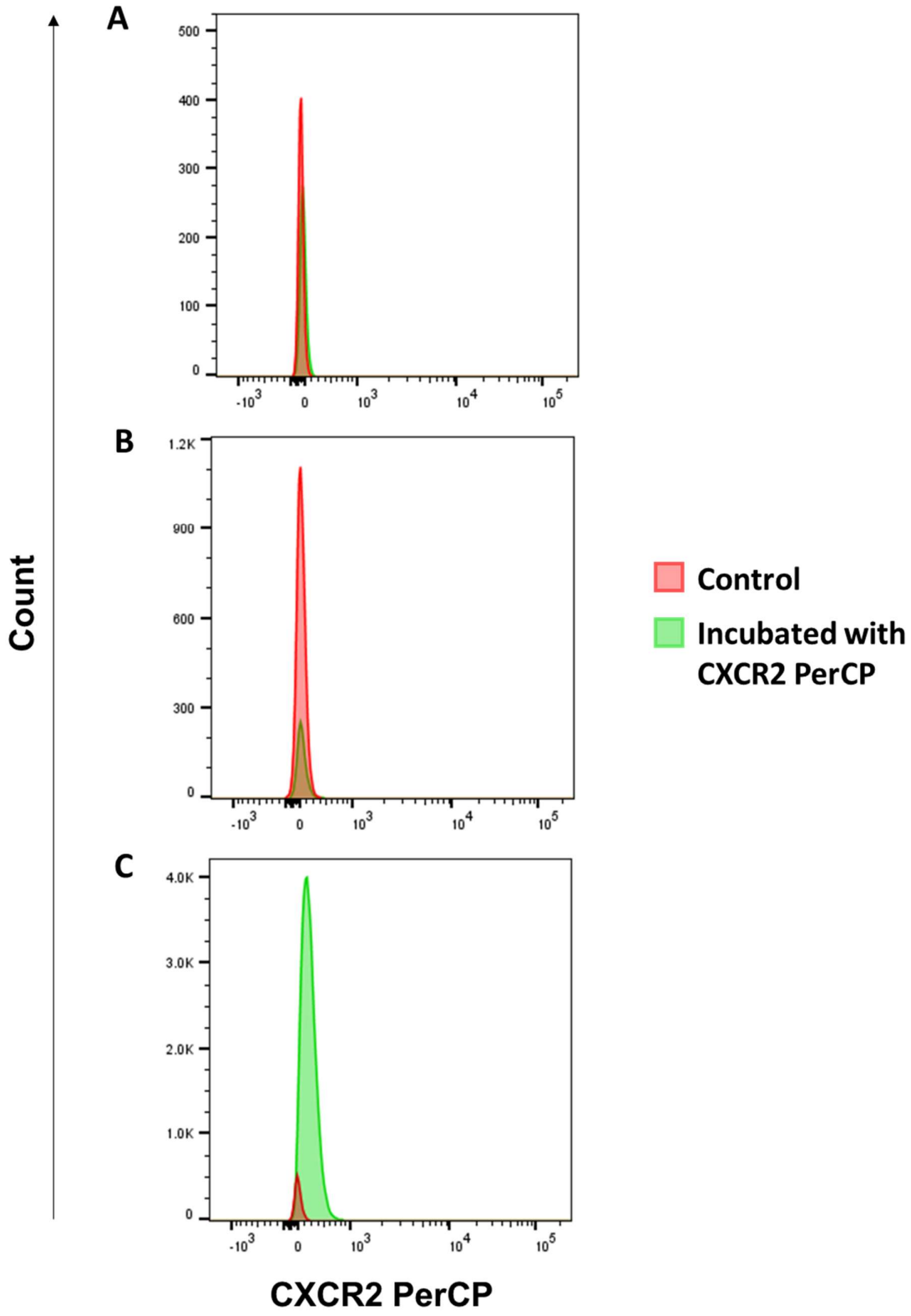

Figure 7.3: CXCR2 is not expressed in HPC at the proteomic level

Post hoc analysis of FACs sorting of HPC, GFP and CXCR2-GFP HPC. All histograms display PerCP expression, the fluorophore associated with the CXCR2 antibody, in HPC incubated with CXCR2 antibody (in green) and those not (in red)

A: Non transfected HPC

B: GFP HPC

C: CXCR2-GFP HPC

Plots A and C underwent sorting on the same day. Plot B was performed on a separate occasion.

7.4 Comparison of GFP expression in CXCR2-GFP and GFP human HPC transplanted into the *Krt19Cre^{ER}Mdm2 $^{fl/fl}$ Rag2$^{-/-}$ Il2rg$^{-/-}$* model.

CXCR2-GFP or GFP HPC were transplanted into the *Krt19Cre^{ER}Mdm2 $^{fl/fl}$ Rag2$^{-/-}$ Il2rg$^{-/-}$* of cholangiopathy via intrasplenic injection. Surgeries were carried out by Dr. Victoria Gadd, whilst the PhD candidate prepared the cells and assisted with the surgeries.

Injury was induced using three doses of tamoxifen followed by 48 hours of DDC diet as described previously. 250,000 CXCR2-GFP or GFP human HPC were transplanted into each mouse.

Although the *Cxcr2-Gfp* plasmid was produced using the same *Gfp* plasmid used to produce the GFP HPC line, there was potential that the addition of a *Cxcr2*transcript could change the efficiency of GFP expression. HPCs would be identified following transplant through expression of GFP, therefore an assessment of the percentage expression of GFP in each HPC line was carried out. Figure 7.4 presents the expression of GFP in the two transplanted HPC lines a single passage following transplantation of the HPC.

93.9% of GFP HPCs were GFP positive one passage following surgery, 91.8% of CXCR2-GFP HPCs were GFP positive. This difference was felt to be negligible and therefore no correction was applied to the analysis of liver tissues post transplantation. It was also noted that the expression of GFP was generally brighter in the GFP HPCs compared with the CXCR2-GFP HPCs, evidenced by the relative shift of cells to the left of the graph on the x axis in Figure 7.4B, compared with Figure 7.4C.

Flow analysis demonstrated that 2.1% of GFP HPCs were also positive for PerCP, despite compensation. This was only seen in cells which had extremely bright GFP expression, it is likely that this represents bleeding of GFP fluorescence into the PerCP channel, as CXCR2 antibody was not added to this sample.

Figure 7.7.4 Comparison of GFP expression in cultured human HPC 1 week following transplant

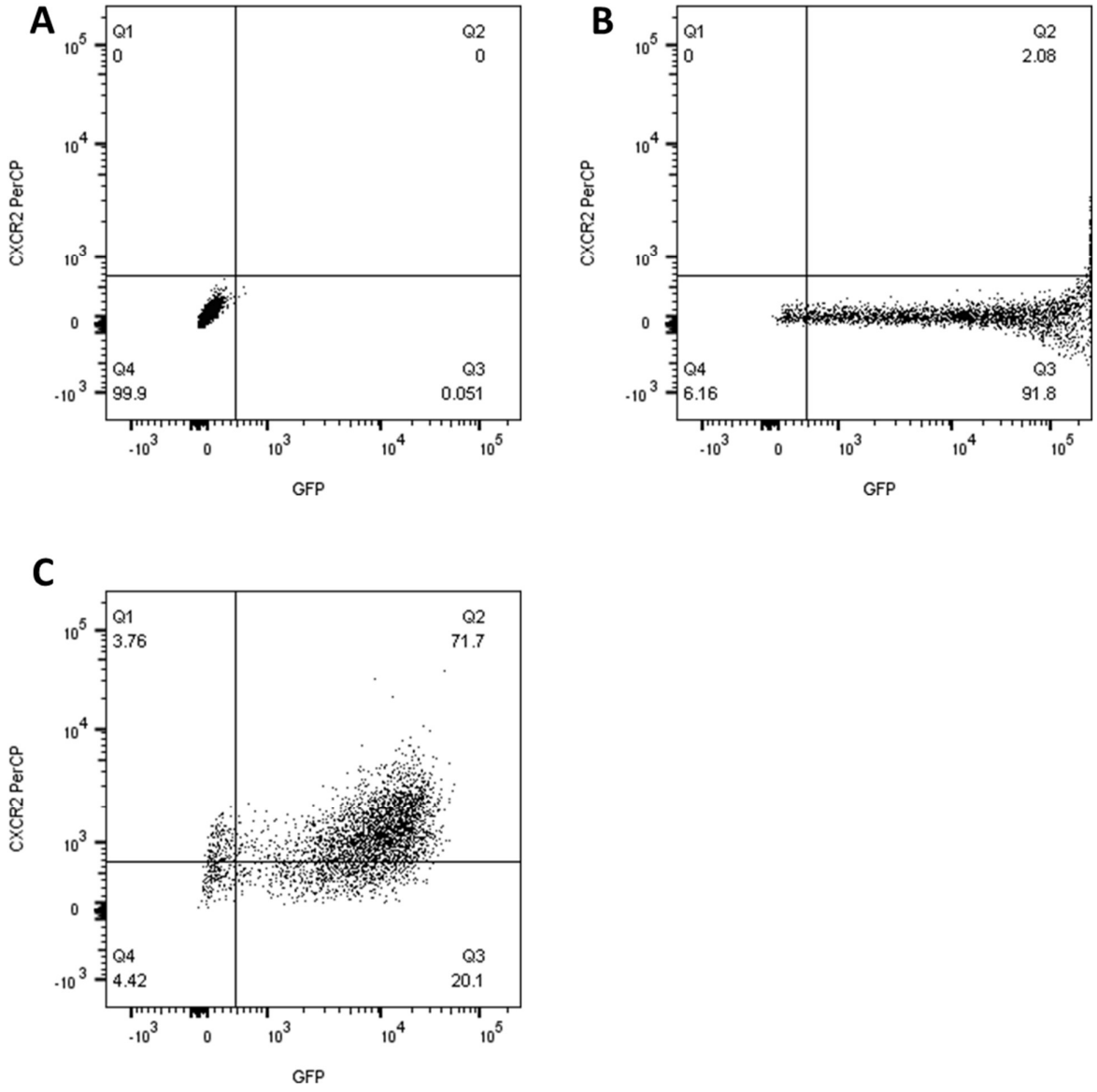

Figure 7.4: Comparison of GFP expression in human HPC 1 week following transplant

Flow cytometry comparing GFP and CXCR2 through PerCP expression, 1 week following transplants.

A: Control human HPCs

B: GFP human HPCs used for transplantation.

C: CXCR2-GFP human HPCs used for transplantation.

7.5 Engraftment and clinical outcomes following transplantation of CXCR2-GFP and GFP cells into the *Krt19Cre^{ER}Mdm2 $^{fl/fl}$ Rag2$^{-/-}$ Il2rg$^{-/-}$* model.

48 hours following transplantation mice were culled, tissue and blood were collected. No significant differences in biochemical markers of liver injury were identified between the groups as shown in Figures 7.5A-F, however it should be noted that using Mann-Whitney test it would be impossible to obtain a significant difference with the number of replicates used. Bilirubin was higher in all four of the mice that received GFP HPCs transplant than the three mice that received CXCR2-GFP HPC, median bilirubin was also more than twice as high in the GFP group compared with CXCR2-GFP. Similarly, AST was more than double in the mice that received GFP HPCs, and all mice individually had higher AST than the mice that received CXCR2-GFP HPCs. There were further trends towards lower levels of ALT and higher levels of GLDH in the mice who received CXCR2-GFP HPCs.

Figure 7.5G and H present images of the livers removed from mice who received GFP and CXCR2-GFP HPCs respectively. Macroscopic areas of palor are seen in the livers of mice that received CXCR2-GFP HPCS and in a single mouse, furthest to the right of Figure 7.5G, that received GFP HPCs. These areas of unclear etiology however areas of infarcted liver have previously been described in this model, and this is one possible explanation [124].

The engraftment of cells was investigated using immunofluorescence and immunohistochemistry. Each individual mouse included in this study had evidence of engraftment at the time of cull, as shown in Figure 7.6. Subjectively, it was felt on immunohistochemistry that more biliary ducts had associated transplanted HPCs in the mice that received GFP HPC transplant. Conversely, when considering only ducts with HPC associated, HPC appeared in larger numbers in mice that received CXCR2-GFP than GFP HPC, reflected in the images in Figure 7.6 and Figure 7.7C.

Using QuPath it was possible to assess the distance of GFP positive cells from the nearest BEC as defined by KRT19 expression. None of the transplanted GFP positive cells were identified by the software as also positive for KRT19, which was convenient and ensured the distance measurements were accurate. This has not been reported previously and indicates the possibility that KRT19 expression is lost in HPC during the culture or transplantation process.

Due to the limited sample size no significant associations could be identified on Mann Whitney test between mice that received GFP HPCs and those that received CXRC2 GFP HPCs. There was a trend towards GFP HPCs having a lower distance to the closest BEC compared with mice who received CXCR2-GFP HPCs, Figure 7.7B. This indicates less efficient cell homing of HPCs to BEC. There was a less clear trend towards a higher proportion of the total cells imaged being positive for GFP in the CXCR2-GFP HPC mice Figure 7.7A, indicating that CXCR2-GFP cells were more likely to become lodged in the liver. Figure 7.7C demonstrates images of typical ducts which were associated with GFP positive cells, as noted in the previous section, these were less common in mice that received CXCR2-GFP transplant.

Figure 7.7.5 Biochemistry of mice who received GFP or CXCR2 cells.

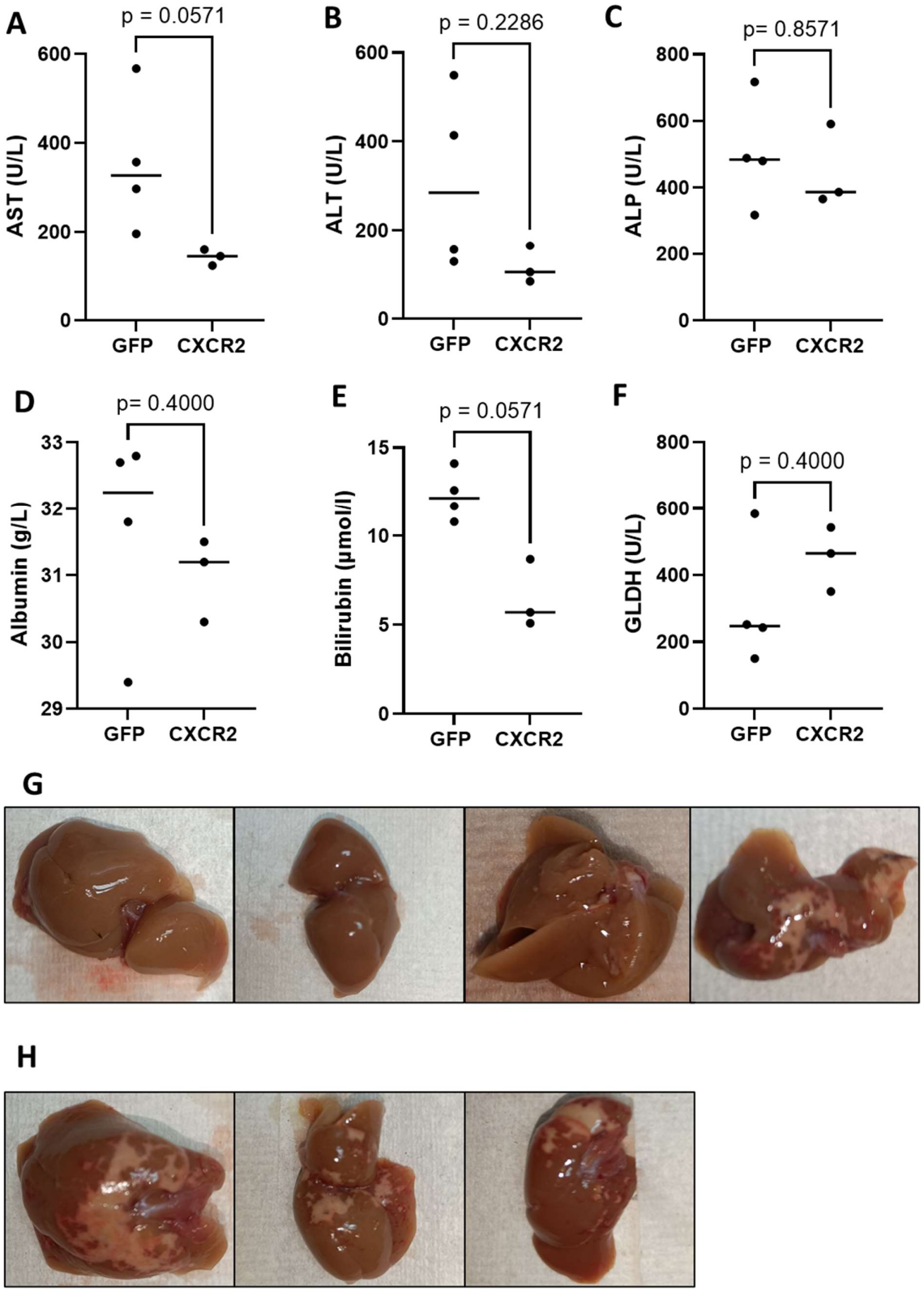

Figure 7.5: Biochemistry of mice who received GFP or CXCR2-GFP HPC.

Graphs indicate individual mice through dots, horizontal lines represent median

A: AST taken at time of cull in mice who received GFP HPCs and CXCR2 GFP HPCs transplant. Median AST in mice who received GFP cell transplant 327 U/L, mice who received CXCR2 transplant 144 U/L. Mann Whitney test p=0.057

B: ALT taken at time of cull in mice who received GFP HPCs and CXCR2 -GFP HPCs transplant. Median ALT in mice who received GFP cell transplant 285 U/L, mice who received CXCR2 transplant 105 U/L. Mann Whitney test p=0.229

C: ALP taken at time of cull in mice who GFP HPCs and CXCR2-GFP HPCs transplant. Median ALP in mice who received GFP cell transplant 484.5 U/L, mice who received CXCR2 transplant 387 U/L. Mann Whitney test p=0.857

D: Albumin taken at time of cull in mice who received GFP HPCs and CXCR2-GFP HPCs transplant. Median Albumin in mice who received GFP cell transplant 12.15 U/L, mice who received CXCR2 transplant 5.7 U/L. Mann Whitney test p=0.4

E: Bilirubin taken at time of cull in mice who received GFP HPCs and CXCR2-GFP HPCs transplant. Median Bilirubin in mice who received GFP cell transplant 32.25 U/L, mice who received CXCR2 transplant 31.2 U/L. Mann Whitney test p=0.057

F: GLDH taken at time of cull in mice who received GFP HPCs and CXCR2-GFP HPCs transplant. Median GLDH in mice who received GFP cell transplant 247.5 U/L, mice who received CXCR2 transplant 465 U/. Mann Whitney test p=0.4

G: Images of livers from mice who received GFP HPC transplant

H: Images of livers from mice who received CXCR2-GFP HPC transplant

Figure 7.7.6 Expression of GFP in mice who received either GFP or CXCR2 transplant

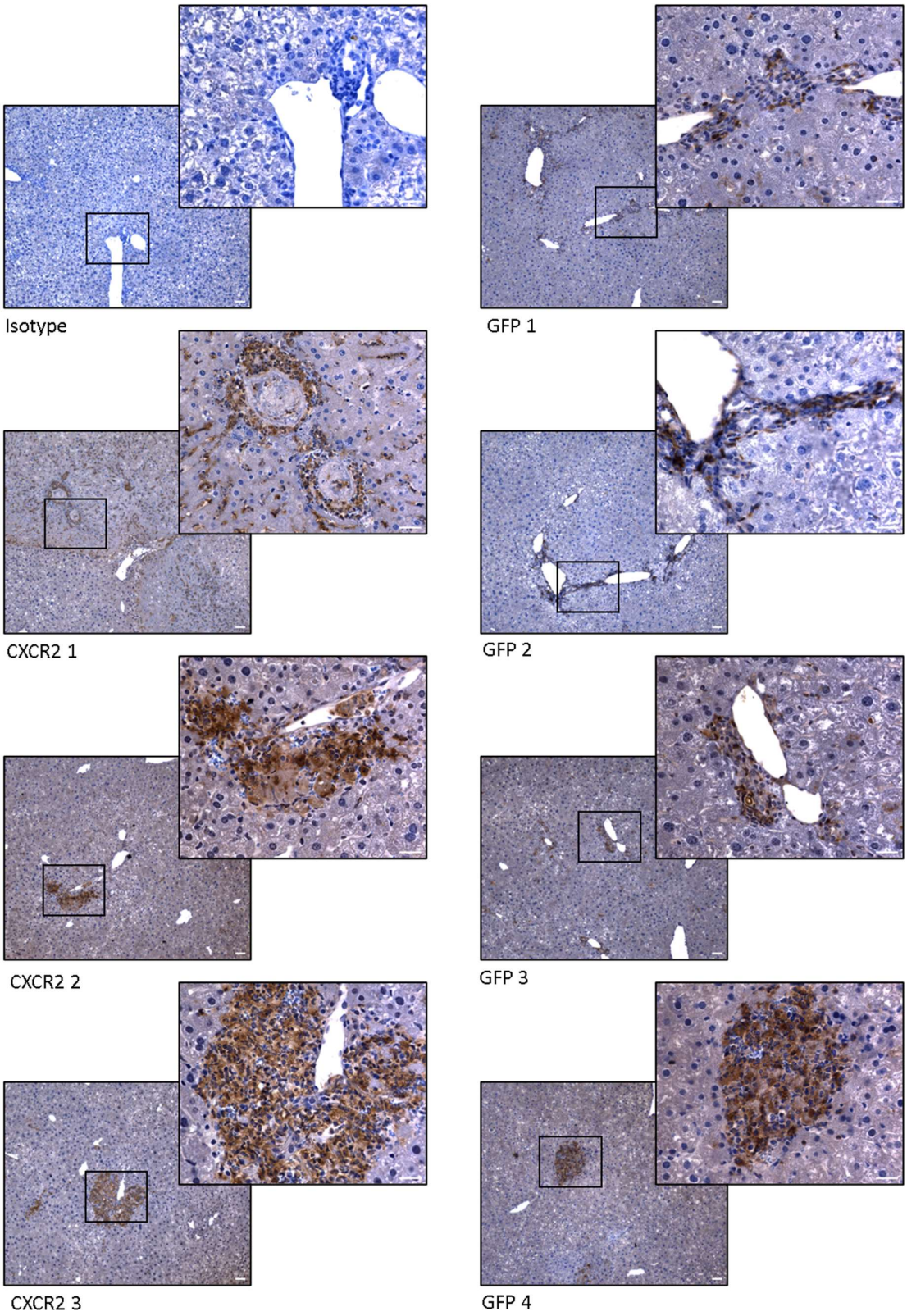

Figure 7.6: Expression of GFP in mice who received either GFP or CXCR2-GFP HPC transplant

Representative images of GFP immunohistochemistry in all 7 of the mice who received either GFP or CXCR2-GFP HPC transplant. Right and superior images are 40x magnification, inferior and left images 10x. All scale bars represent 50μm.

Figure 7.7.7 Expression of GFP relative to biliary ducts

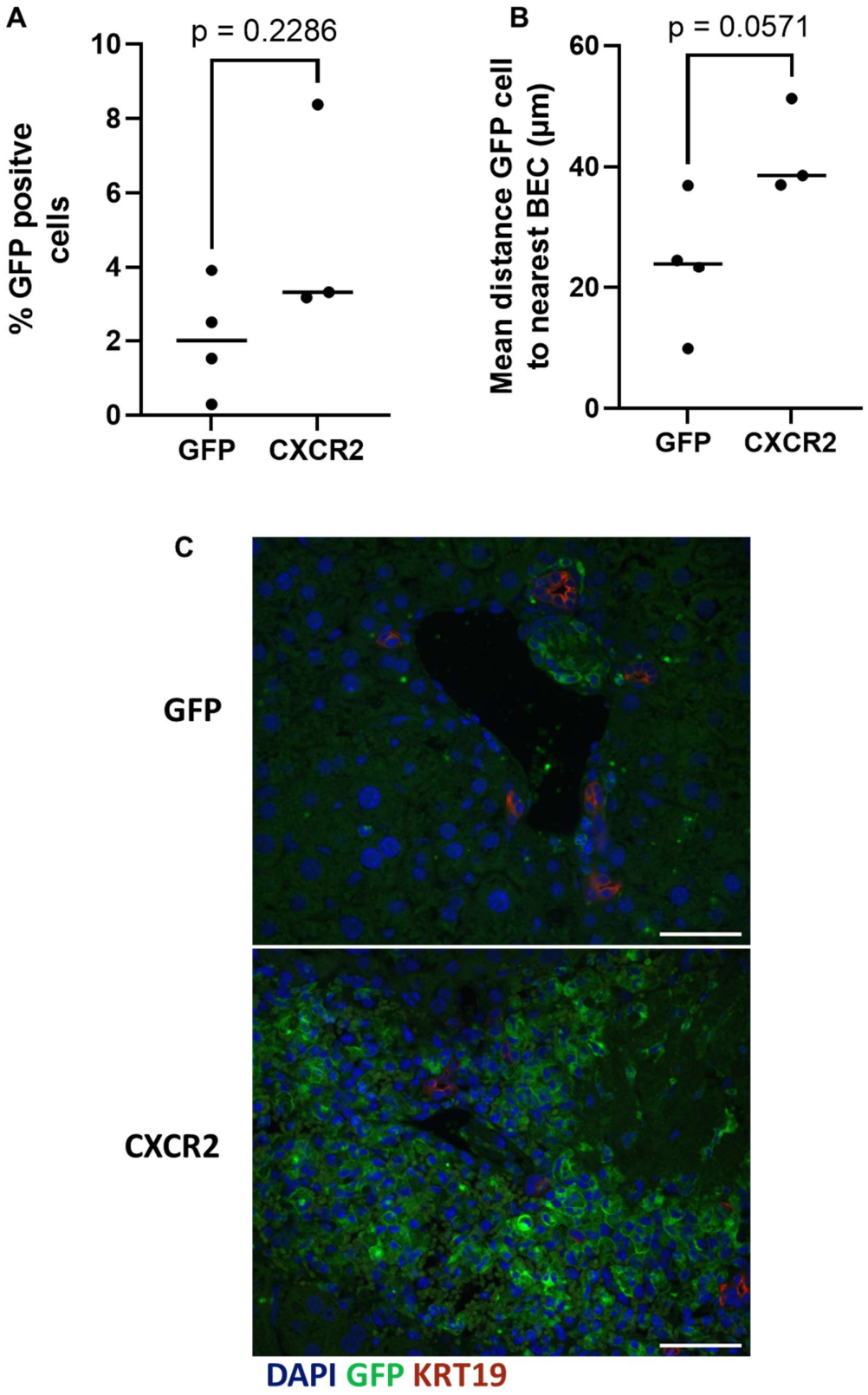

Figure 7.7: Expression of GFP relative to biliary ducts

Graphs indicate individual mice through dots, horizontal lines represent medians.

A QuPath analysis comparing the number of GFP positive cells across 10 images taken containing biliary ducts as defined by KRT19 expression. Median percentage GFP positive cells in mice that received GFP cell transplant 2.016%, in mice that received CXCR2 transplant 3.316%. Mann Whitney test p=0.2269.

B: QuPath analysis comparing the median distance of GFP positive cells across 10 images from the closest KRT19 expressing cell. Median distance in mice who received GFP cell transplant 23.984 μm. Mice that received CXCR2 transplant 38.552. Mann Whitney test p=0.0571.

C: Immunofluoresence images staining for KRT19, GFP and DAPI. All scale bars represent 50μm. Images on immunofluorescence at 40 x magnification.

These images are not representative of a typical duct but are typical of a duct with associated GFP positive cells.

7.6 Host inflammatory response and ACKR2

Whilst the bulk of this thesis has concentrated on homing, immune response of the host against transplanted cells offers an alternate or complimentary cause for poor engraftment[285, 286]. In an ongoing collaboration with Professor G. Graham, University of Glasgow, solutions to this have been investigated. Atypical chemokine receptor 2 (ACKR2) is a transmembrane receptor which transports a multitude of chemokines from the local environment into the cell for degradation[287-289]. The CC-motif family of chemokines such as CCL2 are primarily affected by ACKR2, whereas CXCL1 and CXCL2 are not known to be[290]. An important role of chemokines is the recruitment of immune cells[291]. Currently prevailing consensus postulates that the removal of chemokines by ACKR2 from the local environment reduces the attraction of immune cells. Indeed this theory has garnered support in recent years through the demonstration that neutrophil[292], macrophage[290] and lymphocyte[293] recruitment are modulated by ACKR2 expression. The work of Madigan et al in Journal of Immunology in 2010 indicated that ACKR2 expression in trophoblasts of the placenta reduce the risk of absorption of allogenic embryo transplantation[294]. This study demonstrates the potential of ACKR2 to protect transplanted cells from the host immune response. In this supplementary section we have appropriated this concept for HPC transplant in mice.

As shown in figure 7.1 *Ackr2* expression is low in human HPC. Murine HPC were transduced to expresses ACKR2 and GFP, the production of the plasmid is described in the methods. Figure 7.8 demonstrates that murine HPC do not express ACKR2 at the proteomic level until transduced with lentiviral vector. CCL22- AF647 fluorophore has been used to demonstrate both presence and functionality of ACKR2 as described in methods section 4.30.

The overarching hypothesis of this study was HPC expressing ACKR2 invoke reduced inflammation when transplanted, therefore an immunocompromised model was not an appropriate tool for investigation and experiments were performed on C57BL/6 mice. The IRI model was selected as this is known to induce macrophage infiltration in the liver[225, 295, 296] and cause a mixed biliary and hepatocellular injury[297].

Depicted in Figure 7.9A, is the experimental design. 1 million murine HPC transduced to express ACKR2 and GFP (ACKR2-GFP) or GFP alone were transplanted into mice immediately following IRI.

Il1-β and *Emr-1* were assessed in extracted liver to reflect inflammation and macrophage infiltration respectively. There were no significant differences between the groups Figure 7.9B and C. No significant differences in biochemical markers of hepatic injury were identified following transplantation, Figures 7.9D-I.

Engraftment was assessed through immunohistochemistry for GFP. Figure 7.10 portrays images post transplant indicating in both GFP and the ACKR2-GFP HPC were able to engraft in all cases. No difference was identified in macrophage infiltration as determined by immunohistochemical staining for F4/80 Figure 7.11.

Figure 7.8 Production of an ACKR2 expressing line of murine HPC

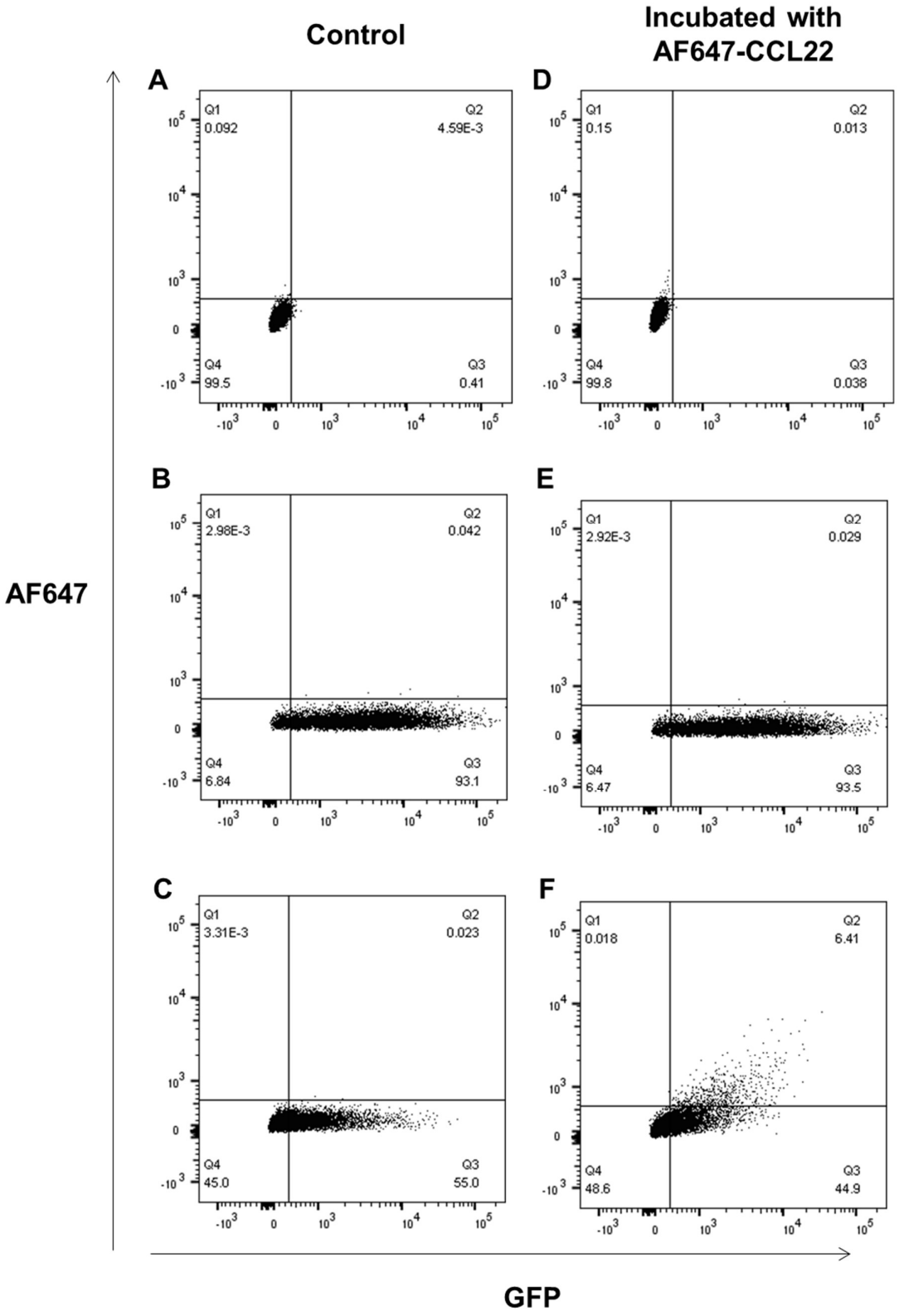

Figure 7.8; Production of an ACKR2 expressing line of murine HPC.

Post hoc analysis of murine HPC comparing GFP and ACKR2 through AF647 expression.

A: Control murine HPC.

B: GFP transduced murine HPC.

C: ACKR2-GFP murine HPC.

D: Control murine HPC incubated with AF647-CCL22.

E: GFP transduced murine HPC incubated with AF647-CCL22.

F: CXCR2-GFP murine HPC incubated with AF647-CCL22.

Figure 7.9 Biochemistry of mice who received GFP or ACKR2-GFP murine HPC.

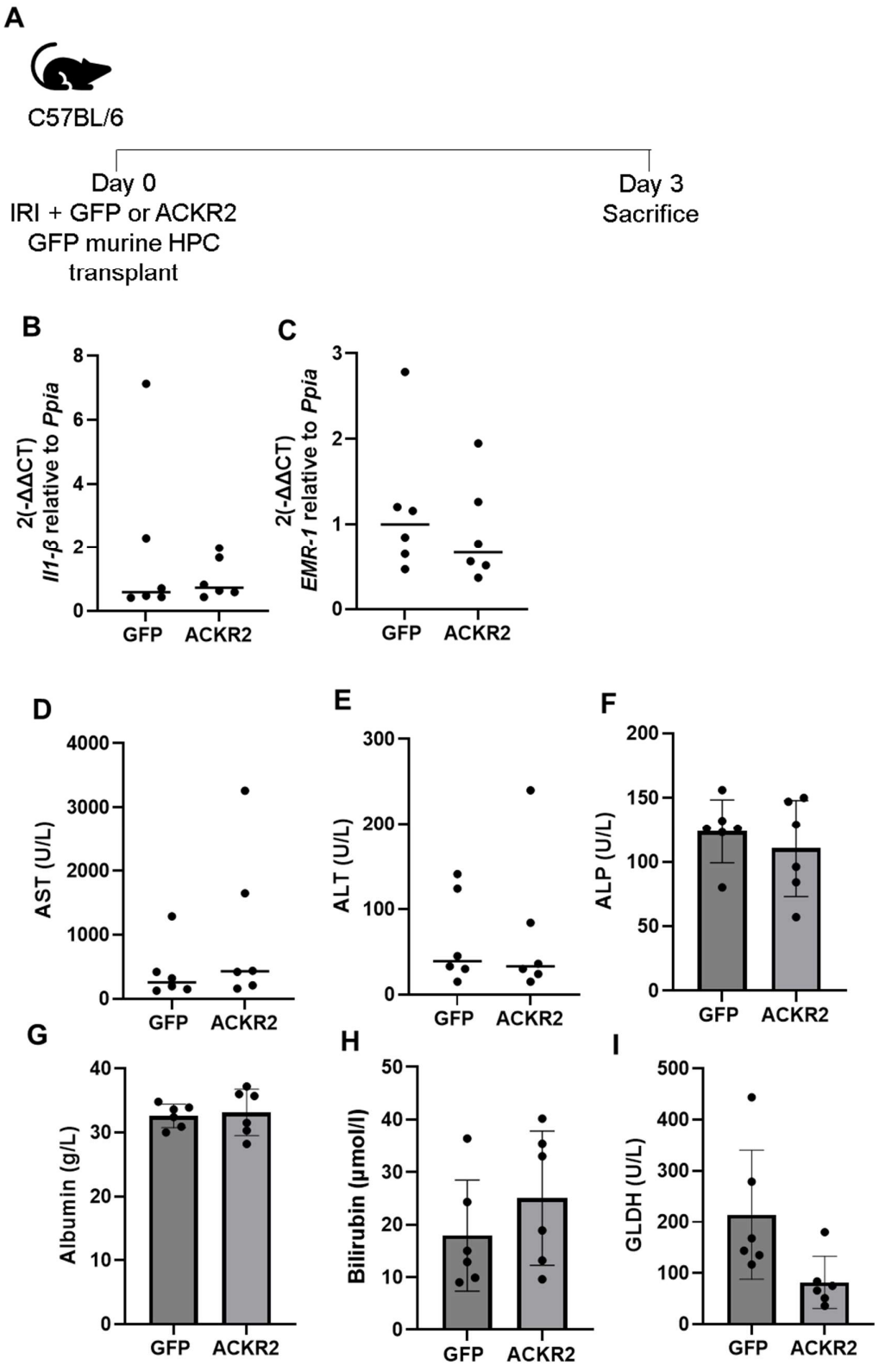

Figure 7.9: Biochemistry of mice who received GFP or ACKR2-GFP murine HPC.

Graphs indicate individual mice through dots. Horizontal lines indicate median. Boxes indicate mean, error bars as standard deviation. Figures have been presented as mean and standard deviation if normality test was passed and parametric testing was used, median if normality test failed and non-parametric testing. n=6

A: Schematic demonstrating experimental design

B: qPCR of *Il1-β* in whole liver of mice treated with GFP or ACKR2-GFP transplant. Median fold change of ACKR2-GFP vs GFP 0.733, p=0.937 using Mann-Whitney test.

C: qPCR of *Emr-1* in whole liver of mice treated with GFP or ACKR2-GFP transplant. Median fold change of ACKR2-GFP vs GFP 0.666, p=0.5887 using Mann-Whitney test.

D: AST taken at time of cull in mice who received GFP cell and ACKR2-GFP transplant. Median AST in mice who received GFP HPC transplant 39 U/L, mice who received ACKR2 transplant 33 U/L. Mann Whitney test p=0.79

E: ALT taken at time of cull in mice who received GFP cell and ACKR2-GFP transplant. Median ALT in mice who received GFP cell transplant 259.5 U/L, mice who received ACKR2 transplant 430.5 U/L. Mann Whitney test p=0.197

F: ALP taken at time of cull in mice who received GFP cell and ACKR2-GFP transplant. Mean and (Standard deviation) of ALP in mice who received GFP cell transplant 123.8U/L (24.63), mice who received ACKR2 transplant 110.5 U/L (37.44). Student's t test with Welch's correction test p=0.485

G: Albumin taken at time of cull in mice who received GFP cell and ACKR2-GFP transplant. Mean and (Standard deviation) of Albumin in mice who received GFP cell transplant 32.6U/L (1.86), mice who received ACKR2 transplant 33.2 U/L (3.64). Student's t test with Welch's correction test p=0.751

H: Bilirubin taken at time of cull in mice who received GFP cell and ACKR2-GFP transplant. Mean and (Standard deviation) of Bilirubin in mice who received GFP cell transplant 17.92 U/L (10.58), mice who received ACKR2 transplant 25.05U/L (12.78). Student's t test with Welch's correction test p=0.3179

I: GLDH taken at time of cull in mice who received GFP cell and ACKR2-GFP transplant. Median Mean and (Standard deviation) of GLDH in mice who received GFP cell transplant 214.5U/L (126.3), mice who received ACKR2 transplant 82.00U/L (50.97). Student's t test with Welch's correction test p=0.051

Transplants were carried out by Dr. S. Ferreira-Gonzalez with assistance from the PhD candidate.

Figure 7.10 Expression of GFP in mice who received either GFP or ACKR2 transplant.

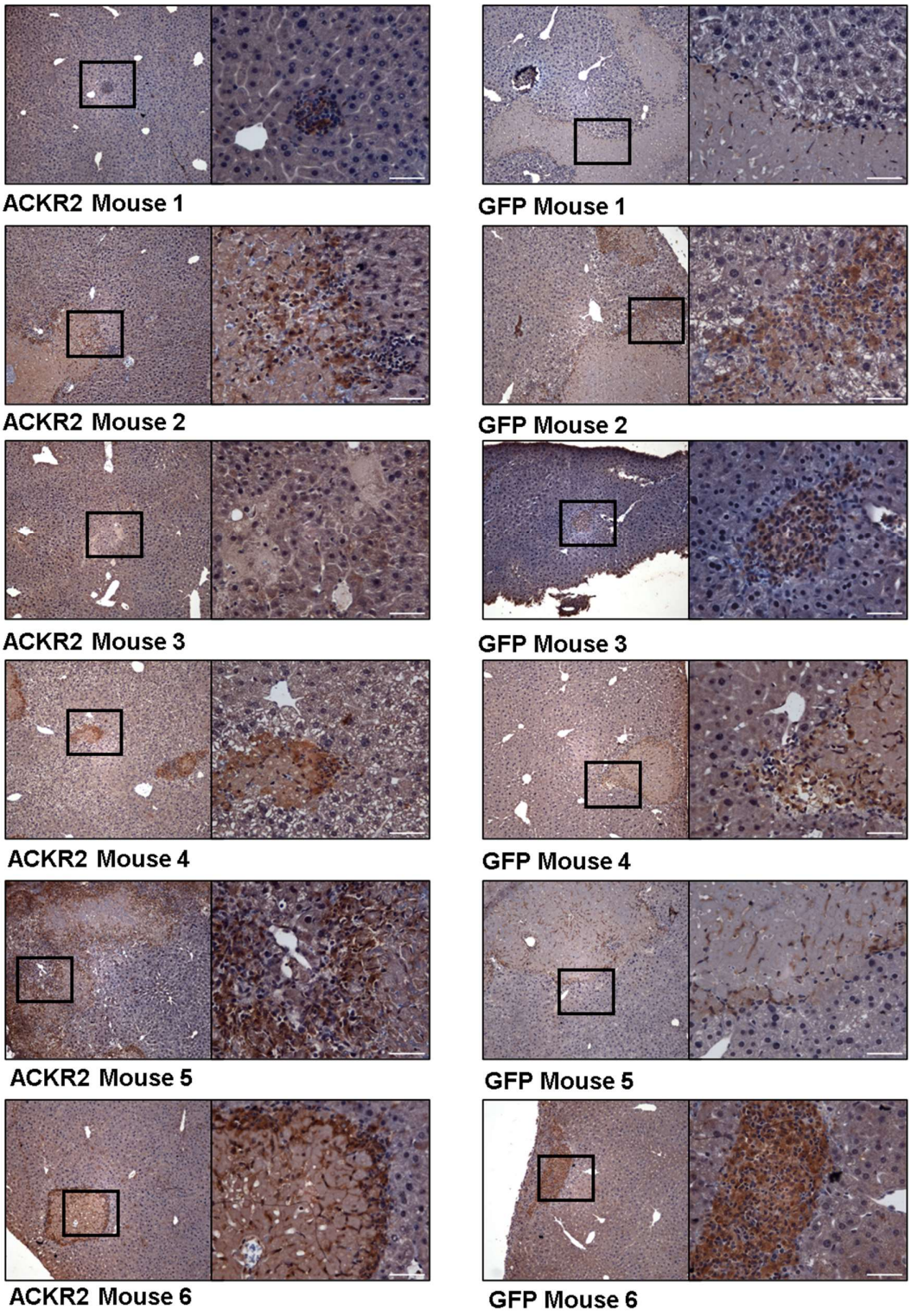

Figure 7.10: Expression of GFP in mice who received either GFP or ACKR2 transplant.

All scale bars represent 50μm. Representative images of GFP immunohistochemistry in all 12 of the mice who received either GFP or ACKR2 transplant. Right images are 40x magnification, left images 10x.

Figure 7.11 Macrophage infiltration following transplantation with GFP or ACKR2-GFP murine HPC.

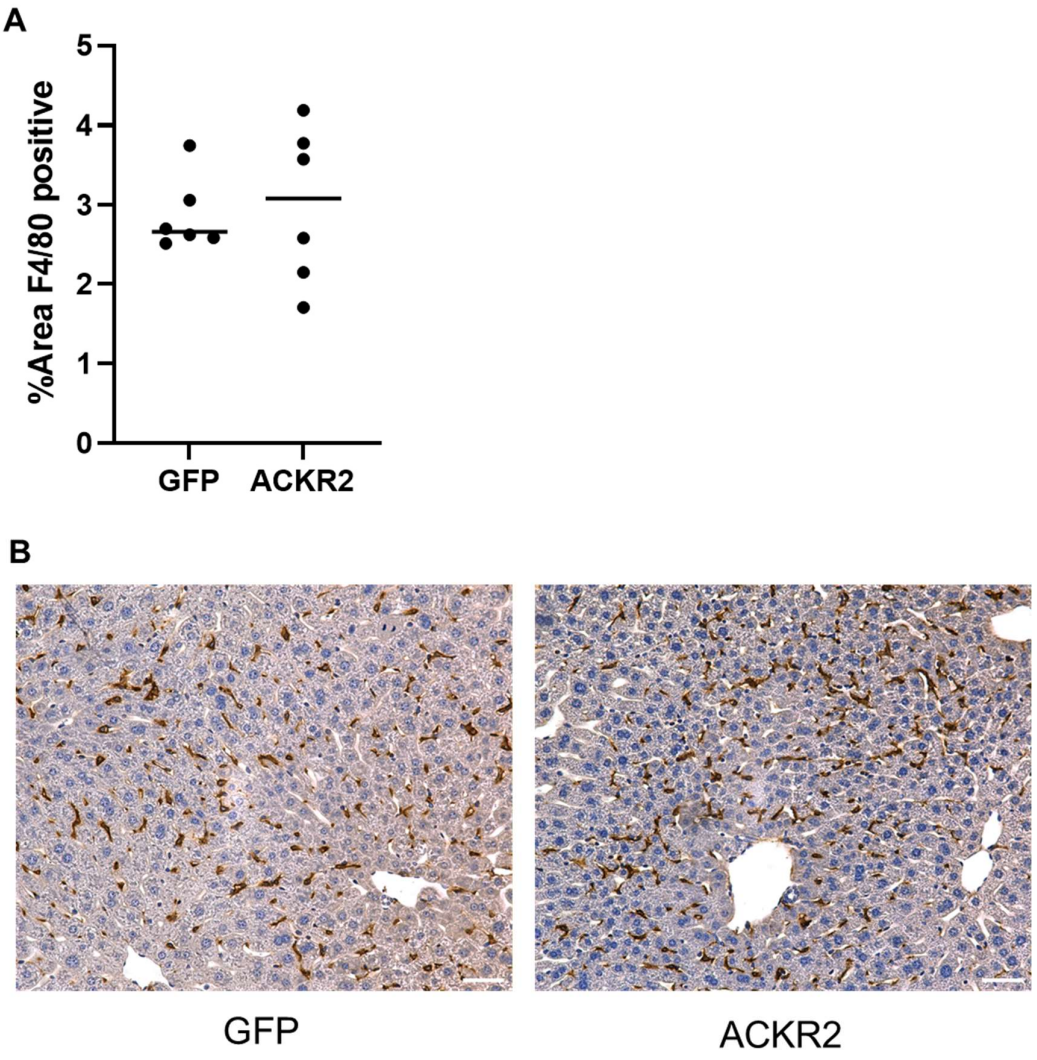

Figure 7.11: Macrophage infiltration following transplantation with GFP or ACKR2-GFP murine HPC.

A: %Area F4/80 positive in mice that received GFP or ACKR2-GFP murine HPC transplant. Dots represent individual mice; horizontal lines represent median. Median GFP expression in mice who received GFP transplant 2.67, and ACKR2-GFP transplant 3.08. Mann Whitney test $p>0.999$

B: Representative images of F4/80 immunohistochemistry in mice that received GFP or ACKR2-GFP murine HPC transplant. Scale bars represent 50μm.

This immunohistochemistry was carried out by Ms Rhona Aird.

7.8 Comparison of murine BEC intrasplenic and portal vein injection

The influence of route of the route of injection may influence the ability of cells to engraft following transplantation. To assess differences in routes of administration comparison was made between the splenic and portal vein routes of injection.

Five million GFP positive murine HPC were injected into the *Krt19Cre^{ER}Mdm2 $^{fl/fl}$ Rag2$^{-/-}$ Il2rg$^{-/-}$* model under terminal anesthetic either via the portal vein or the intrasplenic injection. Mice were injured with three doses of tamoxifen followed by 48 hours DDC diet, prior to transplantation.

Splenic injection was performed using a 30g needle whilst portal vein injection was performed using an intravenous catheter, further description in the methods chapter. Figure 7.12B demonstrated a strong trend towards a higher percentage area GFP positive within the livers of mice who received intrasplenic injection compared with than portal vein. On inspection of the images there was a pattern of cells being contained withing large portal veins in the splenic injection group. In contrast murine HPCs delivered via the portal vein were seen to be more interspersed throughout the hepatic tissue.

Figure 7.12 Comparison of murine BEC intrasplenic and portal vein injection

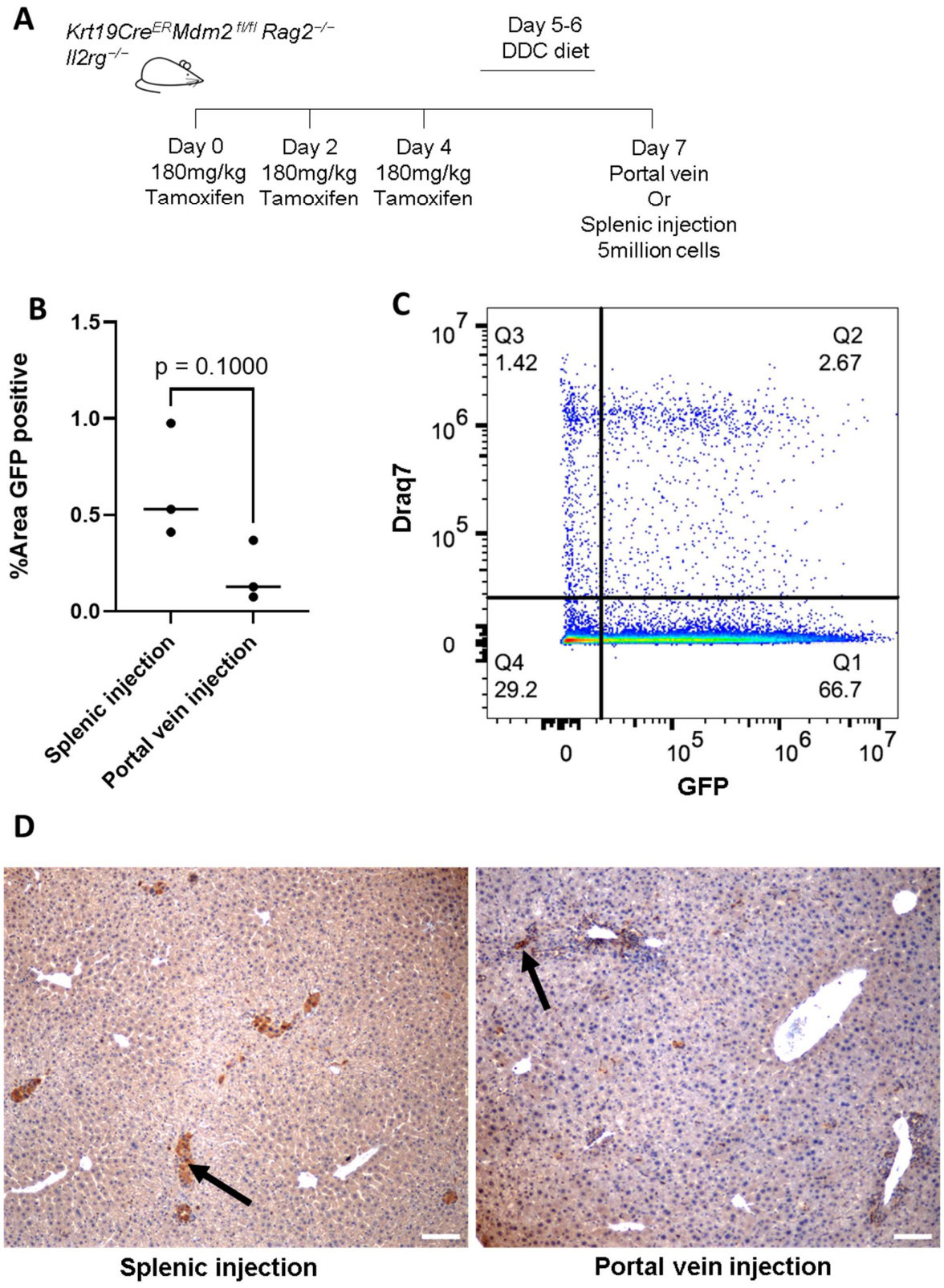

Figure 7.12: Comparison of murine BEC intrasplenic and portal vein injection

A: Schematic demonstrating the experimental plan.

B: Comparison of %Area GFP positive in mice that had transplant via splenic or portal vein injection. Median %Area expression in mice that received splenic injection 0.529%, in mice that received portal vein injection 0.127%. Mann Whitney test p=0.1. Each dot represents data from a single mouse.

C: Flow cytometry comparing GFP and Draq7, Q1 demonstrating live cells positive for GFP.

D: Representative images of immunofluorescence for GFP in mice that received transplant via the portal vein or splenic injection. Scale bars represent 100μm. Black arrows indicate areas of GFP positivity.

7.8 In vitro modelling of CXCR2

In vitro modelling may also be of interest to investigate the ability of CXCR2 HPC migrate to sites of injury. Unfortunately, the in vitro model of biliary injury developed in chapter 5 did not consistently lead to upregulation of CXCL2 and therefore could not act as an appropriate model for cell homing.

Despite this the peroxide model was used to assess the ability of CXCR2 HPC to engraft and to rescue cells from injury. Figure 7.13 displays the results of a single experiment using three wells of 2000 RFP positive murine HPC, plated into a 6 well plate and subsequently treated with peroxide as described in chapter 5. 24 hours following peroxide treatment 5000 murine HPC either GFP or CXCR2-GFP positive were added directly into the media. Cells were subsequently collected for RNA, apoptosis and senescence were assessed through expression of *Casp3* and *p21* respectively. In this limited experiment there was a trend towards a reduction in the expression of both *Casp3 and p21* in wells that received either GFP or CXCR2 HPC, although there was no observed difference between CXCR2 and GFP wells. Images obtained demonstrated the engraftment of both GFP and GFP CXCR2 HPCs in close proximity to RFP BEC.

Figure 7.13 Addition of GFP or CXCR2-GFP murine BEC to the peroxide injury model.

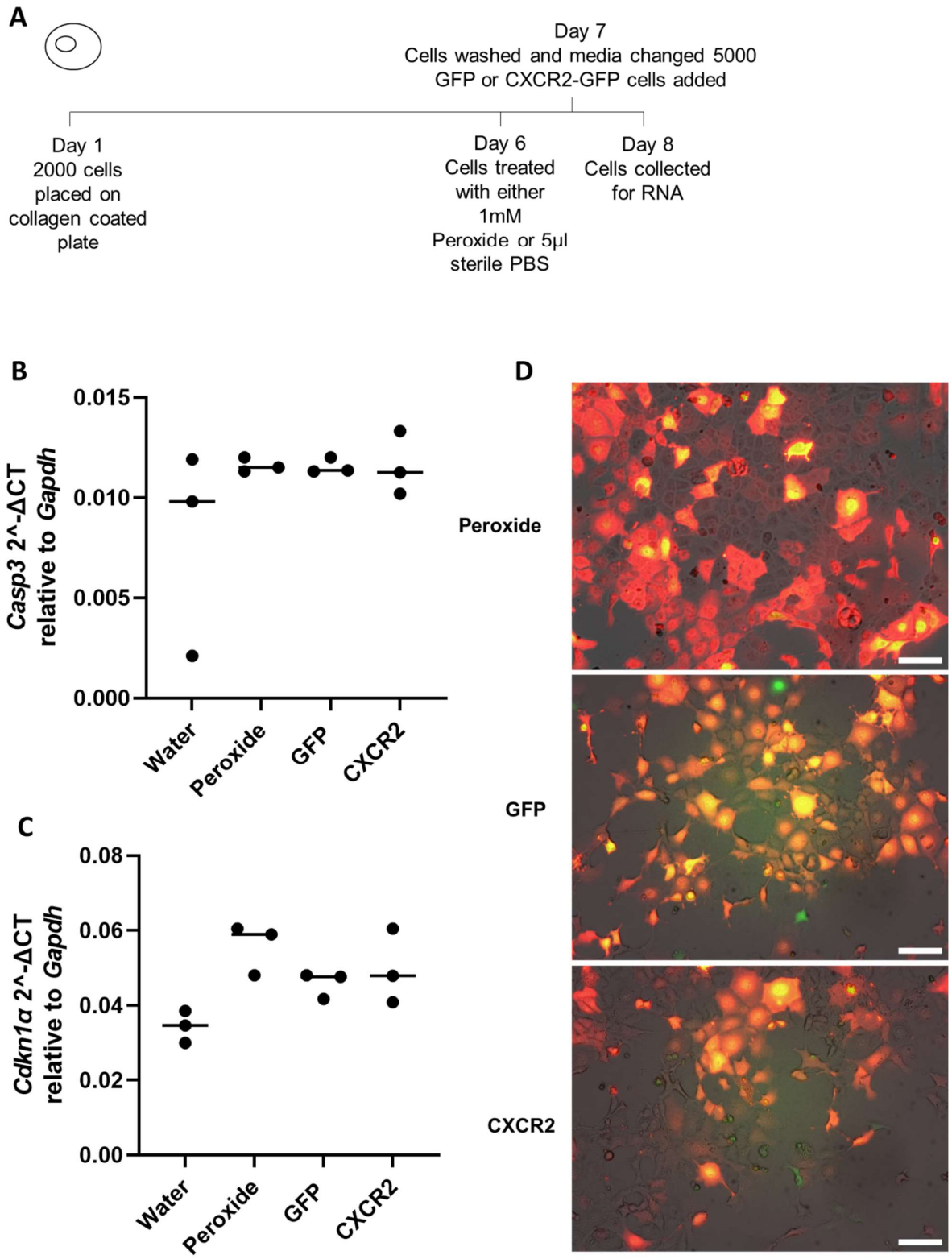

Figure 7.13; Addition of GFP or CXCR2-GFP murine BEC to the peroxide injury model.

Dot plots, individual dots represent technical replicates, n=3 technical and 1 biological replicate. Horizontal lines represent medians.

A: Schematic of experimental design

B: *Casp3* 2^-ΔCT relative to *Gapdh* in cells treated with water or peroxide, not treated with cells and those treated with either GFP or CXCR2-GFP cells. Median expression in that received water 0.01, murine HPC treated with peroxide 0.012, treated with peroxide and GFP HPC 0.011 and peroxide with CXCR2-GFP HPC 0.011.

C: Casp3 2^-ΔCT relative to Gapdh in cells treated with water or peroxide, not treated with cells and those treated with either GFP or CXCR2-GFP cells. Median expression in that received water 0.01, murine HPC treated with peroxide 0.012, treated with peroxide and GFP HPC 0.011 and peroxide with CXCR2-GFP HPC 0.011.

D: Images on day 8 one day following treatment with GFP or GFP-CXCR2 cells. Scale bars represent 100μm.

7.8 Discussion

This chapter aims to improve homing of human HPC to the biliary ducts of mice in the *Krt19Cre^{ER}Mdm2 $^{fl/fl}$ Rag2$^{-/-}$ Il2rg$^{-/-}$* model through the overexpression of CXCR2.

A line of HPCs expressing both CXCR2 and GFP along with a line of HPCs expressing only GFP were produced, and subsequently transplanted into the *Krt19Cre^{ER}Mdm2 $^{fl/fl}$ Rag2$^{-/-}$ Il2rg$^{-/-}$* model.

The major limitation of this chapter is the low number of mice included. This was driven by two factors. Firstly, during my PhD an illness spread through the animal unit leading to the death of many of the immunocompromised mice in the unit. This led to a limited number of mice available for transplantation experiments. There is an uneven number of mice between the groups as one mouse was culled due to ill health during the injury induction process. This was not thought to be secondary to the contagion, but the injury process itself. Secondly it remains challenging to culture primary human HPC. This was even more so the case following viral transduction. Following approximately 25 passages human HPC tend to display reduced growth in culture. The low transduction efficiency coupled with the fact that two episodes of sorting were required to produce high enough proportions of GFP positive HPC made it challenging to produce large enough quantities of cells before a passage number of greater than 20 was reached. It was ensured for transplants that cells were matched in terms of the passage number of controls.

Route of delivery

The splenic route of cell transplantation was used. This route could not be replicated clinically, as injection directly into the spleen would induce a high risk of bleeding. However as detailed in section 1.8, intrasplenic injection is commonly used for pre-clinical cell transplantation as a surrogate for portal vein injection, due to reduced risk of bleeding and improved mortality [150, 164]. It replicates portal vein injection as blood from the spleen drains directly into the portal vein, even if cells are inadvertently injected into a splenic artery this would in theory still direct cells into the portal venous system after passing through the splenic sinusoids. How the intra-splenic and portal vein routes of injection influence a cells proclivity to eventually arrive in the liver, remains to be determined. This has therefore been addressed in

supplementary figure 7.5 comparing the engraftment of GFP positive murine HPC. The results demonstrated a trend towards higher %area positive GFP in the livers of mice that receive HPC via splenic injection compared with portal vein, suggestive of more effective cell delivery to the liver via the intrasplenic route. These results indicate that the splenic route of injection is valid in delivering cells to the liver, which has been shown before[298].

A possible reason for the finding of more HPC arriving in the liver following splenic vs portal injection could be that passing through the splenic sinusoids causes cells to clump together, making them more likely to be lodged in the hepatic vasculature. This in turn raises the question as to whether this is desirable, subjectively it appears that cells were more likely to be into the hepatic parenchyma following portal vein injection, it may be that fewer cells are retained but are retained in more effective areas. To further investigate this hypothesis additional time points would be of use, which would allow the quantification of HPC loss over time, therefore demonstrating if cells had truly engrafted.

In the human HPC transplants described in the main body of this chapter areas of macroscopic palor were identified in the livers of mice that received CXCR2-GFP HPC. These areas are of unclear significance and etiology however one possible explanation are focal areas of hepatic infarction. Whilst this is known to be a feature of the *Krt19Cre^{ER}Mdm2 $^{fl/fl}$ Rag2$^{-/-}$ Il2rg$^{-/-}$* model, the influence of the route of injection should also be considered on the risk of hepatic infarcts developing, as the presence of many cells in the portal veins, as shown in figure 7.12 could lead to blockage of the vein and infarction.

The observed differences in the pattern of delivery of HPC to the liver has implications for both clinical and preclinical research. From a preclinical perspective the present data suggests intrasplenic injection may be superior to portal vein injection in delivering HPC to the liver. As an intrasplenic injection would not be acceptable clinically, preclinical studies using the intrasplenic should consider the possible improved delivery of cells this technique affords compared with portal vein injection, when progressing therapies to clinical research.

Methods of transplanted cell quantification

The production of GFP and CXCR2-GFP HPC lines was challenging in human HPC due to low transduction efficiencies and differences in the brightness of GFP between the two lines. The influence of this latter point is difficult to quantify in the context of cell transplantation. It may be that brighter cells are easier to detect through immunofluorescence and immunohistochemistry which could falsely inflate the number HPC identified in the GFP HPC group.

The quantification of cellular engraftment following transplantation remains a challenging prospect which is framed by resolution and field of view. Several techniques are available to detect cells post transplantation, in this study primarily immunofluorescence and immunohistochemistry were employed. These techniques allow very high resolution as cells can be resolved as singlets and the relations with other cell populations can be defined. Obtaining an adequate field of vein can be more challenging, 4µm slices of fixed liver are taken at images sampling this slice are taken, therefore analysis occurs on a small area of tissue. This inability to focus on specific areas is not of significant concern since, the *Krt19Cre^{ER}Mdm2 $^{fl/fl}$ Rag2$^{-/-}$ Il2rg$^{-/-}$*model leads to a diffuse injury pattern and intrasplenic transplants are expected to deliver cells equally throughout the liver. For this reason, a randomly selected slice of tissue should offer a fair representation of the results of cell transplantation, albeit in only 2 dimensions.

Figures 7.5G and H raised the possibility of hepatic infarcts in the model. These are more difficult to quantify using immunofluorescence and immunohistochemistry as their pattern is geographical and interspersed between areas of non-infarcted tissue. As such these aspects of the injury have been assessed based on biochemical and macroscopic appearances, which is discussed in more depth later in the chapter.

An alternate form of assessment would be through In vivo imaging, using luciferase, or through nuclear imaging such as SPECT or PET. Whilst these techniques allow for live imaging and imaging of the entire liver, they lack the resolution to resolve single cells at present. They are often coupled with a secondary form of imaging such as X-ray, CT or MRI, to allow more accurate localization of the luciferase or gamma ray signal. Even coupled with these secondary imaging techniques it remains challenging to identify biliary ducts confidently. These techniques therefore lack the resolution at present to answer the research question; does CXCR2 expression improve

the ability of HPC to home to biliary ducts. Conversely the resolution may be adequate to assess the progression of transplanted cells via the portal vein and intrasplenic routes. It could assess whether the differences in distribution of cells depicted in Figure S7.5D are transitory or true reflections of the consequences of these methods of delivery.

Live microscopic imaging of organs such as the brain and kidney have been carried out in the past following the insertion of cranial or abdominal windows respectively[299, 300] . This may also be possible in the liver, however in the context of this study it's utility would likely be limited. Whilst these forms of imaging offer the ability to image the process of migration in live time, they have limited field of view[301]BEC constitute a small proportion of the livers cell population and therefore it may be difficult to ensure there are BEC in the field of view. Additionally, it would be less certain that the BEC in the field of view should interact with transplanted HPC, A method for accurately identifying BEC on microscopy without the benefit of KRT19 staining would be required.

The lack of ability to assess the extrahepatic ducts was a limitation of this study, however as noted in chapter 5 the evidence for CXCL2 being an appropriate target for the extrahepatic ducts is limited. Nevertheless, it would have been of interest to compare the presence of HPCs in the extrahepatic ducts.

An unexpected result from the transplantation experiments was raised when transplanted HPC were not found to be positive for KRT19, despite being of BEC origin. The antibody used, which is produced by DSHB as detailed in table 4.3, is known to react with both humans and mouse. Possible explanations for this would include a change in the binding site of KRT19 during the digestion process. This could be assessed by performing immunofluorescence on HPC in culture and those following isolation for transplant. If this hypothesis was demonstrated to be correct, it may have raised concerns regarding the expression of CXCR2 and ACKR2 following digestion, however both have been shown to be present using flow cytometry following digestion in figures 7.3 and 7.8 respectively.

The key findings of this chapter are firstly, both GFP transduced and CXCR2-GFP transduced human HPC can engraft in the *Krt19Cre^{ER}Mdm2 $^{fl/fl}$ Rag2$^{-/-}$ Il2rg$^{-/-}$* model. Subjectively engraftment at 48 hours was significantly greater than that

presented 5 weeks following transplant in the study by Hallett and Ferreira-Gonzalez[124], despite the far fewer cells that were injected in the present study. This suggests that the limited number of human HPC identified in the afore mentioned study is unlikely to be solely due to poor homing. If homing was the sole reason, low numbers of HPC would be expected at 48 hours post-transplantation, which was not the case in the present study.

A target too close

In contrast to the anticipated outcome, GFP human HPC appeared to be found closer to BEC than CXCR2-GFP HPC. The reasons for this are unclear however data from Hallett, Ferreira-Gonzalez et al may provide one potential hypothesis. Human HPC in culture demonstrate high expression of CXCL2, this is not unexpected given the fact that the line of cells is derived from BEC. It is possible that the presence of both the ligand and the receptor in close proximity may have led to cell clumping, particularly in the small vessels of the spleen following injection. This may help to explain the appearance of fewer biliary ducts associated with CXCR2-GFP HPC, but in larger numbers compared with mice that received GFP HPC. This hypothesis presents an existential challenge to homing strategies for human HPC in the cholangiopathies as the transplanted cell and the target cell, namely HPC and BEC, are likely to be very similar in the receptors and ligands they present. One solution to this may be selected a ligand which is exclusively expressed following injury, however as shown in Chapter 6 this is likely to be challenging.

Another possible solution to the problem posed by similarity between transplanted cells and target cells is to move the target site to the adjacent interstitium as opposed to the BEC themselves. Germane to this, section 1.4 described the ductular reaction, which occurs in the cholangiopathies. Associated with the proliferation of BEC, MSC recruitment and the deposition of extracellular matrix develops during this process. Targeting these features of the ductular reaction could allow adequate separation between the target and proteins expressed by the transplanted cell. Biliary duct isolation allows the assessment of BEC and adjacent structures (Figure 4.6D), further vindicating the use of this method for the proteomic analysis featured in Chapter 6.

The results of biochemistry between the two groups showed trends towards lower levels of transaminases and bilirubin in the mice that received CXCR2-GFP HPC, indicative of lower levels of hepatic and biliary injury in these mice. Conversely there was a trend towards higher GLDH in the mice who received CXCR2-GFP HPC. GLDH is contained within the mitochondria, its presence in the blood therefore is indicative of significant cellular damage, for example in necrosis [302]. It was notable that this group also had macroscopic appearances which could suggest infarcts, whilst this was present in only one of the livers in the GFP HPC. It was of interest that the solitary mouse with GLDH greater than 400 in the GFP HPC group also had areas of palor visible macroscopically. The potential that CXCR2-GFP HPC either increases the risk of infarction in the *Krt19Cre^{ER}Mdm2 $^{fl/fl}$ Rag2$^{-/-}$ Il2rg$^{-/-}$* model or directly cause them, would require further investigation.

The improvement in the other biochemical markers described coupled with increased levels of GLDH could be explained in at least two ways. Improved cellular engraftment could lead to resolution of injury and reduced biliary markers. The increased propensity for CXCR2-GFP HPCs to remain in the liver may have led to blockages of portal venules and hepatic infarcts, thus increasing the blood GLDH. Alternately such extensive damage is caused by the CXCR2-GFP HPCs, it has led to a reduced capacity for the liver to produce the enzymes ALT and AST, as is seen in terminal chronic liver disease. The latter explanation would seem unlikely since bilirubin was also lower in the mice who received CXCR2-GFP HPC. One would expect bilirubin to increase in liver injury so severe that ALT and AST production has reduced.

Whilst in Hallett and Ferreira Gonzalez study in 2022, HPC transplantation led to improvements in ALT and bilirubin when compared with PBS or human MSC transplantation[124], it would have also been useful to include further control groups in the experiments detailed in this thesis, particularly given the differences between the present research and the previously published work in terms of the time after surgery LFTs were measured at. A group receiving PBS only would have given information regarding expected LFT levels due to surgery, mice receiving non transduced HPC could have given information regarding the effects of viral transduction. A group receiving another cell type, for example human MSC could have provided information in the expected LFT results from changes incurred by the process of cell transplantation.

Alternative causes of poor engraftment

In this chapter an alternate cause and solution to poor cell engraftment, namely reducing host inflammation through HPC expression of ACKR2, was also investigated. Figures 7.8-11 provided no evidence that ACKR2-GFP HPC reduce inflammation in the liver. Figure 7.11 presented macrophage infiltration in the liver following transplantation and demonstrated no difference in liver macrophage infiltration in mice that received GFP HPC or ACKR2 GFP HPC, however there are important points for consideration, pertinent to the interpretation of these results. Firstly, transplants were performed from C57BL/6 murine HPC into C57BL/6 host mice. This system may lead to reduced immune reaction due to the genetic similarities between transplanted cells and the host. The collaboration with Professor Graham's lab has continued and will assess transplantation of C57BL/6 murine HPC into Balb/c mice. This cross-strain experiment aims to induce a greater immune reaction to transplanted cells and demonstrate more clearly the efficacy of ACKR2 in reducing the immune response. Secondly the assessments performed to date have investigated the liver on a global scale and may lack the granularity to detect how ACKR2+ cells are influencing the host niche locally. Of particular interest is the assessment of the association between macrophages and transplanted HPC, which could be assessed using a similar Qupath analysis to that presented in Figure 7.7. It has been challenging to perform immunofluorescence of GFP and F4/80 together, which would allow the localisation of transplanted HPC and host macrophages in tissue. Finally, it would have also been of interest to include more controls in these experiments including a group receiving only PBS to determine the level of macrophage infiltration in the liver induced by IRI injury and determine whether there was no difference between GFP and ACKR2 GFP transplantation or whether neither had an effect. Beyond this a group receiving a control cell type such as MSC could help to determine whether any differences observed between PBS and HPC transplants were secondary to the cell type or simply due to the process of transplanting cells. Future research should aim to interrogate the relationships between transplanted ACKR2-GFP HPC and host immune cells through other means.

Additionally, the collaboration with Professor Graham also aims to assess the engraftment and local inflammatory response to ACKR2 HPC transplanted into a biliary injury model. This research will allow assessment of the utility of ACKR2 expression

in improving HPC engraftment in biliary injury. This model should not suffer the same difficulties to quantification as described for the ischaemia reperfusion model.

As outlined at the start of this chapter, preclinical cell therapies are aimed at progressing to the clinic. It is therefore important to discuss the status of therapies involving lentivirus in clinical practice. In recent years several lentivirus therapies have been used in major early phase clinical trials. Hematopoietic stem cells have been modified to express specific genes to combat genetic deficiencies such as metachromatic leukodystrophy[303], severe combined immunodeficiency[304], and beta thalassemia, [305]. These studies demonstrate that lentiviral therapies can translate to clinical therapy however there remains strides to be made between replacing a deficiency and upregulating a protein which is not normally expressed in a cell type, as is the case for CXCR2 in HPC. It is not necessary that increased expression of chemokine receptor should be done using lentivirus. Previously CD44 expression has been stimulated in BEC through exposure to CD44[198]. It is possible that culture conditions could be developed that promote the expression of other receptors, including CXCR2, however this is beyond the scope of this research.

Limitations of lentivirus

This chapter employed lentiviral vectors, transducing cells to express GFP alone, or in combination with CXCR2 or ACKR2. Lentiviruses integrate into the genome at random, at 1 or more sites. The effects of this on cell functioning are unpredictable, as the plasmid DNA can disrupt segments of host genetic code leading to dysregulation of host genes. It is therefore possible that the differences observed between mice who received CXCR2 GFP and GFP HPC, could be in part due to changes in expression of host HPC DNA as opposed to a direct result of expression of CXCR2.

To mitigate against this, transduced HPC could have been clonally expanded following FACs from single cells to produce multiple lines of for example CXCR2-GFP HPC each with a unique insertion or insertion points of the lentivirus vector. It would have been possible to perform PCR on DNA from each line to determine the number of times the viral construct had been inserted in each line. Lines with a single insertion could have been selected in order to minimize the risk of off target effects. These lines could have then been sequenced to assess the insertion point of the lentiviral construct, if any of the lines demonstrated insertion points within tumour suppressor

genes, they would be precluded from transplantation experiments. Finally using the remaining cell lines transplant experiments could have been performed comparing the effects of differing insertion points of the lentivirus vector. Unfortunately, due to challenges in culturing HPC, and limitations in the number of mice available for transplant these experiments could not be performed as part of this thesis.

An alternate method for insertion of CXCR2 and ACKR2 into the genome of HPC would be the use of CRISPR/Cas9. This would have allowed for a targeted insertion and have given confidence that any observed differences between the mice that received GFP and CXCR2/GFP HPC were due to CXCR2 and not due to the site of integration.

7.9 Conclusion:

Human HPC do not express CXCR2 however were induced to do so using a lentivirus vector. CXCR2-GFP cells can be transplanted into and engraft within the liver, with trends towards improvements in liver functions test.

Chapter 8: Conclusions and Future Perspectives

8.1 Summary of knowledge preceding this thesis.

The cholangiopathies are a group of conditions which cause injury to the biliary system in the liver. They may lead to hepatic failure; in such cases the only curative therapy is OLT. Unfortunately, limited livers are available for transplantation.

In recent years cell therapy for the cholangiopathies have been proposed as a possible alternate therapy. A subgroup of BEC known as HPC have been transplanted into a mouse model of cholangiopathy demonstrating biochemical and imaging markers of biliary injury[124]. Unfortunately, engraftment was limited in this model.

Cell homing can improve engraftment following transplantation[167, 201, 202, 306]. Homing mechanisms, exploit the interaction between a receptor on the homing cell and a protein specific to the target site. Target proteins are more attractive if they are specific to areas of the disease in question, and not only the anatomy.

The target in cell therapies for the cholangiopathies would be the biliary ducts. Within the context of the liver, several potentially biliary specific proteins have already been identified, including SCTR[37, 98, 187, 307], TFF2[193] and CD44[145, 198].

There are inherent homing mechanisms in the body, particularly within the immune system which have been appropriated previously to improve cell homing. There is evidence that CXCL1[215, 216], CXCL2[217] and CCL2[149] have higher expression in injured biliary ducts.

8.2 Contributions to knowledge by this thesis.

Chapter 5 of this thesis explored the suitability of candidates from previously published research as biliary specific targets. SCTR, TFF2, and CD44 were demonstrated to not be suitable as candidates. No increase in ductal SCTR expression was seen in biliary injury, which rendered SCTR a suboptimal target for the cholangiopathies.

It had already been established that CD44 expression was not limited to BEC in the liver, however in our study the highest expression appeared within cells out with the

biliary tree (Figure 8.1A). CD44 was not seen as an appropriate target for this reason.

TFF2 was previously considered a biliary specific protein, although canalicular expression had been reported in hepatocellular injuries. For the first time cannalicular expression has been shown in biliary injury models and in uninjured mice. This canalicular expression precludes the use of TFF2 as a target, as it may lead to miss direction of transplanted cells.

In the *Krt19Cre^{ER}Mdm2 $^{fl/fl}$ Rag2$^{-/-}$ Il2rg$^{-/-}$* model of cholangiopathy, expression of *Cxcl2* was specific to intrahepatic biliary ducts. There was also a trend towards increased expression in biliary injury. Micro-array data from Rodrigo-Torres and co-workers corroborated this finding, Cxcl2 was the most upregulated gene identified in their DDC diet-based model. In contrast to previous evidence both Ccl2 and Cxcl1 were not seen to be significantly upregulated in injury in the *Krt19Cre^{ER}Mdm2 $^{fl/fl}$ Rag2$^{-/-}$ Il2rg$^{-/-}$* model.

Chapter 6 used a proteomic approach with the aim of identifying plasma membrane proteins specifically expressed in injured biliary ducts in the *Krt19Cre^{ER}Mdm2 $^{fl/fl}$ Rag2$^{-/-}$ Il2rg$^{-/-}$* model. Whilst no appropriate targets were identified for homing, there were other significant findings. MYH14 is a biliary specific protein and is upregulated in biliary injury in the context of the *Krt19Cre^{ER}Mdm2 $^{fl/fl}$ Rag2$^{-/-}$ Il2rg$^{-/-}$* model (Figures 8.2A-D). This had not been reported previously.

In human cholangiopathies BEC express MYH14, however there may also be canalicular expression. MYH14 is a protein associated with cellular contractility suggesting its upregulation is a mechanism to overcome obstructions in the biliary tree.

Annexin V was one of the most abundant proteins identified in the proteomic data, which was expressed in the biliary compartment. The function of this protein remains unclear in the biliary system however, it does not appear to be upregulated in biliary injury and may even be downregulated.

The overarching aim of this thesis was to improve homing in the cholangiopathies, to this end cells presenting CXCR2 were transplanted into the *Krt19Cre^{ER}Mdm2 $^{fl/fl}$ Rag2$^{-/-}$ Il2rg$^{-/-}$* model.

Chapter 7 produced a line of GFP and CXCR2-GFP HPC using lentiviral constructs. This was the first time this had been done in HPC organoids. This thesis has demonstrated that prior to transduction HPC do not express CXCR2.

CXCR2 HPC were subsequently transplanted into the *Krt19Cre^{ER}Mdm2 $^{fl/fl}$ Rag2$^{-/-}$ Il2rg$^{-/-}$* model and were shown to engraft. CXCR2 HPC localised to the ducts in greater numbers but to fewer biliary ducts, which could reflect improved cellular homing (Figures 8.3A and B).

8.3 Future perspectives.

The results of this thesis have suggested that SCTR is not increased in biliary injury. The reasons for this are unclear, however from a prognostication perspective, change in SCTR may be of interest in the liver disease. Future studies could aim to characterise the expression of SCTR and SCT and assess their role in the pathogenesis of biliary diseases.

CD44 presented an exciting prospect as a target for homing however due to wide spread expression in extra-ductal cells following DDC diet, it was not feasible to pursue this as a target. In spite of this, it is of interest why a cell population positive for CD44 should appear within the hepatic parenchyma, after a short period of DDC diet. The main possible cell types considering this model is immunocompromised are resident hepatic macrophages or MSC. The importance of CD44 in the development of early cholangiopathy could be investigated using blockade of this receptor, to determine whether this observation represents an integral part of injury development or an innocent bystander (Figure 8.1C). If CD44 blockade led to a reduction in the degree of biliary injury, this receptor would become implicated in the pathogenesis of the cholangiopathies.

Proteomic analysis uncovered a specific marker of biliary injury in the cholangiopathies in MYH14, which is upregulated in murine BEC in injury and is present in BEC in humans. Interestingly hepatocellular cannalicular expression of MYH14 was also identified in PSC. MYH14 and the other non muscle myosin function through interactions with intracellular actin[308, 309]. Through these interactions cells may contract or change shape. A natural hypothes as to why

expression is increased, would be to help overcome the blockages in the biliary system induced by DDC diet. Increased cellular contractility may raise intraductular pressure, promoting flow. If this hypothesis holds true, it remains to be seen whether this response is detrimental or constructive to the liver or possibly both. The increase in pressure could result in reconstitution of bile flow, however when stricturing becomes too severe it may become counterproductive. The increase pressure could be transmitted to the BEC intercellular junctions leading to bile leak into the hepatic parenchyma.

A Myh14-/- mouse has already been produced[310], and could be used to test this hypothesis. Comparisons between this mouse and wild type mice following DDC diet could reveal whether Myh14 upregulation in biliary injury is detrimental or protective. It would be important to assess this model following short term and long-term exposure to DDC.

MYH14 upregulation in biliary injury may also have clinical implications. Dependant on the effect of MYH14 expression on biliary injury, pharmacological interventions could be designed to promote or block the expression of this protein.

Several proteins were noted to have high abundance in the intra and extrahepatic ducts in the proteomic data presented in chapter 6. Annexin V was investigated further due to the paucity of knowledge surrounding this protein in bile ducts at present. The importance of Annexin V in the biliary ducts remains unclear. In-vivo models of Annexin V knockout have already been developed. This model has not been reported to have a biliary injury phenotype, the suggested reason for this is the functional crossover of the Annexins[268]. Whilst this thesis has not assessed the function of Annexin V in the biliary ducts, it's known role in the binding of PS on the biliary aspect of the plasma membrane is of interest[311]. The importance of the balance of phospholipids for the normal function of the apical plasma membrane has already been discussed in chapter 1.4. It is possible that Annexin V has a role in protecting BEC from the detergent effects of bile. To investigate this hypothesis biliary organoids would be a model of interest. Exposure of organoids to murine bile or bile acids could be performed in controls and organoids with Annexin V knockout using CRISPR/Cas9. Assessment of genes for apoptosis, senescence and necrosis could be assessed as well as proliferation assays.

If the described in vitro model demonstrates Annexin V to be important for the protection of organoids from bile acids, further assessment could be made in vivo. An Annexin V knockout model could be challenged with biliary injury through DDC diet, to assess if more biliary damage occurs in this mouse compared with wild type. One attractive feature of Annexin V is its previous use in clinical research, showing it to be a safe drug[312]. If Annexin V was shown to be effective in preventing biliary injury, supplementation could be an interesting treatment for the cholangiopathies.

Chapter 7 provided data on the transplant of CXCR2-GFP organoids in the *Krt19Cre^{ER}Mdm2 $^{fl/fl}$ Rag2$^{-/-}$ Il2rg$^{-/-}$* model of biliary injury. The primary experiment would be to repeat this experiment to allow a larger n number to be assessed, which would afford more conclusive results. Further in-vitro studies of CXCR2 could also assess the migratory function of CXCR2. Transwell migration assays could be performed comparing GFP and CXCR2-GFP HPC in terms of their ability to migrate towards, CXCL2 ligand, injured BEC or injured extracted ducts. This could help to contextualise the results of transplant experiments, particularly the findings that CXCR2-GFP HPC appeared to localise to fewer ducts in larger numbers.

The described differences in the pattern of engraftment between CXCR2-GFP HPC and GFP HPC, could also be investigated further through the assessment of CXCL2 and CXCL1 spatially within hepatic tissues. This may most require the use of fluorescence in situ hybridisation as immunofluorescence and immunohistochemistry may be challenging for these molecules. These experiments could help to elucidate as to why CXCR2-GFP HPC appear to be attracted to specific biliary ducts in larger numbers, it is possible these ducts have the highest expression of the ligands CXCL1 and 2.

8.4 Remaining barriers to clinical translation of HPC.

The overall goal of research into HPC transplantation is the development of an effective clinical therapy. There are additional challenges beyond those directly relating to engraftment and homing of HPC which were the primary concerns of this thesis. Determining the mechanisms by which HPC affect regeneration, and how a human host environment affect these mechanisms may offer methods to optimize HPC transplantation prior to moving into clinical research. The use explanted livers

could help to answer some of these questions. Transplanting HPC into explanted livers from patients with cholangiopathy following resection in preparation for transplant could give vital information regarding how HPC perform in human tissue with cholangiopathy. Comparing this with engraftment in explanted control livers for example those that have been rejected for transplantation due to anatomical or practical reasons like those used as controls in chapter 6 of this thesis, would identify whether host environment affects the performance of HPC. Single cell RNA sequencing in each of these livers before and after transplantation could identify changes in transplanted cells at the genomic level and identify mechanisms by which HPC could be protected from the host environment. In addition, changes in the recipient cells could also be assessed to develop understanding of how cell transplantation affects native cells. If enough livers were available, transplantation of a control cell type such as MSC could also be performed to determine what observed changes are secondary to HPC specifically or secondary to the process of cell transplantation.

Selecting the correct group of patients for early clinical trials would also be important. Patients with ischaemic cholangiopathy following liver transplantation present a group who often will require further transplantation[100]. This group would be attractive as it would be highly beneficial to develop a method to prevent or delay the need for OLT. In contrast in patients with PSC or PBC it is difficult at present to determine which patients would ultimately require transplantation, HPC transplantation in this context would present a preventative therapy which may be more difficult to justify as a first study for clinical trials. Finally, there are a subgroup of patients who require liver transplantation but have co-morbidities which prevent them from undergoing surgery. HPC could be delivered via minimally invasive means, through placement of a catheter in the hepatic artery or portal vein and may allow patients who otherwise could have no treatment for their failing livers to receive treatment.

Figure 8.1 Schematic pertaining to the findings from CD44 immunofluorescence in chapter 5

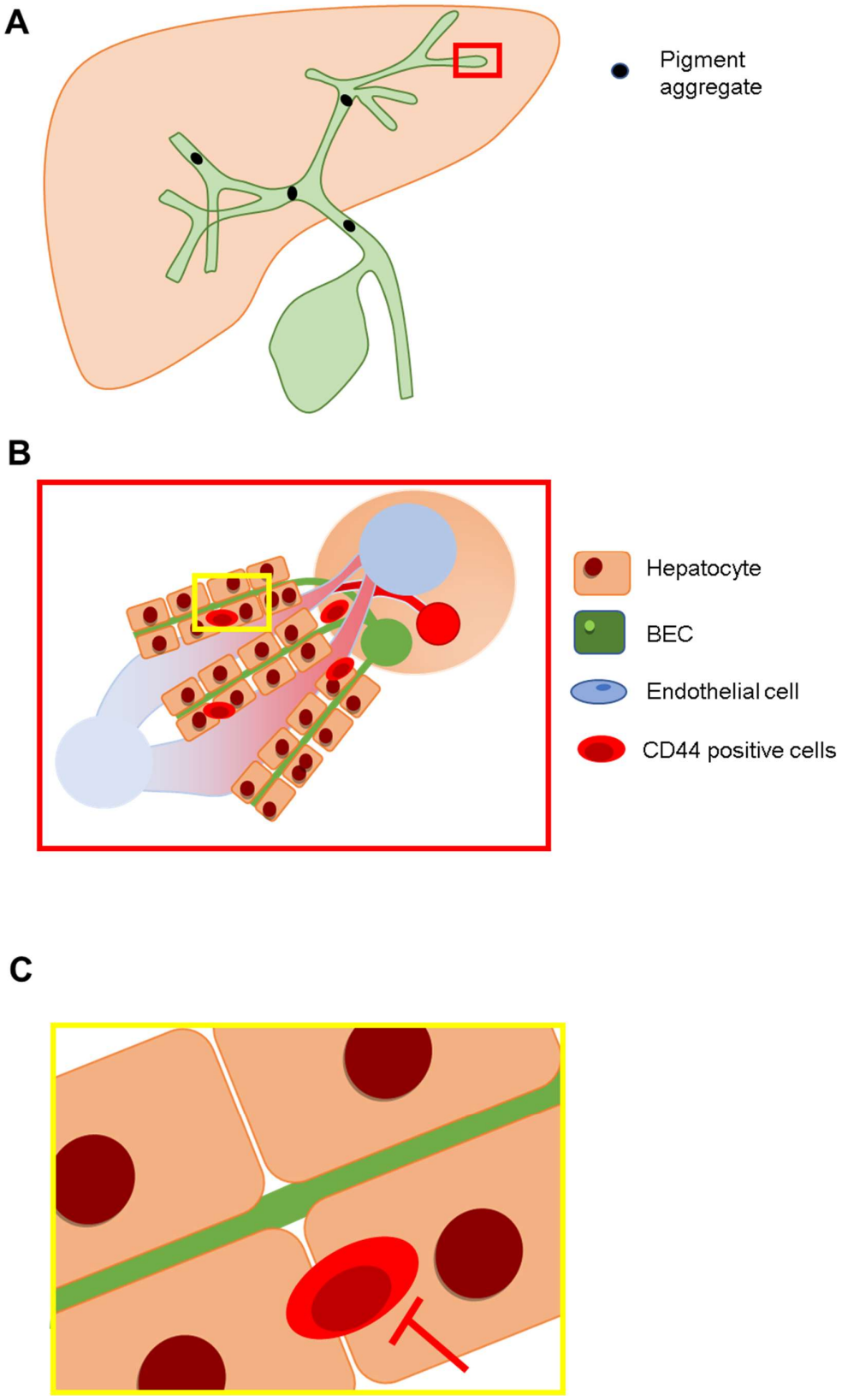

Figure 8.1 Schematic pertaining to the findings from CD44 immunofluorescence in chapter 5

A: Schematic demonstrating injury in the *Krt19Cre^{ER}Mdm2 $^{fl/fl}$ Rag2$^{-/-}$ Il2rg$^{-/-}$* model induced by DDC diet leading to pigment aggregates in the bile ducts

B: View of the hepatic parenchyma as shown in Figure 1.1B, with infiltration of CD44 positive cell population

C: View indicated future perspective, blockade of CD44 to investigate the influence of this receptor in the development of biliary injury.

Figure 8.2 Schematic displaying the discovery of MYH14 as a marker of biliary injury

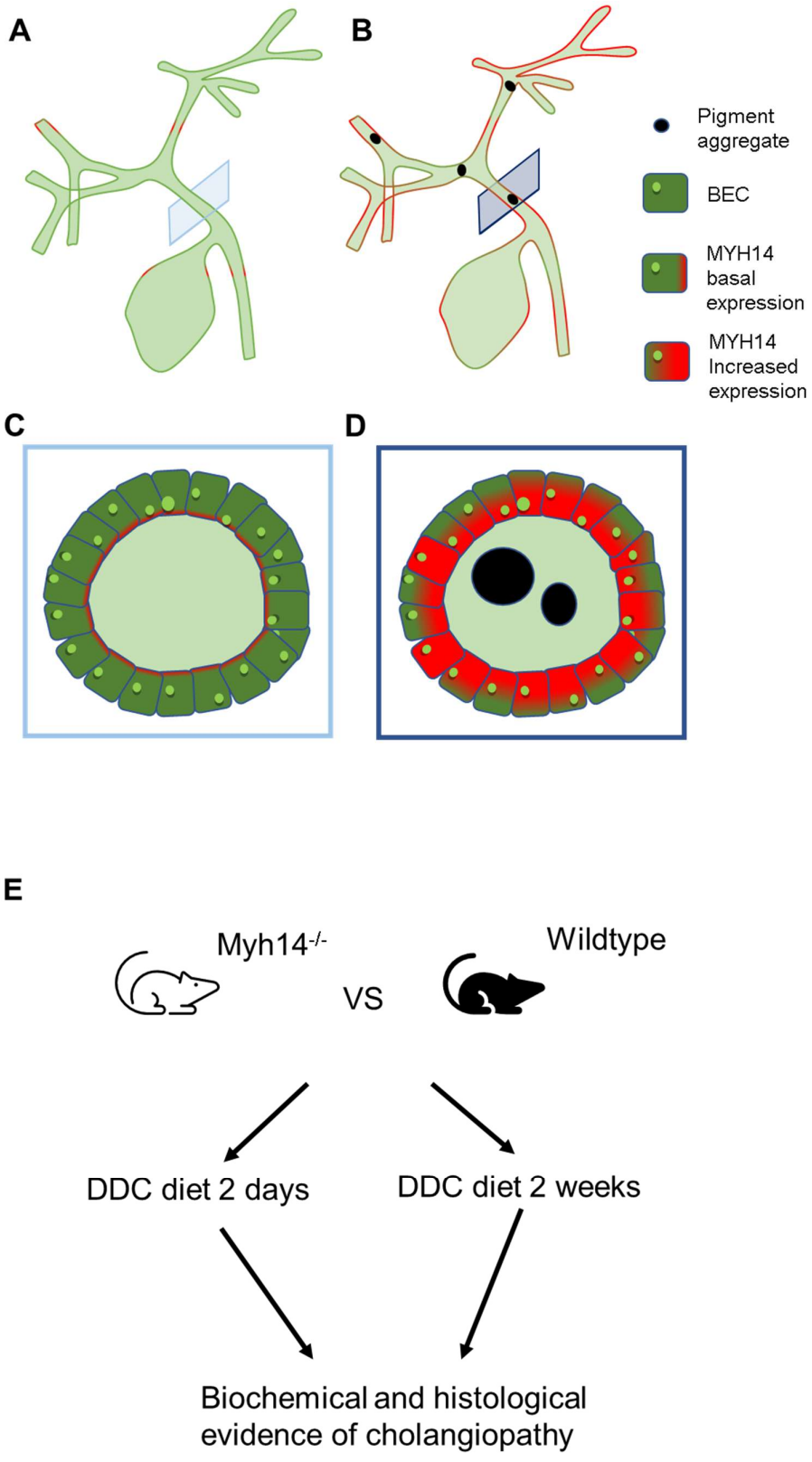

Figure 8.2 Schematic displaying the discovery of MYH14 as a marker of biliary injury

A: Schematic of biliary tree with areas of MYH14 expression displayed in red.

B: Increased expression of MYH14 following biliary injury. Areas of red indicate MYH14 expression.

C: Cross sectional view of the biliary ducts in homeostasis.

D: Cross sectional view of the biliary ducts following injury with increased MYH14 expression.

E: Future perspective design, assessing the effects of MYH14 on biliary injury induced by DDC diet.

Figure 8.3 Summary of CXCR2-GFP transplant and future perspectives

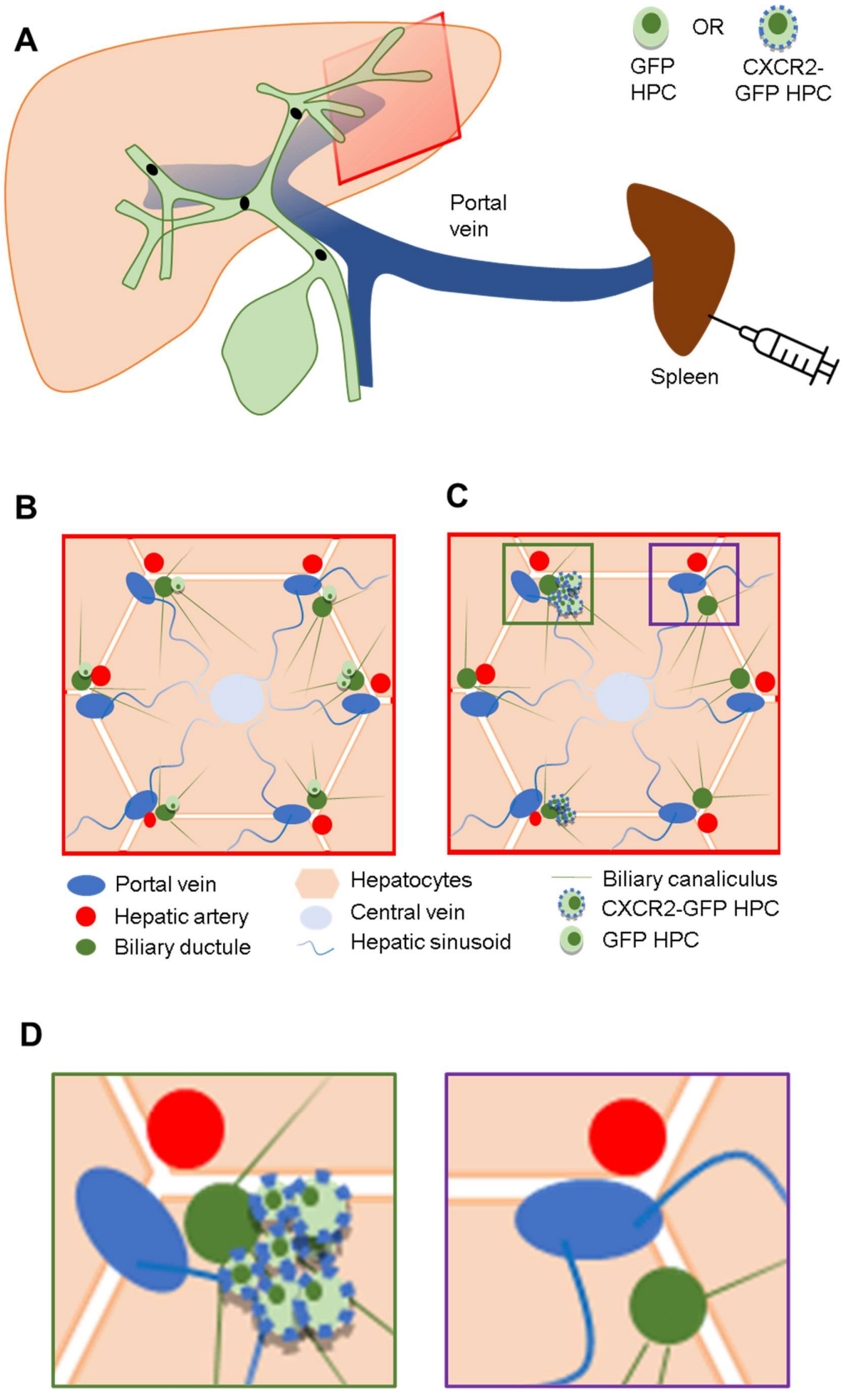

Figure 8.3 Summary of CXCR2-GFP transplant and future perspectives

A: Experimental design, demonstrating intrasplenic injection of GFP or CXCR2-GFP HPC.

B: Simplified diagram of appearances following GFP HPC transplant. Few cells in close proximity to a large number of ducts.

C: Simplified diagram of appearances following CXC2-GFP HPC transplant. Larger numbers of cells associated with fewer biliary ducts.

D: Key question for future experiments, why do some ducts attract large numbers of CXCR2-GFP HPC.

8.5Final Conclusions:

Objective 1: To identify a target protein expressed exclusively on or in close proximity to the plasma membrane of injured BEC.

- TFF2 and CD44 are not specific to BEC in the liver.
- SCTR is not upregulated in BEC following injury.
- Cxcl2 is not expressed in hepatocytes but is in biliary ducts in the *Krt19Cre^{ER}Mdm2 $^{fl/fl}$ Rag2$^{-/-}$ Il2rg$^{-/-}$* model.
- MYH14 is a specific biliary protein and is upregulated in biliary injury
- In human cholangiopathy MYH14 is expressed in both the BEC and in the hepatic canaliculi.
- Annexin V is highly expressed in BEC in both mouse and humans.

Objective 2: To present a ligand specific for the target protein in Objective 1 on the surface of hHPC.

- CXCR2 is not normally expressed on HPC.
- HPC can be induced to express CXCR2.

Objective 3: To demonstrate improvement in cell engraftment of hHPC when transplanted to the *Krt19^{CreER}MDM2$^{fl/fl}$Rag2$^{-/-}$IL2rg$^{-/-}$* model.

- Transplantation of HPC expressing CXCR2 leads to localisation of HPC to fewer biliary ducts in greater numbers.

Bibliography

1. Ezhilarasan, D., *Hepatic stellate cells in the injured liver: Perspectives beyond hepatic fibrosis.* J Cell Physiol, 2022. **237**(1): p. 436-449.
2. Braet, F. and E. Wisse, *Structural and functional aspects of liver sinusoidal endothelial cell fenestrae: a review.* Comp Hepatol, 2002. **1**(1): p. 1.
3. Vartak, N., et al., *On the Mechanisms of Biliary Flux.* Hepatology, 2021. **74**(6): p. 3497-3512.
4. Roskams, T.A., et al., *Nomenclature of the finer branches of the biliary tree: canals, ductules, and ductular reactions in human livers.* Hepatology, 2004. **39**(6): p. 1739-45.
5. Dotan, M., et al., *Periductal bile acid exposure causes cholangiocyte injury and fibrosis.* PLoS One, 2022. **17**(3): p. e0265418.
6. Morell, C.M., L. Fabris, and M. Strazzabosco, *Vascular biology of the biliary epithelium.* J Gastroenterol Hepatol, 2013. **28 Suppl 1**: p. 26-32.
7. Gaudio, E., et al., *Cholangiocytes and blood supply.* World J Gastroenterol, 2006. **12**(22): p. 3546-52.
8. Banales, J.M., et al., *Cholangiocyte pathobiology.* Nat Rev Gastroenterol Hepatol, 2019. **16**(5): p. 269-281.
9. Strazzabosco, M. and L. Fabris, *Development of the bile ducts: essentials for the clinical hepatologist.* J Hepatol, 2012. **56**(5): p. 1159-1170.
10. Bogue, C.W., *Embryology and Development of the Ductal Plate*, in *Fibrocystic Diseases of the Liver*, K.F. Murray and A.M. Larson, Editors. 2010, Humana Press: Totowa, NJ. p. 3-21.
11. Ober, E.A. and F.P. Lemaigre, *Development of the liver: Insights into organ and tissue morphogenesis.* J Hepatol, 2018. **68**(5): p. 1049-1062.
12. Keplinger, K.M. and M. Bloomston, *Anatomy and embryology of the biliary tract.* Surg Clin North Am, 2014. **94**(2): p. 203-17.
13. Si-Tayeb, K., F.P. Lemaigre, and S.A. Duncan, *Organogenesis and development of the liver.* Dev Cell, 2010. **18**(2): p. 175-89.
14. Spence, J.R., et al., *Sox17 regulates organ lineage segregation of ventral foregut progenitor cells.* Developmental cell, 2009. **17**(1): p. 62-74.
15. Poncy, A., et al., *Transcription factors SOX4 and SOX9 cooperatively control development of bile ducts.* Dev Biol, 2015. **404**(2): p. 136-48.
16. Uemura, M., et al., *Sox17 haploinsufficiency results in perinatal biliary atresia and hepatitis in C57BL/6 background mice.* Development, 2013. **140**(3): p. 639-48.
17. Sampaziotis, F., et al., *Cholangiocyte organoids can repair bile ducts after transplantation in the human liver.* Science, 2021. **371**(6531): p. 839-846.
18. Rimland, C.A., et al., *Regional Differences in Human Biliary Tissues and Corresponding In Vitro-Derived Organoids.* Hepatology, 2021. **73**(1): p. 247-267.
19. Kunne, C., et al., *Defective bile salt biosynthesis and hydroxylation in mice with reduced cytochrome P450 activity.* Hepatology, 2013. **57**(4): p. 1509-17.
20. Gerloff, T., et al., *The sister of P-glycoprotein represents the canalicular bile salt export pump of mammalian liver.* J Biol Chem, 1998. **273**(16): p. 10046-50.
21. Boyer, J.L. and C.J. Soroka, *Bile formation and secretion: An update.* J Hepatol, 2021. **75**(1): p. 190-201.
22. Zhou, X., et al., *Structural basis of the alternating-access mechanism in a bile acid transporter.* Nature, 2014. **505**(7484): p. 569-73.
23. Slijepcevic, D., et al., *Hepatic uptake of conjugated bile acids is mediated by both sodium taurocholate cotransporting polypeptide and organic anion transporting polypeptides and modulated by intestinal sensing of plasma bile acid levels in mice.* Hepatology, 2017. **66**(5): p. 1631-1643.

24. Dilger, K., et al., *Effect of ursodeoxycholic acid on bile acid profiles and intestinal detoxification machinery in primary biliary cirrhosis and health.* J Hepatol, 2012. **57**(1): p. 133-40.
25. Ikenaga, N., et al., *A new Mdr2(-/-) mouse model of sclerosing cholangitis with rapid fibrosis progression, early-onset portal hypertension, and liver cancer.* Am J Pathol, 2015. **185**(2): p. 325-34.
26. Vij, M., et al., *Paucity of Interlobular Bile Ducts in Multidrug-Resistant P-Glycoprotein 3 (MDR3) Deficiency.* Int J Surg Pathol, 2019. **27**(3): p. 343-347.
27. Roscam Abbing, R.L.P., et al., *Blocking Sodium-Taurocholate Cotransporting Polypeptide Stimulates Biliary Cholesterol and Phospholipid Secretion in Mice.* Hepatology, 2020. **71**(1): p. 247-258.
28. Brown, S.B., J.C. Docherty, and T.B. Bradley, *Bile-pigment isomers from degradation of haemoglobin M Iwate [proceedings].* Biochem Soc Trans, 1977. **5**(4): p. 1020-2.
29. Lowry, P.T., et al., *The conversion of N15-labeled mesobilirubinogen to stercobilinogen by fecal bacteria.* J Biol Chem, 1954. **208**(2): p. 543-8.
30. Larusso, N.F. and T.V. Masyuk, *The role of cilia in the regulation of bile flow.* Dig Dis, 2011. **29**(1): p. 6-12.
31. Spirli, C., et al., *Posttranslational regulation of polycystin-2 protein expression as a novel mechanism of cholangiocyte reaction and repair from biliary damage.* Hepatology, 2015. **62**(6): p. 1828-39.
32. Chen, J., et al., *Deletion of kif3a in CK19 positive cells leads to primary cilia loss, biliary cell proliferation and cystic liver lesions in TAA-treated mice.* Biochim Biophys Acta Mol Basis Dis, 2022. **1868**(4): p. 166335.
33. Masyuk, A.I., et al., *Cholangiocyte primary cilia are chemosensory organelles that detect biliary nucleotides via P2Y12 purinergic receptors.* Am J Physiol Gastrointest Liver Physiol, 2008. **295**(4): p. G725-34.
34. Masyuk, A.I., T.V. Masyuk, and N.F. LaRusso, *Cholangiocyte primary cilia in liver health and disease.* Dev Dyn, 2008. **237**(8): p. 2007-12.
35. Ulrich, C.D., 2nd, et al., *Cellular distribution of secretin receptor expression in rat pancreas.* Am J Physiol, 1998. **275**(6): p. G1437-44.
36. Alpini, G., et al., *Morphological, molecular, and functional heterogeneity of cholangiocytes from normal rat liver.* Gastroenterology, 1996. **110**(5): p. 1636-43.
37. Alpini, G., et al., *Large but not small intrahepatic bile ducts are involved in secretin-regulated ductal bile secretion.* Am J Physiol, 1997. **272**(5 Pt 1): p. G1064-74.
38. Fiorotto, R. and M. Strazzabosco, *Pathophysiology of Cystic Fibrosis Liver Disease: A Channelopathy Leading to Alterations in Innate Immunity and in Microbiota.* Cell Mol Gastroenterol Hepatol, 2019. **8**(2): p. 197-207.
39. Banales, J.M., et al., *Up-regulation of microRNA 506 leads to decreased Cl-/HCO3- anion exchanger 2 expression in biliary epithelium of patients with primary biliary cirrhosis.* Hepatology, 2012. **56**(2): p. 687-97.
40. Tietz, P.S., et al., *Agonist-induced coordinated trafficking of functionally related transport proteins for water and ions in cholangiocytes.* J Biol Chem, 2003. **278**(22): p. 20413-9.
41. Beuers, U., et al., *The biliary HCO(3)(-) umbrella: a unifying hypothesis on pathogenetic and therapeutic aspects of fibrosing cholangiopathies.* Hepatology, 2010. **52**(4): p. 1489-96.
42. Andrianifahanana, M., N. Moniaux, and S.K. Batra, *Regulation of mucin expression: mechanistic aspects and implications for cancer and inflammatory diseases.* Biochim Biophys Acta, 2006. **1765**(2): p. 189-222.
43. Fitz, J.G., et al., *Regulation of membrane chloride currents in rat bile duct epithelial cells.* J Clin Invest, 1993. **91**(1): p. 319-28.

44. Miettinen, T.A. and M. Siurala, *Bile salts, sterols, sterol esters, glycerides and fatty acids in micellar and oil phases of intestinal contents during fat digestion in man.* Z Klin Chem Klin Biochem, 1971. **9**(1): p. 47-52.
45. Uriarte, I., et al., *Bicarbonate secretion of mouse cholangiocytes involves Na(+)-HCO(3)(-) cotransport in addition to Na(+)-independent Cl(-)/HCO(3)(-) exchange.* Hepatology, 2010. **51**(3): p. 891-902.
46. Minagawa, N., et al., *Cyclic AMP regulates bicarbonate secretion in cholangiocytes through release of ATP into bile.* Gastroenterology, 2007. **133**(5): p. 1592-602.
47. Glaser, S.S., et al., *Gastrin inhibits secretin-induced ductal secretion by interaction with specific receptors on rat cholangiocytes.* Am J Physiol, 1997. **273**(5): p. G1061-70.
48. Kaminski, D.L. and Y.G. Deshpande, *Effect of somatostatin and bombesin on secretin-stimulated ductular bile flow in dogs.* Gastroenterology, 1983. **85**(6): p. 1239-47.
49. Tietz, P.S., et al., *Somatostatin inhibits secretin-induced ductal hypercholeresis and exocytosis by cholangiocytes.* Am J Physiol, 1995. **269**(1 Pt 1): p. G110-8.
50. Okabe, M., et al., *Potential hepatic stem cells reside in EpCAM+ cells of normal and injured mouse liver.* Development, 2009. **136**(11): p. 1951-60.
51. Ku, N.O., et al., *The cytoskeleton of digestive epithelia in health and disease.* Am J Physiol, 1999. **277**(6): p. G1108-37.
52. Li, Y., et al., *Targeted delivery of macromolecular drugs: asialoglycoprotein receptor (ASGPR) expression by selected hepatoma cell lines used in antiviral drug development.* Curr Drug Deliv, 2008. **5**(4): p. 299-302.
53. Alwahsh, S.M., et al., *Fibroblast growth factor 7 releasing particles enhance islet engraftment and improve metabolic control following islet transplantation in mice with diabetes.* Am J Transplant, 2021. **21**(9): p. 2950-2963.
54. de Ville de Goyet, J., et al., *European Liver Transplant Registry: Donor and transplant surgery aspects of 16,641 liver transplantations in children.* Hepatology, 2021.
55. Lazaridis, K.N. and N.F. LaRusso, *The Cholangiopathies.* Mayo Clin Proc, 2015. **90**(6): p. 791-800.
56. Heinemann, M., et al., *Long-term outcome after living donor liver transplantation compared to donation after brain death in autoimmune liver diseases: Experience from the European Liver Transplant Registry.* Am J Transplant, 2021.
57. Gadd, V.L., et al., *The portal inflammatory infiltrate and ductular reaction in human nonalcoholic fatty liver disease.* Hepatology, 2014. **59**(4): p. 1393-405.
58. Gouw, A.S., A.D. Clouston, and N.D. Theise, *Ductular reactions in human liver: diversity at the interface.* Hepatology, 2011. **54**(5): p. 1853-63.
59. Chen, Y., et al., *Mechanisms of ductular reaction in non-alcoholic steatohepatitis.* World J Gastroenterol, 2022. **28**(19): p. 2088-2099.
60. Sancho-Bru, P., et al., *Liver progenitor cell markers correlate with liver damage and predict short-term mortality in patients with alcoholic hepatitis.* Hepatology, 2012. **55**(6): p. 1931-41.
61. Gadd, V.L., et al., *Portal, but not lobular, macrophages express matrix metalloproteinase-9: association with the ductular reaction and fibrosis in chronic hepatitis C.* Liver Int, 2013. **33**(4): p. 569-79.
62. Kinugasa, Y., et al., *Bile ductular proliferation as a prognostic factor in biliary atresia: an immunohistochemical assessment.* J Pediatr Surg, 1999. **34**(11): p. 1715-20.
63. Hamesch, K., et al., *Serum keratin 19 (CYFRA21-1) links ductular reaction with portal hypertension and outcome of various advanced liver diseases.* BMC Med, 2020. **18**(1): p. 336.
64. Vacca, M., et al., *Current treatments of primary sclerosing cholangitis.* Curr Med Chem, 2007. **14**(19): p. 2081-94.
65. Wiesner, R.H., et al., *Comparison of the clinicopathologic features of primary sclerosing cholangitis and primary biliary cirrhosis.* Gastroenterology, 1985. **88**(1 Pt 1): p. 108-14.

66. Biagini, G. and G. Ballardini, *Liver fibrosis and extracellular matrix.* J Hepatol, 1989. **8**(1): p. 115-24.
67. Popper, H., *Pathologic aspects of cirrhosis. A review.* Am J Pathol, 1977. **87**(1): p. 228-64.
68. Salas-Silva, S., et al., *Cholangiocyte death in ductopenic cholestatic cholangiopathies: Mechanistic basis and emerging therapeutic strategies.* Life Sci, 2019. **218**: p. 324-339.
69. Tsuneyama, K., et al., *Primary Biliary Cholangitis: Its Pathological Characteristics and Immunopathological Mechanisms.* J Med Invest, 2017. **64**(1.2): p. 7-13.
70. Vartak, N., et al., *Cholestasis-induced adaptive remodeling of interlobular bile ducts.* Hepatology, 2016. **63**(3): p. 951-64.
71. Sasaki, M. and Y. Nakanuma, *Cellular senescence in biliary pathology. Special emphasis on expression of a polycomb group protein EZH2 and a senescent marker p16INK4a in bile ductular tumors and lesions.* Histol Histopathol, 2015. **30**(3): p. 267-75.
72. Munoz-Espin, D. and M. Serrano, *Cellular senescence: from physiology to pathology.* Nat Rev Mol Cell Biol, 2014. **15**(7): p. 482-96.
73. Meadows, V., et al., *Biliary Epithelial Senescence in Liver Disease: There Will Be SASP.* Front Mol Biosci, 2021. **8**: p. 803098.
74. Bird, T.G., et al., *TGFβ inhibition restores a regenerative response in acute liver injury by suppressing paracrine senescence.* Sci Transl Med, 2018. **10**(454).
75. Ferreira-Gonzalez, S., et al., *Paracrine cellular senescence exacerbates biliary injury and impairs regeneration.* Nat Commun, 2018. **9**(1): p. 1020.
76. Trussoni, C.E., S.P. O'Hara, and N.F. LaRusso, *Correction to: Cellular senescence in the cholangiopathies: a driver of immunopathology and a novel therapeutic target.* Semin Immunopathol, 2022. **44**(4): p. 545-546.
77. Cazzagon, N., et al., *Cholangiocyte senescence in primary sclerosing cholangitis is associated with disease severity and prognosis.* JHEP Rep, 2021. **3**(3): p. 100286.
78. Marschall, H.U., et al., *Incidence, prevalence, and outcome of primary biliary cholangitis in a nationwide Swedish population-based cohort.* Sci Rep, 2019. **9**(1): p. 11525.
79. Wang, L., et al., *CXCR5+ CD4+ T follicular helper cells participate in the pathogenesis of primary biliary cirrhosis.* Hepatology, 2015. **61**(2): p. 627-38.
80. Prieto, J., J.M. Banales, and J.F. Medina, *Primary biliary cholangitis: pathogenic mechanisms.* Curr Opin Gastroenterol, 2021. **37**(2): p. 91-98.
81. Li, H., et al., *The pathogenesis, models and therapeutic advances of primary biliary cholangitis.* Biomed Pharmacother, 2021. **140**: p. 111754.
82. Medina, J.F., et al., *Decreased anion exchanger 2 immunoreactivity in the liver of patients with primary biliary cirrhosis.* Hepatology, 1997. **25**(1): p. 12-7.
83. Rudic, J.S., et al., *Ursodeoxycholic acid for primary biliary cirrhosis.* Cochrane Database of Systematic Reviews, 2012(12).
84. Angulo, P. and K.D. Lindor, *Primary sclerosing cholangitis.* Hepatology, 1999. **30**(1): p. 325-32.
85. Loftus, E.V., Jr., et al., *PSC-IBD: a unique form of inflammatory bowel disease associated with primary sclerosing cholangitis.* Gut, 2005. **54**(1): p. 91-6.
86. Schrumpf, E., et al., *The gut microbiota contributes to a mouse model of spontaneous bile duct inflammation.* J Hepatol, 2017. **66**(2): p. 382-389.
87. Sheth, S., et al., *Increased prevalence of CFTR mutations and variants and decreased chloride secretion in primary sclerosing cholangitis.* Hum Genet, 2003. **113**(3): p. 286-92.
88. Werlin, S., et al., *Primary sclerosing cholangitis is associated with abnormalities in CFTR.* J Cyst Fibros, 2018. **17**(5): p. 666-671.
89. McBennett, K.A., P.B. Davis, and M.W. Konstan, *Increasing life expectancy in cystic fibrosis: Advances and challenges.* Pediatr Pulmonol, 2022. **57 Suppl 1**(Suppl 1): p. S5-s12.
90. Colombo, C., et al., *Liver disease in cystic fibrosis: A prospective study on incidence, risk factors, and outcome.* Hepatology, 2002. **36**(6): p. 1374-82.

91. Asai, A., A. Miethke, and J.A. Bezerra, *Pathogenesis of biliary atresia: defining biology to understand clinical phenotypes.* Nat Rev Gastroenterol Hepatol, 2015. **12**(6): p. 342-52.
92. Schreiber, R.A., et al., *Biliary atresia: the Canadian experience.* J Pediatr, 2007. **151**(6): p. 659-65, 665.e1.
93. Berauer, J.P., et al., *Identification of Polycystic Kidney Disease 1 Like 1 Gene Variants in Children With Biliary Atresia Splenic Malformation Syndrome.* Hepatology, 2019. **70**(3): p. 899-910.
94. Millwala, F., D.L. Segev, and P.J. Thuluvath, *Caroli's disease and outcomes after liver transplantation.* Liver Transpl, 2008. **14**(1): p. 11-7.
95. Hankeova, S., et al., *DUCT reveals architectural mechanisms contributing to bile duct recovery in a mouse model for Alagille syndrome.* Elife, 2021. **10**.
96. Turnpenny, P.D. and S. Ellard, *Alagille syndrome: pathogenesis, diagnosis and management.* Eur J Hum Genet, 2012. **20**(3): p. 251-7.
97. Emerick, K.M., et al., *Features of Alagille syndrome in 92 patients: frequency and relation to prognosis.* Hepatology, 1999. **29**(3): p. 822-9.
98. de Jong, I.E.M., et al., *Persistent biliary hypoxia and lack of regeneration are key mechanisms in the pathogenesis of posttransplant nonanastomotic strictures.* Hepatology, 2021.
99. Mourad, M.M., et al., *Aetiology and risk factors of ischaemic cholangiopathy after liver transplantation.* World J Gastroenterol, 2014. **20**(20): p. 6159-69.
100. Goria, O., et al., *Ischemic cholangiopathy: An update.* Clin Res Hepatol Gastroenterol, 2020. **44**(4): p. 486-490.
101. Leithead, J.A., et al., *The evolving use of higher risk grafts is associated with an increased incidence of acute kidney injury after liver transplantation.* J Hepatol, 2014. **60**(6): p. 1180-6.
102. Gómez-Mellado, V.E., et al., *ATP8B1 Deficiency Results in Elevated Mitochondrial Phosphatidylethanolamine Levels and Increased Mitochondrial Oxidative Phosphorylation in Human Hepatoma Cells.* Int J Mol Sci, 2022. **23**(20).
103. Groen, A., et al., *Complementary functions of the flippase ATP8B1 and the floppase ABCB4 in maintaining canalicular membrane integrity.* Gastroenterology, 2011. **141**(5): p. 1927-37.e1-4.
104. de Waart, D.R., et al., *ATP11C targets basolateral bile salt transporter proteins in mouse central hepatocytes.* Hepatology, 2016. **64**(1): p. 161-74.
105. Varma, S., et al., *Retargeting of bile salt export pump and favorable outcome in children with progressive familial intrahepatic cholestasis type 2.* Hepatology, 2015. **62**(1): p. 198-206.
106. Busuttil, R.W., et al., *Analysis of long-term outcomes of 3200 liver transplantations over two decades: a single-center experience.* Ann Surg, 2005. **241**(6): p. 905-16; discussion 916-8.
107. Caiado, A.H., et al., *Complications of liver transplantation: multimodality imaging approach.* Radiographics, 2007. **27**(5): p. 1401-17.
108. Ueda, Y., et al., *Long-term Prognosis and Recurrence of Primary Sclerosing Cholangitis After Liver Transplantation: A Single-Center Experience.* Transplant Direct, 2017. **3**(12): p. e334.
109. Manousou, P., et al., *Primary biliary cirrhosis after liver transplantation: influence of immunosuppression and human leukocyte antigen locus disparity.* Liver Transpl, 2010. **16**(1): p. 64-73.
110. Hargrove, L., et al., *Bile duct ligation-induced biliary hyperplasia, hepatic injury, and fibrosis are reduced in mast cell-deficient Kit(W-sh) mice.* Hepatology, 2017. **65**(6): p. 1991-2004.
111. Mancinelli, R., et al., *Ischemia reperfusion of the hepatic artery induces the functional damage of large bile ducts by changes in the expression of angiogenic factors.* Am J Physiol Gastrointest Liver Physiol, 2015. **309**(11): p. G865-73.
112. Jiang, J., et al., *Partial Portal Vein Arterialization Attenuates Acute Bile Duct Injury Induced by Hepatic Dearterialization in a Rat Model.* Biomed Res Int, 2016. **2016**: p. 7427246.
113. Vištejnová, L., et al., *Mesenchymal Stromal Cell Therapy in Novel Porcine Model of Diffuse Liver Damage Induced by Repeated Biliary Obstruction.* Int J Mol Sci, 2021. **22**(9).

114. Liem, H.H., K. Miyai, and U. Muller-Eberhard, *Effect of porphyrinogenic agents on protein synthesis and bilirubin formation by the isolated perfused rat liver.* Biochim Biophys Acta, 1977. **496**(1): p. 52-64.
115. Boonstra, K., U. Beuers, and C.Y. Ponsioen, *Epidemiology of primary sclerosing cholangitis and primary biliary cirrhosis: a systematic review.* J Hepatol, 2012. **56**(5): p. 1181-1188.
116. Gow, P.J. and R.W. Chapman, *Liver transplantation for primary sclerosing cholangitis.* Liver, 2000. **20**(2): p. 97-103.
117. Low, T.Y., et al., *A proteomic analysis of thioacetamide-induced hepatotoxicity and cirrhosis in rat livers.* Proteomics, 2004. **4**(12): p. 3960-74.
118. Unsal, V., M. Cicek, and İ. Sabancilar, *Toxicity of carbon tetrachloride, free radicals and role of antioxidants.* Rev Environ Health, 2021. **36**(2): p. 279-295.
119. Guicciardi, M.E., et al., *Biliary tract instillation of a SMAC mimetic induces TRAIL-dependent acute sclerosing cholangitis-like injury in mice.* Cell Death Dis, 2017. **8**(1): p. e2535.
120. Dickinson, P., J.R. Dorin, and D.J. Porteous, *Modelling cystic fibrosis in the mouse.* Mol Med Today, 1995. **1**(3): p. 140-8.
121. Concepcion, A.R., et al., *CD8+ T cells undergo activation and programmed death-1 repression in the liver of aged Ae2a,b-/- mice favoring autoimmune cholangitis.* Oncotarget, 2015. **6**(30): p. 28588-606.
122. Zhao, C., et al., *Intrahepatic cholangiocyte regeneration from an Fgf-dependent extrahepatic progenitor niche in a zebrafish model of Alagille Syndrome.* Hepatology (Baltimore, Md.), 2022. **75**(3): p. 567-583.
123. Nakagawa, H., et al., *Loss of liver E-cadherin induces sclerosing cholangitis and promotes carcinogenesis.* Proc Natl Acad Sci U S A, 2014. **111**(3): p. 1090-5.
124. Hallett, J.M., et al., *Human biliary epithelial cells from discarded donor livers rescue bile duct structure and function in a mouse model of biliary disease.* Cell Stem Cell, 2022. **29**(3): p. 355-371.e10.
125. Funaki, B., *Islet cell transplantation.* Semin Intervent Radiol, 2006. **23**(3): p. 295-7.
126. Bensinger, W., *Individual patient data meta-analysis of allogeneic peripheral blood stem cell transplant vs bone marrow transplant in the management of hematological malignancies: indirect assessment of the effect of day 11 methotrexate administration.* Bone Marrow Transplant, 2006. **38**(8): p. 539-46.
127. Forbes, S.J., S. Gupta, and A. Dhawan, *Cell therapy for liver disease: From liver transplantation to cell factory.* J Hepatol, 2015. **62**(1 Suppl): p. S157-69.
128. Meier, R.P., et al., *Microencapsulated human mesenchymal stem cells decrease liver fibrosis in mice.* J Hepatol, 2015. **62**(3): p. 634-41.
129. Moroni, F., et al., *Safety profile of autologous macrophage therapy for liver cirrhosis.* Nat Med, 2019. **25**(10): p. 1560-1565.
130. Weismüller, T.J., et al., *Patient Age, Sex, and Inflammatory Bowel Disease Phenotype Associate With Course of Primary Sclerosing Cholangitis.* Gastroenterology, 2017. **152**(8): p. 1975-1984.e8.
131. Lammers, W.J., et al., *Levels of alkaline phosphatase and bilirubin are surrogate end points of outcomes of patients with primary biliary cirrhosis: an international follow-up study.* Gastroenterology, 2014. **147**(6): p. 1338-49.e5; quiz e15.
132. Khan, A.A., et al., *Human fetal liver-derived stem cell transplantation as supportive modality in the management of end-stage decompensated liver cirrhosis.* Cell Transplant, 2010. **19**(4): p. 409-18.
133. Cardinale, V., et al., *Transplantation of human fetal biliary tree stem/progenitor cells into two patients with advanced liver cirrhosis.* BMC Gastroenterol, 2014. **14**: p. 204.
134. Khandekar, G., et al., *Coordinated development of the mouse extrahepatic bile duct: Implications for neonatal susceptibility to biliary injury.* J Hepatol, 2020. **72**(1): p. 135-145.

135. Nevi, L., et al., *Hyaluronan coating improves liver engraftment of transplanted human biliary tree stem/progenitor cells.* Stem Cell Res Ther, 2017. **8**(1): p. 68.
136. Carpino, G., et al., *Peribiliary Gland Niche Participates in Biliary Tree Regeneration in Mouse and in Human Primary Sclerosing Cholangitis.* Hepatology, 2020. **71**(3): p. 972-989.
137. de Jong, I.E.M., et al., *Peribiliary Glands Are Key in Regeneration of the Human Biliary Epithelium After Severe Bile Duct Injury.* Hepatology, 2019. **69**(4): p. 1719-1734.
138. Tarlow, B.D., et al., *Bipotential adult liver progenitors are derived from chronically injured mature hepatocytes.* Cell Stem Cell, 2014. **15**(5): p. 605-18.
139. Schaub, J.R., et al., *De novo formation of the biliary system by TGFbeta-mediated hepatocyte transdifferentiation.* Nature, 2018. **557**(7704): p. 247-251.
140. Furuyama, K., et al., *Continuous cell supply from a Sox9-expressing progenitor zone in adult liver, exocrine pancreas and intestine.* Nat Genet, 2011. **43**(1): p. 34-41.
141. Tarlow, B.D., M.J. Finegold, and M. Grompe, *Clonal tracing of Sox9+ liver progenitors in mouse oval cell injury.* Hepatology, 2014. **60**(1): p. 278-89.
142. Malato, Y., et al., *Fate tracing of mature hepatocytes in mouse liver homeostasis and regeneration.* J Clin Invest, 2011. **121**(12): p. 4850-60.
143. Raven, A., et al., *Cholangiocytes act as facultative liver stem cells during impaired hepatocyte regeneration.* Nature, 2017. **547**(7663): p. 350-354.
144. Zhang, J., et al., *miR-21 Inhibition Reduces Liver Fibrosis and Prevents Tumor Development by Inducing Apoptosis of CD24+ Progenitor Cells.* Cancer Res, 2015. **75**(9): p. 1859-67.
145. Kon, J., et al., *Expression of CD44 in rat hepatic progenitor cells.* J Hepatol, 2006. **45**(1): p. 90-8.
146. Sackett, S.D., et al., *Foxl1 is a marker of bipotential hepatic progenitor cells in mice.* Hepatology, 2009. **49**(3): p. 920-9.
147. Kordes, C., et al., *CD133+ hepatic stellate cells are progenitor cells.* Biochem Biophys Res Commun, 2007. **352**(2): p. 410-7.
148. Aizarani, N., et al., *A human liver cell atlas reveals heterogeneity and epithelial progenitors.* Nature, 2019. **572**(7768): p. 199-204.
149. Pepe-Mooney, B.J., et al., *Single-Cell Analysis of the Liver Epithelium Reveals Dynamic Heterogeneity and an Essential Role for YAP in Homeostasis and Regeneration.* Cell Stem Cell, 2019. **25**(1): p. 23-38.e8.
150. Lu, W.Y., et al., *Hepatic progenitor cells of biliary origin with liver repopulation capacity.* Nat Cell Biol, 2015. **17**(8): p. 971-983.
151. Han, B., et al., *Fat-associated lymphoid clusters as expandable niches for ectopic liver development.* Hepatology, 2021.
152. Newsome, P.N., et al., *Granulocyte colony-stimulating factor and autologous CD133-positive stem-cell therapy in liver cirrhosis (REALISTIC): an open-label, randomised, controlled phase 2 trial.* Lancet Gastroenterol Hepatol, 2018. **3**(1): p. 25-36.
153. Mansini, A.P., et al., *The Chemosensory Function of Primary Cilia Regulates Cholangiocyte Migration, Invasion, and Tumor Growth.* Hepatology, 2019. **69**(4): p. 1582-1598.
154. Mine, T., et al., *Clinical practice guideline for post-ERCP pancreatitis.* J Gastroenterol, 2017. **52**(9): p. 1013-1022.
155. Turan, A.S., et al., *Complications of percutaneous transhepatic cholangiography and biliary drainage, a multicenter observational study.* Abdom Radiol (NY), 2022. **47**(9): p. 3338-3344.
156. Farid, W.R., et al., *Relationship between the histological appearance of the portal vein and development of ischemic-type biliary lesions after liver transplantation.* Liver Transpl, 2013. **19**(10): p. 1088-98.
157. Laing, R.W., et al., *The Delivery of Multipotent Adult Progenitor Cells to Extended Criteria Human Donor Livers Using Normothermic Machine Perfusion.* Front Immunol, 2020. **11**: p. 1226.

158. Seki, A., et al., *Transcatheter arterial chemoembolization with epirubicin-loaded superabsorbent polymer microspheres for 135 hepatocellular carcinoma patients: Single-center experience.* CardioVascular and Interventional Radiology, 2011. **34**(3): p. 557-565.
159. Makary, M.S., et al., *Yttrium-90 microsphere selective internal radiation therapy for liver metastases following systemic chemotherapy and surgical resection for metastatic adrenocortical carcinoma.* World J Clin Oncol, 2018. **9**(1): p. 20-25.
160. Marcacuzco Quinto, A., et al., *Complications of transarterial chemoembolization (TACE) in the treatment of liver tumors.* Cir Esp, 2018. **96**(9): p. 560-567.
161. Kruepunga, N., et al., *Anatomy of rodent and human livers: What are the differences?* Biochim Biophys Acta Mol Basis Dis, 2019. **1865**(5): p. 869-878.
162. Shapiro, A.M., et al., *International trial of the Edmonton protocol for islet transplantation.* N Engl J Med, 2006. **355**(13): p. 1318-30.
163. Haddad, M.M., et al., *Comparison of Bleeding Complications between Transplenic versus Transhepatic Access of the Portal Venous System.* J Vasc Interv Radiol, 2018. **29**(10): p. 1383-1391.
164. Thalheimer, A., et al., *Tumor cell dissemination in a human colon cancer animal model: orthotopic implantation or intraportal injection?* Eur Surg Res, 2009. **42**(3): p. 195-200.
165. He, H., et al., *Leutusome: A Biomimetic Nanoplatform Integrating Plasma Membrane Components of Leukocytes and Tumor Cells for Remarkably Enhanced Solid Tumor Homing.* Nano Lett, 2018. **18**(10): p. 6164-6174.
166. Li, X., et al., *Improving Cell Engraftment in Cardiac Stem Cell Therapy.* Stem Cells Int, 2016. **2016**: p. 7168797.
167. Chavakis, E., C. Urbich, and S. Dimmeler, *Homing and engraftment of progenitor cells: a prerequisite for cell therapy.* J Mol Cell Cardiol, 2008. **45**(4): p. 514-22.
168. Sarkar, D., et al., *Engineered mesenchymal stem cells with self-assembled vesicles for systemic cell targeting.* Biomaterials, 2010. **31**(19): p. 5266-74.
169. Sarkar, D., et al., *Cell surface engineering of mesenchymal stem cells.* Methods Mol Biol, 2011. **698**: p. 505-23.
170. Dollet, P.E., et al., *Evaluation of Strategies Aimed at Improving Liver Progenitor Cell Rolling and Subsequent Adhesion to the Endothelium.* Cell Transplant, 2020. **29**: p. 963689720912707.
171. Ko, I.K., et al., *Targeting improves MSC treatment of inflammatory bowel disease.* Mol Ther, 2010. **18**(7): p. 1365-72.
172. Jeong, J.H., et al., *Leukocyte-mimicking stem cell delivery via in situ coating of cells with a bioactive hyperbranched polyglycerol.* J Am Chem Soc, 2013. **135**(24): p. 8770-3.
173. Corradetti, B., et al., *Hyaluronic acid coatings as a simple and efficient approach to improve MSC homing toward the site of inflammation.* Sci Rep, 2017. **7**(1): p. 7991.
174. Yoneten, K.K., et al., *Comparative Proteomics Analysis of Four Commonly Used Methods for Identification of Novel Plasma Membrane Proteins.* J Membr Biol, 2019.
175. Akpinar, G., et al., *Search for Novel Plasma Membrane Proteins as Potential Biomarkers in Human Mesenchymal Stem Cells Derived from Dental Pulp, Adipose Tissue, Bone Marrow, and Hair Follicle.* J Membr Biol, 2021. **254**(4): p. 409-422.
176. Kumar, V., et al., *Optimization and Application of a Biotinylation Method for Quantification of Plasma Membrane Expression of Transporters in Cells.* Aaps j, 2017. **19**(5): p. 1377-1386.
177. Weekes, M.P., et al., *Comparative analysis of techniques to purify plasma membrane proteins.* J Biomol Tech, 2010. **21**(3): p. 108-15.
178. Ducret, A., et al., *Identification of six cell surface proteins for specific liver targeting.* Proteomics Clin Appl, 2015. **9**(7-8): p. 651-61.
179. Eichacker, L.A., et al., *Hiding behind hydrophobicity. Transmembrane segments in mass spectrometry.* J Biol Chem, 2004. **279**(49): p. 50915-22.

180. Lee, S.H., et al., *Bioinformatic analysis of membrane and associated proteins in murine cardiomyocytes and human myocardium.* Sci Data, 2020. **7**(1): p. 425.
181. Tietz, P.S., et al., *Isolation and characterization of rat cholangiocyte vesicles enriched in apical or basolateral plasma membrane domains.* Biochemistry, 1995. **34**(47): p. 15436-43.
182. Wiśniewski, J.R., et al., *In-depth quantitative analysis and comparison of the human hepatocyte and hepatoma cell line HepG2 proteomes.* J Proteomics, 2016. **136**: p. 234-47.
183. Miszczuk, G.S., et al., *Adaptive downregulation of Cl-/HCO3- exchange activity in rat hepatocytes under experimental obstructive cholestasis.* PLoS One, 2019. **14**(2): p. e0212215.
184. Rodrigues, P.M., et al., *Primary biliary cholangitis: A tale of epigenetically-induced secretory failure?* J Hepatol, 2018. **69**(6): p. 1371-1383.
185. Afroze, S., et al., *The physiological roles of secretin and its receptor.* Ann Transl Med, 2013. **1**(3): p. 29.
186. Chow, B.K., *Molecular cloning and functional characterization of a human secretin receptor.* Biochem Biophys Res Commun, 1995. **212**(1): p. 204-11.
187. Körner, M., et al., *Secretin receptors in the human liver: expression in biliary tract and cholangiocarcinoma, but not in hepatocytes or hepatocellular carcinoma.* J Hepatol, 2006. **45**(6): p. 825-35.
188. McDaniel, K., et al., *Forkhead box A2 regulates biliary heterogeneity and senescence during cholestatic liver injury in mice‡.* Hepatology, 2017. **65**(2): p. 544-559.
189. Wu, N., et al., *The secretin/secretin receptor axis modulates liver fibrosis through changes in transforming growth factor-β1 biliary secretion in mice.* Hepatology, 2016. **64**(3): p. 865-79.
190. Kennedy, L., et al., *Secretin/secretin receptor signaling mediates biliary damage and liver fibrosis in early-stage primary biliary cholangitis.* FASEB J, 2019: p. fj201802606R.
191. Hayashi, Y., et al., *Loss of trefoil factor 1 inhibits biliary regeneration but accelerates the hepatic differentiation of progenitor cells in mice.* Biochem Biophys Res Commun, 2018. **506**(1): p. 12-19.
192. Zhang, B., et al., *Trefoil factor 2 secreted from damaged hepatocytes activates hepatic stellate cells to induce fibrogenesis.* J Biol Chem, 2021. **297**(1): p. 100887.
193. Sasaki, M., et al., *Site-characteristic expression and induction of trefoil factor family 1, 2 and 3 and malignant brain tumor-1 in normal and diseased intrahepatic bile ducts relates to biliary pathophysiology.* Liver Int, 2004. **24**(1): p. 29-37.
194. Engevik, K.A., et al., *Trefoil factor 2 activation of CXCR4 requires calcium mobilization to drive epithelial repair in gastric organoids.* J Physiol, 2019. **597**(10): p. 2673-2690.
195. Stamenkovic, I., et al., *A lymphocyte molecule implicated in lymph node homing is a member of the cartilage link protein family.* Cell, 1989. **56**(6): p. 1057-62.
196. Yamaguchi, Y. and E. Ruoslahti, *Expression of human proteoglycan in Chinese hamster ovary cells inhibits cell proliferation.* Nature, 1988. **336**(6196): p. 244-6.
197. Zuo, X., et al., *Spheroids of Endothelial Cells and Vascular Smooth Muscle Cells Promote Cell Migration in Hyaluronic Acid and Fibrinogen Composite Hydrogels.* Research (Wash D C), 2020. **2020**: p. 8970480.
198. He, Y., et al., *Interaction of CD44 and hyaluronic acid enhances biliary epithelial proliferation in cholestatic livers.* Am J Physiol Gastrointest Liver Physiol, 2008. **295**(2): p. G305-12.
199. Brenner, S., et al., *CXCR4-transgene expression significantly improves marrow engraftment of cultured hematopoietic stem cells.* Stem Cells, 2004. **22**(7): p. 1128-33.
200. Bonacina, F., et al., *Adoptive transfer of CX3CR1 transduced-T regulatory cells improves homing to the atherosclerotic plaques and dampens atherosclerosis progression.* Cardiovasc Res, 2021. **117**(9): p. 2069-2082.
201. Zhang, X., et al., *CXCR5-Overexpressing Mesenchymal Stromal Cells Exhibit Enhanced Homing and Can Decrease Contact Hypersensitivity.* Mol Ther, 2017. **25**(6): p. 1434-1447.
202. Xu, R., et al., *CCR2-overexpressing mesenchymal stem cells targeting damaged liver enhance recovery of acute liver failure.* Stem Cell Res Ther, 2022. **13**(1): p. 55.

203. Jiang, H.H., et al., *Combined Treatment With CCR1-Overexpressing Mesenchymal Stem Cells and CCL7 Enhances Engraftment and Promotes the Recovery of Simulated Birth Injury-Induced Stress Urinary Incontinence in Rats.* Front Surg, 2020. **7**: p. 40.
204. Kurzejamska, E., et al., *Effect of Chemokine (C-C Motif) Ligand 7 (CCL7) and Its Receptor (CCR2) Expression on Colorectal Cancer Behaviors.* Int J Mol Sci, 2019. **20**(3).
205. Lee, Y.S., et al., *Crosstalk between CCL7 and CCR3 promotes metastasis of colon cancer cells via ERK-JNK signaling pathways.* Oncotarget, 2016. **7**(24): p. 36842-36853.
206. Ford, J., et al., *CCL7 Is a Negative Regulator of Cutaneous Inflammation Following Leishmania major Infection.* Front Immunol, 2018. **9**: p. 3063.
207. Sokulsky, L.A., et al., *A Critical Role for the CXCL3/CXCL5/CXCR2 Neutrophilic Chemotactic Axis in the Regulation of Type 2 Responses in a Model of Rhinoviral-Induced Asthma Exacerbation.* J Immunol, 2020. **205**(9): p. 2468-2478.
208. Tylaska, L.A., et al., *Ccr2 regulates the level of MCP-1/CCL2 in vitro and at inflammatory sites and controls T cell activation in response to alloantigen.* Cytokine, 2002. **18**(4): p. 184-90.
209. Zhang, T., et al., *Migration of cytotoxic T lymphocytes toward melanoma cells in three-dimensional organotypic culture is dependent on CCL2 and CCR4.* Eur J Immunol, 2006. **36**(2): p. 457-67.
210. Yamazaki, C., et al., *Conservation of a chemokine system, XCR1 and its ligand, XCL1, between human and mice.* Biochem Biophys Res Commun, 2010. **397**(4): p. 756-61.
211. Schutyser, E., S. Struyf, and J. Van Damme, *The CC chemokine CCL20 and its receptor CCR6.* Cytokine Growth Factor Rev, 2003. **14**(5): p. 409-26.
212. Guilliams, M., et al., *Spatial proteogenomics reveals distinct and evolutionarily conserved hepatic macrophage niches.* Cell, 2022. **185**(2): p. 379-396.e38.
213. Sasaki, M., et al., *Modulation of the microenvironment by senescent biliary epithelial cells may be involved in the pathogenesis of primary biliary cirrhosis.* J Hepatol, 2010. **53**(2): p. 318-25.
214. Guicciardi, M.E., et al., *Macrophages contribute to the pathogenesis of sclerosing cholangitis in mice.* J Hepatol, 2018. **69**(3): p. 676-686.
215. Konishi, T., et al., *Cell-specific regulatory effects of CXCR2 on cholestatic liver injury.* Am J Physiol Gastrointest Liver Physiol, 2019. **317**(6): p. G773-g783.
216. Mohamad Zaki, N.H., et al., *C-X-C motif chemokine ligand 1 induced by Hedgehog signaling promotes mouse extrahepatic bile duct repair after acute injury.* Hepatology, 2022.
217. Rodrigo-Torres, D., et al., *The biliary epithelium gives rise to liver progenitor cells.* Hepatology, 2014. **60**(4): p. 1367-77.
218. Suski, J.M., et al., *Isolation of plasma membrane-associated membranes from rat liver.* Nat Protoc, 2014. **9**(2): p. 312-22.
219. Lund, R., et al., *Efficient isolation and quantitative proteomic analysis of cancer cell plasma membrane proteins for identification of metastasis-associated cell surface markers.* J Proteome Res, 2009. **8**(6): p. 3078-90.
220. Law, C.W., et al., *voom: Precision weights unlock linear model analysis tools for RNA-seq read counts.* Genome Biol, 2014. **15**(2): p. R29.
221. Shinkai, Y., et al., *RAG-2-deficient mice lack mature lymphocytes owing to inability to initiate V(D)J rearrangement.* Cell, 1992. **68**(5): p. 855-67.
222. Cao, X., et al., *Defective lymphoid development in mice lacking expression of the common cytokine receptor gamma chain.* Immunity, 1995. **2**(3): p. 223-38.
223. Tsuchida, T., et al., *A simple diet- and chemical-induced murine NASH model with rapid progression of steatohepatitis, fibrosis and liver cancer.* J Hepatol, 2018. **69**(2): p. 385-395.
224. Marcolin, E., et al., *Methionine- and choline-deficient diet induces hepatic changes characteristic of non-alcoholic steatohepatitis.* Arq Gastroenterol, 2011. **48**(1): p. 72-9.
225. Pretzsch, E., et al., *Molecular Mechanisms of Ischaemia-Reperfusion Injury and Regeneration in the Liver-Shock and Surgery-Associated Changes.* Int J Mol Sci, 2022. **23**(21).

226. Datta, G., B.J. Fuller, and B.R. Davidson, *Molecular mechanisms of liver ischemia reperfusion injury: insights from transgenic knockout models.* World J Gastroenterol, 2013. **19**(11): p. 1683-98.
227. Maru, Y., K. Orihashi, and Y. Hippo, *Lentivirus-Based Stable Gene Delivery into Intestinal Organoids.* Methods Mol Biol, 2016. **1422**: p. 13-21.
228. Hansell, C.A.H., et al., *Analysis of lung stromal expression of the atypical chemokine receptor ACKR2 reveals unanticipated expression in murine blood endothelial cells.* Eur J Immunol, 2020. **50**(5): p. 666-675.
229. Dwivedi, A.K., I. Mallawaarachchi, and L.A. Alvarado, *Analysis of small sample size studies using nonparametric bootstrap test with pooled resampling method.* Stat Med, 2017. **36**(14): p. 2187-2205.
230. Terada, R., et al., *Stromal cell-derived factor-1 from biliary epithelial cells recruits CXCR4-positive cells: implications for inflammatory liver diseases.* Lab Invest, 2003. **83**(5): p. 665-72.
231. Sánchez-Martínez, D., et al., *Enforced sialyl-Lewis-X (sLeX) display in E-selectin ligands by exofucosylation is dispensable for CD19-CAR T-cell activity and bone marrow homing.* Clin Transl Med, 2021. **11**(2): p. e280.
232. Stastna, M. and J.E. Van Eyk, *Secreted proteins as a fundamental source for biomarker discovery.* Proteomics, 2012. **12**(4-5): p. 722-35.
233. Loarca, L., et al., *Development and characterization of cholangioids from normal and diseased human cholangiocytes as an in vitro model to study primary sclerosing cholangitis.* Lab Invest, 2017. **97**(11): p. 1385-1396.
234. Cheng, Y., et al., *Autophagy is Required for the Maintenance of Liver Progenitor Cell Functionality.* Cell Physiol Biochem, 2015. **36**(3): p. 1163-74.
235. Nagano, T., et al., *Identification of cellular senescence-specific genes by comparative transcriptomics.* Sci Rep, 2016. **6**: p. 31758.
236. Bankhead, P., et al., *QuPath: Open source software for digital pathology image analysis.* Sci Rep, 2017. **7**(1): p. 16878.
237. Kruidering, M. and G.I. Evan, *Caspase-8 in apoptosis: the beginning of "the end"?* IUBMB Life, 2000. **50**(2): p. 85-90.
238. Porter, A.G. and R.U. Jänicke, *Emerging roles of caspase-3 in apoptosis.* Cell Death Differ, 1999. **6**(2): p. 99-104.
239. Wagner, K.D. and N. Wagner, *The Senescence Markers p16INK4A, p14ARF/p19ARF, and p21 in Organ Development and Homeostasis.* Cells, 2022. **11**(12).
240. Sheekey, E. and M. Narita, *p53 in senescence - it's a marathon not a sprint.* Febs j, 2021.
241. Schlegel, A., et al., *Hypothermic oxygenated perfusion (HOPE) protects from biliary injury in a rodent model of DCD liver transplantation.* J Hepatol, 2013. **59**(5): p. 984-91.
242. Toki, M.I., et al., *Proof of the quantitative potential of immunofluorescence by mass spectrometry.* Lab Invest, 2017. **97**(3): p. 329-334.
243. Hirata, K. and M.H. Nathanson, *Bile duct epithelia regulate biliary bicarbonate excretion in normal rat liver.* Gastroenterology, 2001. **121**(2): p. 396-406.
244. Ishii, M., et al., *Hepatocytic parental progenitor cells of rat small hepatocytes maintain self-renewal capability after long-term culture.* Sci Rep, 2017. **7**: p. 46177.
245. Yin, Q., et al., *CD44 promotes the migration of bone marrow-derived mesenchymal stem cells toward glioma.* Oncol Lett, 2016. **11**(4): p. 2353-2358.
246. López-Ortega, O. and L. Santos-Argumedo, *Myosin 1g Contributes to CD44 Adhesion Protein and Lipid Rafts Recycling and Controls CD44 Capping and Cell Migration in B Lymphocytes.* Front Immunol, 2017. **8**: p. 1731.
247. Girbl, T., et al., *Distinct Compartmentalization of the Chemokines CXCL1 and CXCL2 and the Atypical Receptor ACKR1 Determine Discrete Stages of Neutrophil Diapedesis.* Immunity, 2018. **49**(6): p. 1062-1076.e6.

248. De Filippo, K., et al., *Mast cell and macrophage chemokines CXCL1/CXCL2 control the early stage of neutrophil recruitment during tissue inflammation.* Blood, 2013. **121**(24): p. 4930-7.
249. Ding, J., et al., *Overexpression of CXCL2 inhibits cell proliferation and promotes apoptosis in hepatocellular carcinoma.* BMB Rep, 2018. **51**(12): p. 630-635.
250. Han, K.Q., et al., *Targeted silencing of CXCL1 by siRNA inhibits tumor growth and apoptosis in hepatocellular carcinoma.* Int J Oncol, 2015. **47**(6): p. 2131-40.
251. Prašnikar, E., J. Borišek, and A. Perdih, *Senescent cells as promising targets to tackle age-related diseases.* Ageing Res Rev, 2021. **66**: p. 101251.
252. Sabbagh, L., et al., *Selective up-regulation of caspase-3 gene expression following TCR engagement.* Mol Immunol, 2005. **42**(11): p. 1345-54.
253. González-Gualda, E., et al., *A guide to assessing cellular senescence in vitro and in vivo.* Febs j, 2021. **288**(1): p. 56-80.
254. Taniguchi, Y., et al., *Quantifying E. coli proteome and transcriptome with single-molecule sensitivity in single cells.* Science, 2010. **329**(5991): p. 533-8.
255. Vogel, C. and E.M. Marcotte, *Insights into the regulation of protein abundance from proteomic and transcriptomic analyses.* Nat Rev Genet, 2012. **13**(4): p. 227-32.
256. Liu, Y., A. Beyer, and R. Aebersold, *On the Dependency of Cellular Protein Levels on mRNA Abundance.* Cell, 2016. **165**(3): p. 535-50.
257. Krogh, A., et al., *Predicting transmembrane protein topology with a hidden Markov model: application to complete genomes.* J Mol Biol, 2001. **305**(3): p. 567-80.
258. Ritchie, M.E., et al., *limma powers differential expression analyses for RNA-sequencing and microarray studies.* Nucleic Acids Res, 2015. **43**(7): p. e47.
259. Smyth, G.K. and T. Speed, *Normalization of cDNA microarray data.* Methods, 2003. **31**(4): p. 265-73.
260. Thomas, P.D., et al., *PANTHER: a browsable database of gene products organized by biological function, using curated protein family and subfamily classification.* Nucleic Acids Res, 2003. **31**(1): p. 334-41.
261. Nakanuma, Y. and N. Kono, *Expression of vimentin in proliferating and damaged bile ductules and interlobular bile ducts in nonneoplastic hepatobiliary diseases.* Mod Pathol, 1992. **5**(5): p. 550-4.
262. Paulsen, J.D., et al., *Keratin 19 and mesenchymal markers for evaluation of epithelial-mesenchymal transition and stem cell niche components in primary biliary cholangitis by sequential elution-stripping multiplex immunohistochemistry.* J Histotechnol, 2020. **43**(4): p. 163-173.
263. Lalioti, V., et al., *Cell surface detection of vimentin, ACE2 and SARS-CoV-2 Spike proteins reveals selective colocalization at primary cilia.* Sci Rep, 2022. **12**(1): p. 7063.
264. Paulin, D., et al., *Vimentin: Regulation and pathogenesis.* Biochimie, 2022. **197**: p. 96-112.
265. Välikangas, T., T. Suomi, and L.L. Elo, *A systematic evaluation of normalization methods in quantitative label-free proteomics.* Brief Bioinform, 2018. **19**(1): p. 1-11.
266. Betapudi, V., *Life without double-headed non-muscle myosin II motor proteins.* Front Chem, 2014. **2**: p. 45.
267. Katayanagi, K., et al., *Generation of monoclonal antibodies to murine bile duct epithelial cells: identification of annexin V as a new marker of small intrahepatic bile ducts.* Hepatology, 1999. **29**(4): p. 1019-25.
268. Grewal, T., et al., *Annexins - insights from knockout mice.* Biol Chem, 2016. **397**(10): p. 1031-53.
269. Nuerzhati, Y., et al., *Role of the long non-coding RNA-Annexin A2 pseudogene 3/Annexin A2 signaling pathway in biliary atresia-associated hepatic injury.* Int J Mol Med, 2019. **43**(2): p. 739-748.
270. Yao, H.S., et al., *Annexin A4-nuclear factor-κB feedback circuit regulates cell malignant behavior and tumor growth in gallbladder cancer.* Sci Rep, 2016. **6**: p. 31056.

271. Shao, Y.Y., et al., *Association of annexin A10 expression with poor prognosis of intrahepatic cholangiocarcinoma.* BMC Cancer, 2022. **22**(1): p. 219.
272. Herta, T., et al., *Role of the IgG4-related cholangitis autoantigen annexin A11 in cholangiocyte protection.* J Hepatol, 2022. **76**(2): p. 319-331.
273. Hubers, L.M., et al., *Annexin A11 is targeted by IgG4 and IgG1 autoantibodies in IgG4-related disease.* Gut, 2018. **67**(4): p. 728-735.
274. Koopman, G., et al., *Annexin V for flow cytometric detection of phosphatidylserine expression on B cells undergoing apoptosis.* Blood, 1994. **84**(5): p. 1415-20.
275. Vermes, I., et al., *A novel assay for apoptosis. Flow cytometric detection of phosphatidylserine expression on early apoptotic cells using fluorescein labelled Annexin V.* J Immunol Methods, 1995. **184**(1): p. 39-51.
276. Ewing, M.M., et al., *Annexin A5 therapy attenuates vascular inflammation and remodeling and improves endothelial function in mice.* Arterioscler Thromb Vasc Biol, 2011. **31**(1): p. 95-101.
277. Faria, D., et al., *Effect of Annexin A5 on CFTR: regulated traffic or scaffolding?* Mol Membr Biol, 2011. **28**(1): p. 14-29.
278. Martin, L., et al., *How much do clinical trials cost?* Nat Rev Drug Discov, 2017. **16**(6): p. 381-382.
279. Mitrousis, N., A. Fokina, and M.S. Shoichet, *Biomaterials for cell transplantation.* Nature Reviews Materials, 2018. **3**(11): p. 441-456.
280. Kharbikar, B.N., P. Mohindra, and T.A. Desai, *Biomaterials to enhance stem cell transplantation.* Cell Stem Cell, 2022. **29**(5): p. 692-721.
281. Ohya, T., et al., *Degeneration of intrahepatic bile duct with lymphocyte infiltration into biliary epithelial cells in biliary atresia.* J Pediatr Surg, 1995. **30**(4): p. 515-8.
282. Terasaki, S., et al., *Eosinophilic infiltration of the liver in primary biliary cirrhosis: a morphological study.* Hepatology, 1993. **17**(2): p. 206-12.
283. Du, Z., et al., *Mesenchymal stem cells overexpressing C-X-C chemokine receptor type 4 improve early liver regeneration of small-for-size liver grafts.* Liver Transpl, 2013. **19**(2): p. 215-25.
284. Love, M.I., W. Huber, and S. Anders, *Moderated estimation of fold change and dispersion for RNA-seq data with DESeq2.* Genome Biol, 2014. **15**(12): p. 550.
285. Vimalesvaran, S., J. Nulty, and A. Dhawan, *Cellular Therapies in Pediatric Liver Diseases.* Cells, 2022. **11**(16).
286. Dhawan, A., et al., *Alginate microencapsulated human hepatocytes for the treatment of acute liver failure in children.* J Hepatol, 2020. **72**(5): p. 877-884.
287. Graham, G.J., *D6/ACKR2.* Front Immunol, 2015. **6**: p. 280.
288. Lee, K.M., R.J. Nibbs, and G.J. Graham, *D6: the 'crowd controller' at the immune gateway.* Trends Immunol, 2013. **34**(1): p. 7-12.
289. Graham, G.J., *D6 and the atypical chemokine receptor family: novel regulators of immune and inflammatory processes.* Eur J Immunol, 2009. **39**(2): p. 342-51.
290. Wilson, G.J., et al., *Chemokine receptors coordinately regulate macrophage dynamics and mammary gland development.* Development, 2020. **147**(12).
291. Hughes, C.E. and R.J.B. Nibbs, *A guide to chemokines and their receptors.* Febs j, 2018. **285**(16): p. 2944-2971.
292. Castanheira, F., et al., *The Atypical Chemokine Receptor ACKR2 is Protective Against Sepsis.* Shock, 2018. **49**(6): p. 682-689.
293. Tavares, L.P., et al., *ACKR2 contributes to pulmonary dysfunction by shaping CCL5:CCR5-dependent recruitment of lymphocytes during influenza A infection in mice.* Am J Physiol Lung Cell Mol Physiol, 2020. **318**(4): p. L655-l670.

294. Madigan, J., et al., *Chemokine scavenger D6 is expressed by trophoblasts and aids the survival of mouse embryos transferred into allogeneic recipients.* J Immunol, 2010. **184**(6): p. 3202-12.
295. Chen, R.X., et al., *Apolipoprotein A-1 protected hepatic ischaemia-reperfusion injury through suppressing macrophage pyroptosis via TLR4-NF-κB pathway.* Liver Int, 2023. **43**(1): p. 234-248.
296. Wu, S., et al., *Macrophage extracellular traps aggravate iron overload-related liver ischaemia/reperfusion injury.* Br J Pharmacol, 2021. **178**(18): p. 3783-3796.
297. Reiling, J., et al., *The role of macrophages in the development of biliary injury in a lipopolysaccharide-aggravated hepatic ischaemia-reperfusion model.* Biochim Biophys Acta Mol Basis Dis, 2018. **1864**(4 Pt B): p. 1284-1292.
298. Gupta, S., et al., *111Indium labeling of hepatocytes for analysis of short-term biodistribution of transplanted cells.* Hepatology, 1994. **19**(3): p. 750-7.
299. Revell, D.Z. and B.K. Yoder, *Intravital visualization of the primary cilium, tubule flow, and innate immune cells in the kidney utilizing an abdominal window imaging approach.* Methods Cell Biol, 2019. **154**: p. 67-83.
300. Coelho-Santos, V., T. Tieu, and A.Y. Shih, *Reinforced thinned-skull window for repeated imaging of the neonatal mouse brain.* Neurophotonics, 2022. **9**(3): p. 031918.
301. Stoletov, K., et al., *Intravital imaging of Wnt/β-catenin and ATF2-dependent signalling pathways during tumour cell invasion and metastasis.* J Cell Sci, 2023.
302. Schmidt, E.S. and F.W. Schmidt, *Glutamate dehydrogenase: biochemical and clinical aspects of an interesting enzyme.* Clin Chim Acta, 1988. **173**(1): p. 43-55.
303. Fumagalli, F., et al., *Lentiviral haematopoietic stem-cell gene therapy for early-onset metachromatic leukodystrophy: long-term results from a non-randomised, open-label, phase 1/2 trial and expanded access.* Lancet, 2022. **399**(10322): p. 372-383.
304. Kohn, D.B., et al., *Autologous Ex Vivo Lentiviral Gene Therapy for Adenosine Deaminase Deficiency.* N Engl J Med, 2021. **384**(21): p. 2002-2013.
305. Thompson, A.A., et al., *Gene Therapy in Patients with Transfusion-Dependent β-Thalassemia.* N Engl J Med, 2018. **378**(16): p. 1479-1493.
306. Poch, C.M., et al., *Migratory and anti-fibrotic programmes define the regenerative potential of human cardiac progenitors.* Nat Cell Biol, 2022. **24**(5): p. 659-671.
307. Ueno, Y., et al., *Evaluation of differential gene expression by microarray analysis in small and large cholangiocytes isolated from normal mice.* Liver Int, 2003. **23**(6): p. 449-59.
308. Leal, A., et al., *A novel myosin heavy chain gene in human chromosome 19q13.3.* Gene, 2003. **312**: p. 165-71.
309. Vicente-Manzanares, M., et al., *Non-muscle myosin II takes centre stage in cell adhesion and migration.* Nat Rev Mol Cell Biol, 2009. **10**(11): p. 778-90.
310. Fu, X., et al., *Loss of Myh14 Increases Susceptibility to Noise-Induced Hearing Loss in CBA/CaJ Mice.* Neural Plast, 2016. **2016**: p. 6720420.
311. Grewal, T., et al., *Annexin Animal Models-From Fundamental Principles to Translational Research.* Int J Mol Sci, 2021. **22**(7).
312. Boersma, H.H., et al., *Past, present, and future of annexin A5: from protein discovery to clinical applications.* J Nucl Med, 2005. **46**(12): p. 2035-50.